Measurement and quantification of CO$_2$ from space.

Thesis is submitted for the degree of

Doctor of Philosophy

at the University of Leicester

by

Rhian Llinos Evans MPhys

Department of Physics and Astronomy

University of Leicester

September 2008

Declaration

I herby declare that no part of this thesis has been previously submitted to this or any other University as part of the requirement for a higher degree. The work within this document has been conducted by the undersigned except for contributions where acknowledged in this text.

Rhian Llinos Evans

September, 2008.

Measurement and quantification of CO$_2$ from space

by Rhian Llinos Evans

Abstract

Satellite retrievals are used to observe the distribution of CO$_2$ in the troposphere and to determine if the net surface fluxes in the lower troposphere can be calculated through combining normalised column CO$_2$ data. Satellites used are the Atmospheric Infrared Sounder (AIRS) and Scanning Imaging Absorption spectrometer for Atmospheric CHartographY (SCIAMACHY), which are sensitive to the upper and lower troposphere respectively. Annual variations in CO$_2$ concentrations are small in the upper troposphere producing seasonal cycle amplitudes between 1.1 and 7.7 ppmv, lower tropospheric seasonal cycles are much greater with amplitudes ranging from 6.7 and 22.6 ppmv.

Subtracting the CO$_2$ column data (SCIAMACHY – AIRS), the residual variability reflects in part the surface CO$_2$ variations. Comparisons are made with fractional green vegetation (FGV), the agreement between the data is very good, producing correlation values up to 0.96. SCIAMACHY column data also produced good agreement with the FGV data, suggesting that the subtracted data can measure the net surface fluxes, it is unclear whether the subtracted data represents the net surface fluxes better or worse than the SCIAMACHY data, further investigations are proposed.

Numerical Atmospheric Dispersion Model (NAME) is used to calculate the origin of tropospheric over different vegetation types. Results showed that lower tropospheric data originated from the surface beneath, upper tropospheric data emanated from multiple areas, indicating that the CO$_2$ in the upper troposphere is well mixed.

Acknowledgements

The past four years has been a great experience, I've met many interesting people and have made some fabulous friends!

There are lots of people I'd like to say thanks, firstly I want to thank you my supervisor Paul Monks for giving me this opportunity and his support throughout my PhD and also letting me go to conferences/holidays in some fabulous places. I'd also like to say thanks to Hartmut Boesch for his help and support, and also to NERC for funding me. I'd also like thank all of EOS members both past and present for their support and a big thank you to Mr Hewitt for all his help with IDL. Alan, you're a star!

Becks you were a fab housemate (except for the fact that you made me watch bad girls), thank you for putting up with me and for taking me with you to the Star Wars convention it was Amazing!

I'd especially like to give a big thanks to my parents and family for supporting me through my student years, (of which there have been many!) and will be glad to hear that I'll finally be getting a job.

And last but not least I'd like to say thank you to McDreamy, just because he's so damn gorgeous!

Table of Contents

Chapter 3: Comparisons of CO_2 in the upper and lower troposphere for 2003 measured by AIRS (4D-var method) and SCIAMACHY

Chapter 4: Comparisons of SCIAMACHY (FSI) WFM-DOAS and AIRS (LSQ method) column CO_2 data

Chapter 5: Tropospheric CO_2 comparisons with vegetation types over Africa for 2004

Chapter 6: Conclusions and future work

Chapter 1

Carbon dioxide in our atmosphere.

1.1 Climate change.

Earth's climate is a complex interactive system whose major components are the atmosphere, land, oceans, snow and ice. Climate is the 'average weather' or the mean value of temperature, precipitation and wind over a period of time [IPCC, 2007]. Over the past 150 years there has been a change in our climate, likely caused by factors such as increased use of fossil fuels, deforestation, change in land surface usage and an increase in population. The vast consumption of fossil fuels has increased the rate of anthropogenic emissions secreted into the atmosphere, which in turn effects the environment. Increasing evidence shows that glaciers are melting, weather systems are becoming more extreme, with increasing numbers of hurricanes and storms and localised areas of increased precipitation or drought. It's no coincidence that the increase of anthropogenic emissions is causing the changes in the climate.

Increased anthropogenic emissions, such as CO_2, NO_2, and many other greenhouse gases have a profound effect on the amount of infrared radiation trapped in the atmosphere. Increasing the radiation trapped in the atmosphere increases the global temperature, which in turn warms the oceans and melts the polar ice. Ice is a great reflector of incoming solar radiation. With decreasing ice volume, less radiation is reflected back out to space, which leads to increased atmospheric temperature, which in turn leads to greater amounts of ice melting, thus causing a positive feedback. If the anthropogenic emissions continue to rise the effect on the climate could be catastrophic.

Changes in the climate can be natural or induced through increased anthropogenic sources. Some may believe that the recent increases in the global temperatures, hurricanes, droughts and other deviations in 'typical' regional weather patterns are simply caused by natural changes of the planet. Measurements accumulated over the past 150 years shows that there is a direct correlation between the climate change and usage of fossil fuels [IPCC, 2007].

1.2 Greenhouse gases.

The earth reflects roughly one-third of the incoming solar radiation and absorbs approximately two-thirds of the solar radiation at the surface, (Figure 1.1) [IPCC 2007]. The energy radiated from the surface are at longer wavelengths which are located mainly in the Infrared region of the spectrum. Thermal Infrared radiation (TIR) is the radiation which is re-emitted back into space, from the land and oceans, some of which are trapped in the atmosphere by greenhouse gases (GHGs) and clouds and reradiated back to the surface. The re-radiated TIR radiation is called the greenhouse effect.

The compounds in the atmosphere which cause the greenhouse effect are primarily water vapour and CO_2. Increasing the amount of GHGs emitted into the atmosphere will increase the greenhouse effect, which in turn increase the mean global temperature.
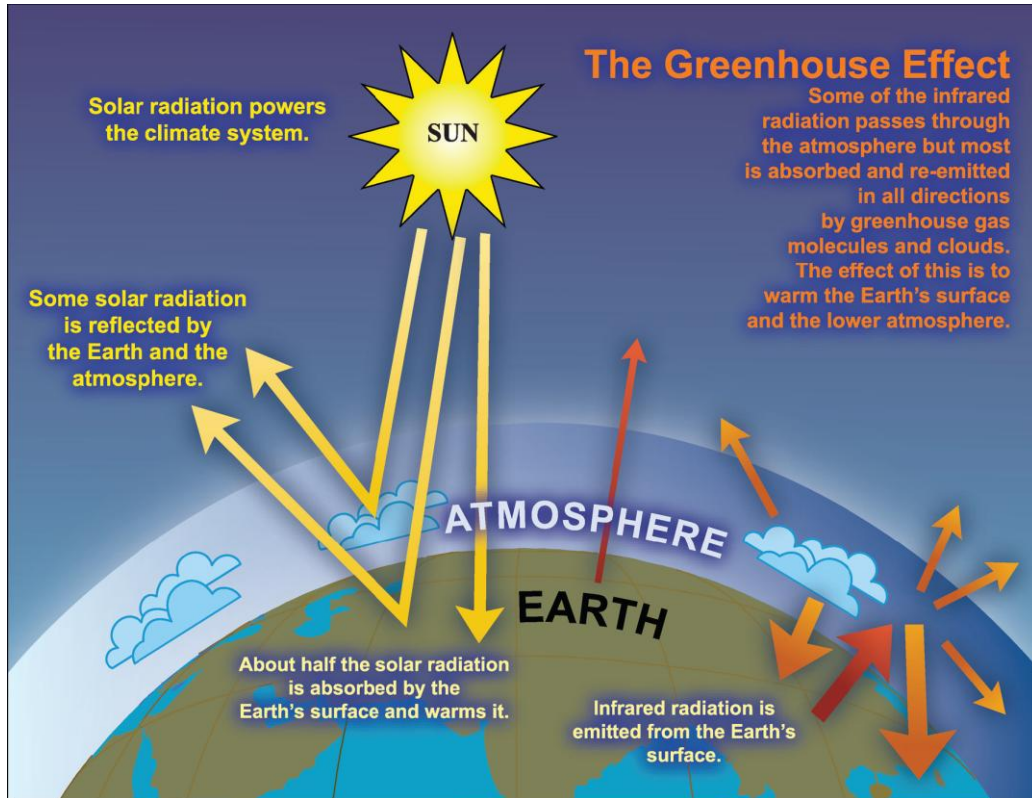
Figure 1.1. An idealised model of the natural greenhouse effect. (FAQ3 IPCC 2001)

The radiation emitted by the sun which enters the atmosphere, most of which is in the visible part of the spectrum. The visible light passes through the atmosphere (which is transparent to visible light), and is absorbed by the surface. The surface radiates energy in the thermal spectral range, which is not transparent to the atmosphere. Greenhouse gases absorb the infrared radiation emitted which is re-emitted in all directions within the atmosphere, where some escapes out to space and same is re-radiated back to the surface.

Greenhouse gases play a vital part to trapping heat in our atmosphere, without such gases the mean global temperature would be much lower than current values. [Peixoto, 1992]. The energy absorbed by the earths surface is approximately 240 Wm^{-2}. Through using the Stefan-Boltzman equation (equation 1.1) the mean global temperature is calculated to be -19 °C.

$$\sigma T_e^4 \approx 240 Wm^{-2} \qquad (1.1)$$

$$T_e = -19^o C \qquad (1.2)$$

The measured average global temperature is approximately 14^oC [IPCC 2004], the difference between the calculated and measured temperatures are due to the greenhouse effect, which increases the temperature by 33^oC [IPCC, 2004].

1.3 Radiative forcing

Radiative forcing (RF) is the radiative balance in the climate system at the top of the atmosphere caused by variations in GHGs [IPCC 2004].   In essence, 'radiative' is the change caused by factors that alter the balance between incoming and outgoing radiation within earth's atmosphere and the 'forcing' is the balance deviating from its normal state [Houghton et al., 2001.; IPCC 2001].   The contribution of each greenhouse gas to radiative forcing over a particular period of time is determined by the change in its concentration in the atmosphere over that period and the effectiveness of the gas in perturbing the radiative balance [IPCC, 2007].

Carbon dioxide is the GHG with the highest concentration in the atmosphere which is continuing to rise, and also has the greatest radiative forcing trapping radiation in the atmosphere causing the atmospheric temperature to rise. (Table 1.1)

Gas	Concentration	Radiative Forcing (W/m^2)	Lifetime (years)	GWP* 100 years
CO_2	365 ppmv	1.46	$\sim 100 \times 10^4$	1
CH_4	1745 ppbv	0.48	12×10^4	23
N_2O	314 ppbv	0.15	114×10^4	296
HFC-23	14 ppbv	0.002	260	12000
CF_4	80 ppbv	0.003	50000	5700
SF_6	4.2 pptv	0.002	3200	22200
CFC-11	268 pptv	0.07	45	4600

Table 1.1: Important Greenhouse Gases. Table show the concentration of various greenhouse gases in our atmosphere and also the increase of radiative forcing each has in the atmosphere. The lifetime shows how long each gas molecule stays in the atmosphere and GWP shows the global warming potential that each gas has in our environment. (adapted from Bréon and Peylin, 2003; http://cdiac.ornl.gov/pns/current_ghg.html)

Radiative forcing (RF) can be direct or indirect, the direct forcing is caused by a sudden change in the atmospheric GHG concentration and indirectly by chemical processes and their distribution throughout the atmosphere. Formulae derived for global RF by Ramaswamy et al, (2001) calculate that an increase of 3.7 Wm^{-2} is produced for a doubling in the CO_2 mixing ratio, [IPCC, 2004.; IPCC, 1990]. Atmospheric CO_2 concentrations in 2005 were measured at 379 ppm, using Ramaswamy equation produced a RF of +1.66 ± 0.17 Wm^{-2}, which is an increase of ~14% since 1998, [Ramaswamy et al,. 2001]

$$\Delta T_s = \lambda \cdot RF \qquad (1.3)$$

Radiative forcing can be related to the global mean surface temperature T_s using a linear equation (equation 1.3) where λ is the climate sensitivity parameter [Ramaswamy et al., 2001]. A positive forcing causes a warming at the Earth's surface and a negative forcing creates a cooling effect.
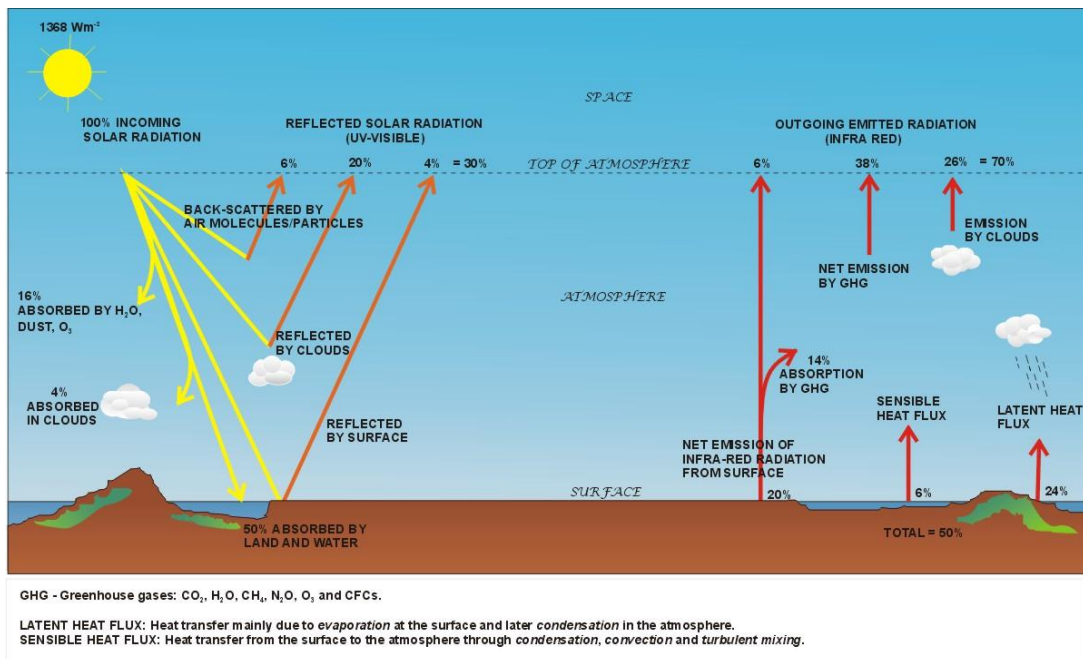
Figure 1.2; Global mean energy balance. Figure shows the amount of incoming and outgoing radiation through the atmosphere. [Courtesy of H. Sembhi and J. Remedios].

It is clear that there has been an increase in the climate's RF since the 1750s. CO_2 is one of the atmospheric gases responsible for the increase of RF. Anthropogenic emissions have significantly increased over the past few centuries, as a result the overall radiative forcing has increased. Not all aerosols cause an increase in the RF. The change in global land cover through changes in forests, croplands and reflective properties of snow and ice, produces a negative RF.
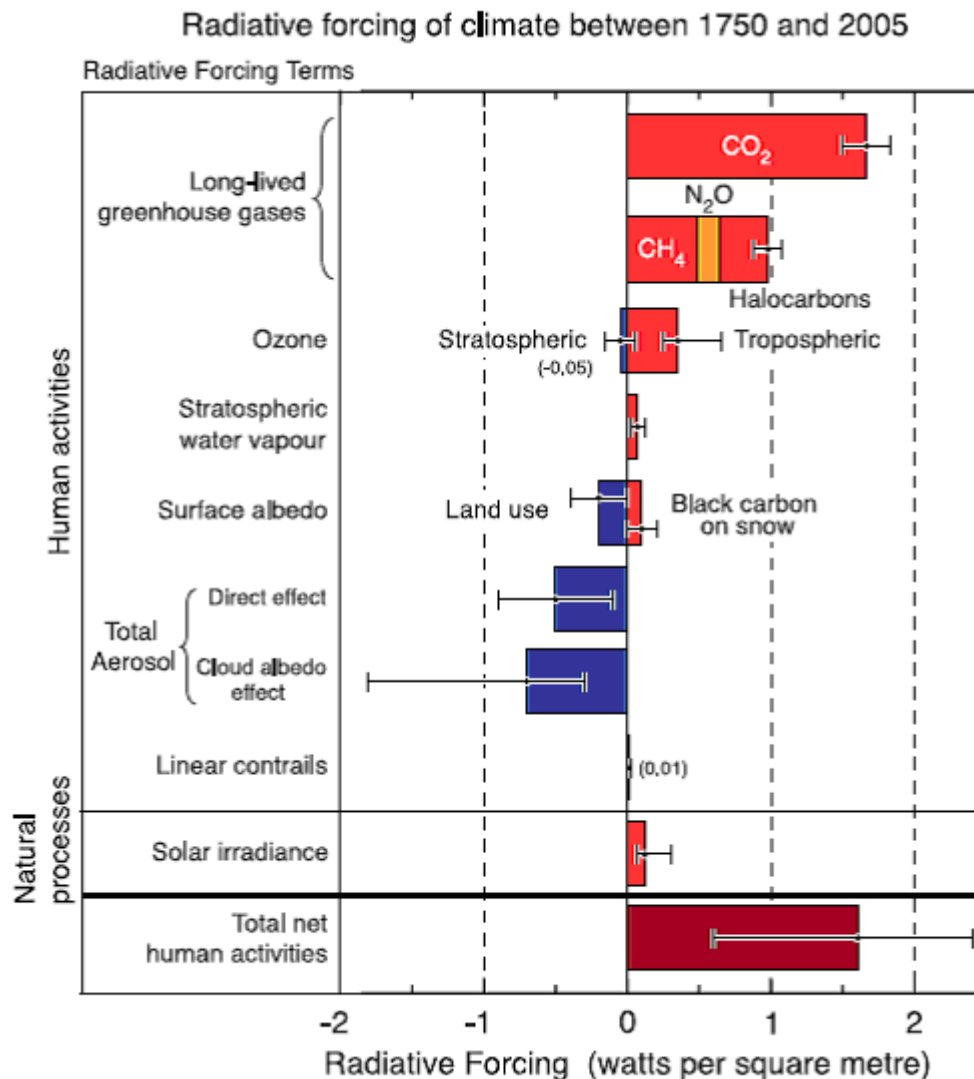
Figure 1.3 Change in GHGs cause a change in radiative forcing in our atmosphere. Radiative forcings shown result from natural or human activities. The values represent the change in the radiative forcing in 2005 compared to those in 1750 (the pre-industrial era). Human activities have caused significant changes in the radiative forcings since the pre-industrial era, due to the changes in long-lived gases such as ozone, water vapour, surface albedo, aerosols and carbon dioxide emissions into the atmosphere. Positive forcings lead to a warming of the climate and a negative forcing leads to a cooling. The error bars associated to each radiative forcing term represents an uncertainty for the respective value. [IPCC, 2007].

Carbon is also directly emitted into the atmosphere as particles. There are two different types of carbon emitted into the atmosphere contributing to the increased RF, which are organic carbon and black carbon. Organic carbon primarily consists of fossil fuel burning, emissions have been estimated to be 10 to 30 TgC yr^{-1} [Liousse et al., 1996; Cooke et al., 1999; Scholes and Andreae, 2000]. More recently, Bond et al. (2004) provided a detailed analysis of primary organic carbon emissions from fossil fuels, biofuels and open burning, and suggested that contained burning (approximately the sum of fossil fuel and biofuel) emissions are in the range of 5 to 17 TgC yr^{-1}, with fossil fuel contributing only 2.4 TgC yr^{-1} [IPCC., 2001]. Incomplete combustion of fossil fuels produces black carbon, global atmospheric estimates are 8 TgC yr^{-1}, 4.6 TgC yr^{-1} from bio and fossil fuels and 3.3 TgC yr^{-1} from open biomass burning, [Bond et al., 2004].

1.4 Atmospheric concentrations of carbon dioxide.

Carbon dioxide is one of the main contributors in global warming (Section 1.3), but with concentrations continually rising the true effects of the CO_2 emissions on global warming are yet unknown.

Atmospheric carbon dioxide concentrations can be measured as far back as 420,000 years [Petit et al, 1999]. Ice core samples are retrieved from Antarctica by drilling through the ice to depths up to 3626 m [Petit et al., 1997]. From the ice core samples CO_2 gas trapped in bubbles within the ice are extracted and its concentration measured. Figure 1.4 shows the CO_2 measurements retrieved from Antarctica ice core, which show that the CO_2 concentrations have varied dramatically over the past several thousand years varying between 180 ppmv to 280 ppmv $\pm$ 20 ppmv [Indermühle et al., 1999].

Carbon Dioxide Variations

The Industrial Revolution Has Caused A Dramatic Rise in CO_2

Ice Age Cycles
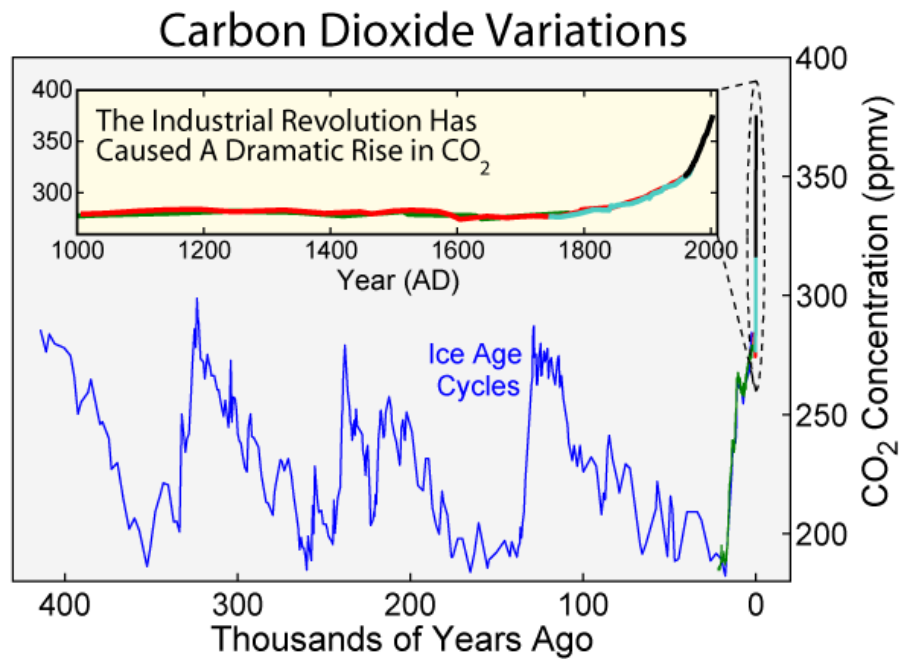
Figure 1.4. Variations of CO_2. Data retrieved from ice core samples in Antarctica. Data shows the change in CO_2 concentration over a period of 400 years. A sharp increase in atmospheric CO_2 levels are measured from circa 1750 to present, levels are much greater than those measured before the industrial revolution [IPCC, 2001]

The Vostok ice core represents a glacial/inter-glacial time-scale of the past four cycles spanning 420 Kyr (Figure 1.4). Measurements from the ice cores also show that with increasing atmospheric CO_2 concentrations there is an increase in the global temperature (Figure 1.5) which in turn prompts the melting of the ice [Fischer et al., 1999].

Antarctic Ice Core Data 1

Temperature Variation — CO2 Concentration
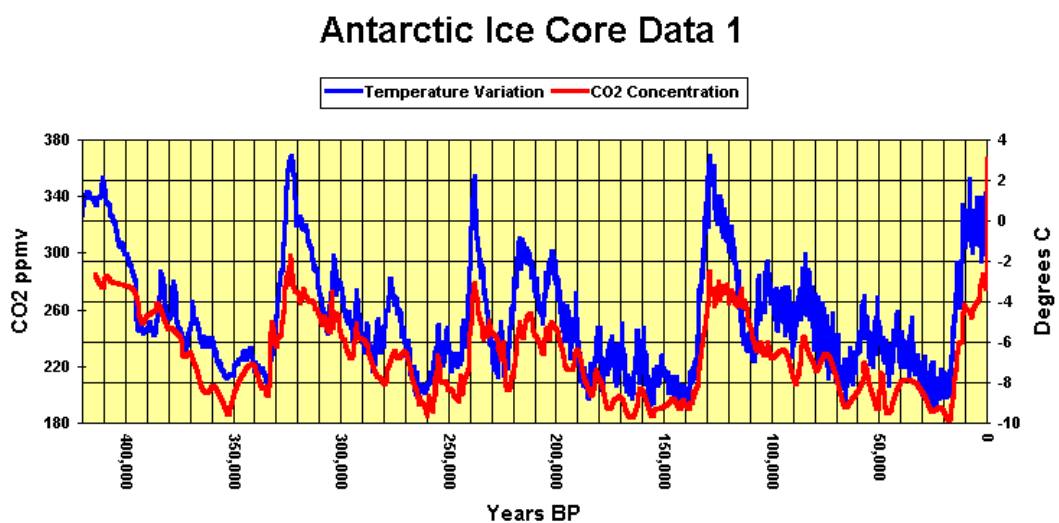
Figure 1.5; Temperature and CO_2 data retrieved from Antarctic ice core, [Petit et al., 1997].

17

Atmospheric CO_2 levels from 1750 to 10 Kyr ago, which is before the industrial revolution, have varied between 180 ppmv to 280 ppmv ± 20 ppmv (Indermühle et al., 1999) but in the last 150 years levels have increased from 280 to 380 ppmv in 2005 [Tiwari et al., 2006; Indermuhle et al., 1999; Conway et al., 1994], and are still rising [Indermuhle et al., 1999; Conway et al., 1994].   Research conducted on the ice core bubbles and the information gathered from Mauna Loa indicates that the burning of fossil fuels has had a considerable effect on the levels of CO_2 in the atmosphere [Keeling and Whorf., 2000].   The average rate of increase in CO_2 determined by these direct instrumental measurements over the period 1960 to 2005 is 1.4 ppm yr^{-1} [IPCC, 2007], contributing to an increase in radiative forcing of 1.66 ± 0.17 Wm^{-2} [IPCC 2001, Tiwari et al., 2006].

In 1958 Keeling began measuring the CO_2 in the atmosphere and discovered that fifty years later, the atmospheric CO_2 levels have been steadily increasing [Keeling et al., 1995].   Studies in Canada and Australia [Manning and Keeling, 2006] show that the O_2 concentration has been decreasing with the increasing CO_2, (Figure 1.6) burning fossil fuels requires O_2 for combustion. As we increase our usage of fossil fuels, the O_2 levels in our atmosphere will continue to decrease [IPCC, 2001].
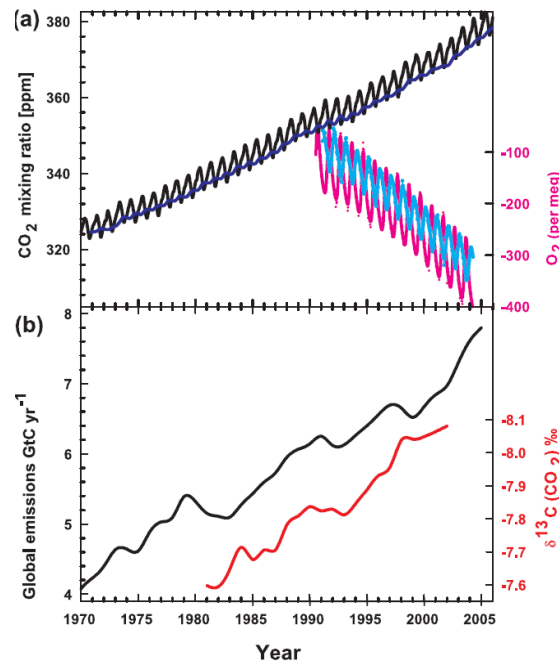
Figure 1.6; Recent CO_2 concentrations and emissions. (a) CO_2 concentrations (monthly averages) measured by continuous analysers over the period 1970 to 2005 from Mauna Loa, Hawaii (19°N, black; Keeling and Whorf, 2005) and Baring Head, New Zealand (41°S, blue; following techniques by Manning et al., 1997). Due to the larger amount of terrestrial biosphere in the NH, seasonal cycles in CO_2 are larger there than in the SH. In the lower right of the panel, atmospheric oxygen (O_2) measurements from fl ask samples are shown from Alert, Canada (82°N, pink) and Cape Grim, Australia (41°S, cyan) (Manning and Keeling, 2006). The O_2 concentration is measured as 'per meg' deviations in the O_2 / N_2 ratio from an arbitrary reference, analogous to the 'per mil' unit typically used in stable isotope work, but where the ratio is multiplied by 10^6 instead of 10^3 because much smaller changes are measured. (b) Annual global CO_2 emissions from fossil fuel burning and cement manufacture in GtC yr^{-1} (black) through 2005, using data from the CDIAC website (Marland et al, 2006) to 2003. Emissions data for 2004 and 2005 are extrapolated from CDIAC using data from the BP Statistical Review of World Energy (BP, 2006). Land use emissions are not shown; these are estimated to be between 0.5 and 2.7 GtC yr^{-1} for the 1990s Annual averages of the 13C/12C ratio measured in atmospheric CO_2 at Mauna Loa from 1981 to 2002 (red) are also shown (Keeling et al, 2005). The isotope data are expressed as $\delta 13C(CO_2)$ ‰ (per mil) deviation from a calibration standard. Note that this scale is inverted to improve clarity. [IPCC 2004., figure 2.3].

Not only does the CO_2 concentration increase each year, there is also a seasonal variation which is seen in Figure 1.7. CO_2 levels increase during the respective hemispheric winter months owing to less vegetation being able to absorb the CO_2 from the atmosphere. CO_2 concentrations decrease as the vegetation begins to blossom during the spring/summer months. Atmospheric oxygen concentrations also show seasonal variations, O_2 levels increase with increasing vegetative growth as green plants remove CO_2 from the atmosphere via photosynthesis and O_2 is released as a by-product. CO_2 and O_2 seasonal cycles are out of phase due to the absorption and respiration of the vegetation, an increase in vegetation produces an increase in atmospheric O_2 and a decrease in atmospheric CO_2 concentration. Owing to the increased land mass and anthropogenic sources in the northern

19

hemisphere the amplitude of the seasonal cycle is greater than the southern seasonal cycle, the two hemispheric cycles are approximately six months out of phase with each other, owing to the difference in their summer/winter months.
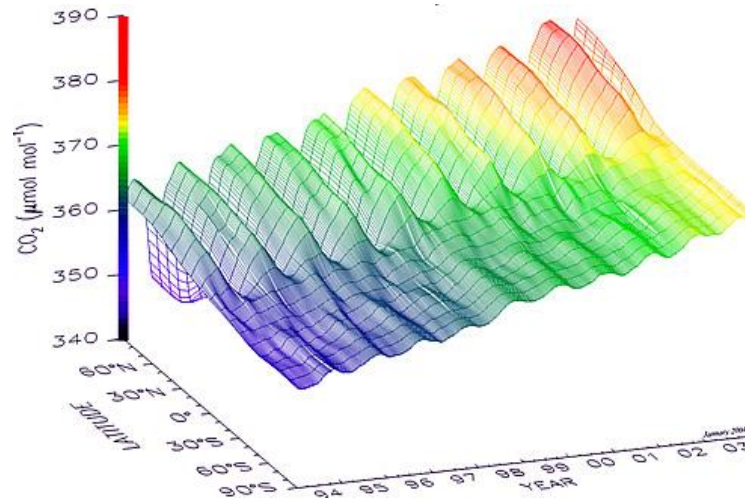
Figure 1.7. Change in atmospheric CO_2 between 1993 and 2003. Differences can be seen between the atmospheric CO_2 concentration in the northern and southern hemispheres, with the CO_2 concentration in the sourthern hemisphere lower than those measured in the northern hemisphere. A general increase in CO_2 concentrations can be seen in both hemispheres over the 10 year period (NOAA ERSL GMD).

1.5 The carbon cycle.

The oceans, land and atmosphere maintain a balance of CO_2 entering and leaving each system. This balance is maintained through the uptake and release of CO_2 to and from each system.

Global Flows of Carbon
(Petagrams of Carbon/Year)
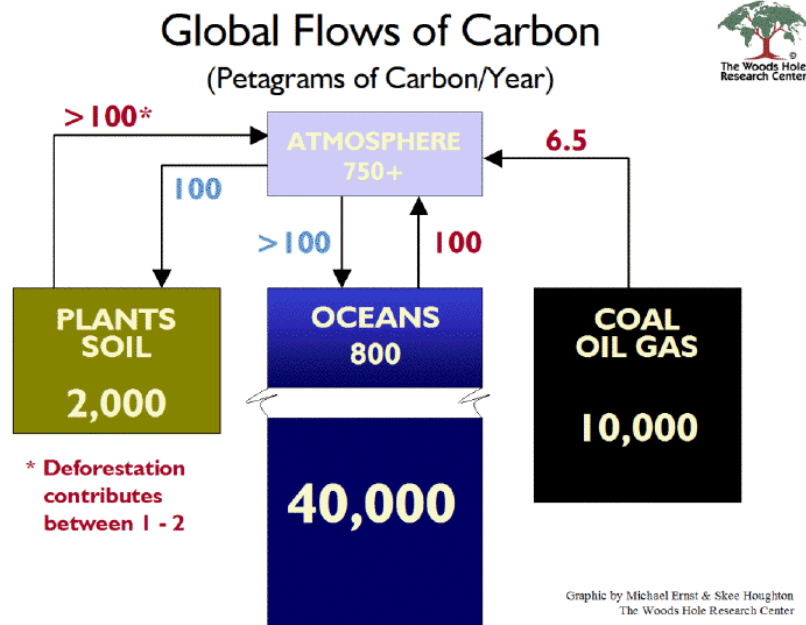
Figure 1.8; The flow of Carbon ($GtCyr^{-1}$) through our environment per year. Diagram shows the amount of carbon stored in each system and also the amount of carbon ($GtCyr^{-1}$) released into the atmosphere in red and the quantity absorbed by the oceans and vegetation in blue (NASA website www.nasa.gov).

Carbon exists in many forms within our environment, these include CO_2, carbonate rocks ($CaCO_3$) and dead organic matter. Carbon is emitted naturally from the land and oceans through plant and animal respiration and forest fires. Carbon dioxide is also released anthropogenically into the atmosphere through the consumption of fossil fuels. Before the industrial revolution, the carbon cycle maintained a balance of emission and absorption of CO_2. The increase of fossil fuel consumption has significantly increased the quantity of anthropogenic CO_2 being expelled into the atmosphere. The carbon cycle is continually adjusting its equilibriative state in order to compensate, with increasing amounts of CO_2 being absorbed by vegetation and the oceans.
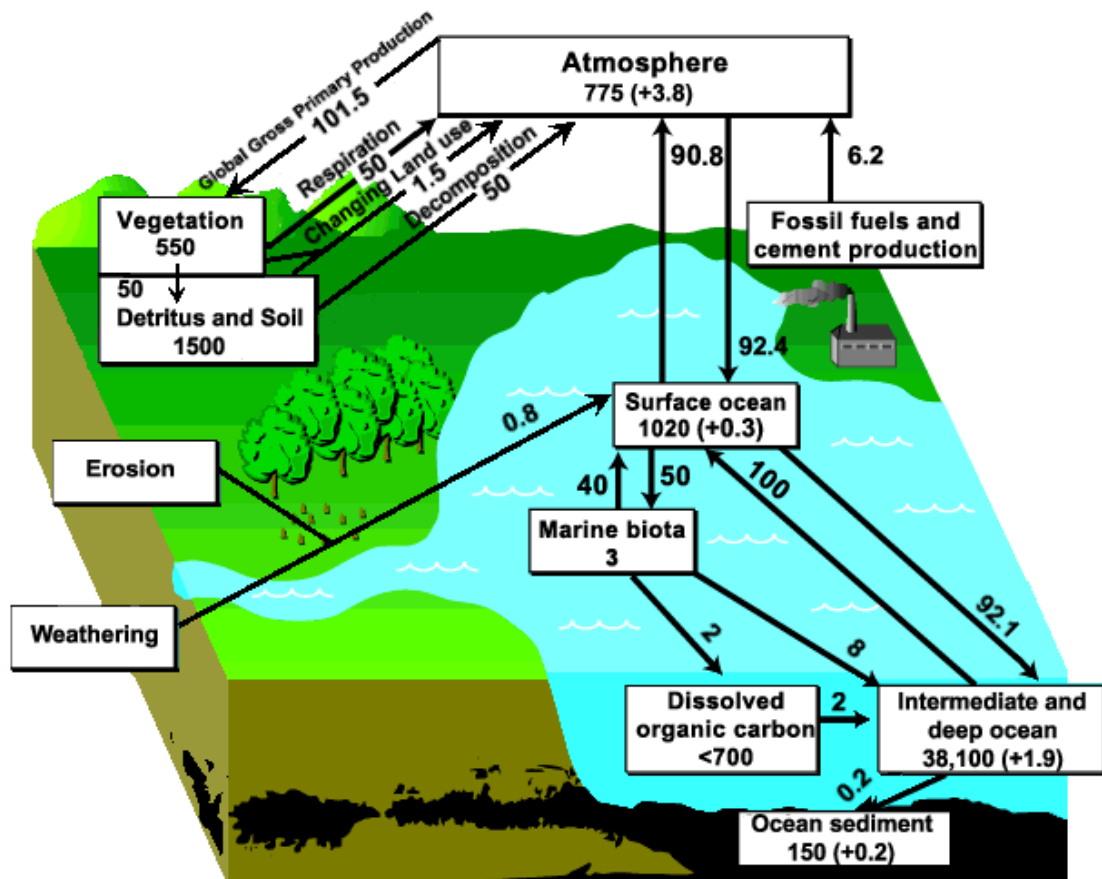
Figure 1.9; Global carbon cycle, Shows carbon yearly carbon flux in gigatones (GtC). [CDIAC: www.cdiac.ornl.gov/images/carbon_cycle]

1.5.1 Terrestrial CO_2

Carbon is transferred from land to the atmosphere through respiration, biomass burning, land use change and burning of fossil fuels. Anthropogenic emissions have continually increased between 1999 and 2005, the emission rate rose steadily from 6.5 to 7.8 GtC yr^{-1} (Marland et al., 2006) or about 3.0% yr^{-1}. The terrestrial biosphere attempts to compensate for the increase of emissions through additional uptake of CO_2 via photosynthesis in green vegetation.

The terrestrial carbon cycle component is comprised of two reservoirs; vegetation and soil. Vegetation and soil comprise of four fluxes; photosynthesis, plant respiration, litter-fall turnover and soil respiration. Carbon is absorbed by vegetation through photosynthetic uptake and is released beck into the atmosphere via plant respiration, soil respiration and turnover (litter fall). The amount of

carbon stored and emitted by the soil varies depending on the litter fall (carbon absorbed) soil respiration (carbon emitted) [Lenton and Huntingford., 2003].

Present-day global vegetation is estimated to contain about 450 GtC [Bolin et al., 2000], approximately 150 GtC of which is released into the environment as CO_2 due to a change in land-usage [Houghton, 2005]. Excess carbon is also released into the atmosphere owing to nitrogen fertilization. Present-day carbon soil reservoirs have increased, with values ranging from 1200-1600 GtC for surface soils [Post et al., 1990] and 2000 GtC for soils up to 1 meter in depth [Bolin et al., 2000], indicating a good sink for CO_2.

Vegetation in the terrestrial sink removes carbon from the atmosphere through photosynthesis.

$$6CO_2 + 6H_2O \rightarrow C_2H_{12}O_6 + 6O_2 \qquad (1.4)$$

Within the biome carbon exists not only as CO_2, but is also in the leaves, animals and microbes in various forms. Carbon can be stored in the biome for many tens of years. The amount of carbon within the biome is defined as the Net Biome Productivity (NBP). NBP is a measure of the net flux of CO_2 (the uptake and release of CO_2) between the land into the atmosphere.

Vegetation plays a vital role in absorbing CO_2 from the atmosphere, approximately 60 GtC yr^{-1} is drawn down by global vegetation. CO_2 is also released by the plants via respiration, more CO_2 is absorbed than respired by the vegetation into the atmosphere, which makes the global vegetation a natural sink of carbon. The greatest influence on the carbon flux within the land cycle is owing to the plants absorbing and respiring CO_2. However, there are a whole myriad of sources of CO_2, such as fires both natural and anthropogenic, change in land usage, animal respiration, anthropogenic emissions from industrial usage are just a few to mention. The only terrestrial CO_2 sink is the vegetation, which absorbs around 2190 GtC yr^{-1}, which is currently decreasing. Between 1890 and

1990, forest cover had decreased by roughly 11 million km^2 [Ramankutty and Foley., 1999; IPCC, 2004].

Small variations of CO_2 in the environment can be compensated by the cycle adjusting itself, through increasing or decreasing the amount of CO_2 absorbed. Over the last century, the carbon cycle has needed to compensate for increasing anthropogenic CO_2 emissions and decreasing forests, which has resulted in excess CO_2 in the atmosphere. However, the oceans have absorbed a significant amount of CO_2 and have the capacity to store CO_2 for many years, before it is upwelled and released back into the atmosphere. During the 1990s fossil fuels and industrial emissions were estimated to be +6.4 ± 0.4 $PgC\ yr^{-1}$, the oceanic flux was -2.2 ± 0.4 $PgC\ yr^{-1}$ (uptake) and the terrestrial flux was -1.0 ± 0.6 $PgC\ yr^{-1}$ [Denman et al., 1996, 2007].

Unbalancing the carbon cycle through increased amounts of anthropogenic CO_2 emitted into the atmosphere each year could have dire effects on our environment. Projections indicate an atmospheric CO_2 concentration of 450 ppmv by the year 2100, this will result in a global equilibrium warming of 1.4°C to 3.1°C, which translates as an additional 105 to 300 GtC released into the atmosphere (IPCC 2007).

1.5.2 Oceanic Carbon dioxide.

The oceanic water column is vertically stratified, which strongly inhibits vertical water movements. The water column can be separated into 3 layers: the surface ocean, pycnocline and the deep ocean. These layers are determined by the oceanic density distribution, which are governed by salinity and temperature distributions [Wright and Colling., 1995]. The most important layer is the surface mixing layer, as this is where the CO_2 enters and exits the oceans. Understanding how the CO_2 circulates within the ocean is essential in understanding how the CO_2 concentrations vary within the ocean.

The surface mixing layer is located between the oceanic surface up to a depth of 100m. It contains the least dense water, which is well mixed by the action of the winds and waves. This region is the main region for biological production. The pycnocline lies beneath the mixing layer, which extends to an approximate depth of 1000m. Water density rapidly increases with depth; this is typically associated with the thermocline. (The thermocline is the zone where temperature quickly decreases from the surface values to the top temperature of the underlying deep-water zone). The deep ocean, which contains the denser water, extends from a depth of 1000m to the bottom. Neither temperature nor salinity are affected by seasonal variations. This zone is characterized by the absence of vertical gradients in the chemical composition.

Figure 1.10 portrays the oceanic carbon cycle. The ocean absorbs CO_2 from the atmosphere in an attempt to reach equilibrium by direct air-to-sea exchange. This process takes place at extremely low rate, measured in hundreds to thousands of years. However, once dissolved in the ocean, a carbon atom will stay there, on average, more than 500 years [McElroy., 2002., IPCC, 2001]. There are two 'pumps' which circulate the CO_2 around the ocean, these are the 'solubility pump' and the 'Biological pump'. Before describing these pumps in detail, it is important to understand what is happening to the CO_2 as it enters the boundary layer.
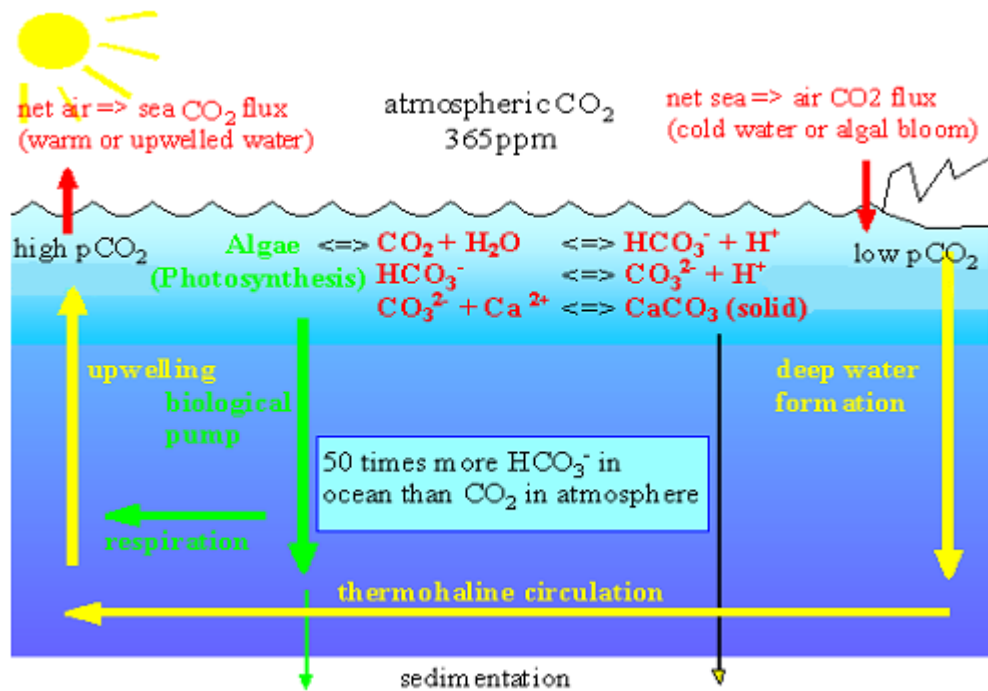
Figure 1.10; The two main processes which transfer carbon between the mixed layer and the deep water. Biological pump; occurs between the oceanic vegetation and the uptake of CO_2 from the ocean and CO_2 released back into the ocean via its respiration. Solubility pump; occurs in the top 1 meter layer of the ocean where CO_2 enters the ocean and through a series of chemical processes it is dissociated into its ions and can be changed into calcium carbonate. The amount of CO_2 entering the ocean at the polar regions is less than those upwelled back into the atmosphere at the equator. [www.chooseclimate.org]

The chemical reactions, which occur in the seawater, are referred to as the carbonate system. The chemical reactions that occur explain why the ocean can store more CO_2 than the atmosphere. There are three main parts of the dissociation of CO_2 these thermodynamic equilibria are;

$$CO_{2(aq)} + H_2O \leftrightarrow H_2CO_3^- + H^+ \tag{1.5}$$

$$H_2CO_3 \leftrightarrow HCO_3^- + H^+ K^1 \cong 10^{-6} \text{ mol l}^{-1} \tag{1.6}$$

$$HCO_3^- \leftrightarrow CO_3^{2-} + H^+ K^2 \cong 10^{-10} \text{ mol l}^{-1} \tag{1.7}$$
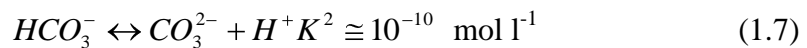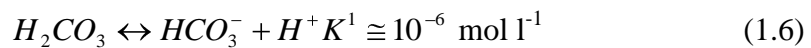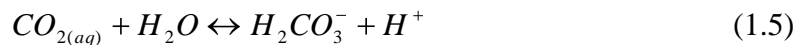
The CO_2 reacts with water to form carbonic acid (Equation 1.5). Carbonic acid can lose a proton to form bicarbonate ions (Equation 1.6), which can lose another proton to form carbonate ions (Equation 1.7).

Only about one in every ten molecules of CO_2 added to the current ocean remain as dissolved CO_2 and thereby contribute to increasing the water pCO_2, the other

nine molecules mainly form bicarbonate ions. The oceans have a high capacity to store CO_2. An increase in natural or anthropogenic CO_2 emitted into the atmosphere can potentially be absorbed by the ocean. However, the transfer CO_2 from the atmosphere into the ocean is slow. Model simulations indicate that 100 to 200 years would be required to absorb two-thirds of the carbon emitted into our environment since the industrial revolution. Although the ocean can absorb significant amounts of the anthropogenic CO_2 emitted into our atmosphere, the time required for the CO_2 to dissociate into its ions is extensive. Much of the CO_2 is re-emitted back into the atmosphere before it has time to dissolve into the ocean. The oceans are helping to diminish the rate of CO_2 emitted into the atmosphere. However due to the lengthy absorption rate, the uptake of CO_2 is not immediate, hence the continual increase of CO_2 in our atmosphere.

The oceanic carbon cycle is complex, the amount of CO_2 entering and leaving the ocean is dependent on many components. The rate determining factors for transfer of CO_2 between the atmosphere and the ocean are the solubility and biological pumps. Since the solubility of CO_2 in seawater at 0 °C is approximately twice that at 30 °C, the surface mixed layer can contain more CO_2 in equilibrium with the atmosphere in the cold polar seas where it's subducted, than it can in warm equatorial regions where it is upwelled, as shown in Figure 1.10.

The Solubility pump is, as the name suggests, how carbon dissolves in the ocean and how it is pumped around the ocean, (The chemical process of how the CO_2 dissolves in the oceans water has been explained in Equations 1.5 to 1.7). The surface waters evaporate and some water forms ice, leaving remaining sea water with higher salinity content. The sea water with higher salinity content is denser than the surrounding water it begins to sink down through the pycnocline towards the deep ocean. Here the temperature and salinity does not vary, this is also known as the thermohaline circulation. The water moves very slowly towards lower latitudes where further carbonate ions are added to the deep waters. Travelling to lower latitudes where the water is slightly warmer at these depths, the water begins to rise and is heated further as it enters the pycnocline and upper levels, where the CO_2 is finally degassed back into the atmosphere. However,

owing to the uptake of additional CO_2 molecules throughout the ocean, the amount of CO_2 being degassed into the atmosphere is significantly greater at lower latitudes than the amount absorbed at the polar regions.

Contributing to the CO_2 levels being degassed is the biological pump. As the name suggests it involves the marine life of the ocean that is the flora and fauna. The oceanic vegetation absorbs CO_2 via photosynthesis, and respire CO_2. When the vegetation dies, carbon is contributed to the sedimentation at the base of the ocean. Fish and other aquatic life that respire CO_2 also contribute to the thermohaline circulation and hence the amount of CO_2 degassed into the atmosphere. These two oceanic pumps determine how much carbonate is dissolved into the ocean and how much CO_2 is dissolves and degassed.

1.6 Climate change.

1.6.1 Future CO_2 levels

Anthropogenic emissions are the main cause of the continual increase in atmospheric CO_2 levels. Each year, excess CO_2 emissions are accumulating in the troposphere where more heat can be trapped in our atmosphere, some CO_2 is absorbed by vegetation and the Oceans, but due to the decrease in rainforests and forests globally less CO_2 is removed from the atmosphere. With the decrease in global vegetation and increase in anthropogenic CO_2 along with the long lifetime of CO_2, the atmospheric levels will increase exponentially. Models run to calculate future atmospheric levels with various scenarios, predict that the future levels will increase between 20 and 220 ppmv by 2100. Atmospheric CO_2 concentrations simulated by these coupled climate-carbon cycle models range between 730 and 1020 ppmv by 2100 [IPCC., 2007]

1.6.2 Kyoto protocol

On the 11th December 1997 in Kyoto, Japan a protocol to the international framework convention on climate change with the objective of reducing greenhouse gases was agreed. The Kyoto protocol is an agreement between various countries to commit to reducing their emissions of CO_2 and 5 other greenhouse gasses. Globally there are more than 170 countries endorsing the protocol, which is greater than 60% of global countries willing to reduce their emissions of global greenhouse gasses[1] into the atmosphere. The primary objective of the Kyoto[1] protocol is to achieve "stabilization of GHG concentrations in the atmosphere at a level that would prevent dangerous anthropogenic interference with climate change[2]. All Annex I (developed countries) from January 2008 through 2012 have agreed to reduce their GHG emissions by a collective average of 5% below their 1990 levels.
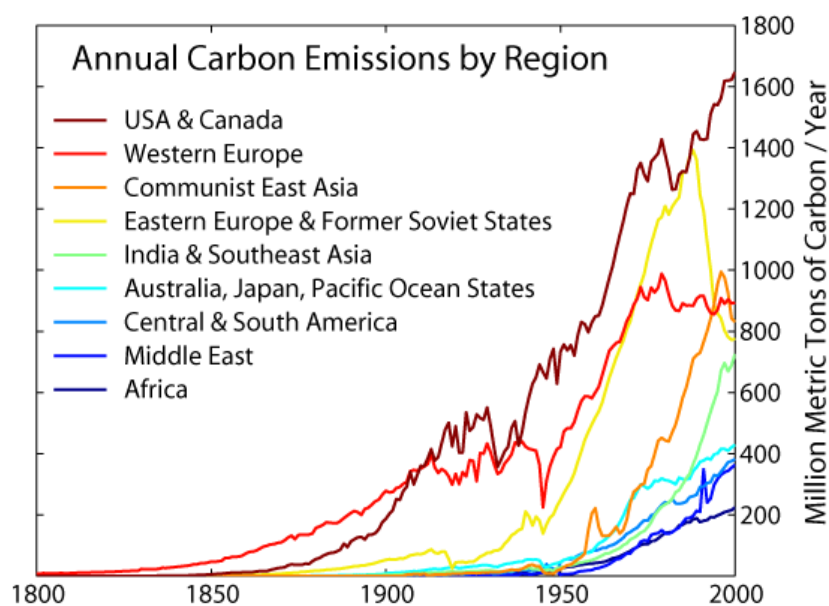
Figure 1.11; Regional anthropogenic carbon emissions in GtC from 1800 – 2000 [image created by Robert A. Rhode/global warming art: www.globalwarmingart.com].

---

[1] Climate talks face international hurdles, by Arthur Max, Associated press, 5/14/07

2. Article 2 *The United Nations Framework Convention on Climate Change*. Retrieved on November 15, 2005

1.6.3 Model predictions.

As the climate continues to change, models project an increase in extreme weather such as rainfall intensity, especially in the northern hemispheric land which is likely to cause very wet winters over central and northern Europe. Similar results are projected for summer precipitation with implications for more flooding in tropical areas and the Asian monsoon region, [IPCC 2001]. Multi-model projections based on SRES scenarios give reductions of oceanic pH of between 0.14 and 0.35 units in the 21st century, adding to the present decrease of 0.1 units from pre-industrial times [IPCC, 2007].
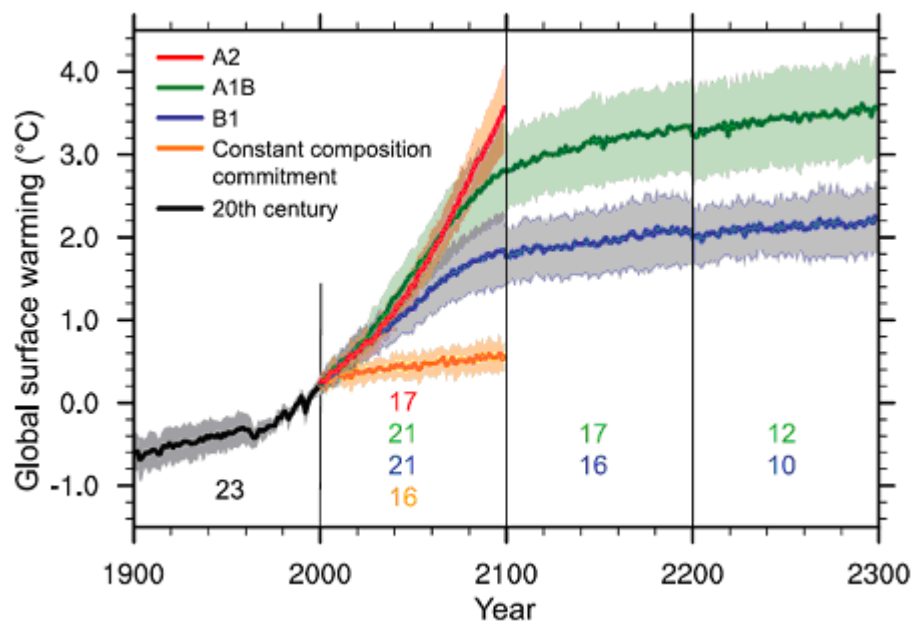
Figure 1.12; Model predictions of future global surface warming (relative to 1980 – 1999). Lines show the multi-model means, shading denotes between the $\pm$ 1 standard deviation range of individual model annual means. Discontinuities between different periods have no physical meaning and are caused by the face that the number of models that have run a given scenario is different for each period and scenario, as indicated by the coloured numbers given for each period and scenario at the bottom of the panel. A2 scenario; a rapid increase in population, development of technology which is non-dependant on fossil fuels but population is slow and fragmented to use the technology. Scenario A1B; balance of non- fossil fuel energy sources caused by need to stop use of fossil fuel energy sources. Scenario B1; rapid economical growth of global population , which declines after 2050, use of clean, resource efficient technologies. Scenario 'constant composition commitment'; use of non-fossil fuel technologies. [IPCC 2007].

Atmospheric CO_2 concentrations simulated by these coupled climate-carbon cycle models range between 730 and 1,020 ppmv by 2100 [IPCC 2007]. Constant CO_2

emissions at year 2000 values would lead to concentrations reaching about 520 ppmv by 2100 [Friedlingstein et al., 2001, 2006; IPCC 2007]. For a doubling of atmospheric carbon dioxide (CO_2), or 'equilibrium climate sensitivity', is *likely* to lie in the range 2°C to 4.5°C, with a most likely value of about 3 °C.

1.7 Summary.

Increasing the amount of carbon dioxide emitted into the atmosphere is clearly impacting the earth's climate. Carbon dioxide is a greenhouse gas which traps thermal radiation in the atmosphere, which is radiated by the earth's surface. With increasing amounts of CO_2 being expelled into our atmosphere each year, the mean global temperature has increased by approximately 1.33 °C between 1900 and 2005, which in turn is causing the polar ice caps to melt and hence increasing sea levels [IPCC, 2007]. Anthropogenic emissions are clearly responsible for the rise in the atmospheric CO_2 levels, their long term effects on the climate are uncertain, but it is clear that the climate is changing as a result of the additional emissions.

1.8 Thesis outline.

Atmospheric CO_2 concentrations are measured by satellites, aircraft and ground based instruments. Each method has its merits, satellites are able to cover large areas within a small time frame, where as in-situ measurements are able to measure specific areas and altitudes with greater accuracy. Combining the various methods a greater understanding of how CO_2 is mixed through the atmosphere can be attained.

This thesis aims are to measure the distribution of CO_2 concentrations both globally and regionally within the troposphere. Subtracting upper tropospheric normalised column CO_2 data (retrieved from AIRS) from a full column normalised CO_2 data (retrieved from SCIAMACHY) is calculated to determine if

the data remaining produces a better representation of the surface fluxes, which are validated with in-situ measurements.

Two satellites are used to measure the tropospheric CO_2 concentrations these are; the Scanning Imaging Absorption spectrometer for Atmospheric CHartographY (SCIAMACHY) on board ENVISAT and Atmospheric Infrared Sounder (AIRS) which is on board AQUA. Each satellite is sensitive to different tropospheric regions, SCIAMACHY is sensitive to the lower troposphere and AIRS the mid-upper troposphere, Chapters 3 and 4 compare the retrievals from the two satellites to determine if the CO_2 is well mixed through the troposphere or if sinks and sources can be detected. Through combining the satellite retrievals with in-situ measurements a greater accuracy can be attained in the measurements produced by the satellites.

Global and regional seasonal cycles measured each year are influenced by vegetative growth, the magnitude of the change of CO_2 concentrations in the upper and lower troposphere are uncertain. Chapter 5 examines the comparisons of fractional green vegetation with CO_2 concentrations measured in the upper and lower troposphere to determine how much influence the local vegetation has on the CO_2 concentration in the troposphere over Africa. Numerical Atmospheric ModEl (NAME) is used to calculate the likely origin of CO_2 measured in the upper and lower troposphere. The NAME model will aid in establishing if the CO_2 measured in the upper and lower troposphere were emitted from the surface directly beneath were the measurements taken or if the CO_2 concentrations originated from another location.

Chapter 2

Atmospheric Carbon dioxide retrievals from space-borne instruments.

2.1 Introduction.

Satellites are a major contributor to our understanding of how CO_2 is distributed throughout the atmosphere. Atmospheric CO_2 concentrations have been continuously rising since the industrial revolution [IPCC, 2007]. Determining where the major emissions and absorptions of CO_2 to and from the atmosphere with greater accuracy is vital to our understanding of climate change. The CO_2 retrievals from two satellite instruments which are sensitive to different tropospheric regions are used to determine how CO_2 is distributed throughout the atmosphere. The two satellites used are; Atmospheric Infrared Sounder (AIRS) and Scanning Imaging Absorption spectrometer for Atmospheric CHartographY (SCIAMACHY), which are sensitive to the upper and lower troposphere respectively.

2.2 Measuring CO_2.

Atmospheric CO_2 is measured by a variety of instruments which are situated in space, airborne, on the ground or on ships. Combinations of in-situ and satellite data are used to attain an accurate representation of the CO_2 distribution through the atmosphere. Satellites are able to attain global coverage within 3 to 6 days depending on the instrument used and its orbit. Due to the time taken to attain

global coverage daily variations of CO_2 are not seen, weekly and monthly mean concentrations are calculated globally from which annual variations can be determined globally and regionally.

2.2.1 Precision requirements of satellite data.

GLOBALVIEW - CO_2 network consists of around 120 stations worldwide, the instruments measures CO_2 on a daily basis to improve our understanding of the atmospheric CO_2 budget [GLOBALVIEW- CO_2, 2005].   Ground based measurements are also used to determine regional scale exchanges of CO_2, [Rodenbeck et al., 2006; Macatangay et al., 2008], however these measurements are spatially limited, and given that some of the measurements sites are in close proximity to sources and sinks the results could be bias [Washenfelder et al., 2006]. The retrievals measured within the network have uncertainties of around 0.1 ppm (0.03%), [Miller et al., 2007].

Space-based instruments may offer a solution to the spatial and temporal distributions of CO_2 sources and sinks, by providing global column measurements of CO_2 [Yang et al., 2002]. Satellites are able to measure column averaged CO_2, which is the mean distribution of CO_2 through the troposphere (and stratosphere). Spatial resolution of satellite measurements are much less than those retrieved from in-situ measurements, the 'footprint' (or area) measured by each satellite varies. SCIAMACHY at nadir measures 30 x 60 km and AIRS is 13.5 km^2. Rayner and O'Brien [2001] showed that if the measurements of space-based XCO_2 are of adequate precision and spatial coverage the data could dramatically improve our understanding of CO_2 sources and sinks. The dry air mole fraction (XCO_2) can be calculated from the simultaneous measurements of CO_2 and O_2 soundings. XCO_2 (the ratio of the CO_2 to O_2) will eliminate the environmental variables from the measurements, such as clouds, surface pressure, humidity and temperature [Crisp et al., 2004]. Precisions for XCO_2 global coverage retrievals measured by space-based instruments would need to be less than 2.5 ppm (0.7% of 375 ppmv) on a 8° x 10° scale in order to match the performance of the existing

ground based network at monthly or annually timescales [Rayner and O'Brien., 2001].

2.2.2 Thermal infrared measurements.

Measurements from the AIRS instrument have been used to derive CO_2 concentrations either by incorporating AIRS radiances into a 4d-variational (4D-var) assimilation calculated by Engelen et al, (2004, 2005) or by Barnet et al, (2005) devised a retrieval scheme of 'Least squares method'(LSQ).

The thermal IR radiance $I(\lambda)$ reaching a satellite instrument is governed by both the composition and temperature of the atmosphere directly beneath it. This can be represented using the Schwarchild equation:

$$I(\lambda) = \varepsilon_s B(\lambda, T_s) \cdot \Gamma(\lambda, T) + \int_{z=0}^{\infty} B(\lambda, T) \cdot \frac{d\Gamma(\lambda, p, T)}{dz} dz + R_s I_{down}(atm) \tau(\lambda, \infty) \quad (2.1)$$

where ε_s is the surface emissivity, $B(\lambda, T)$ is the Planck function, Γ is the atmospheric transmission (equal to $e\text{-}^{\tau\lambda}$ where $\tau\lambda$ is the optical depth) and where p, T and λ indicate the pressure, temperature (the subscript S denotes the surface temperature) and wavelength respectively. R_s is the radiation reflected at the surface, $I_{down}(atm)$ is the intensity of the radiation at the surface and τ (λ, ∞) transmission of the atmosphere between the ground and space.

The first term represents the contribution from the surface whilst the second represents the atmospheric contribution and the third term is the radiation emitted by the atmosphere towards the surface and reflected back towards space. The atmospheric component is equal to the integral, from the surface to the top of the atmosphere (i.e. $z = \infty$), of the Planck function weighted by the corresponding derivative of the transmission for each individual height layer within the atmosphere. The derivative of the transmission, otherwise known as the weighting function, determines how much each height layer of thickness dz contributes to the

total radiance leaving the top of the atmosphere. Data which are sensitive to different altitude regions (i.e. where the weighting function peaks) can be retrieved through selecting specific wavelengths.

CO_2 within the mid–upper troposphere has typically been transported and mixed so that the original CO_2 surface flux signal is diluted. The vertical profile measured represents an area spanning several kilometers, as the weighting functions retrieved typically covers several kilometers thus only a column integral over a specific altitude region is usually possible [Engelen et al., 2004; Engelen and McNally, 2005]. Although the results of these works show good agreement with large scale trends, the use of CO_2 data derived from thermal IR instruments to reduce the uncertainties in the global carbon cycle fluxes is somewhat limited (e.g. Chevallier et al. (2005) or Tiwari et al. (2006)). This is because thermal IR sensors are only sensitive to light originating from CO_2 emissions in the mid-upper troposphere (as indicated by the arbitrary averaging kernels shown in Figure. 2.1..

2.2.3 Near infrared Techniques

The advantage of the using NIR wavelengths to determine CO_2 concentrations is that the (solar) light is sensitive to changes in the CO_2 concentration near the surface as photons (in the absence of scattering) traverse the atmosphere twice before being detected by satellite. Thus, the near surface sensitivity of the NIR makes it the ideal spectral region for observing surface fluxes. To a first order approximation [Breon and Peylin, 2003], the NIR radiance $I(\lambda)$ measured by a satellite-borne instrument is given by:

$$I(\lambda) = I_0(\lambda) \cdot R(\lambda) \cdot \Gamma(\lambda) \qquad (2.2)$$

where $I_0(\lambda)$ is the solar irradiance, $R(\lambda)$ is the surface reflectance (or albedo) and $\Gamma(\lambda)$ is the atmospheric transmission. Whilst both the solar irradiance and surface

reflectance vary with wavelength for a limited spectral interval, the transmission will exhibit many spectral features due to the absorption of light. The depth of each absorption line (or feature) of a given trace gas is directly dependent on its concentration along the observational line of sight. Therefore by examining the depths of the absorption lines it is possible to infer the amounts of various trace gases present in the atmosphere using common retrieval techniques such as differential optical absorption spectroscopy [Platt and Stutz, 2006] and optimal estimation [Rodgers, 2000].
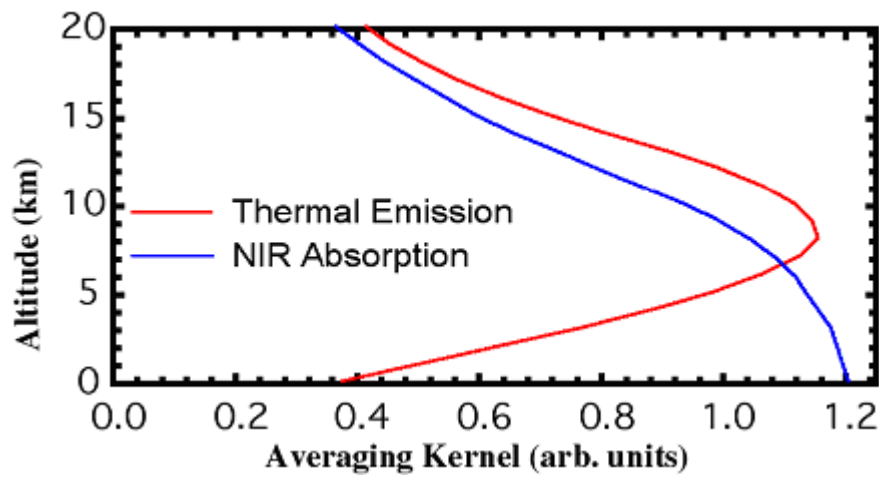
Figure 2.1: Averaging kernels of thermal IR (AIRS; red) and NIR (SCIAMACHY;blue) retrievals [Crisp et al., 2004].

The advantage of using the thermal IR is that measurements can be made both day and night and also over the oceans over which NIR measurements can be retrieved in a sun-glint viewing geometry, but measurements taken are limited to day-light hours only [Dufour and Breon, 2003].

Two instruments will be considered here which measure tropospheric CO_2, these are AIRS and SCIAMACHY. Each instrument are sensitive to different tropospheric regions, AIRS measures (TIR) CO_2 and SCIAMACHY in the (NIR) spectral region, (Figure 2.1) located at 3.7 - 15.4 μm and 1.57 μm respectively. TIR measurements are sensitive in the middle troposphere at an altitude between

8-14 km [Engelen et al., 2005] NIR is sensitive to CO_2 variations in the lower troposphere which are around an altitude of 1-5 km [Barkley et al., 2006].

2.3 Atmospheric InfraRed Sounder (AIRS).

2.3.1 AIRS instrument.

The Atmospheric InfraRed Sounder (AIRS) was launched May 4th 2002 on the EOS AQUA spacecraft, AIRS is designed to provide both new and more accurate data regarding the atmosphere, land and oceans. AIRS looks down at the Earth and measures the infrared brightness coming up through and from the atmosphere. The simultaneous measurements form AMSU, HSB and AIRS provide both new and improved measurements of cloud properties, atmospheric temperature and humidity, land and ocean skin temperature with the accuracy resolution and coverage required by numerical weather prediction and climate models. AQUA is situated at an altitude of 705 km at an inclination of $98.2^{o} \pm 0.1°$, which crosses the equator twice daily descending at 1:30am and 1:30 pm ascending. AIRS coverage is pole-to-pole, the swaths do not overlap at low latitudes, and some points at the equator are missed, but are scanned within 2-3 days.
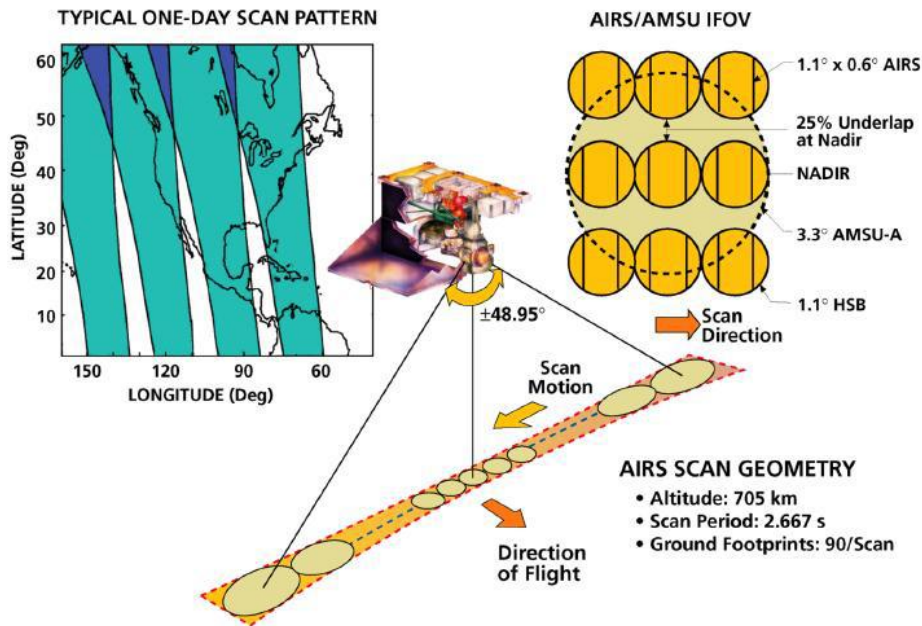
Figure 2.2. AIRS scanning geometry. [www-AIRS.jpl.nasa.gov/]

AIRS uses a cross-track rotary scan mirror to look towards the ground, which provides a ± 49.5 degrees from nadir ground coverage along with views to cold space and to on-board spectral and radiometric calibration sources every scan cycle. Ninety ground footprints are observed with each scan, which repeats every 2.67 seconds (2 second scan followed by a rapid scan in 0.67 seconds comprising a routine calibration) and produces one spectrum with 2378 spectral samples obtained within each footprint.

The AIRS IR spatial resolution is 13.5 km^2 at nadir and 41.0 x 21.4 km at the scan extremes from a nominal 705.3 km orbit. A set of visible and near infrared detectors (Vis/NIR) with a resolution of approximately 2.3 km is also measured by AIRS. These channels provide a diagnostic imaging capability for observing low-level clouds.

AIRS uses a cooled (155 K) array grating spectrometer which operates between 3.7 and 15.4 μm at a spectral resolution of $\lambda/\Delta\lambda = 1200$. The spectroscopic approach uses a grating to disperse infrared energy across arrays of HgCdTe detectors operating at 58 K. All 2378 spectral samples are measured simultaneously in space and time, this measurement is essential for accurate

temperature retrievals under partially cloudy conditions. The AIRS spectrometer is a pupil imaging, multi-aperture, Echelle grating design that utilizes a coarse 13 l/mm grating at high orders to disperse infrared energy across a series of detector arrays. The grating spectrally disperses each image, which is overlaid onto the HgCdTe detector array with each detector viewing a unique wavelength by virtue of a grating dispersion.

The AIRS optical system splits infrared radiation into its constituent colors (Figure 2.3). The wavelengths used are sensitive to temperature and water vapour over a range of heights in the atmosphere, from the surface up into the stratosphere. The term sounder refers to the fact that temperature and water vapour are measured as functions of height, AIRS also measures clouds, abundances of trace components in the atmosphere including ozone, carbon monoxide, carbon dioxide, methane, and sulfur dioxide, and detects suspended dust particles.
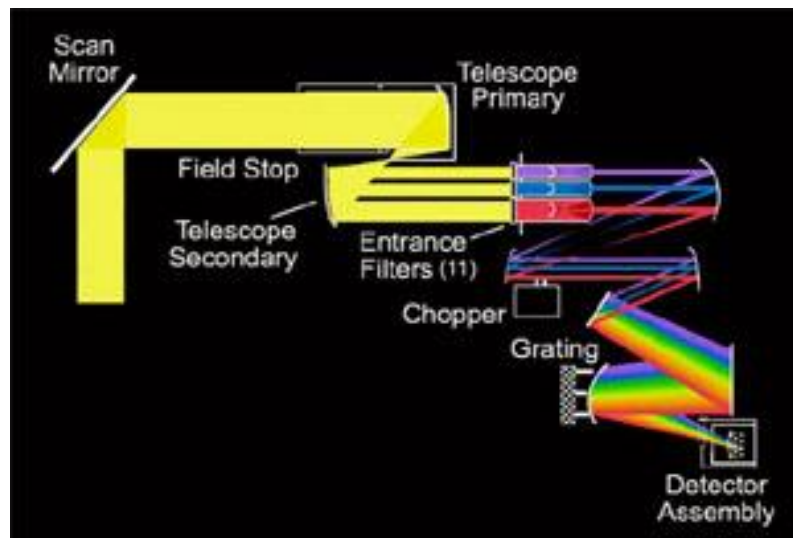
Figure 2.3. Light travels through AIRS optics.
Credit: Zareth Gorjian, Jet Propulsion Laboratory.

Upwelling radiance enters the system via the cross track scan mirror, where it's directed into a 4-mirror off-axis telescope assembly. The collimated energy exciting the telescope is incident on the spectrometer entrance slit plane containing 11 individual apertures arranged in two staggered columns. These eleven slits are

imaged onto the focal plane, where each slit image contains the energy from one selected grating order.
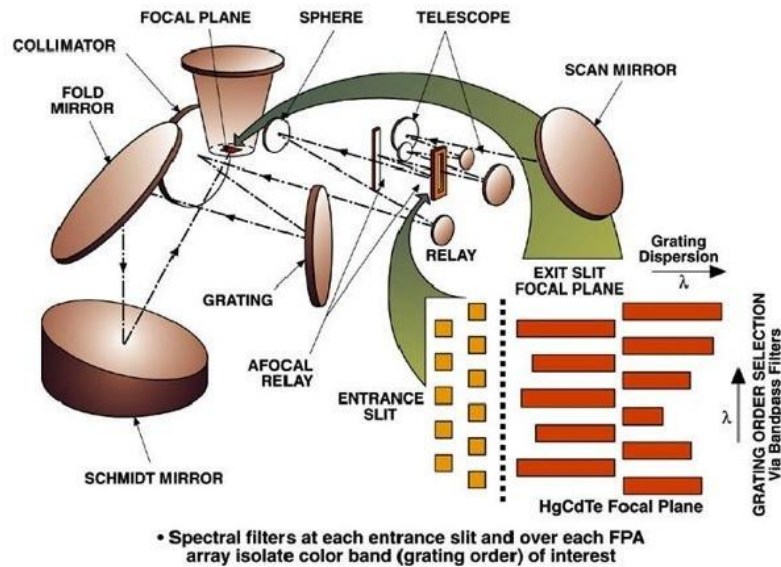
Figure 2.4. Infrared spectrometer assembly. The multi-aperture, array grating spectrometer is an advanced pupil-imaging design providing high spectral resolution, wide spectral coverage and full spectral multiplex operation The design approach uses a coarse echelle grating in combination with high definition bandpass filters to create a two-dimensional color map compatible with state of the art IR FPA technology. Image from NASA website.

AIRS infrared spectrum provides information on various gases in the atmosphere, it forms a "fingerprint" of the state of the atmosphere for a given place and time. AIRS provides column abundances of minor atmospheric gases; CO_2, CH_4 and ozone. The retrieval accuracy in the presence of clouds is $1°$ K for 1 km, with each footprint being $1°$ x $1°$ which corresponds to a 13.5 km footprint.

2.4 Calculating CO_2 column data from AIRS retrievals.

AIRS is capable of measuring variations of atmospheric trace gases such as carbon dioxide, water vapour, ozone and temperature. This capability coupled with AIRS broad swath pattern, low and well characterized instrument noise and global coverage afforded by a method of cloud clearing [Susskind et al., 2003] enables

the derivation of the distribution of CO_2 in the mid-upper troposphere on global scales, twice daily.

Two AIRS CO_2 products are used to examine the distribution of CO_2 in the mid-upper tropospheric regions. The first method of retrieval uses a four dimensional variation (4D-var) assimilation method (AIRS-4D) [Engelen et al., 2004] and the second uses a least squares method (AIRS-LSQ) [Maddy et al., 2008].

2.4.1 Four-dimensional variation (4D-var) data assimilation system.

Four-dimensional variation (4D-var) data assimilation system is a practical formulation of Bayesian estimation theory for the particular case of a new linear problem with unbiased Gaussian errors [Lorenc, 1986]. 4D-var is a method of estimating a set of parameters by optimizing a fit between observations (CO_2 retrievals from AIRS) and the solution of the model (RTTOV radiative transfer model [Matricardi et al., 2004]). The 4D-var seeks a model trajectory that is statistically consistent with the information provided by the observations y^0 which are available for the analysis time window [t_0, t_n] and the information provided by an a-priori model state x_b which is the background state, which is taken from a short-range weather forecast.

The model trajectory is defined by the initial state x_0 at time t_0. An analysis correction $(\delta x/(t_0))$ is retrieved from a combination of the initial state and the background analysis through using an objective cost function $J(\delta x/(t_0))$ [Courtier et al., 1994].

$$J(\delta x/(t_0)) = \frac{1}{2}\delta x(t_0)^T B^{-1}\delta x(t_0) + \frac{1}{2}\sum_{i=0}^{n}[H_i\delta x(t_i) - d_i]^T R^{-1}[H_i\delta x(t_i) - d_i] \quad (2.3)$$

The cost function (Equation 2.3) is made up of two terms, the first term is the background and the second the initial state, where d_i are the observation

departures, which are the differences calculated between the observed radiances retrieved from AIRS and the simulated model radiance (calculated from a radiative transfer model). H is the full nonlinear observation operator and B and R are the background and observation error covariance matrices [Engelen et al., 2004].

2.4.1.1 Analysis error

For CO_2, each analysis uses a climatological background state of CO_2, where the CO_2 information from the model used in the 4D-var assimilation is not carried over from one analysis to the next, a new background state is used for each retrieval in order to reduce errors.

Each individual retrieval produced from the 4D-var assimilation comes with its own analysis error (σ_a), which is calculated from the background error (σ_b), the observation error covariance (R) and the CO_2 Jacobians (H):

$$\sigma_a^2 = [\sigma_b^{-2} + H^T R^{-1} H]^{-1} \tag{2.4}$$

Separate calculations of the Jacobians (H) are made for each observation.

The value of the analysis error relative to the background error shows how much information is gained from the observations and can be formally represented by the averaging kernel (Figure 2.5) [Rodgers, 2000]. For a single scalar analysis the tropospheric column averaging kernel is defined as;

$$A = 1 - \frac{\sigma_a^2}{\sigma_b^2} \tag{2.5}$$

Values of *A* obtained are between 0 and 1. Zero represents areas where background data only is used and values of unity are pure observational retrievals.
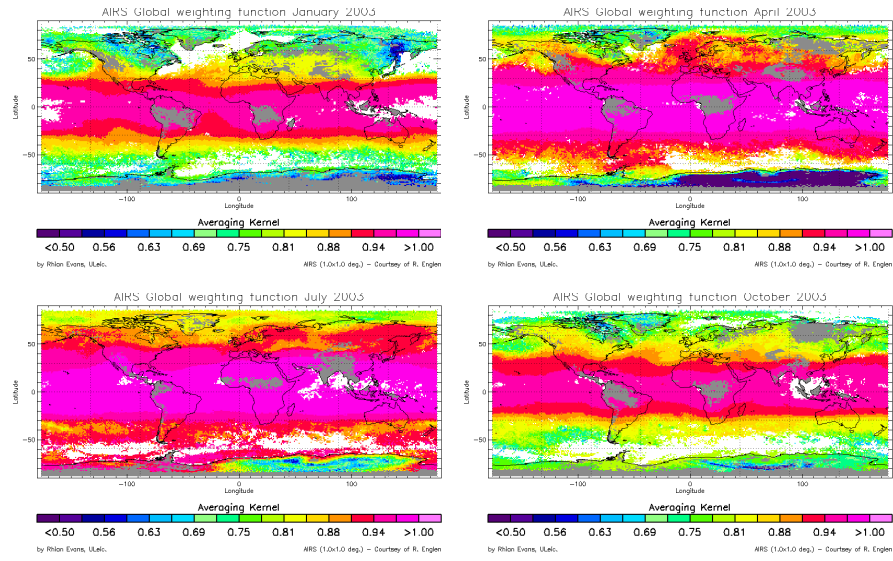
Figure 2.5 Averaging kernels from 2003 on a 1° x 1° grid. Calculated using the 4D-var method.

Figure 2.5 shows how the calculated averaging kernels vary globally and annually, showing that the retrievals are more accurate at the tropics (± 30°). With increasing latitude there is also a decrease in the information used from AIRS, the background values contribute more to the retrievals at higher latitudes, caused by a lower tropopause and smaller temperature lapse rates at higher latitudes.

2.4.1.2 Constraints on the AIRS data available for processing in the 4D-var system.

ECMWF receives data from 324 out of the 2378 channels available to measure CO_2, these channels are further reduced to avoid problems specific to certain spectral bands. Channels which are sensitive to the upper stratosphere were excluded as they have large temperature biases in the mesosphere and polar winters; channels sensitive to water vapour and ozone were removed to minimize their effect on the CO_2 retrievals. The removal of these biases reduces the number of channels available to 55 in the long-wave CO_2 absorption band, of which 31 are sensitive to tropospheric CO_2.

 The tropospheric CO_2 column data calculated by the 4D-var assimilation system uses cloud cleared data only, which further reduces the number of channels used.

The detection algorithm used was developed by McNally and Watts [2003], which detects AIRS channels which are affected by clouds and removes those channels from the assimilation, while keeping the channels unaffected by clouds.

2.4.2 AIRS CO_2 retrieval: Least squares method.

For the retrieval of CO_2 and other geophysical parameters a regularized non-linear least squares solution [Susskind et al., 2003] is used to minimize the AIRS observations in the form of cloud-cleared radiances [Maddy et al., 2008].

The Advanced Microwave sounding unit (AMSU) (which is also onboard AQUA) utilizes an O_2 absorption band for temperature sounding. The addition of the O_2 dependent microwave measurements to the CO_2 sensitive IR measurements will decouple the temperature/CO_2 interdependence. To reduce the interdependence between the temperature and CO_2 for AIRS retrievals, a covariance term is introduced for the temperature retrieval and cloud clearing steps, due to the variability in the CO_2 in the covariance matrix noise channel [Susskind et al., 2003].

For each retrieval the channel noise covariance matrix also includes errors due to instrument noise, radiative transfer modelling errors and uncertainties in various other trace gas concentrations.

Physical retrieval of the AIRS CO_2 radiances and other trace gas radiances requires several processes. The retrieval process begins with a cloud clearing step, where CO_2 is held constant at a background value based on ESRL/GMD fit. Using the cloud-cleared radiances, retrievals for temperature, moisture, surface properties and ozone are determined. Addition of noise covariance term due to CO_2 in the cloud-cleared and temperature retrieval steps minimizes the impact of systematic errors in the assumed background CO_2 value on the retrieved CO_2. The CO_2 channels respond to temperature changes more rapidly in the 4.3 μm band than in the 15 μm band, to take advantage of this the CO_2 AIRS retrievals utilize

68 channels in the 15 μm band and 1 in the 4.3 μm band. The 69 channels produce four coarse layers in the troposphere and one in the stratosphere.

The 69 channels used are sensitive to the CO_2, O_3, T and water vapour in addition to an estimate of the instrument noise, the algorithm used weights each channel by expectation of variability of the parameters in the least square inversion. These channels are selected based on the simulations as well as signal-to-noise ratio considerations due to interfering species.

.
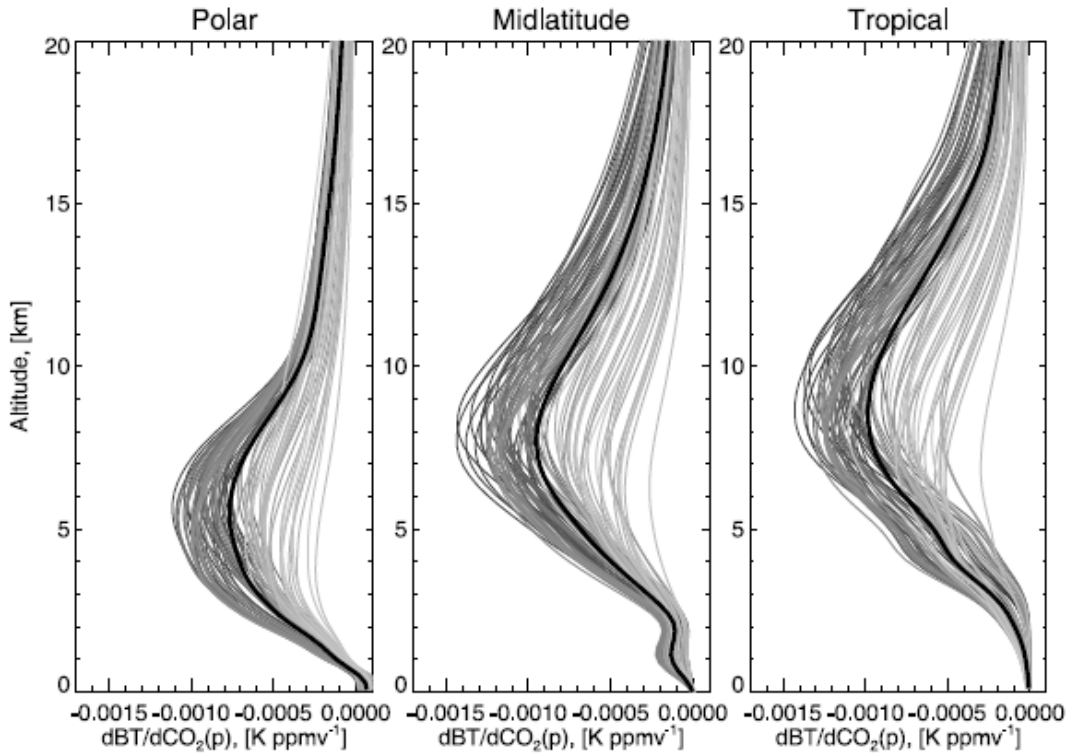
Figure 2.6: CO_2 Jacobians for a 1 ppmv layer perturbation for the 69 AIRS channels used in the NOAA retrieval. Polar, midlatitude, and tropical situations shown to illustrate the effect of H_2O displacement onthe peak altitude. The average Jacobian over all channels is shown as the thick black line [Maddy et al., 2008].

Perturbing the atmospheric CO_2 concentration by 1 ppmv induces a change in the brightness temperature. Figure 2.6 illustrates the change in brightness temperature for a 1 ppmv CO_2 change. The brightness temperature decreases where the CO_2 is most sensitive in the atmosphere. As shown in Figure 2.6 the AIRS CO_2 radiances

are most sensitive at different altitudes in the tropics, mid-latitudes and at the polar region, these sensitivity changes are due to water vapour, clouds geophysical parameters such as ozone and lapse rate.

The AIRS measurements possess approximately one piece of information on the vertical distribution of CO_2, Figure 2.6 shows that the maximum sensitivity of the CO_2 Jacobians in the vertical position. The CO_2 Jacobians are a function of temperature, water vapour and other geophysical parameters, which causes the change in maximum sensitivity with altitude. The mean Jacobian in Figure 2.6 is plotted in black which is the average value of the 69 channels used in the retrieval process (plotted in gray) [Maddy et al., 2008].

2.5 SCIAMACHY (Scanning Imaging Absorption spectrometer for Atmospheric CHartographY).

2.5.1 SCIAMACHY instrument.

Scanning Imaging Absorption spectrometer for Atmospheric CHartographY (SCIAMACHY) was launched March 2002 onboard ENVISAT. SCIAMACHY is a passive UV – VIS – NIR hyper-spectral spectrometer designed to measure tropospheric and stratospheric composition and processes. SCIAMACHY was launched on, into a sun-synchronous polar orbit, crossing the equator on its descending node (southwards) 10:00 am local time. Eight separate grating spectrometers are used to measure the scattered sunlight from the earths surface, covering the spectral range 240 – 2380 nm. Near polar sun-synchronous orbit irradiance and lunar radiance are measured using solar/lunar occultation. The Vertical column densities (VCDs), of various trace gasses, whose absorption features lie within SCIAMACHY's spectral range, can then be determined through the inversion of the logarithmic ratio of the earthshine radiance and solar irradiance via differential absorption spectroscopy (DOAS). [Barkley et al., 2006]. Atmospheric distributions are determined by retrieving CO_2 VCDs from nadir observations made in the NIR, specifically at the CO_2 band at 1.57 μm. Each

pixel within the swath is 60 by 30 km^2 corresponding to an integration time of 0.25 s. Global coverage is achieved at the equator within 6 days.
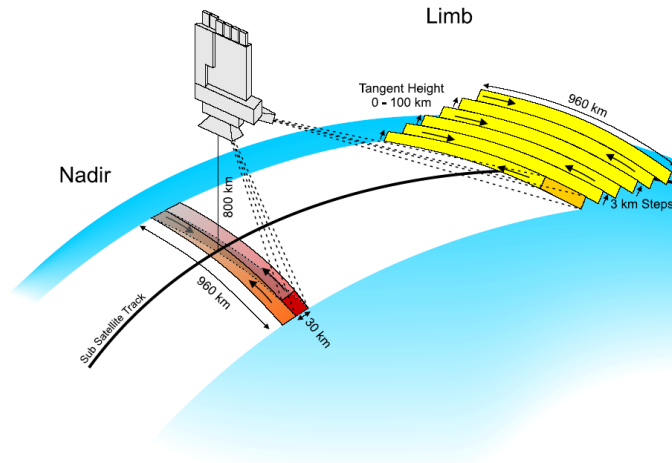
Figure 2.7: Nadir and limb viewing geometries[http://www.iup.uni-bremen.de/sciamachy/instrument/introduction/index.html]

SCIAMACHY's prime objective is to investigate the chemistry and dynamics of the Earth's atmosphere from the retrieval of a wide range of atmospheric gases, aerosols, pressure, temperature, radiation field, cloud parameters and surface reflectance.
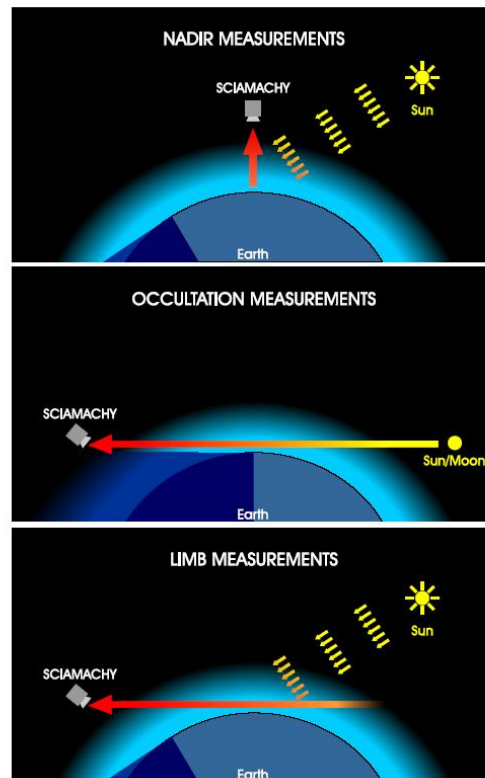
Figure 2.8: Viewing geometries of the SCIAMACHY instrument [http://www.iup.uni-bremen.de/sciamachy/instrument/introduction/index.html]

SCIAMACHY measures atmosphere in three different modes. These are; Nadir, Limb and occultation (Figure 2.8) In Nadir mode the atmosphere directly below the sensor is viewed producing retrievals with good spatial but poor vertical resolution. Radiation incident on the sensor is reflected sunlight from the surface and scattered from the atmosphere. A characteristic scan consists of the nadir mirror scanning across track for 4 s followed by a fast 1 s backscan. This is repeated for 65 or 80 s according to the orbital region. The ground swath viewed is 960 x 30 km, across/along track.

Limb mode looks tangentially into the atmosphere detecting scattered solar radiation. This produces observations with good vertical but poor spatial resolution. A typical scan consists of 34 horizontal scans, starting at 3 km below the horizon. Each scan lasts for 1.5 s where a 3 km jump in elevation before a scan is performed in the reverse direction. This gives a swath width of 960 km at the tangent point, consistent with nadir observations.

In solar occultation mode the sun is observed, in lunar mode the moon is viewed. The SCIAMACHY instrument actively tracks the sun and moon giving an improved performance. The sun is followed with scans performed up to an altitude of 100 km with a horizontal and vertical resolution of 30 km and 2.6 km respectively.

2.5.2 SCIAMACHY CO_2 retrieval method: FSI WFM-DOAS.

Differential Optical Absorption spectroscopy (DOAS), is a widely used technique to derive atmospheric concentrations of trace gases. Here a summary of how the DOAS retrieval calculates the atmospheric concentration of trace gases and the modified version which is used to determine the Volume Column Density (VCD) of CO_2 from SCIAMACHY radiances is given.

DOAS is a technique that identifies and quantifies trace gas abundances with narrow band absorption structures in the near UV and visible wavelength region in the atmosphere [Platt et al., 1994].

The change in intensity of light $dI(\lambda, r)$ which traverses through an infinitesimally small volume element (or atmosphere) of thickness dr at a specific location defined by r is given by:

$$dI(\lambda, r) = -I(\lambda, r) \sum_i \rho_i(r) \sigma_i(\lambda, r) dr \qquad (2.6)$$

Where $\sigma_i(\lambda, r) \equiv \sigma_i(\lambda, T(r), p(r))$ is the wavelength, temperature and pressure dependent absorption cross section, $\rho_i(r)$ is the density or concentration of absorbing (i^{th}) trace gas species within the volume element. Integrating Equation 2.6 gives the Beer-Lambert law which states that the intensity of a light beam decreases exponentially with optical density $\tau(\lambda)$:

$$I(\lambda) = I_0(\lambda)\exp\left[-\int_0^L \sum_i \rho_i(r)\sigma_i(\lambda,r)dr\right] \qquad (2.7)$$

Where Equation 2.8 is the optical density of the volume element

$$\tau(\lambda) = \frac{\ln(I_0(\lambda))}{\ln(I(\lambda))} = \int_0^L \sum_i \rho_i(r)\sigma_i(\lambda,r)dr \qquad (2.8)$$

If the absorption cross section is constant over the light path or the effect of the temperature and pressure on the absorption cross section is small, so that the dependency of r is assumed to be negligible. Therefore Equation 2.8 is re-written as:

$$\tau(\lambda) = \frac{\ln(I_0(\lambda))}{\ln(I(\lambda))} = \sum_i \sigma_i(\lambda) \cdot \int_0^L \rho_i(r)dr = \sum_i \sigma_i(\lambda) \cdot S_i = \sum_i \tau_i(\lambda) \qquad (2.9)$$

Where the slant column density S_i (molecules cm^{-2}) is defined as the integrated concentration of each trace gas species along the light path:

$$S_i = \int_0^L \rho_i(r)dr \qquad (2.10)$$

Thus for a given absorber, the slant column density can be obtained through the ratio of the optical density and its absorption cross section:

$$S = \frac{\tau(\lambda)}{\sigma(\lambda)} \qquad (2.11)$$

Differential absorption is used to overcome the effects of Mie and Rayleigh scattering which can cause a modulation of the signal. The absorption cross section is split into its high frequency $\sigma_i'(\lambda,r)$ and its broadband $\sigma_b(\lambda,r)$ components:

$$\sigma(\lambda, r) = \sigma_i^{'}(\lambda, r) + \sigma_{ib}(\lambda, r) \tag{2.12}$$

Addition of the high frequency and broadband structure into the Beer Lambert law and accounting for Rayleigh and Mie scattering, we can calculate the intensity of the incident light and thus the differential optical density, which is defined as:

$$\tau^{'}(\lambda) = \frac{\ln(I_0^{'}(\lambda))}{\ln(I(\lambda))} = \sum_i \sigma_i^{'}(\lambda) \cdot S_i = \sum \tau_i^{'}(\lambda) \tag{2.13}$$

From which the slant column density can be obtained without knowledge of the true initial intensity $I_0(\lambda)$ for a given absorber:

$$S = \frac{\tau^{'}(\lambda)}{\sigma^{'}(\lambda)} = \frac{\tau(\lambda)}{\sigma(\lambda)} \tag{2.14}$$

Slant column density, gives the integrated concentration of the trace gas along the light path which is dependant on the observation viewing geometry, we convert this into the vertical column density (VCD) which is the integrated concentration of the trace gas as a function of altitude z, VCD (or *V* denoted in equation 2.15 and 2.16) is the amount of molecules cm^{-2}.

$$V = \int_0^z \rho_z dz \tag{2.15}$$

VCD is used as it depends only on the vertical trace gas profile which is independent of its observation geometry. VCD can be calculated through dividing the slant column density *s* by the appropriate Air Mass Factor (AMF) which is calculated by a radiative transfer model, which is a function of wavelength and observation geometry:

$$V = \frac{s(\Phi, \lambda)}{AMF(\Phi, \lambda)} \tag{2.16}$$

AMF gives the ratio pf the two different path lengths describing the absorption due to the slant path viewing geometry and the solar elevation angle [Platt and Stutz., 2006].

DOAS assumes that temperature and pressure dependence of the absorption is negligible and that absorption from scattered light is weak. However in the NIR the absorption is strong and the temperature and pressure decreases with altitude giving a greater dependence on the absorption cross section. Using a cross section which is valid for one altitude will introduce errors into the total column. WFM-DOAS algorithm, [Buchwitz et al., 2000] was developed to improve the retrieval method.
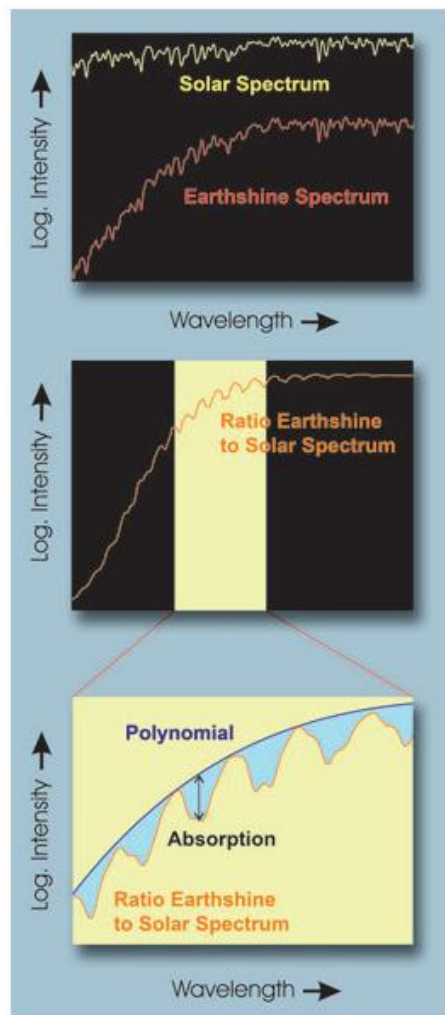
Fig 2.9 main steps of the DOAS retrieval.
(graphics: IUP-IFE, University of Bremen)

Summary of the DOAS analysis method, (Figure 2.9).

- Radiance from earth and direct Solar irradiance (this provides the absorption background), is measured.
- The total amount of absorption and scattering is determined through dividing the earthshine radiance by the direct solar irradiance.
- Molecular absorption cross section and a polynomial is fitted to the logarithm of this ratio, which produces the slant column density, (trace gas concentration along the light path).
- The average light path is calculated using a radiative transfer model, where the light path is usually expressed as Air Mass Factor (AMF), which is the light path enhancement factor relative to a vertical transaction of the atmosphere.
- The vertical column concentration of the absorber (i.e CO_2) is calculated from the AMF.

2.5.3 WFM-DOAS

WFM-DOAS (Weighting Function Modified Differential Optical Absorption Spectroscopy) [Buchwitz et al., 2000] method used to retrieve VCDs of trace gases in the NIR. WFM-DOAS is based on a linear least squares fit of the logarithm of a model reference spectrum I_i^{ref} and its derivatives, plus a quadratic polynomial $P_i a_m$ to the logarithm of the measured sun normalized intensity I_i^{meas}

$$
\left\| \ln I_i^{meas}(V^t) - \left[\begin{array}{l} \ln I_i^{ref}(\overline{V}) + \dfrac{\partial \ln I_i^{ref}}{\partial \overline{V}_{co_2}} \cdot (\hat{V}_{CO_2} - \overline{V}_{CO_2}) + \dfrac{\partial \ln I_i^{ref}}{\partial \overline{V}_{H_2O}} \cdot (\hat{V}_{H_2O} - \overline{V}_{H_2O}) \\ + \dfrac{\partial \ln I_i^{ref}}{\partial \overline{V}_{Temp}} \cdot (\hat{V}_{Temp} - \overline{V}_{Temp}) + P_i a_m \end{array} \right] \right\|^2 \equiv \left\| RES_i \right\|^2
$$

$\rightarrow$ min w.r.t $\hat{V}_j$ & a_m (2.17)

Subscript i refers to each detector pixel of wavelength λ_i. The polynomial $P_i a_m$ which has coefficients a_0, a_1 and a_2 is included to account for the spectral continuum and broadband scattering. The true model and retrieved vertical columns are represented by:

$$V^t = (V^t_{CO_2}, V^t_{H_2O}, V^t_{temp})$$ (2.18)

$$\overline{V} = (\overline{V}_{CO_2} \overline{V}_{H_2O} \overline{V}_{Temp})$$ (2.19)

$\hat{V}_j$, where j represents the variables, CO_2, H_2O and Temperature.

Each derivative or column weighting function represents the change in radiance as a function of relative scaling of the corresponding trace gas or temperature profile.

Basically the column weighting functions are replacing the absorption cross sections in the DOAS retrieval method. The temperature and water profiles are required to retrieve the CO_2 derivatives.

For the WFM-DOAS a reference spectrum is introduced, and the trace gas absorption cross sections have been replaced by total column weighting functions that relate the change in intensity to a relative scaling of the trace gas concentration profile, these are obtained by vertically integrating altitude resolved weighting functions, each of which is a function of wavelength, that shows the absolute change in radiance for a relative change in atmospheric parameter [Buchwitz et al., 2000]. i.e. assuming a given atmospheric state with a trace gas vertical column V=V$_1$ yields an intensity I$_1$ and has a weighting function W$_1$. Then for a second scenario where the vertical column has been perturbed by a small amount δ so the second vertical column is V$_2$=V$_1$+ δ, which yields a new intensity I$_2$;

$$I_2 = I_1 + W_1 \times \frac{\delta}{V_1}$$ (2.20)

Where each weighting function is defined by:

$$W_1 = \left(\frac{I_2 - I_1}{V_2 - V_1} \right) \cdot V_1 = \frac{\partial I}{\partial V} \cdot V_1 \qquad (2.21)$$

Weighting functions vary with altitude due to a change in the trace gas concentration and change in the spectral effects such as line broadening.

Weighting functions and reference spectra are computed using a forward model, such as SCIATRAN, [Rozanov et al., 2002] which was used for the WFM-DOAS retrieval. The SCIATRAN model is designed to calculate the weighting functions for the retrievals used.

There are many parameters which need to be taken into account when calculating the CO_2 retrievals, these include; surface reflection, elevation and pressure, cloud coverage, aerosols, temperature profiles and Water vapour.

2.5.4   Full Spectral Initiation (FSI) WFM-DOAS

The FSI algorithm was developed by Barkley et al, (2006) to specifically retrieve atmospheric CO_2 from NIR measurements taken from SCIAMACHY. (FSI) WFM-DOAS (Full Spectral Initiation Weighting Function Modified Differential Optical Absorption Spectroscopy) differs from the WFM-DOAS in that rather than using a look-up table approach, it generates a reference spectrum for each individual observation, based on the known properties of the atmosphere and surface at the time of the measurement [Barkley et al., 2006].

The WFM-DOAS method doesn't account for contributions made by surface albedo, pressure aerosols and vertical profiles of CO_2, water vapour and temperature which affect the calculated model spectrum. Each contributes a small error in the column which is around 2% or less (Barkley et al., 2006). These potential errors can be reduced through introducing explicit a-priori information in

the retrieval. This gives the new method of calculating CO_2 vertical columns. For the Full spectral initiation WFM-DOAS method a reference spectrum is generated for each SCIAMACHY measurement in order to obtain the best linearization point for the retrieval [Rozanov et al.,2002].

Several input sources are used to generate each spectrum produced by the RTM SCIATRAN. For each SCIAMACHY observation a reference spectrum is created from atmospheric and surface data, where the CO_2 profile is selected from the climatology at the time and latitude of observation is made. 6-hourly ECMWF date are interpolated onto the local overpass time and centre of the SCIAMACHY pixel is used to obtain the closest atmospheric state to the observation temperature, pressure and water vapour profile. A look-up table of radiances for each window as a function of surface reflectance and solar zenith angle is used to determine the linearization point for the surface albedo. Cloud screening for all SCIAMACHY pixels is done prior to the retrieval processing, where the cloud contaminated pixels are discarded. Three aerosol scenarios are introduced into the algorithm to reduce systematic errors, using the LOWTRAN aerosol model [Kneizys et al., 1996]. These are Rural, urban and maritime which are implemented over land, urban areas and oceans respectively. Once the retrieval process is complete, a filter is applied to retrieve VMRs with retrieval errors less then 5% and are within the range of 340-400ppmv.
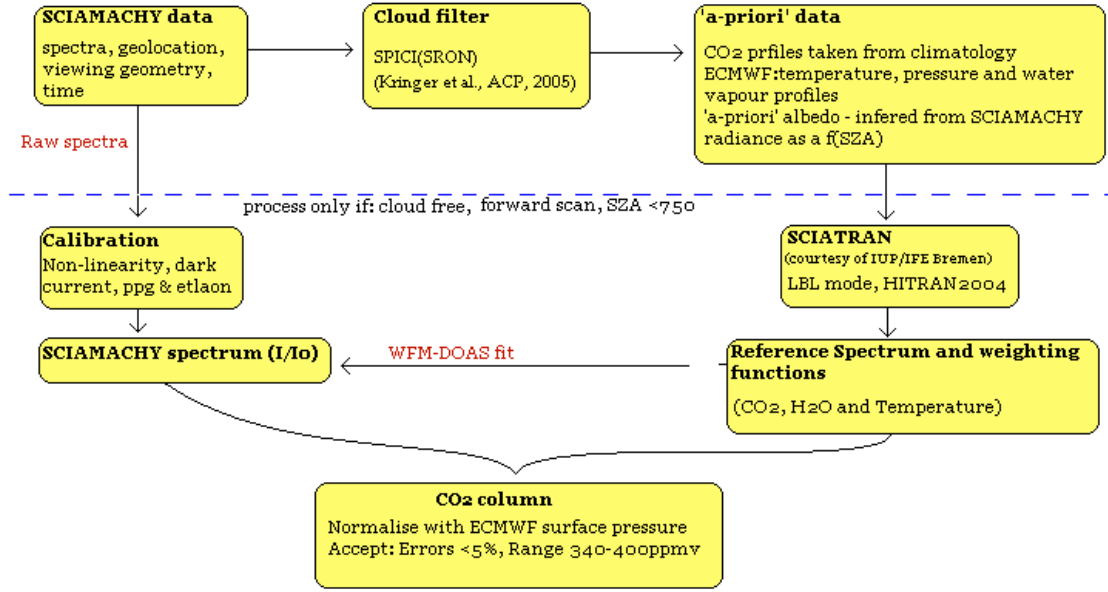
Figure 2.10: Schematic flow diagram of FSI algorithm, [courtesy of M. Barkley].

Errors associated with each of the retrieved variables are given by:

$$\sigma_{\hat{V}_j} = \sqrt{\frac{(C_X)_{jj} \times \sum_i RES_i^2}{(m-n)}}$$

(2.22)

$(C_x)_{jj}$ is the jth diagonal element from the least squares fit covariance, matrix RES_i is the fit residual, m is the number of spectral points within the fitting window and n is the number of fit parameters, [Barkley et al., 2006a].

Barkley et al. (2006) showed that the error associated with retrieved CO_2 VCD is significantly reduced when the reference spectrum is created from an *a-priori* scenario that closely resembles the true conditions.

The VCDs retrieved from the (FSI) WFM-DOAS method are the number of molecules per cm^{-2}. To obtain a better representation of the total column of CO_2 in the atmosphere the VCDs are normalized using the surface pressure. The surface pressure from ECMWF is used to normalize the VCD column. Pressure exerted by 1 molecule of air on the atmospheric column is:

$$p = \frac{F}{A} = \frac{mg}{A} = \frac{M_{air}g}{A_v A} \tag{2.23}$$

Where m is the average mass of an air molecule, g is the acceleration due to gravity, M_{air} is the molecular weight of air (28.97×10^6 kg mol^{-1}) A_v is Avogadro's constant (6.023×10^{26} molecules kmol^{-1}), inputting these values into Equation 2.23 gives a value of p = 4.72×10^{-26} mb.

The column CO_2 volume mixing ratio (VMR) is calculated using:

$$CO_2[VMR] = CO_2[VCD] \times \frac{4.72 \times 10^{-26}(mb)}{p(mb)} \tag{2.24}$$

Using the VMR is beneficial as we can determine how much CO_2 is in the whole column and not just how high the concentration is per cm^{-2}.

2.6 Summary.

Both SCIAMACHY and AIRS data will be used in order to calculate global and regional CO_2 in the troposphere. CO_2 is said to be well mixed through the atmosphere using these two instruments this can be investigated, if CO_2 is uniformly mixed throughout the troposphere the two instruments should agree, however studies have been made and it's clear that CO_2 varies considerably more in the lower troposphere due to different land types, [Barkley et al., (2007)], than in the middle-upper troposphere where there are no influences on the uptake or emission of CO_2. Studies have also been carried out with the AIRS instrument [Engelen et al, 2004; Barnet et al., 2005] which show that the CO_2 doesn't vary regionally but rather with changes in latitude. Results indicate that CO_2 is mixed thoroughly in the middle-upper troposphere but in the lower troposphere the CO_2 varies considerably [Buchwitz et al., 2007; Barkley et al., 2006c].

Different methods have been used to calculate the CO_2 in the troposphere, these retrievals will be used and validated with in-situ measurements. Comparison of the NIR and TIR instruments will be made to determine the magnitude of the difference between their measurements and to determine if the CO_2 measured in the lower troposphere has any influence over the CO_2 concentration in the tropospheric region directly above or if it is well mixed and hence influenced by the surrounding regions emissions and absorptions. Data from the two tropospheric regions are used to ascertain if a more accurate value for the CO_2 concentration in the lower troposphere can be deduced from subtracting the upper CO_2 (AIRS) column value from the whole column value (SCIAMACHY) by comparing the results with in-situ data.

Chapter 3.

Comparisons of CO_2 in the upper and lower troposphere for 2003 measured by AIRS (4d-var method) and SCIAMACHY.

3.1 Introduction.

SCIAMACHY and AIRS are sensitive to CO_2 measurements in the lower and upper troposphere respectively, where SCIAMACHY retrievals are measured in the NIR (Near infrared) and AIRS in the TIR (thermal infrared) spectral region (see Chapter 2). Comparisons of the two retrievals are not for validation, but to determine how different the distribution and concentration of CO_2 are in the two tropospheric regions. Comparisons are made on a global and on regional scales for 2003, global CO_2 distributions are plotted, seasonal cycles and their respective amplitudes (the difference between the maximum and minimum values of CO_2 of the measured seasonal cycle over a one year period) are determined for both instruments. AIRS and SCIAMACHY data are also compared to ground based measurements which are primarily located in northern America, one station in China and another in South Africa.

Measuring CO_2 at different altitudes could provide a greater understanding of how CO_2 is distributed through the atmosphere; results can help indicate if CO_2 is evenly distributed globally or whether there are sinks and sources and if so are these CO_2 variations translated into the upper troposphere?

3.2 Global Comparisons of AIRS and SCIAMACHY CO_2.

SCIAMACHY measurements are most sensitive to CO_2 variations near the surface peaking in the planetary boundary layer [Barkley et al., 2007]. AIRS retrievals are most sensitive between 10 and 15 km, with maximum sensitivity around 13 km (200 hPa), [Engelen et al., 2004] (Figure 3.1).
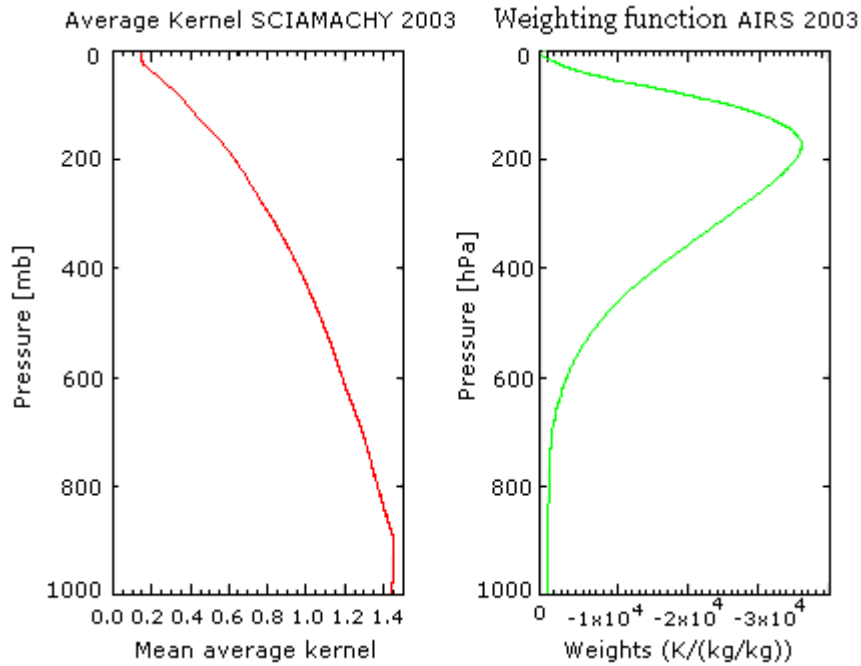
Figure 3.1: Mean average kernel for SCIAMACHY (left) and weighting function AIRS (right). These show where the instruments measurements are most sensitive in the atmosphere.

Figure 3.1 shows that direct comparisons for validation of the two data sets is not possible as they each represent different atmospheric regions (and they are two very different retrieval approaches). The atmospheric measurements attained from AIRS and SCIAMACHY can be used to determine if the CO_2 variations in the lower troposphere influence the tropospheric region directly above or if the CO_2 measured in the upper tropospheric region is a mean value of the concentration fluxes from the surface of the surrounding region.

Fluctuations of the surface CO_2 concentrations are caused by respiration of plants and animals, land usage change and anthropogenic sources [IPCC, 2007]. CO_2 is

an inert gas whose seasonal cycle propagates primarily from the surface, the differences between the CO_2 mixing ratios in the upper and lower troposphere are determined by the processes that transport surface air through the atmosphere, these include advection, convection and eddy mixing [Run-Lie Shia et al., 2006; Park et al., 2007].

SCIAMACHY and AIRS (4D-var method, hereafter referred to as AIRS-4d) CO_2 global maps for 2003 have been produced to determine the distribution of global CO_2 in the upper and lower troposphere. Both data sets are gridded on a 3 x 3 degree scale by averaging results (the AIRS data were pre-gridded at source), AIRS retrievals are most accurate within $\pm$ 30° latitude of the equator (Figure 3.2), with errors increasing with increasing latitude. Averaging kernel values vary between 0 and 1, where 1 represents values of observational retrieved data and 0 correspond to a background value. The SCIAMACHY averaging kernel varies little with latitude therefore retrievals are not biased by a change in latitude [Barkley et al., 2006a].
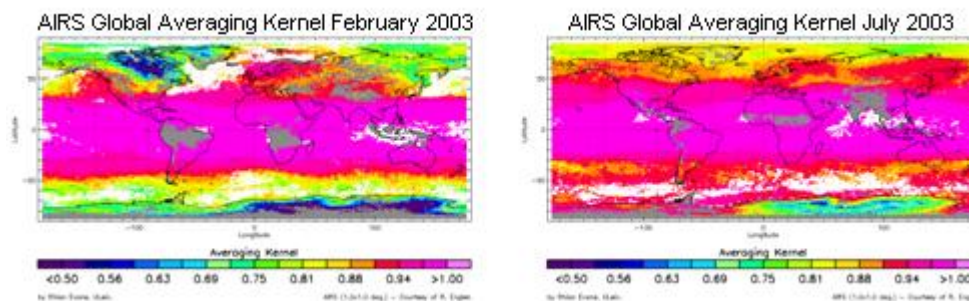
Figure 3.2: Total column average kernels for AIRS-4D ECMWF data for February (left) and July (right) 2003. 1 = where data is retrieved from AIRS-4D. <1 increasing amounts of data used from the a-priori.

SCIAMACHY data retrieved are limited to specific regions owing to the time taken to process each pixel. Data retrieved by SCIAMACHY are primarily retrieved over land as the albedo over the oceans is low which make it difficult to retrieve CO_2 radiances in nadir mode. Global coverage of the AIRS-4D data are available. However some data are missing due to cloud and water contamination

which are more prominent over the tropical regions and also at high latitudes; clouds are filtered out of the AIRS-4D retrievals using the method of McNally and Watts., 2003. The information content is highest at the tropics and degrades at higher latitudes (Figure 3.2), the degradation is caused by a lower tropopause and smaller temperature lapse rate at higher latitudes [Engelen et al., 2004].
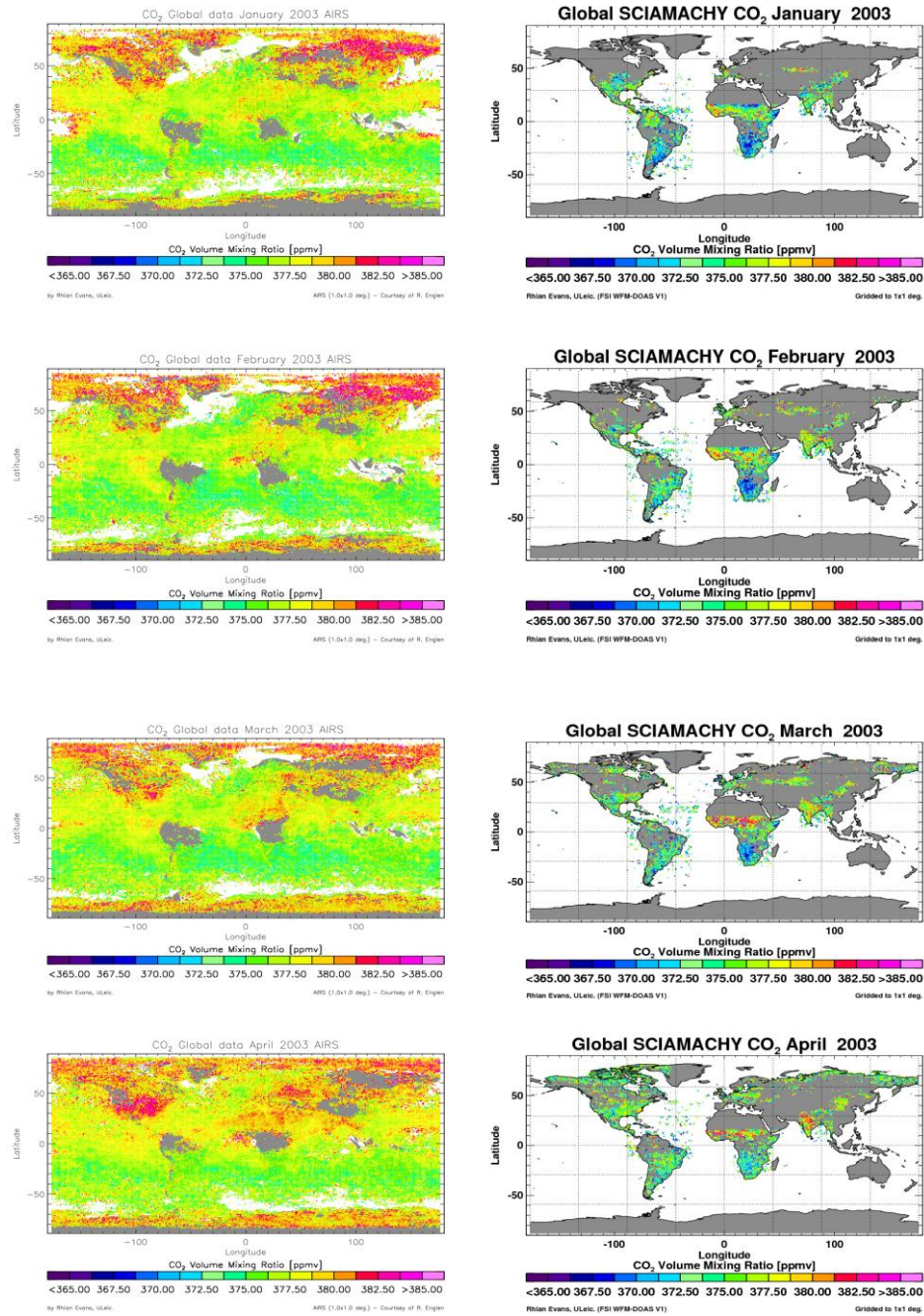
Figure 3.3a: Global distribution of atmospheric CO_2 columns; January through April 2003 measured by AIRS-4D (left column) and SCIAMACHY (right column).
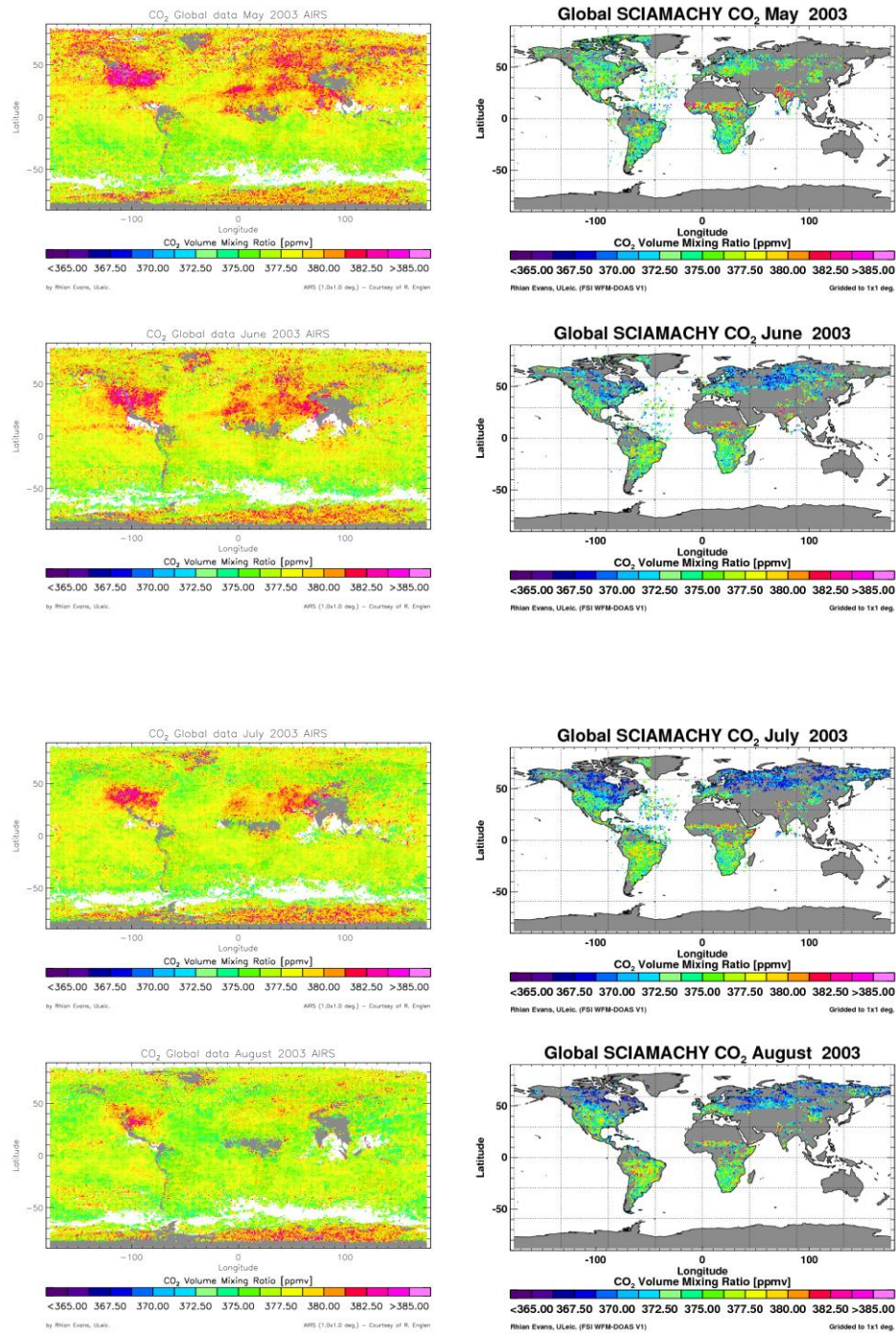
Figure 3.3b: Global distribution of atmospheric CO_2 columns; May through August 2003 measured by AIRS-4D (left column) and SCIAMACHY (right column).
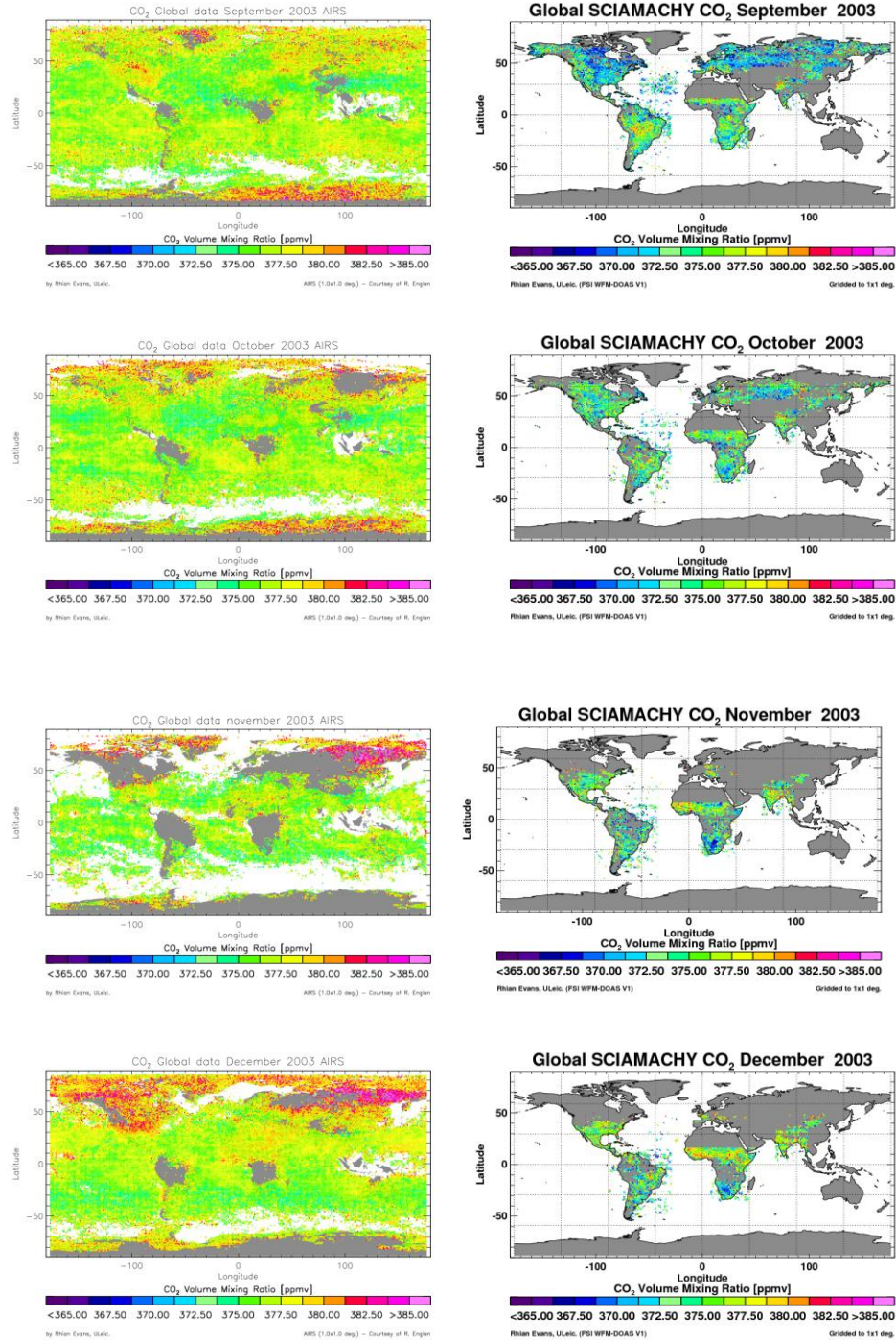
Figure 3.3c: Global distribution of atmospheric CO_2 columns during 2003 measured by AIRS-4D (left column) and SCIAMACHY (right column).

AIRS-4D global data shows a distinct northern and southern hemispheric divide with significantly higher tropospheric CO_2 concentrations at higher northern latitudes. The greatest upper tropospheric CO_2 concentrations are seen over North America and Siberia, with concentrations decreasing between June and

September. CO_2 concentrations vary little annually in the upper troposphere. Over the southern hemisphere, CO_2 values increase from May through September (southern hemispheric winter) by a few ppmv. With the exception of Antarctica, there are no distinct regions of high or low CO_2 measured over the southern hemisphere, the CO_2 concentration is relatively well mixed through the upper troposphere. Error constraints applied on the retrievals acquired from AIRS-4D and SCIAMACHY are $\pm$ 5 ppmv and $\pm$ 10 ppmv respectively; data are rejected if errors are higher.

The data retrieved by SCIAMACHY shows definite structure to the distribution of the CO_2 in the lower troposphere. Data for North America shows a CO_2 gradient with higher values seen in the south west which gradually decrease moving in a north easterly direction, in June through September. Barkley et al, (2007) showed that the CO_2 change over North America is correlated with the regional vegetative growth. Owing to a lack of SCIAMACHY data at higher latitudes determining how much the CO_2 increases over the winter months and if this increase correlates to the quantity of vegetative decrease is impossible.

SCIAMACHY data shows greater structure to the distribution of CO_2 compared to the measurements retrieved from AIRS-4D. CO_2 measured over South Africa and South America show localized regions of high and low tropospheric CO_2 concentration throughout the year in the lower troposphere, AIRD-4d measurements show no CO_2 structure within these regions in the upper troposphere. An increase of CO_2 in both the upper and lower troposphere can be seen over India and the Himalayas from April through to July.

Measurements are made over oceanic regions but due to lack of retrievals from SCIAMACHY it is difficult to determine if there are any sinks or sources in the lower troposphere. Greater global coverage of CO_2 are retrieved in the upper troposphere, their distribution shows no distinct structure over the ocean compared to the CO_2 over land as the CO_2 is distributed uniformly throughout the atmosphere.

Different seasonal cycles can be seen in the two data sets, AIRS-4D produces a general seasonal cycle for the northern and southern hemispheres, with the CO_2 peaking in opposite hemispheres approx six months apart. SCIAMACHY shows that along with a north and south seasonal cycles, areas within the hemispheres can have drastically different cycles. Central Africa for example shows areas of high and low concentrations between $0°$ N and $15°$ N within the same month, also the east and west coast of North America shows a 5 ppmv difference.

Distributions of CO_2 in the upper troposphere are well mixed whilst AIRS-4D is unable to measure the surface fluxes, SCIAMACHY is sensitive to lower tropospheric measurements and is able to observe the seasonal variations. Measurements from the two instruments provide valuable information on how the CO_2 is distributed through the troposphere. In the lower troposphere the CO_2 concentrations are influenced by the surface fluxes and the upper tropospheric concentrations are an average of the surface fluxes, which indicates that the CO_2 is not well mixes through the whole column.

AIRS-4D retrievals show that the CO_2 in the upper troposphere lack the structure and definition compared to the retrievals in the lower troposphere. This suggests that the CO_2 is well mixed in the middle-upper troposphere but it is not thoroughly mixed throughout the whole tropospheric column as surface fluxes clearly influence the CO_2 concentration in the lower troposphere.
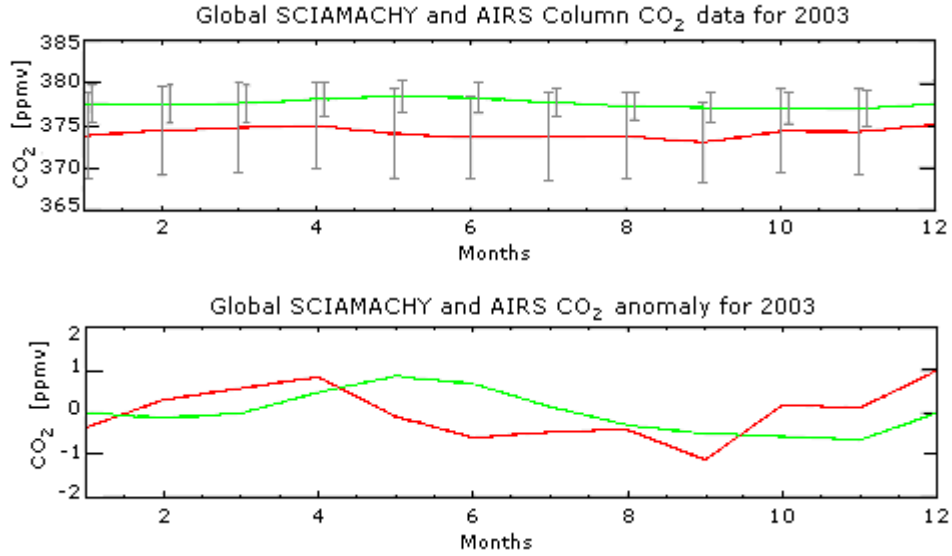
Figure 3.4: Top: Global seasonal cycles of AIRS-4D (green) and SCIAMACHY (red) for 2003, Bottom: AIRS-4D and SCIAMACHY anomaly (mean yearly value subtracted from monthly mean CO_2 column data).

The global seasonal cycles measured by AIRS-4D and SCIAMACHY (figure 3.4) show that the data measured in the upper troposphere lags the CO_2 concentrations in the lower troposphere by approximately 2 months. The mean CO_2 concentration of the two measurements are similar, with AIRS-4D maximum at 378.45 ± 1.92 ppmv and SCIAMACHY at 375.16 ± 5.18 ppmv. The phase lag of the AIRS-4D measurements indicates that the average global CO_2 concentration in the lower troposphere translates to the upper troposphere within 2 months.

Figure 3.4 represents globally averaged CO_2 values. The amplitude of the seasonal cycles (the difference between the maximum and minimum values of CO_2 of the measured seasonal cycle over a one year period) measured by AIRS-4D and SCIAMACHY are between 4.75 and 2.48 ppmv respectively (Figure 3.4). Olsen and Randerson, (2004) determined that the difference between the column averaged CO_2 mixing ratio and the surface value varies between 2 and 10 ppmv, depending on location. The correlation between the AIRS-4D and SCIAMACHY global CO_2 data is 0.097, which shows that the CO_2 in the two tropospheric regions are distinctly different (Figure 3.4). Park et al., (2004) determined that the CO_2 in the tropopause (altitude of 12 to 19 km) travels monotonically and takes 26

± 3 days to travel through the layer. AIRS-4D retrievals lie within this region, which would account for the lag in the seasonal cycle with regard to SCIAMACHY concentrations and the low correlation value.

3.3 Column subtraction of AIRS-4D and SCIAMACHY.

The AIRS-4D and SCIAMACHY data are sensitive to different tropospheric regions, the Averaging Kernels (AK) produced are weighted differently, with SCIAMACHY retrievals sensitive to lower tropospheric regions and AIRS-4D to mid-upper tropospheric regions.
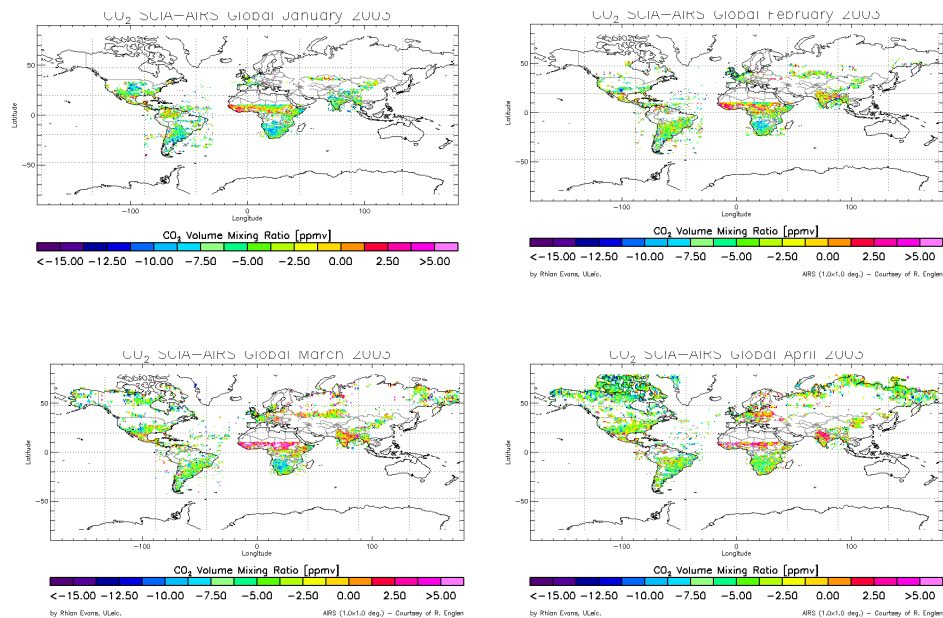
Figure 3.5a: Global data of AIRS-4D CO_2 column data subtracted from SCIAMACHY column data January through April 2003.
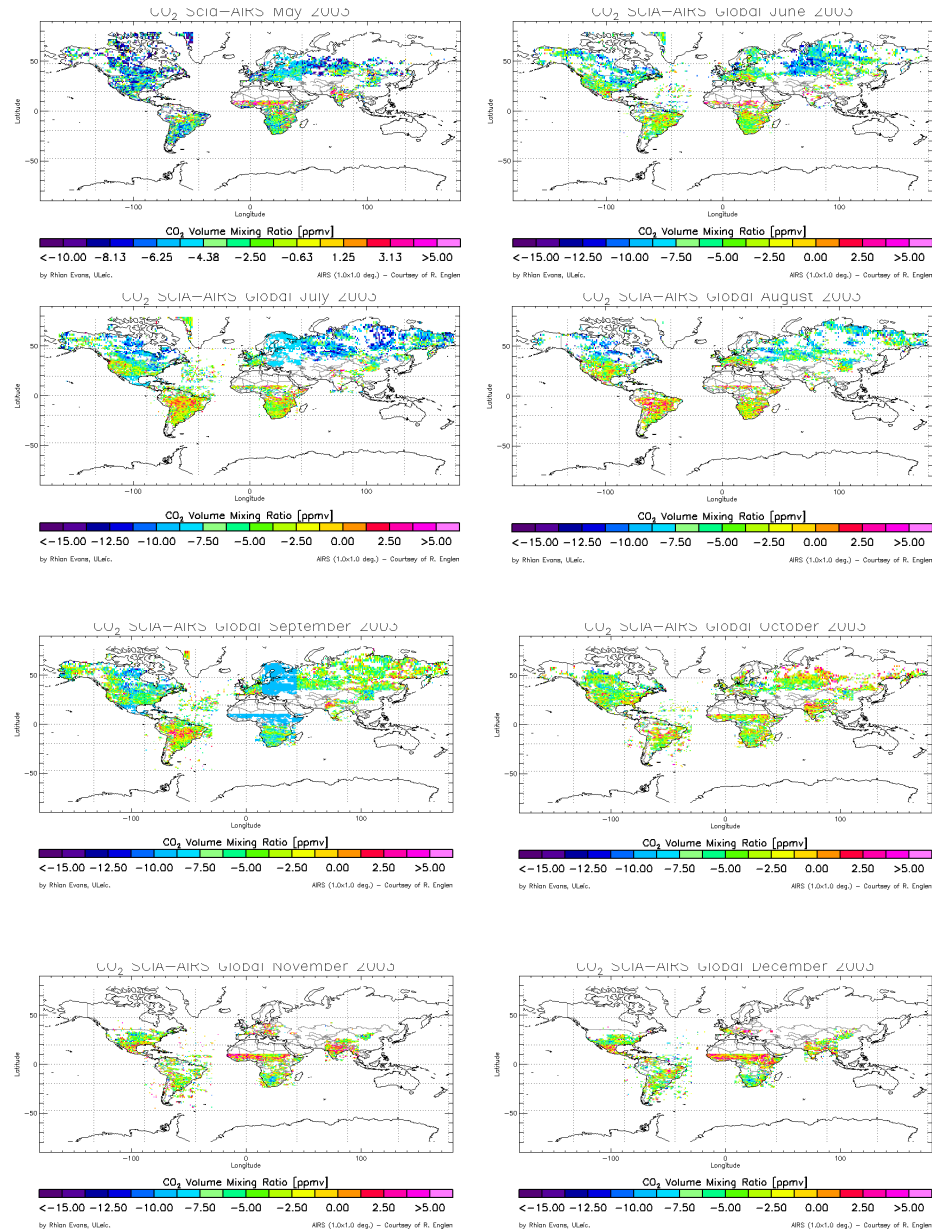
Figure 3.5b: Global data of AIRS-4D CO_2 column data subtracted from SCIAMACHY column data May through December 2003.

Global normalised column CO_2 of the subtracted (SCIAMACHY(CO_2) – AIRS-4D(CO_2)) data are plotted in Figure 3.5 for 2003, where red represents an increase in concentration in the lower troposphere and blue shows a deficit of CO_2 in the lower troposphere. Implicit sinks and sources of CO_2 are clearly visible over southern Africa, central Africa, Amazonia, India, North America and Siberia during 2003. These flux variations are seen in the SCIAMACHY data, but not in the AIRS-4D data (figure 3.3), which suggests that the CO_2 fluxes in the lower

troposphere dominate the column values retrieved from the SCIAMACHY instrument. AIRS-4D CO_2 measurements are sensitive in the troposphere from 9 km and upward [Engelen et al., 2004] these measurements represent the mean background CO_2 value and not the high flux variations from the surface directly below. CO_2 data in the upper troposphere are comparatively well mixed, these values are influenced by the surrounding area, subtracting the upper tropospheric data leaves us with a more accurate image of the fluxes produced at the surface.

May through September show a northern and southern hemispheric divide with the northern hemisphere CO_2 values decreasing and the southern hemispheric values increasing during this period. The decrease of CO_2 in the northern hemisphere is most likely due to the increased vegetative growth over the hemisphere's spring/summer months, whereas the southern hemisphere experiences a decrease in CO_2 as the vegetation is dying owing to its autumn/winter period.

The subtracted (SCIAMACHY – AIRS-4D) data shows greater variation in the surface flux where the sinks and sources are more prominent than is seen in the SCIAMACHY data alone. Sinks and sources are particularly prominent over the Amazon in South America during July and August.

The advantages of subtracting the two columns produces a greater representation of the CO_2 fluxes in the lower troposphere without the influence of the upper tropospheric mean CO_2 values. The subtracted data shows that the CO_2 is in a constant state of flux at the surface, but is thoroughly mixed in the upper troposphere where the CO_2 values at each grid point are an average of the surrounding area, thus the upper troposphere is not representative of the CO_2 emissions from the surface below. To determine if this method of subtracting the two data columns are valid in-situ comparisons are required. To increase the accuracy of determining the CO_2 in the lower troposphere, from subtracting the two data columns, processing the CO_2 data using the same retrieval method is essential (See section 6.3).

3.4 Regional comparisons of AIRS-4D and SCIAMACHY CO$_2$ during 2003.
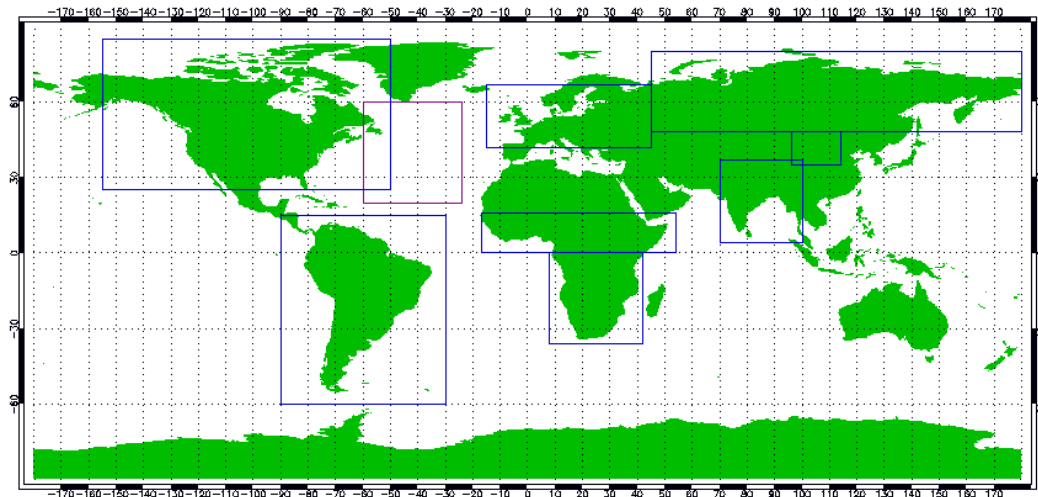
Figure 3.6 : Regions selected to compare AIRS-4D and SCIAMACHY column CO$_2$ for 2003

Global data shows that there are regions of high and low CO$_2$ concentrations which could be natural variations in the concentrations caused by changing seasons or they could be permanent sinks and sources for example the ocean (see Section 1.5.2). Analysis of smaller regions will help determine how variable the seasonal cycles are in the two tropospheric regions and how much they vary between locations.

Nine locations are selected which are split into three regions, northern hemisphere (north America, Siberia, north Atlantic, UK & Europe and the Gobi dessert), tropics (central Africa and India) and the southern hemisphere (south America and southern Africa). The regions are separated as the regional areas have different seasons, the north and southern hemispheres have temperate weather (spring, summer, autumn and winter) which are six months out of phase, and the tropical regions have two or three seasons (depending on its location to the ITCZ) which are wet and dry (but can also have hot and cold wet seasons).

3.4.1 Northern hemisphere regions: North America, Siberia, Northern Atlantic, UK/Europe and the Gobi dessert.
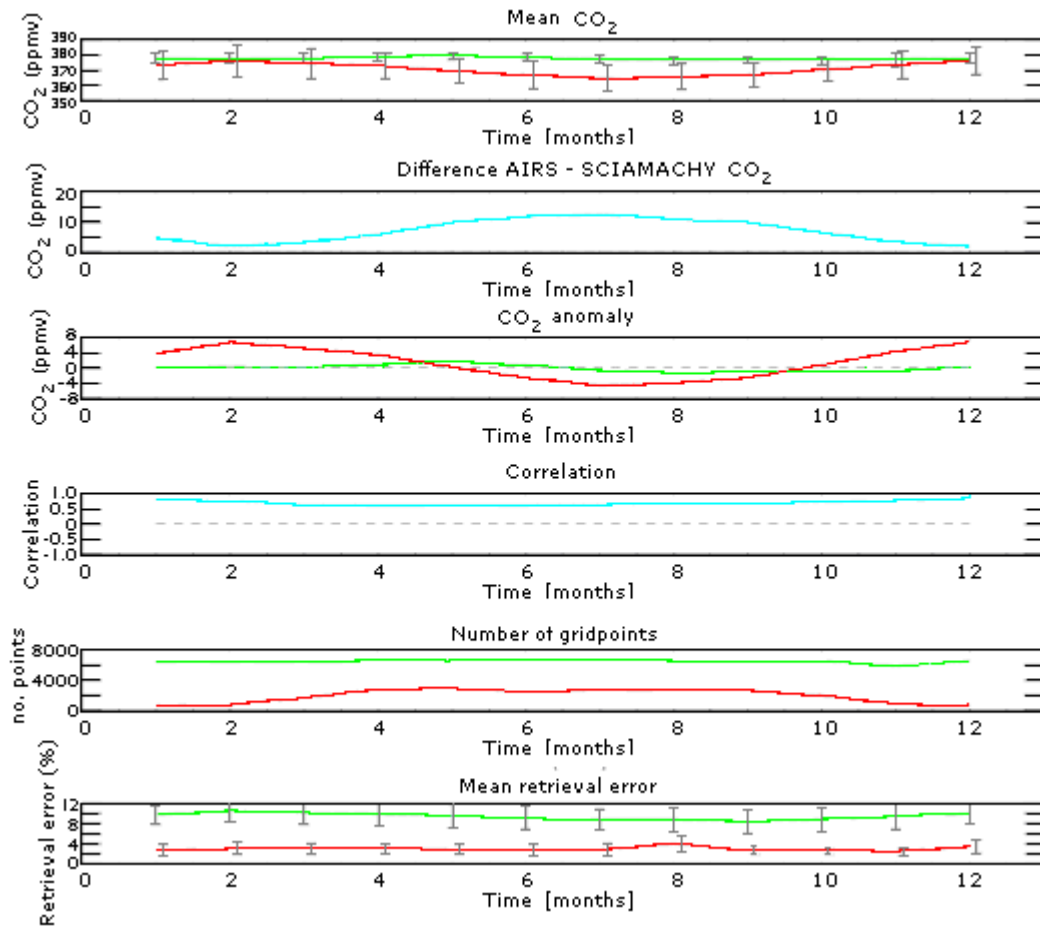
Figure 3.7: North America 2003 AIRS-4D (green) and SCIAMACHY (red) column CO_2 data. First box; SCIAMACHY and AIRS column CO_2. Second box; is the difference between AIRS and SCIAMACHY CO_2 column data. Third box; represents the CO_2 data for AIRS and SCIAMACHY subtracted from their respective annual mean subtracted. Fourth box; is the correlation values between the AIRS and SCIAMACHY data. Fifth box; shows the number of grid points available each month for the data. Sixth box; shows the errors associated with the two data sets.
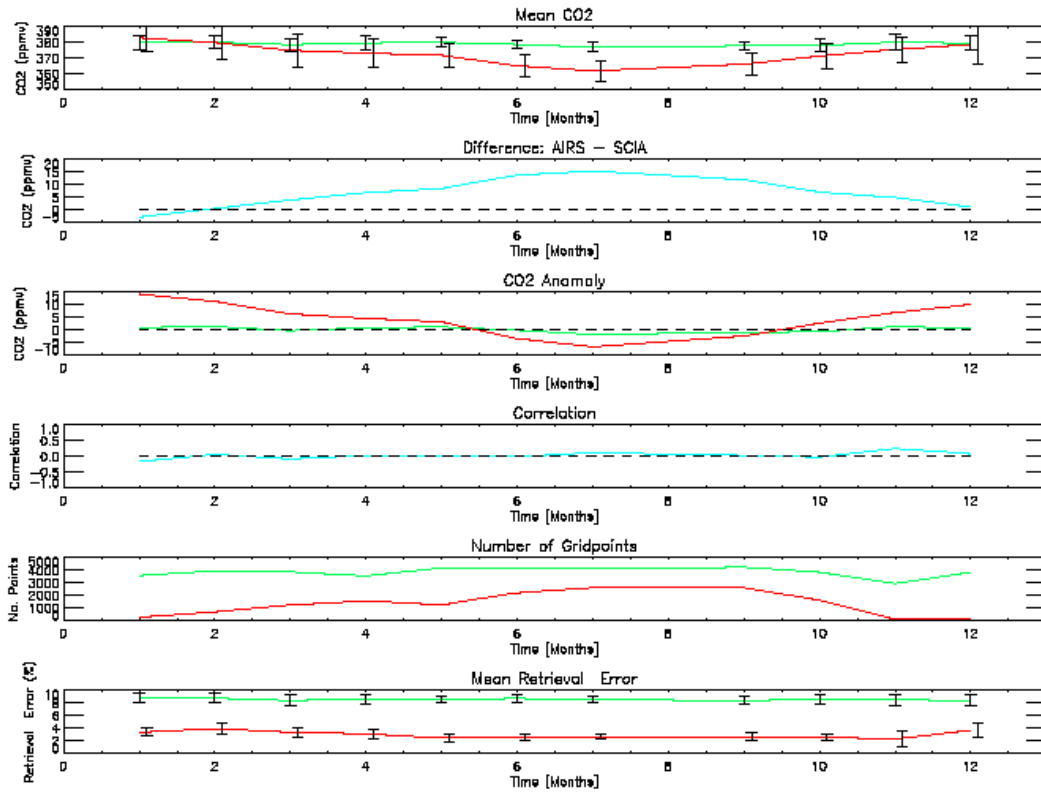
Figure 3.8: Siberia 2003 AIRS-4D (green) and SCIAMACHY (red) column CO_2 data; see figure 3.7 caption for more details.
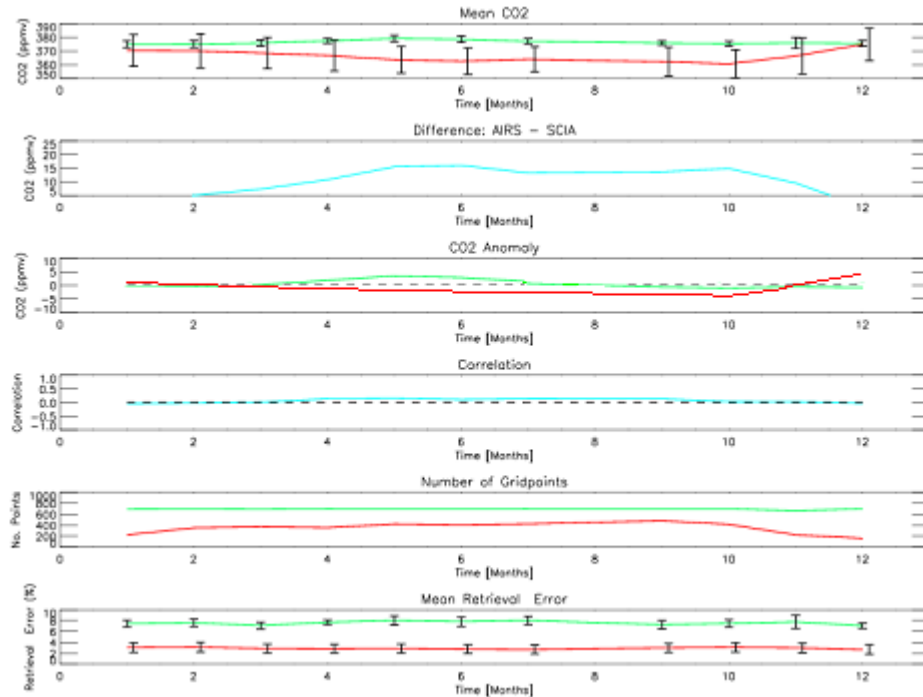
Figure 3.9: Uk & Europe 2003 AIRS-4D (green) and SCIAMACHY (red) column CO_2 data; see figure 3.7 caption for more details.
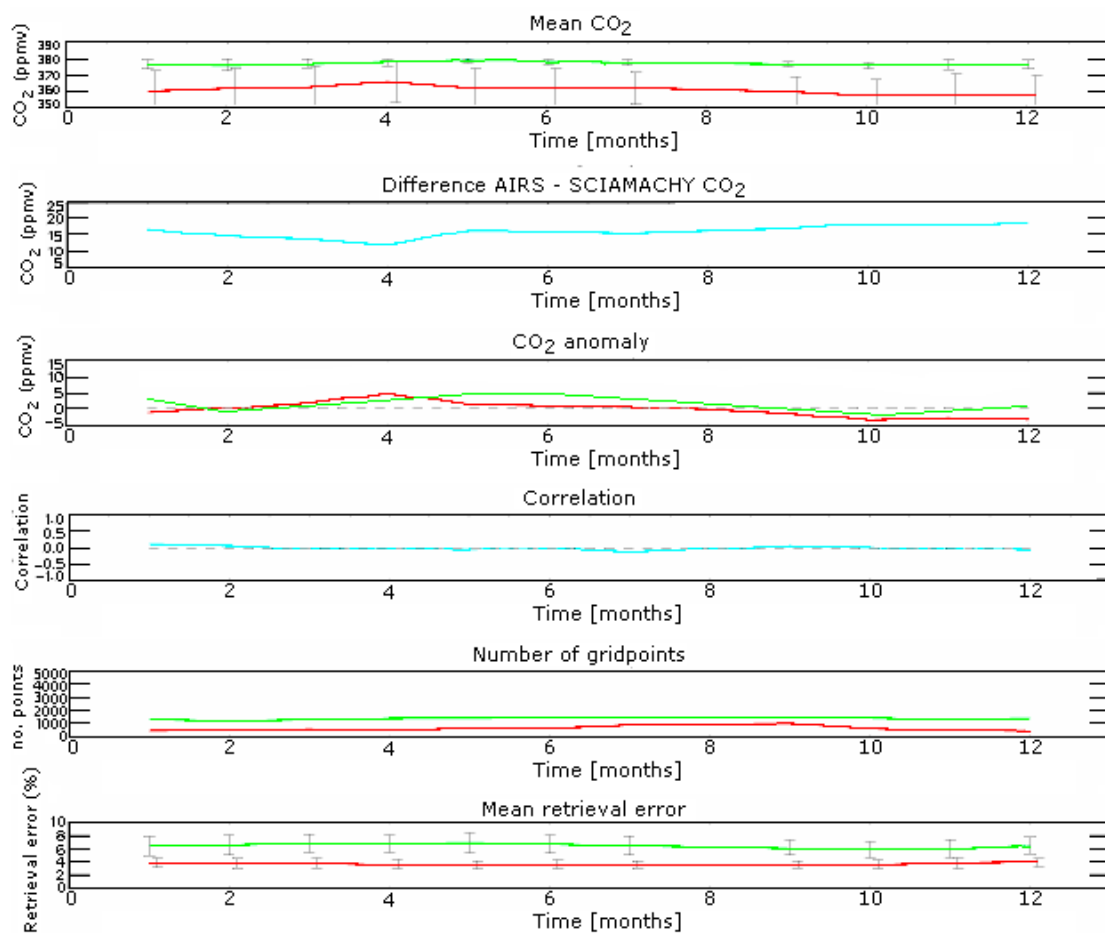
Figure 3.10: North Atlantic 2003 AIRS-4D (green) and SCIAMACHY (red) column CO_2 data; see figure 3.7 caption for more details.
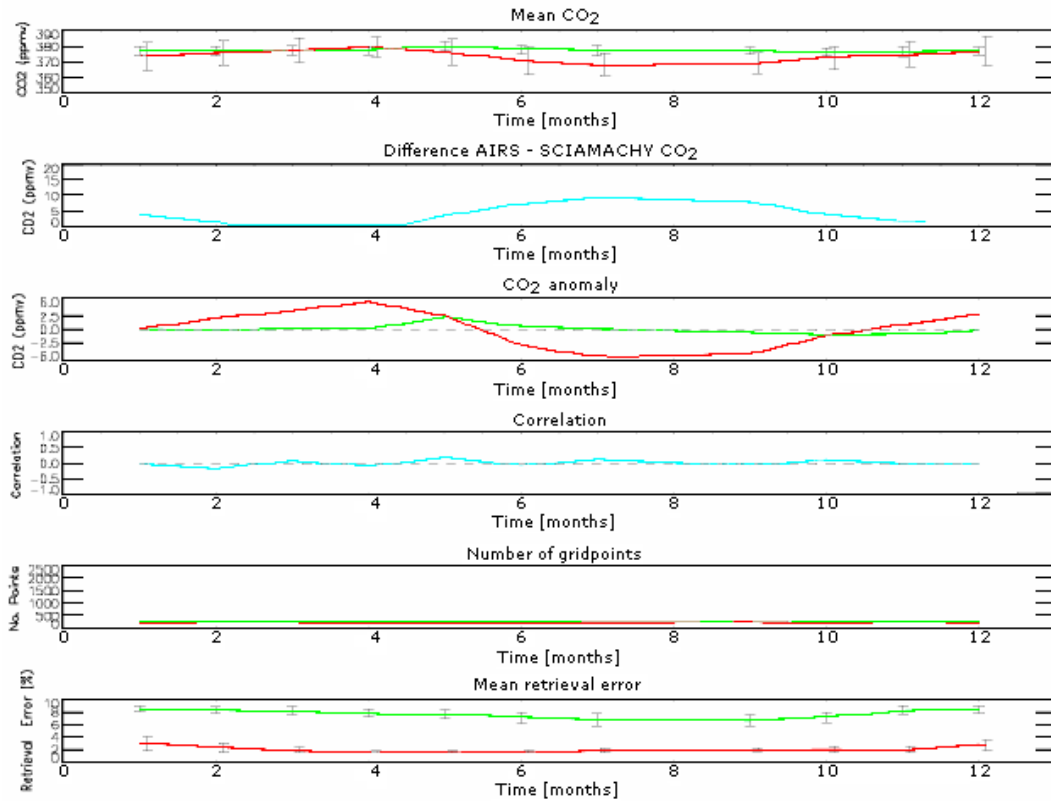
Figure 3.11: Gobi Desert 2003 AIRS-4D (green) and SCIAMACHY (red) column CO_2 data; see figure 3.7 caption for more details.

The five regions analysed in the northern hemisphere show that in all cases the AIRS-4D seasonal cycle lags the SCIAMACHY seasonal cycle peak by 1 to 3 months. SCIAMACHY data shows the CO_2 max occurring between April and June which are in the hemisphere's spring months. The CO_2 concentrations continue to decrease until September/October where the quantity of vegetation decreases at the same time. Increasing CO_2 concentrations coincides with an increase in vegetation. AIRS-4D data for all regions show a much smaller variation in the CO_2 concentration, with the amplitude (difference between maximum and minimum CO_2 value) typically more than 5 ppmv smaller than the seasonal cycles measured by SCIAMACHY. Each seasonal cycle is dependent on the air transport and local vegetation. Latitude also seems to affect the amplitude of the seasonal cycle, with north America and Siberia located at the highest latitudes, SCIAMACHY measures amplitudes of 11.5 ± 3.9 ppmv and 21.3 ± 5.9 ppmv respectively. UK, north Atlantic and Gobi measure 10.1 ± 5.1, 8.2 ± 2.0, 2.9 ± 3.5 ppmv respectively, indicating that the amplitudes decrease with

decreasing latitude. The decrease of amplitude could be caused by many factors such as different vegetation absorbing and emitting different amounts of CO_2, land usage, population size and anthropogenic sources.

3.4.2 Tropical regions: India, Central Africa.
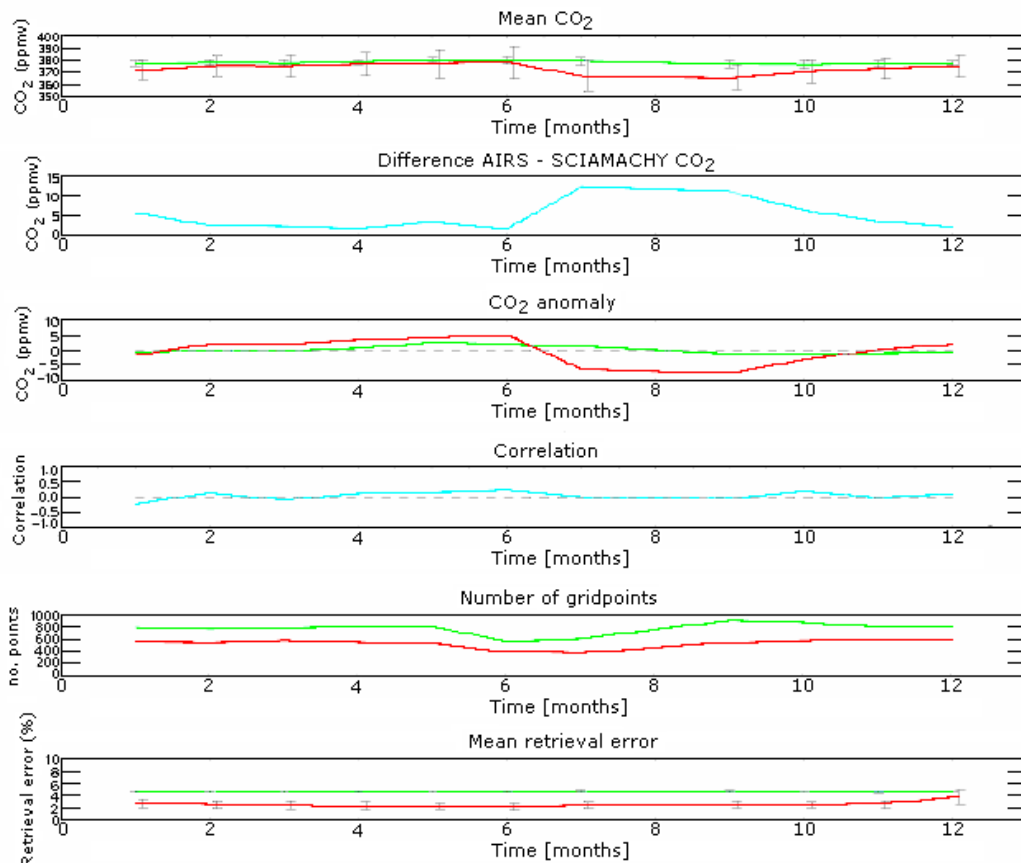
Figure 3.12: India 2003 AIRS-4D (green) and SCIAMACHY (red) column CO_2 data; see figure 3.7 caption for more details.
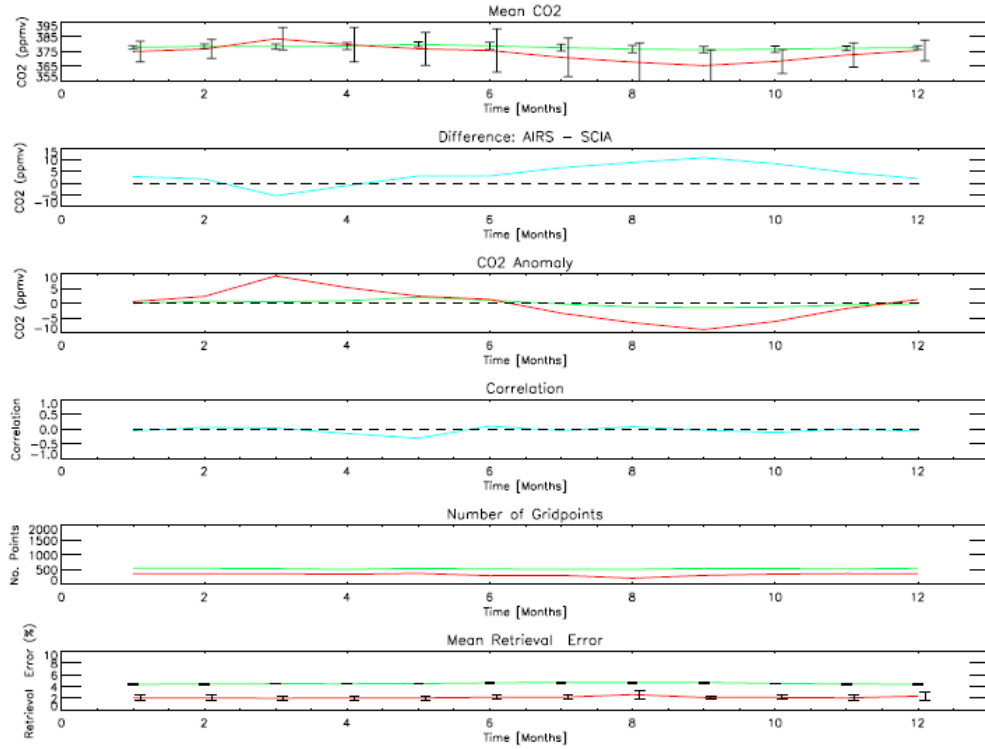
Figure 3.13: Central Africa 2003 AIRS-4D (green) and SCIAMACHY (red) column CO_2 data; see figure 3.7 caption for more details.

India and Central Africa are located within the northern tropics (Tropic of Cancer). India is situated slightly north of the equator, whereas central Africa is positioned on and around the equator. The weather at the tropics is different to the weather at higher latitudes. In the tropics there are two seasons wet and dry, compared to the four seasons at higher latitudes. Within the tropics the vegetation typically grows during the wet season.

The CO_2 seasonal cycle measured over India is one typically found at high northern latitudes with the CO_2 reaching maximum value around May-June and minimum between August and September. The AIRS-4D CO_2 measurements vary little during the year, reaching maximum in July and minimum in October. SCIAMACHY measurements show greater flux change with a maximum value measured in June and a minimum in September. These measurements show that the AIRS-4D measurements lag behind the SCIAMACHY measurements by approximately one month, indicating that the time for the change in CO_2 at the

lower troposphere affect the upper tropospheric concentrations is approximately one month.

Central African atmospheric CO_2 concentrations in the lower troposphere peak in March and reach minimum in September, and peak in May and reach minimum in October in the upper troposphere. Again there is a lag of approximately one month between the measurements in the upper and lower troposphere, with the upper tropospheric concentrations lagging behind the lower tropospheric concentrations. The lag could be due to the time required for the mixing of the CO_2 through the troposphere.

CO_2 anomaly values are greatest in June in India with a value of 8.9 ± 3.7 ppmv. In central Africa maximum CO_2 value in the lower troposphere is measured in March with an of 18.3 ± 4.7 ppmv. Central Africa is primarily covered with woody savannahs and grassland, whereas India vegetation consists primarily of cropland which absorbs less CO_2. The different types of vegetation coverage within the two regions, would be expected to influence the amount of CO_2 absorbed and emitted into the atmosphere (see chapter 5).

3.4.3 Southern Hemisphere: South America & Southern Africa
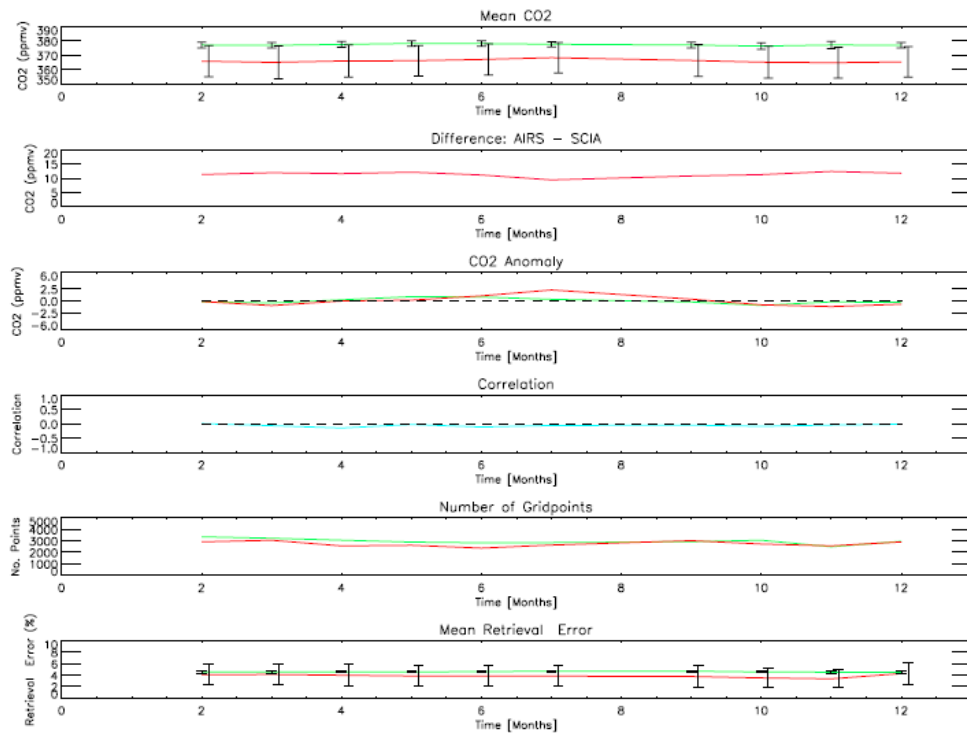
Figure 3.14: South America 2003 AIRS-4D and SCIAMACHY column CO_2 data; see figure 3.7 caption for more details.
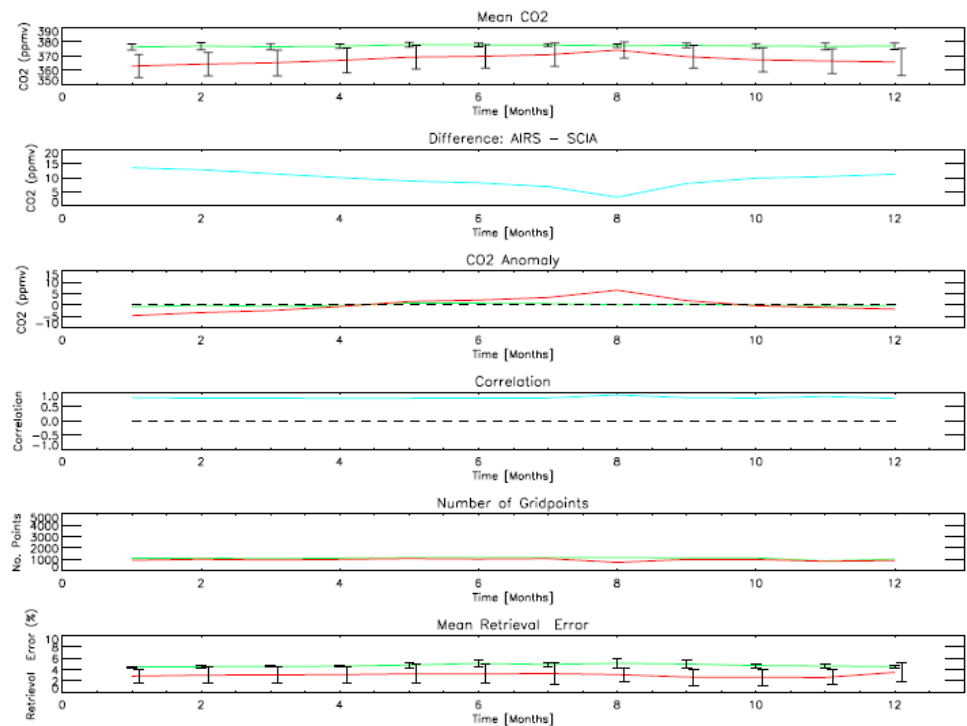
Figure 3.15: Southern Africa 2003 AIRS-4D and SCIAMACHY column CO_2 data; see figure 3.7 caption for more details.

Seasons in the southern hemisphere occur approx. 6 months out of phase compared to those in the northern hemisphere. SCIAMACHY data shows that the CO_2 values peak in July for south America (3.2 ± 1.6 ppmv) and August over southern Africa (6.7 ± 2.5 ppmv), which are the region's winter months. AIRS-4D data shows a seasonal cycle similar to those measured in the northern hemisphere, with the maximum CO_2 value reached around May which is 2-3 months before the maximum measured over the regions in the southern hemisphere. The CO_2 surface emissions in the northern hemisphere are typically larger than those in the southern hemisphere which appear to be influencing the global CO_2 concentrations in the upper troposphere. The lower tropospheric data show seasonal variations caused by changes in the surface fluxes which are out of phase with the upper troposphere.

Comparisons of the AIRS-4D and SCIAMACHY data over the selected regions show that the amplitude (difference between maximum and minimum CO_2 values) of the CO_2 seasonal cycle in the lower troposphere is much larger than those measured in the upper troposphere. The CO_2 in the upper troposphere is the mean CO_2 value from the surrounding area, where it has been transported from the surface through convection, advection and eddy mixing [Shia et al., 2006]. In the northern hemisphere the AIRS-4D seasonal cycle data lags the SCIAMACHY measurements whereas in the southern hemisphere the reverse is true (albeit that the AIRS amplitudes are smaller), indicating that the CO_2 fluxes in the northern hemisphere dominate in the upper troposphere. This could be due to the transport of the CO_2 emissions from the northern hemisphere to the southern hemisphere, biomass burning could also contribute to the CO_2 concentrations. Subtracting the upper tropospheric column (AIRS-4D data) from the whole column (SCIAMACHY) data is essential in determining the CO_2 fluxes at the surface and not from the surrounding regions, which are more noticeable when evaluating the data in the southern hemisphere as they have different seasonal cycles in the different tropospheric regions, where the upper tropospheric concentrations could influence the values measured in the lower troposphere.

3.4.4 Regional correlation values of AIRS-4D vs. SCIAMACHY

Region	Correlation
Central Africa	0.78
Gobi	0.22
India	0.49
North America	0.35
North Atlantic	-0.46
Southern Africa	0.71
South America	0.03
Siberia	0.81
UK & Europe	-0.17

Table 3.2; correlation values of SCIAMACHY vs. AIRS-4D column data for 2003.

Correlation values are variable over the regions analysed, varying between 0.03 and 0.81. The correlation calculated for North America is small, the seasonal cycle (Figure 3.7) shows that the seasonal cycles in the tropospheric regions are out of phase by approximately four months. The regions that produce seasonal cycles in the upper and lower troposphere that are approximately in phase tend to generate higher correlation values, while the lower values show a lag between the two measurements. Correlation values indicate that comparisons between the AIRS-4D and SCIAMACHY data are variable, with some regions producing good agreement such as Siberia and Southern Africa, while the UK and the North Atlantic produce poor agreements. Areas which show good correlation are also regions where biomass burning occur (this theory has not been examined in this thesis).

3.5 Satellite comparisons with in-situ data for 2003.

Comparisons of the satellite data with ground data are made to determine how sensitive the data are with regard to the surface fluxes. In section 3.4 AIRS-4D and SCIAMACHY data were compared over large areas so that we were able to see unique seasonal cycles over each region. Using ground data from WMO WDCGG network we can determine if SCIAMACHY can measure CO_2 variations

on a small scale or if the spatial averaging of the instrument is too large. AIRS-4D measurements are also compared even though their measurements are unable to measure surface fluxes, in order to see how much the CO_2 concentrations change from the surface to 9 km and from 9 km and the upper troposphere.

Eight ground stations with data available for comparisons during 2003 [WMO WDCGG http://gaw.kishou.go.jp/wdcgg/)] are used to validate the satellite data, six are located in North America and Canada, one in China and one in southern Africa. Data used are measured from ground based measurements all between 0.03 and 3.81 km in altitude. Differences are expected between the in-situ and the satellite data as the satellites measure a column of atmosphere whereas the in-situ measure at a specific altitude. Seasonal cycles produced by in-situ and SCIAMCHY measurements are expected to be roughly in phase. However the concentrations could be different as the satellite measures over a greater region, thus it will be susceptible to the surrounding CO_2 fluxes.

	Latitude	Longitude	Altitude (m)
Cape point, South Africa	-34.35°	18.48°	230
Estivan Point, Canada	49.38°	-126.55°	39
Key Biscayne, Florida	25.67°	-80.02°	3
Wendover, California	39.88°	113.72°	1320
Point Arena, California	38.95°	-123.73°	17
Southern Great Plains, Oklahoma	36.8°	-97.5°	374
Trinidad Head, California	41.05°	-124.15°	107
Mt. Waliguan, China	36.29°	100.9°	3810

Table 3.2: WMO WDGCC 2003 ground data, coordinates and altitudes of each station used.

AIRS-4D and SCIAMACHY data used are centred on the coordinates of the ground station where a 3 x 3 degree grid surrounding the station was chosen. Smaller measurement area for the satellite data resulted in an increase in the random errors associated with the CO_2 measurements. To reduce these errors a larger area centred on the in-situ measurements are used.

3.5.1 SCIAMACHY and AIRS-4D CO$_2$ comparisons over the in-situ sites for 2003
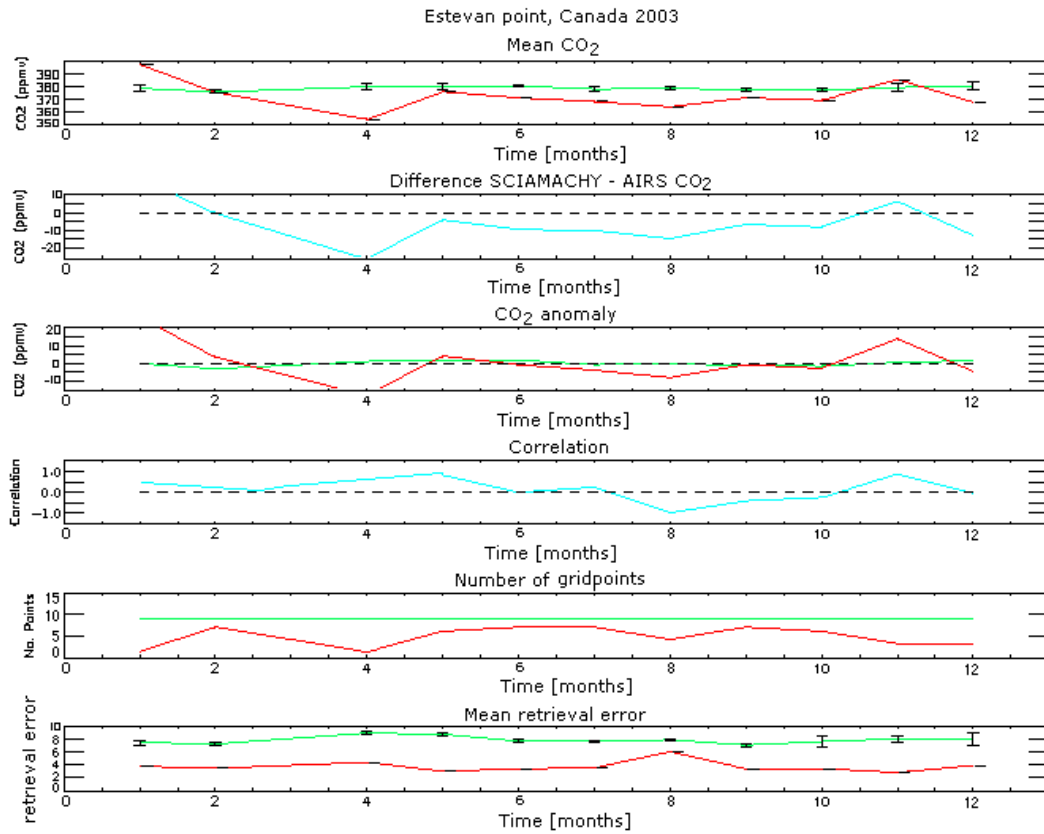
Figure 3.16: AIRS-4D (green) and SCIAMACHY (red) 2003 CO$_2$ data for Estevan point, Canada (WMO WDGCC ground data); see figure 3.7 caption for more details.
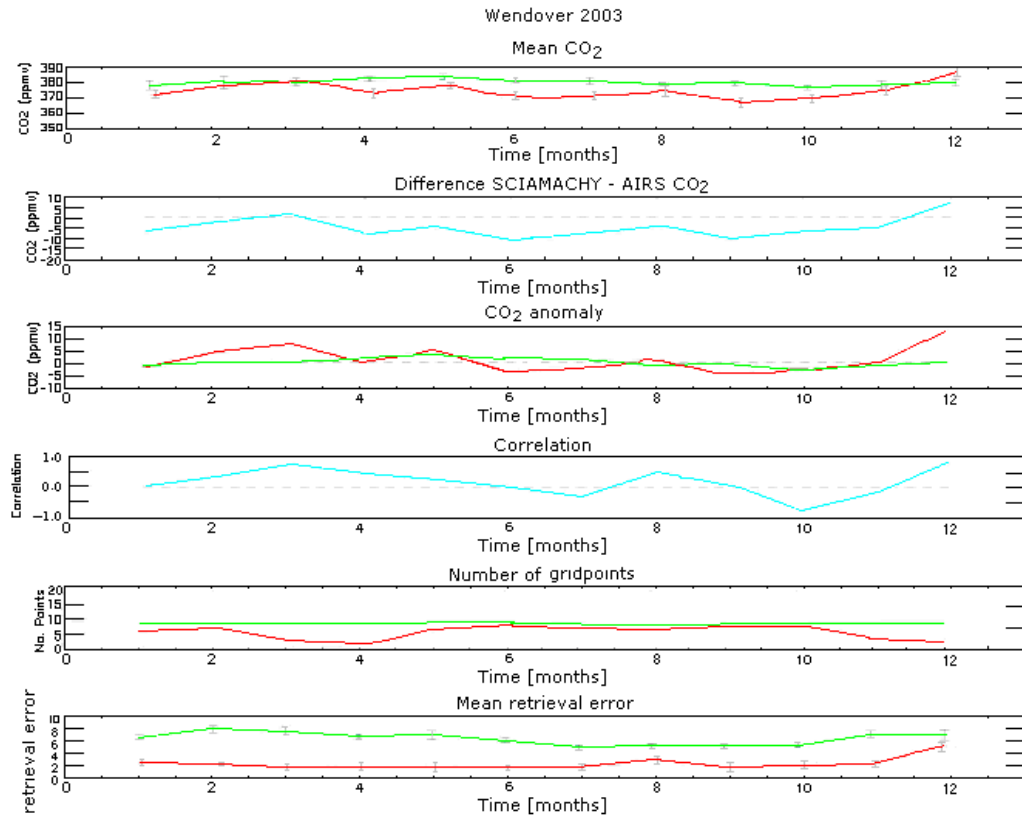
Figure 3.17: AIRS-4D (green) and SCIAMACHY (red) 2003 CO_2 data for Wendover (WMO WDGCC ground data); see figure 3.7 caption for more details.
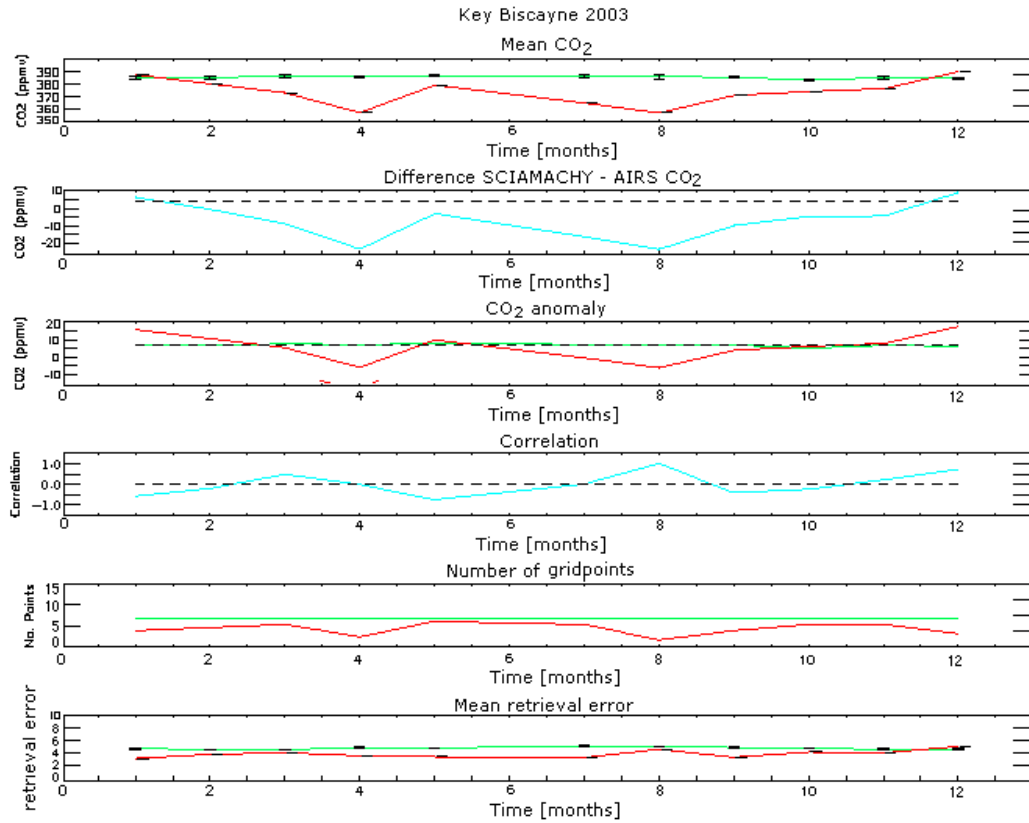
Figure 3.18: AIRS-4D (green) and SCIAMACHY (red) 2003 CO_2 data for Key Biscayne (WMO WDGCC ground data); see figure 3.7 caption for more details.
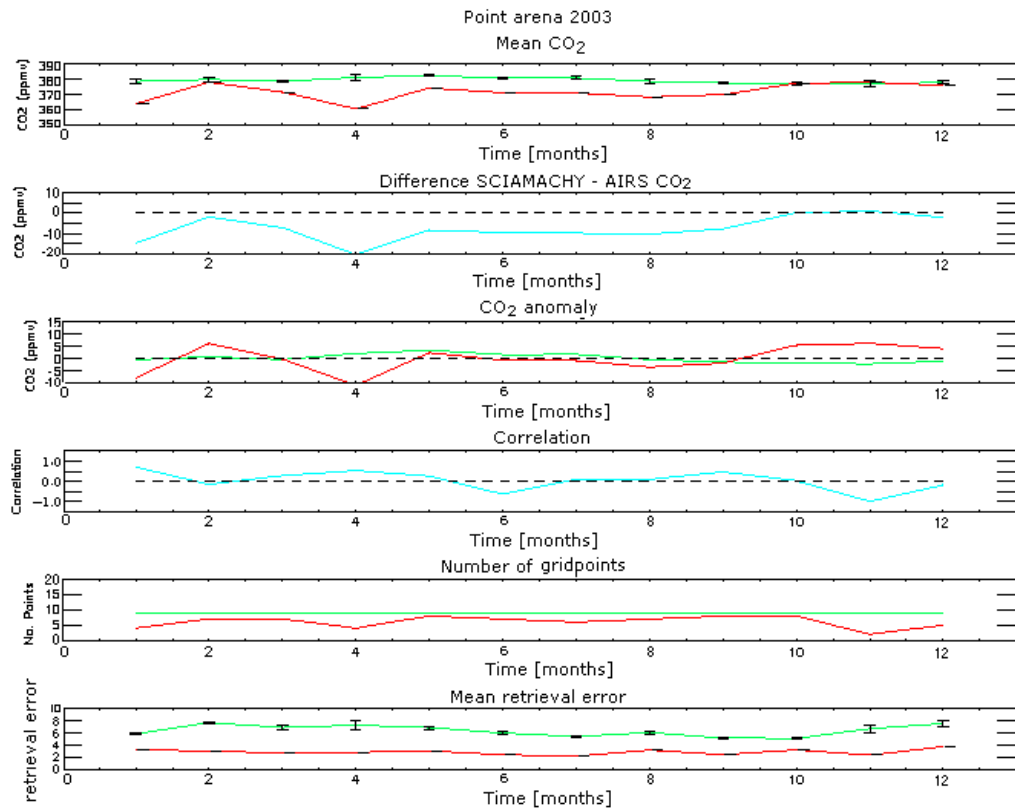
Figure 3.19: AIRS-4D (green) and SCIAMACHY (red) 2003 CO_2 data for Point arena (WMO WDGCC ground data); see figure 3.7 caption for more details.
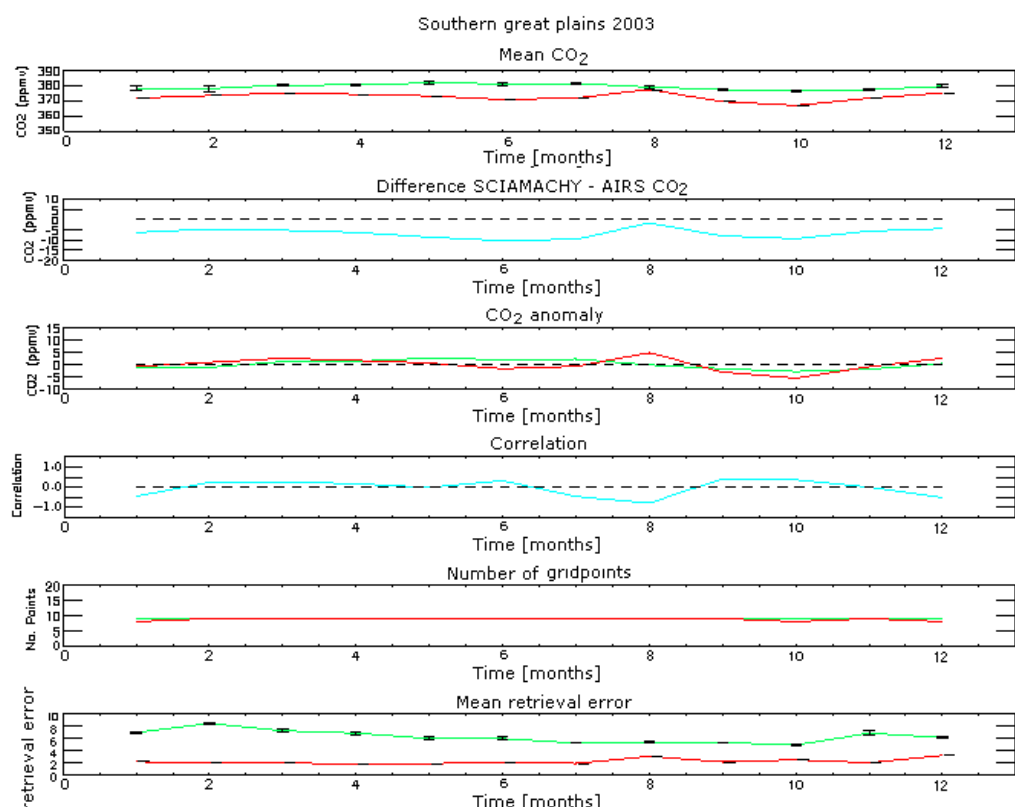
Figure 3.20: AIRS-4D (green) and SCIAMACHY (red) 2003 CO_2 data for Southern great plains (WMO WDGCC ground data); see figure 3.7 caption for more details.
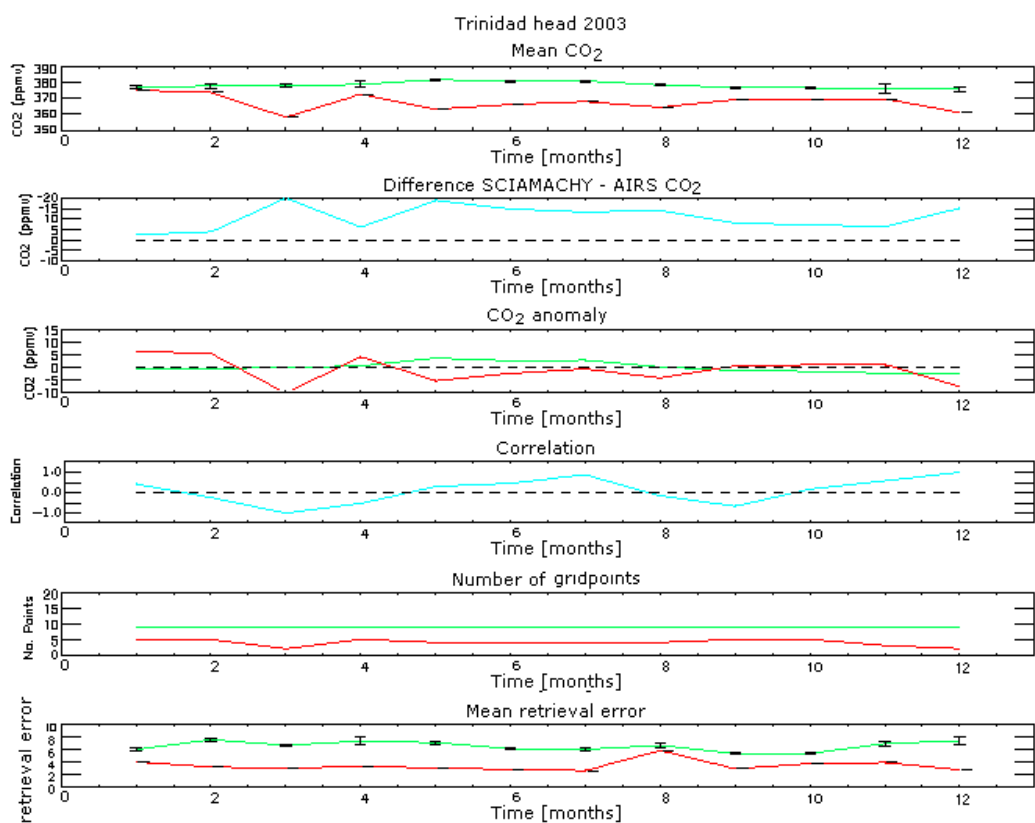
Figure 3.21: AIRS-4D (green) and SCIAMACHY (red) 2003 CO_2 data for Trinidad head (WMO WDGCC ground data); see figure 3.7 caption for more details.
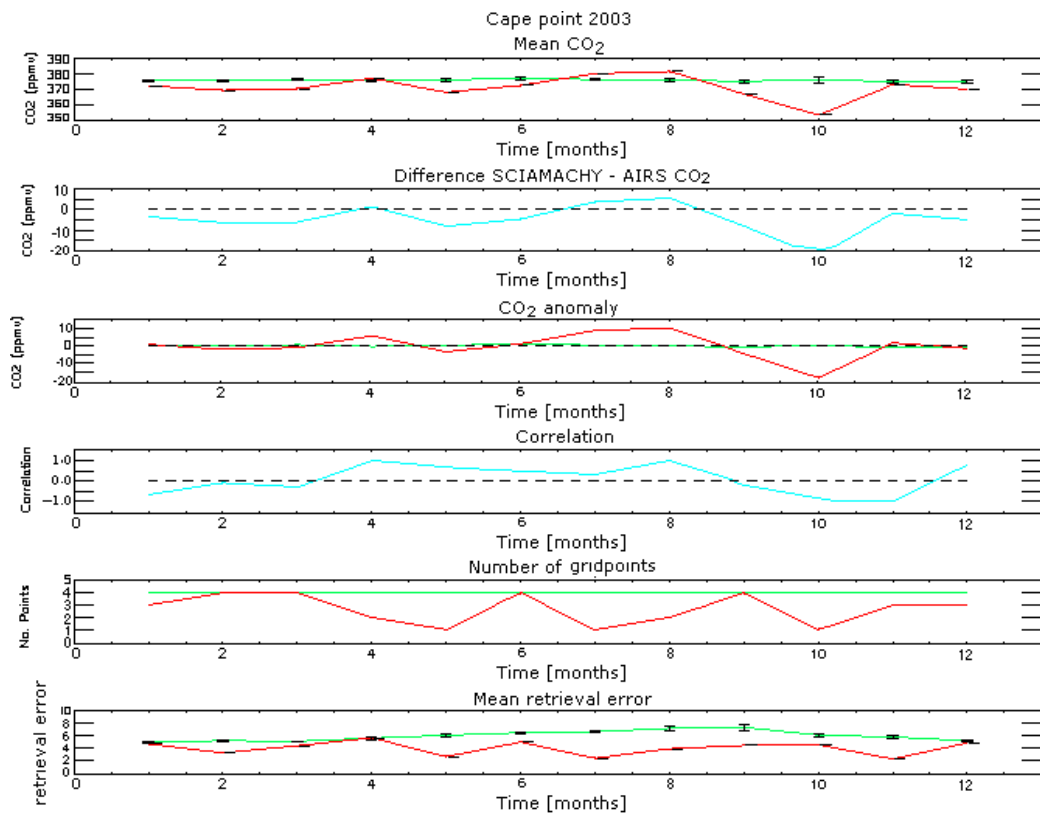
Figure 3.22: AIRS-4D (green) and SCIAMACHY (red) 2003 CO_2 data for Cape point (WMO WDGCC ground data); see figure 3.7 caption for more details.
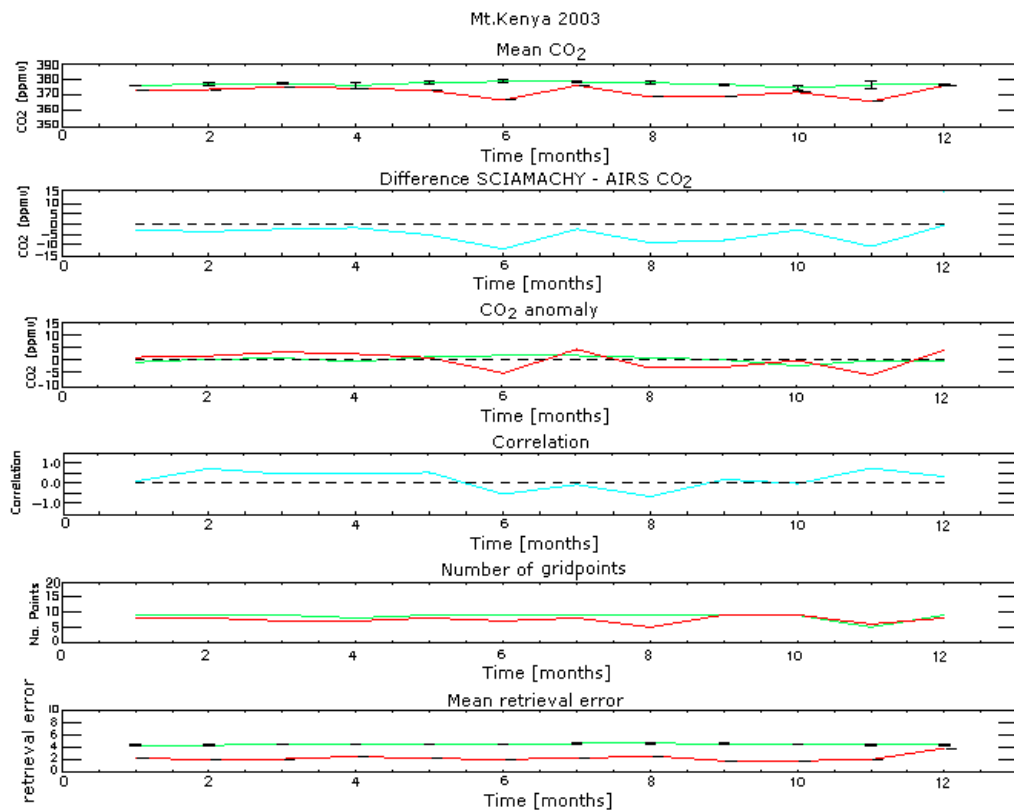
Figure 3.23: AIRS-4D (green) and SCIAMACHY (red) 2003 CO_2 data for Mt. Kenya (WMO WDGCC ground data); see figure 3.7 caption for more details.
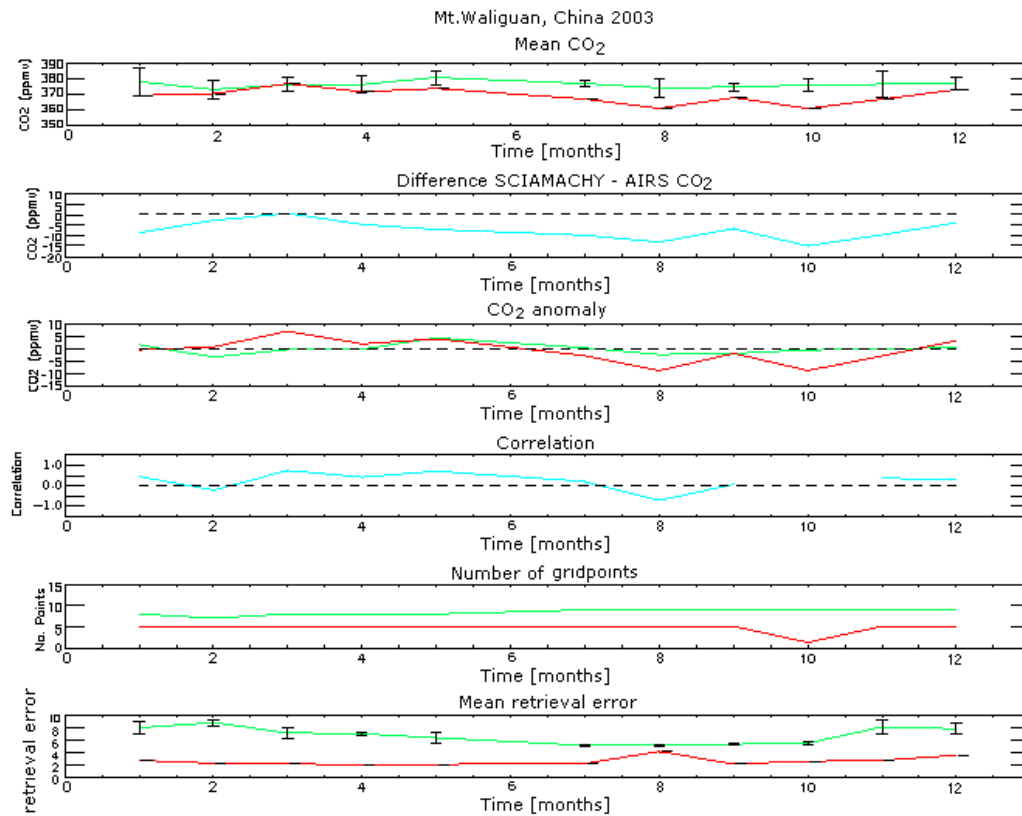
Figure 3.24: AIRS-4D (green) and SCIAMACHY (red) 2003 CO_2 data for Mt. Waliguan, Chiana (WMO WDGCC ground data); see figure 3.7 caption for more details.

Measuring the CO_2 concentrations over each in-situ location shows that the AIRS-4D measurements are fairly consistent, with each seasonal cycle reaching maximum concentration between April and June. Amplitudes (difference between the maximum and minimum CO_2 value during a one year period) of the AIRS-4D seasonal cycles vary between 2.2 and 7.3 ppmv with a retrieval error up to $\pm$ 9.2 ppmv. The AIRS-4D data shows that the seasonal cycle in the upper troposphere is fairly uniform in the upper troposphere, varying little over each region in both the northern and southern hemisphere. SCIAMACHY retrievals over the small areas show massive changes in the concentrations over each location and from month to month within a location area. Amplitudes of the seasonal cycles measured in the lower troposphere vary between 10.4 and 44.4 ppmv with a retrieval error up to $\pm$ 5 ppmv. Measurements retrieved in the lower atmosphere do not produce 'typical' seasonal cycles, where the CO_2 concentration increases during the area's winter months and decreases over the summer months. The seasonal cycles produced have no definite structure. Figures 3.16 to 3.24 show

that the CO_2 concentration can vary greatly from one month to the next, showing no seasonal variation over any location. The seasonal cycle amplitude measured over Estevan was 44.4 ppmv, Canada amplitudes of these magnitudes are unrealistic as CO_2 values within such a small area are unlikely to produce amplitudes of this size, unless there have been forest fires or substantial changes in the land usage. The area measured by SCIAMACHY is a 3 x 3 degree grid which covers a large area which could cover a wide variety of land usage such as vegetation, urban areas and forest fires. Each months measurement could be dominated by these different land types causing the abnormal seasonal cycles.

3.5.2 Satellite comparisons with in-situ ground (WMO WDGCC) CO_2 data.

To determine if the SCIAMACHY data measures the fluxes from the surface or if the measurements are caused by the variations in the surrounding areas, comparisons are made between the SCIAMACHY retrievals and ground based measurements from WMO WDGCC (http://gaw.kishou.go.jp/wdcgg/). AIRS-4D data are also compared to the in-situ data to determine if the CO_2 seasonal cycle is in or out of phase with the lower tropospheric seasonal cycle.
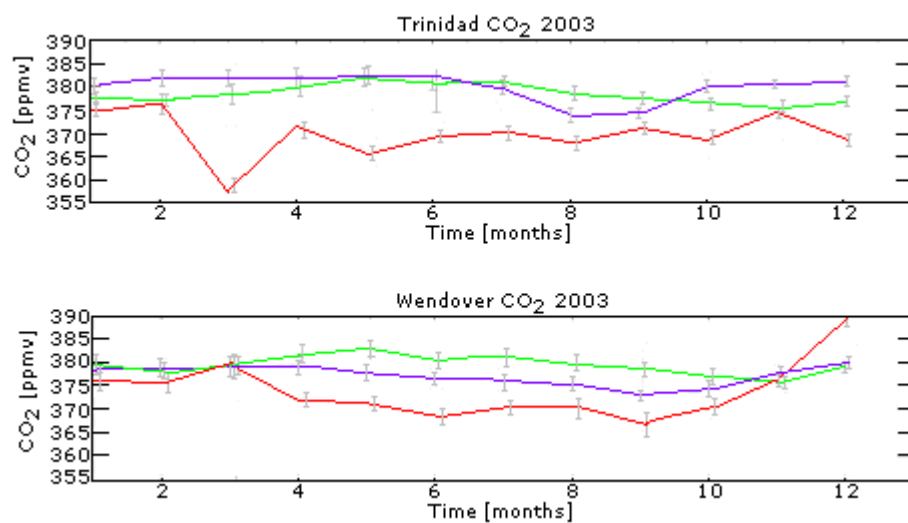
Figure 3.25: Seasonal cycles with 1σ errors for 2003, AIRS-4D (green), SCIAMACHY (red) and in-situ (purple). Top: Trinidad head, California, Bottom: Wendover, California.
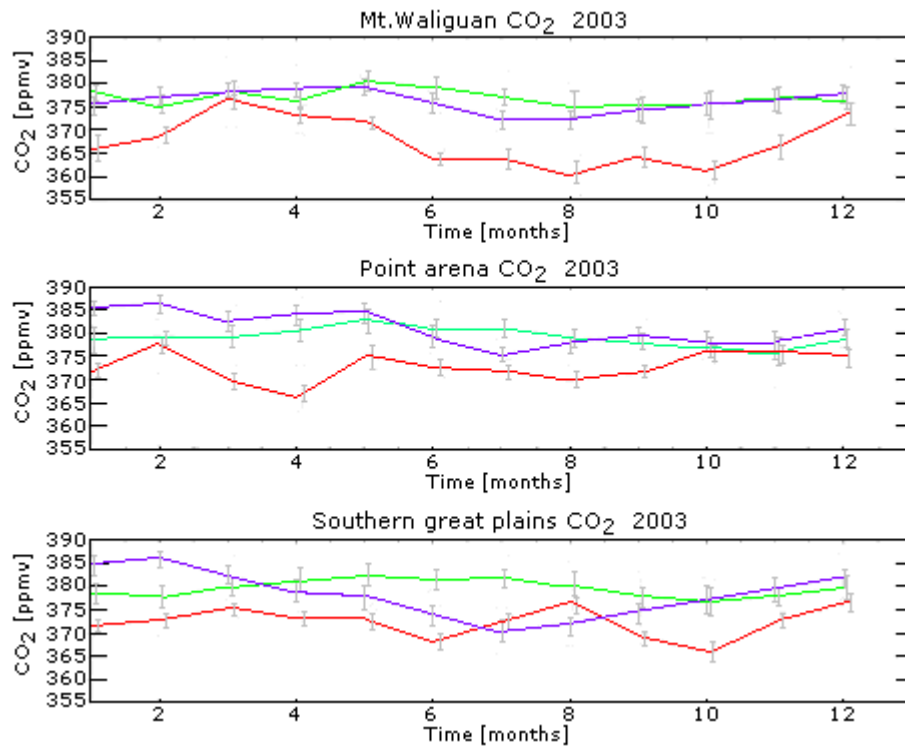
Figure 3.26: Seasonal cycles with 1σ errors for 2003, AIRS-4D (green), SCIAMACHY (red) and in-situ (purple). Top: Mt.Waliguan, Peoples republic of China, Middle: Point Arena, California, Bottom: Southern Great Plains, Oklahoma.
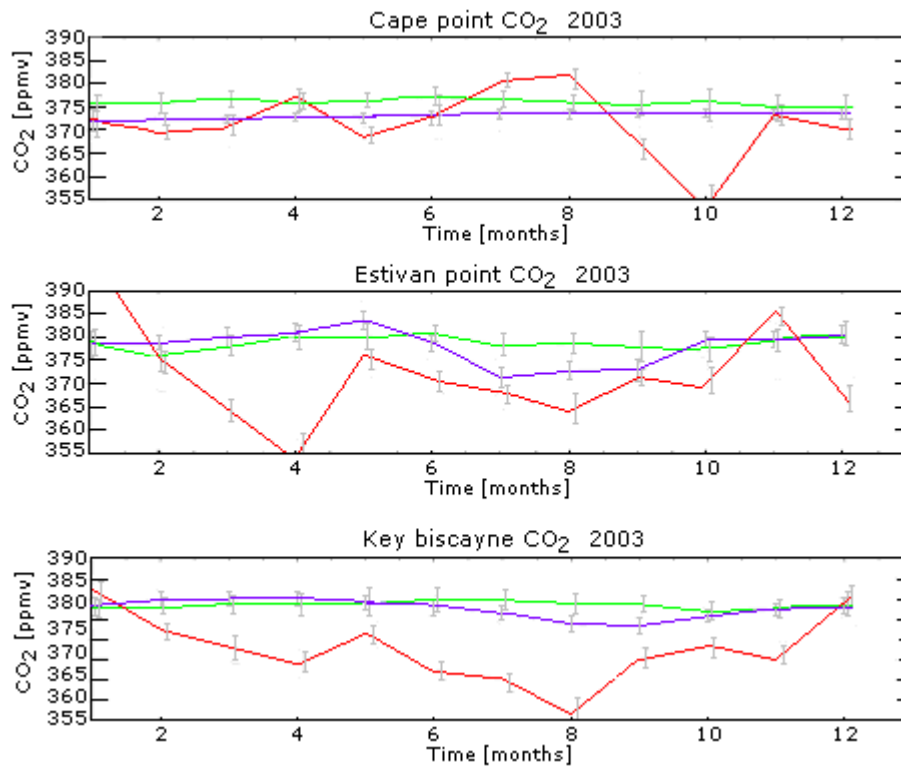
Figure 3.27: Seasonal cycles with 1σ errors for 2003, AIRS-4D (green), SCIAMACHY (red) and in-situ (purple). Top: Cape Point, South Africa. Middle: Estevan Point, Canada. Bottom: Key Biscayne, Florida.

CO_2 measurements from the ground instruments show that the CO_2 concentration varies with the regional changes in seasons, increasing during the winter months and decreasing over the summer months. The SCIAMACHY data show some similarities with the ground measurements for, Mt. Waliguan, Wendover, and Key Biscayne. The seasonal cycles are not smooth, there are unexpected changes in the CO_2 concentration, for example, Trinidad, California show a sharp decline in CO_2 measured by SCIAMACHY in March, which is not measured by either of the other instruments. These comparisons on a 3 x 3 degree grid show that SCIAMACHY measurements are too erratic to produce accurate results. AIRS-4D measurements produce seasonal cycles of varying amplitude and phase with regard to the ground measurements. The AIRS-4D seasonal cycle for Cape Point, peaks approximately 2 months before the CO_2 concentration peaks at ground level (in-situ measurement), for all other locations which are situated in the northern hemisphere the AIRS-4D seasonal cycle peak CO_2 concentration lags between one and three months with respect to the ground measurements. These comparisons of the upper and lower tropospheric CO_2 concentrations show that the upper troposphere is clearly dominated by the CO_2 fluxes in the northern hemisphere. Southern hemispheric regions show seasonal cycles representative of the northern hemisphere, they are weaker (smaller amplitudes), but due to the northern hemisphere emitting more CO_2 per year than the southern hemisphere [IPCC, 2007] the upper troposphere is influenced globally by the northern hemisphere emissions.

	AIRS-4D vs. SCIAMACHY	Ground vs. SCIAMACHY	Ground vs. AIRS-4D
Cape point	-0.015	0.011	-0.210
Estevan	-0.10	0.169	0.423
Key Biscayne	-0.487	0.474	0.069
Mt. Waliguan	0.341	0.824	0.377
Point arena	-0.275	0.017	0.292
Southern great plains	0.327	0.191	-0.414
Trinidad Head	-0.270	-0.072	0.210
Wendover	-0.185	0.731	0.225

Table 3.3: Regional correlation values for 2003: Right: Ground measurements vs. AIRS-4D data. Middle: Ground data vs. SCIAMACHY data. Left: SCIAMACHY data vs. AIRS-4D data.

Correlations between each of the data measured produced highly variable results (Table 3.3). As expected from the seasonal cycles produced the SCIAMACHY and AIRS-4D data showed little correlation over any region with the greatest correlation for Mt. Waliguan and Southern Great Plains.

Ground and SCIAMACHY correlations are varied, with some regions such as Wendover, Mt. Waliguan and Key Biscayne showing reasonable correlation. All other regions showed very little correlation, which is due to the erratic results produced by SCIAMACHY, clear seasonal cycles were not seen over these regions. It is uncertain why the data produced by SCIAMACHY are inconsistent; this could be caused by high or low emissions from the surrounding areas dominating the regional areas measured or that the spatial gridding of the instrument data is too coarse. It is also possible that the instrument errors are affecting the CO_2 measurements.

Correlating the AIRS-4D and ground measurements are pointless as they measure CO_2 concentrations at different points in the atmosphere. Comparisons are made to highlight that the CO_2 concentration in the upper troposphere are influenced by the ground fluxes, but due to the time taken for CO_2 to reach the upper troposphere [Park et al., 2007] and atmospheric mixing [Shia et al., 2006], CO_2 seasonal cycles are out of phase and vary in amplitude compared to the lower troposphere.

3.6 Summary.

Measuring CO_2 at different tropospheric heights produce vastly different results. The upper troposphere global results show that the CO_2 is uniformly distributed, with some regions of varying concentration, which are generally seen in the northern hemisphere. The lower troposphere measurements produce contrasting results compared to the upper tropospheric region, sinks and sources are clearly visible over many regions. Seasonal variations which differ in the north and southern hemisphere are evident. Comparisons of CO_2 data from the two instruments provide a better understanding of how CO_2 is distributed throughout the troposphere. CO_2 is highly variable in the lower troposphere which is

influenced by surface emissions and absorptions and the type of the land usage. Whereas the upper troposphere shows that CO_2 is well mixed globally, indicating that it is not influenced primarily by the continuous surface emissions and absorptions, rather the time taken for the surface CO_2 to mix through the troposphere.

Seasonal cycle amplitudes are much greater in the northern hemisphere than those measured in the southern hemisphere, these differences are due to greater CO_2 emissions and absorptions from the surface vegetation and urbanisation in the northern hemisphere. Lower tropospheric seasonal cycles deduced from SCIAMACHY data indicate that CO_2 concentrations peak between April and May in the northern hemisphere and in August (Southern Africa) and July (South America) in the southern hemisphere, which are representative of the respective winter months where the vegetation mass is decreased. In contrast the upper tropospheric seasonal cycle shows similar trends in both hemispheres with CO_2 concentrations at maximum between May and June.

The seasonal cycle measured in the upper troposphere shows little to no variation over the nine regions analysed. The amplitude of the cycles are small in the upper troposphere with a max amplitude measured over UK and Europe at 4.2 ± 7.6 ppmv compared to the max amplitude in the lower troposphere of 21.3 ± 2.6 ppmv over Siberia, which suggests that the CO_2 in the upper troposphere is well mixed and that small fluxes from the surface have little effect on the upper tropospheric concentrations. Large surface fluxes are seen over North America and Siberia from January through to May which are translated up into the upper troposphere where the higher CO_2 concentrations is added to the current CO_2 levels.

The CO_2 measurements of the lower troposphere show that not only do the seasonal changes effect the CO_2 concentration, the land usage also influences the amount emitted and absorbed. High urbanization areas (cities) produce greater amounts of CO_2 compared to areas of dense vegetation. The fluxes measured by SCIAMACHY in the lower troposphere help determine where the sinks and sources are located.

Owing to the high variability of the SCIAMACHY data over small areas, comparisons with in-situ ground data showed that small scale SCIAMACHY

measurements were not good. AIRS-4D comparisons with in-situ data were also shown to be poor as the AIRS-4D measurements are sensitive to different tropospheric region, indicating that validation comparisons between the upper and lower tropospheric regions are futile.

Previous evaluation studies between in-situ and satellite measurements show that there is some good agreement between the two data types [buchwitz et al., 2005, Barkley et al., 2006]. Comparisons between SCIAMACHY and in-situ data have also shown some promising results, with good agreement between ground stations in Bremen and Park Falls and in Darwin [Schneising et al., 2008]. AIRS-4D measurements are most sensitive in the mid-upper troposphere where comparisons with the CO_2 data have been made with aircraft data. Results between AIRS-4D and aircraft (CMDL flight data) data for Cook islands, Hawaii, Brazil and Harvard forest show reasonable results, with correlation values varying between 0.56 and 0.96 [Engelen and McNally, 2005]. To improve the satellite data for comparison with in-situ based measurements, smaller grid areas would likely improve the comparisons, as 3 x 3 degree grid encompasses a vast area of varying land usage which can profoundly influence the atmospheric CO_2 concentration measured by the satellite.

Chapter 4.

Comparisons of SCIAMACHY (FSI) WFM-DOAS CO_2 column data with AIRS (LSQ method) column CO_2 data.

4.1 Introduction.

This chapter compares the (FSI) WFM-DOAS SCIAMACHY CO_2 data [Barkley et al., 2006] with the AIRS data retrieved via the LSQ method (hereafter referred to as AIRS-LSQ) from Barnet et al (2005) and Maddy et al (2008). SCIAMACHY CO_2 column (CO_2) data covers the whole tropospheric region with its greatest sensitivity between one and five kilometres. The AIRS data extends from the stratosphere down to the tropospheric boundary layer, in five discrete layers which can be used individually or combined to calculate a vertical column density of CO_2.

AIRS measures Thermal InfraRed (TIR) radiation which are sensitive to measurements in the mid–upper troposphere (Section 2.3) and SCIAMACHY measure in the Near InfraRed (NIR) spectral region (Section 2.4) which are sensitive to measurements in the lower troposphere. AIRS-LSQ data is far more versatile than the AIRS-4d product (chapter 3). The AIRS-LSQ data provided is unfiltered, which is the CO_2 data before cloud clearing, application of averaging kernels and other filters. From the data provided various filters are applied to attain the best results. The 4d-var method provided was already processed and

had a background error of ± 30 ppmv which could drastically effect the CO_2 retrievals. The use of the LSQ data is to attain more accurate measurements of the upper tropospheric CO_2. AIRS (Section 2.3.3) and SCIAMACHY (Section 2.4) are examined globally and regionally to determine if the data are similar or if there are clear differences in the CO_2 concentrations in the upper and lower atmosphere. Column data are calculated from the AIRS-LSQ and SCIAMACHY retrievals where the CO_2 distributions for August 2003 to December 2004 are shown and compared. Seven global regions are analysed using the AIRS-LSQ and SCIAMACHY CO_2 data to determine if there are differences in the seasonal cycle between the upper and lower troposphere and how do they vary with latitude and in the northern and southern hemispheres. Subtraction of the AIRS-LSQ column from the SCIAMACHY CO_2 column is calculated to determine if the remaining data is representative of the surface flux, through comparisons with in-situ data.

4.2 Filtering the AIRS data.

Data retrieved from AIRS-LSQ (or the unfiltered data) include cloud and water vapour measurements from the troposphere. To reduce the errors caused by the clouds, water vapour and low signal retrieval (or high noise signal) constraints are applied to the retrieved data. Removal of measurements with unprecedented high (>400 ppmv)/low (<350 ppmv) CO_2 concentrations are included to increase the quality of data analysed.

Carbon dioxide (CO_2) data calculated are the average values within each layer retrieved, there are 5 layers extending from the boundary layer to the top of the stratosphere (where L represents a layer boundary in the atmosphere):

$$CO_2 (L) = Average(CO_2 (L\text{-}1\text{:}L)) \qquad\qquad (4.1)$$

CO_2 values for each layer (L) are assigned at the effective pressure or average pressure of the layer. The CO_2 values calculated are the average concentration retrieved per level not the CO_2 concentration value at the centre of the layer.

Calculating CO_2 concentration within each layer assumes a thin layer approximation, which is a constant scale height between boundary levels, yielding:

$$P_{eff}(L) = \frac{(P(L-1) - P(L))}{A * Log(P(L)) * P(L-1)} \qquad (4.2)$$

For the effective pressure where P(L) and P(L-1) are the pressure level boundaries of each retrieval layer, A is the average pressure layer. The upper and lower boundaries of the retrieval layers are:

Layer level	Lower atmospheric layer P[hPa]	Upper atmospheric layer P[hPa]
1	0.0	103.0
2	103.0	201.0
3	201.0	300.0
4	300.0	496.6
5	496.6	Psurface

Table 4.1: AIRS-LSQ layers and their respective pressures.
(where psurf is the surface pressure).

There are 5 layers throughout the troposphere and stratosphere that can be used to calculate column CO_2 (Table 4.1), the lower tropospheric layer is not used as AIRS-LSQ is not sensitive to the lower tropospheric region, therefore only 4 pressure layers are used, as these layers have absolute pressure layer boundaries. The column CO_2 values for each 3° x 3° area were calculated for each day for every month processed. The data were then summed and averaged over each month. The bottom layer (layer 5) which is sensitive to CO_2 in the middle-lower troposphere is not used as the surface pressure layer varies considerably over different surface types, such as different land types and oceans. In order to limit the errors in the AIRS-LSQ column data, this layer is not used.

The initial CO_2 retrievals are unfiltered which means that all radiances utilised have a high concentration of cloud and water vapour, which increase the errors in the retrievals. Therefore the CO_2 retrievals are filtered, to reduce the errors and to

remove contaminants in the data. The remaining data, once filtered better represents the tropospheric CO_2 as the errors are reduced and uncharacteristic high/low values are removed.

4.2.1 AIRS-LSQ global unfiltered CO_2 data.

To determine how much effect various atmospheric components, such as cloud, water vapour etc. have on the quality of the CO_2 data produced, the data is plotted with and without filters. In Figure 4.1 unfiltered global CO_2 data for tropospheric CO_2 are plotted.
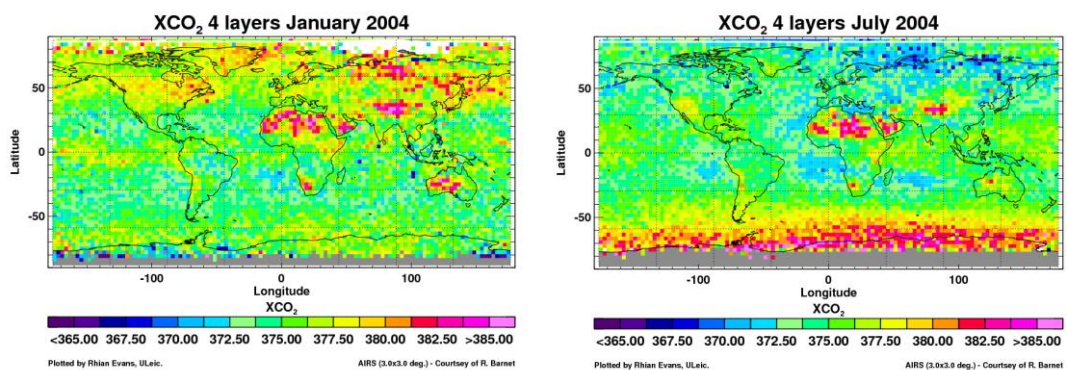
Figure 4.1, AIRS-LSQ data (courtesy of C. Barnet) is plotted for January (left) and July (right) 2004, no filters are applied and values greater than 340 ppmv are used.

The global data shows high concentrations of CO_2 in Antarctica in July and low concentrations in January which indicates that there are anomalies in the data retrieved causing these high values. There are no significant anthropogenic or natural CO_2 emissions which could cause such high CO_2 values over this region. The high concentrations could be due to cloud or water in the atmosphere as July is the southern hemisphere's winter, where it would have a greater amount of cloud in the atmosphere. There are also high concentrations of CO_2 over the Saharan desert in both July and January (Figure 4.1). There are no excessive natural or anthropogenic emissions from the surrounding area which could account for such high concentrations in the upper troposphere.

4.2.2 Cloud filtered AIRS-LSQ CO_2 data.

Cloud fraction is retrieved and calculated from data from AMSU FOV (which is also on board AQUA and measures the same area as AIRS). This is used to filter the cloud data from the global CO_2 values. The cloud fraction has values from 1 (no cloud) to 0 (full cloud coverage).
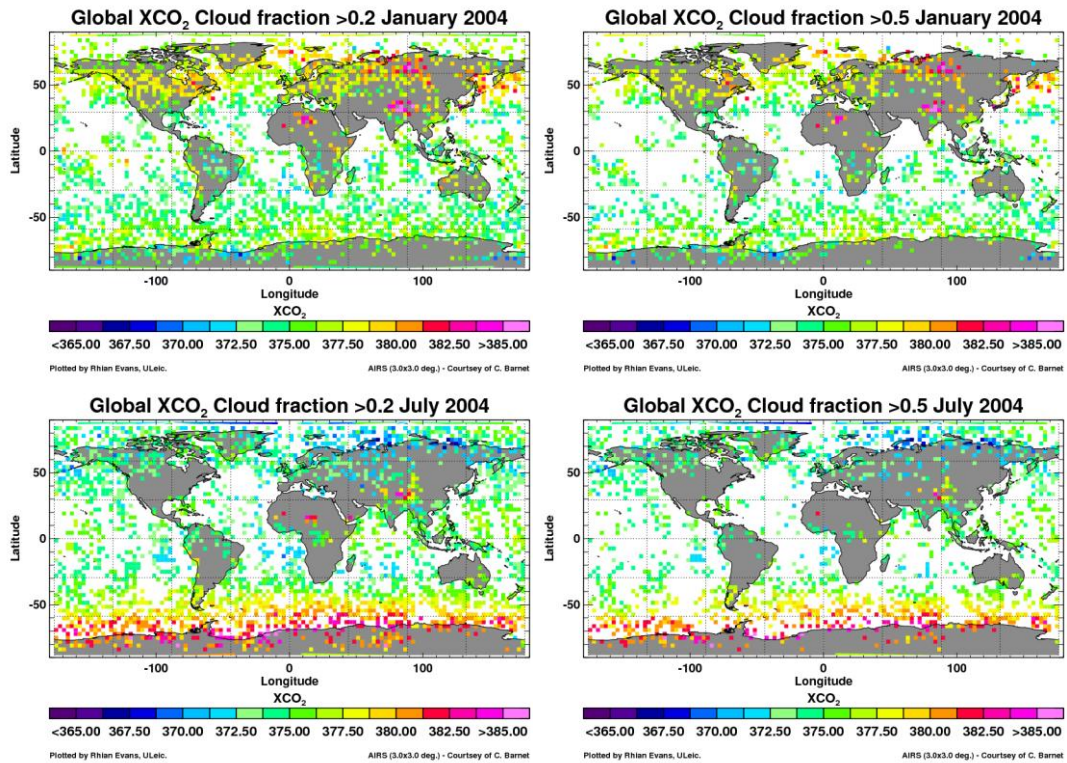
Figure 4.2. Filtering for cloud fraction left top and bottom are CO_2 data with cloud fractions greater than 0.2 for January and July respectively. Right: Filtered data for cloud fractions greater than 0.5 for January and July respectively.

AIRS-LSQ data retrieved with cloud fraction greater than 0.2 and 0.5 are plotted in Figure 4.2. Global data shows that significant amounts of data are removed when filtering the retrievals for cloud fraction greater than 0.2 and 0.5. The data remaining is sporadic from which no definite conclusions can be made.

4.2.3 Water filtered CO$_2$ data

The CO$_2$ data is filtered through the fraction of water retrieved where the water fraction values range from 0 to 3. Three represents the greatest amount of water retrieved and zero where no water is retrieved. Filtering the data for fractions less than 2.5 and 1.5 (Figure 4.3) shows that significant amounts of data are lost over the Sahara dessert for both cases.
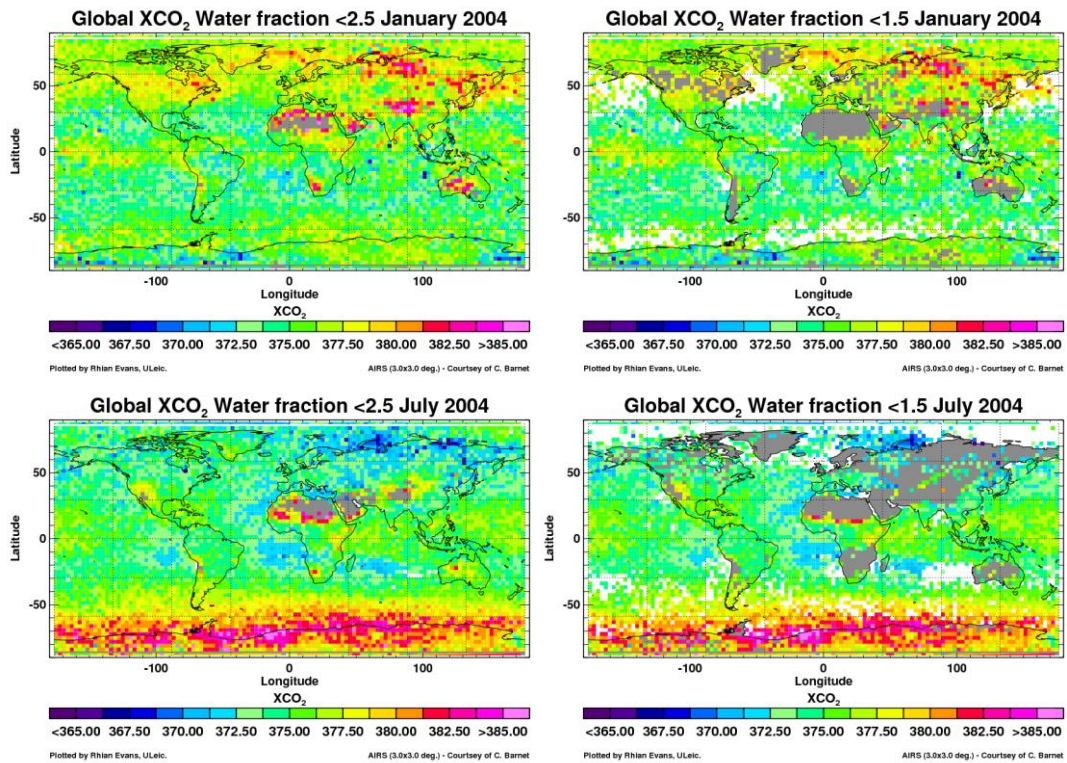
Figure 4.3; Global CO$_2$ data filtered through water retrieval residual (signal to noise ratio). Left: water fraction less than 2.5, right: water fraction less than 1.5.

Figure 4.1 shows high concentrations of CO$_2$ over northern Africa which could not be explained, as there are no great natural sources of CO$_2$ (or high anthropogenic emissions) over this region which would account for such high values. Eliminating the retrievals with high water content the high concentrations of carbon dioxide over Africa are removed from analysis. Further reductions to the amount of data accepted occurred with increasing water fraction value, where data is lost over southern Africa, Russia, Australia and the west coast of America.

Filtering the data for water content the high CO_2 values retrieved over the southern hemisphere at latitudes greater than 50^oS remain. CO_2 concentrations within this region should be much smaller as there are very little if any anthropogenic and natural CO_2 emissions. Figure 4.2 shows that the poor data in this region could be due to cloud contamination.

4.2.4 Averaging Kernels and degree of freedom (DOF).

The information content within each measurement describes the amount by which that measurement reduces the uncertainty in the value of interest [Feldman., 2004], this is a generalization of the signal to noise ratio. The degree of freedom (DOF) is the information content which describes the number of independent pieces of information in each measurement [Rodgers, 2000].

$$DOF = tr(A) \qquad (4.3)$$

where tr(A) is the trace of the averaging kernel matrix. This quantity is important in order to establish an appropriate co-ordinate system for a successful retrieval. The averaging kernel shows how sensitive the retrieval is with regard to the atmospheric state and provides the relative weighting between the true and a-priori profile. The averaging kernel is basically the retrieval produced from a combination of factors; the vertical resolution, sensitivity of the retrieval and influence of the a-priori, which contribute to the retrieval performance.

$$A = I - (C_a^{-1} + K^T C_e^{-1} K)^{-1} C_a^{-1} \qquad (4.4)$$

where I is the identity matrix, C_a is the a-priori covariance matrix, C_x is the retrieval covariance error matrix, K is the weighting function, and C_e is the radiance error matrix. The averaging kernel is directly related to the weighting

function, which describes the sensitivity of the measurement of the vertical distribution of the species of interest in the atmosphere.

The amount of independent data available in the retrieved AIRS-LSQ data is represented by the average kernel values. The data provided represents 5 layers in the atmosphere, which gives a 5 x 5 matrix. The trace of the average kernel matrix is calculated (Equation 4.3) for each latitude and longitude measured by AIRS-LSQ.
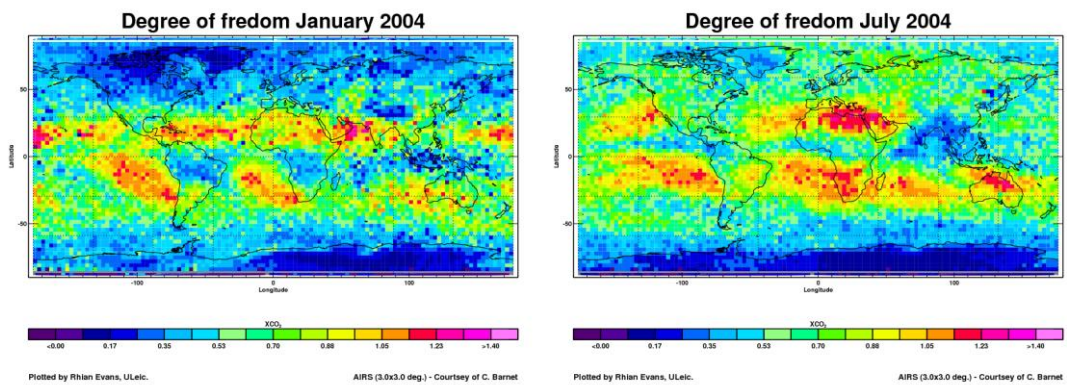
Figure 4.4: AIRS-LSQ DOF for January (left) and July (right) 2004.

Figure 4.4 shows the global values of the DOF, the areas where the information content is greatest are located within the tropics. Values in these regions are typically greater than 1.0. The amount of data available with values of one decreases with increasing latitudes, in both northern and southern hemispheres. Data with greater DOF values have a higher content of the retrieval from the measurements taken by the instrument, those with lower values have a higher noise to signal ratio. DOF value of 0.3 receives 30% from the instrument measurement and 70% from a-priori data.

The DOF (or trace array) calculated from the averaging kernel is used to filter the CO_2 column data. Several values were used to determine how much data is available once filtered; DOF values used are: >0.4, >0.5 and >1.0.
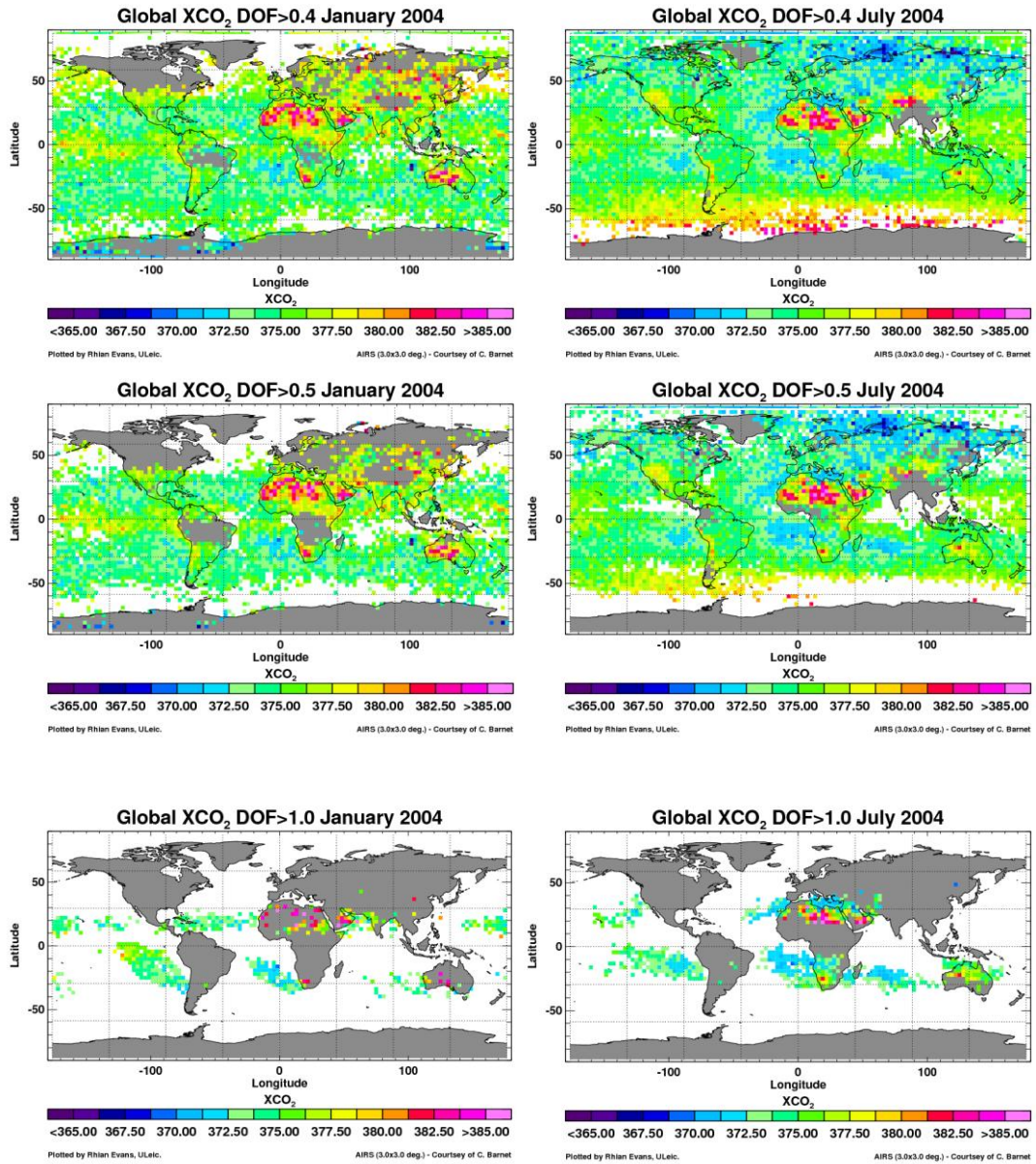
Figure 4.5; calculating the degrees of freedom (DOF) from the data retrieved, top: DOF >0.4, middle > 0.5, bottom >1.0.

Figure 4.5 shows the CO_2 data with DOF greater than 0.4, 0.5 and 1.0 (top to bottom respectively). Increasing the quality of the information content decreases the amount of data available. DOF greater than 1.0 will not be used as the data is sparse and producing data for a whole year over one region is unlikely. Data available for DOF greater than 0.4 and 0.5 are considerable, although using a DOF greater than 0.5 much data is lost at higher latitudes over North America and also over the tropical areas in South America and Africa.

4.2.5 Combining filters to reduce errors in the retrieved data.
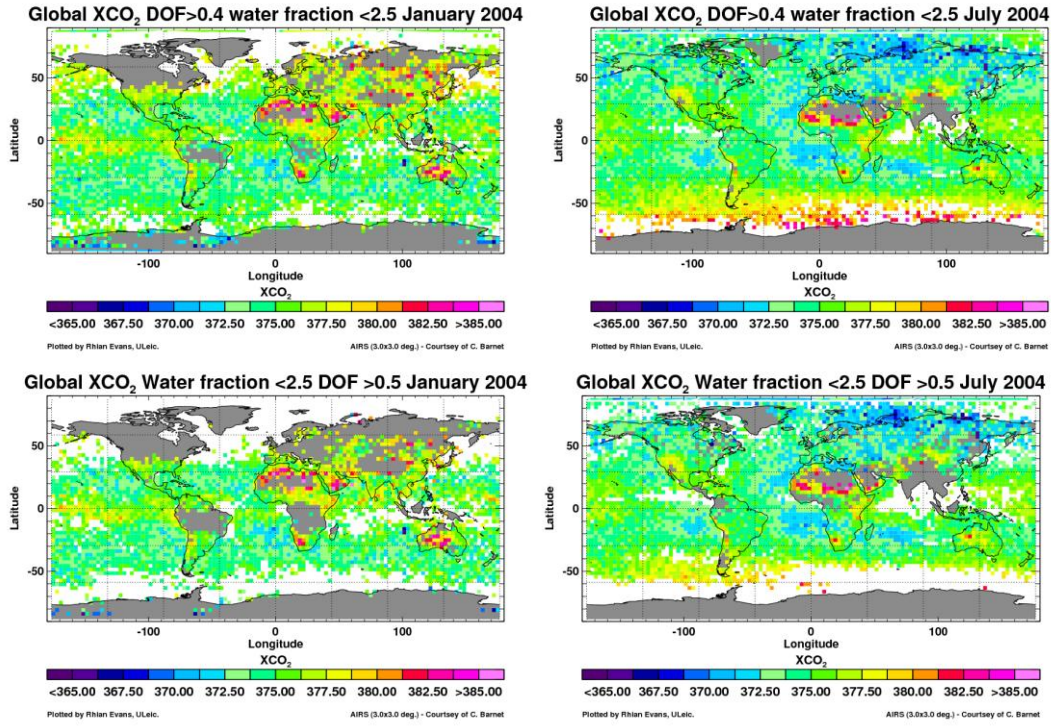
Figure 4.6; Global CO_2 plots with filtering. Top: DOF > 0.4 and water fraction < 2.5. Bottom: DOF > 0.5 and water fraction < 2.5.

Determining the best filters to use to attain good global coverage of CO_2, a mix of both water fraction and DOF was used to reduce the high concentrations of CO_2 over Africa and Antarctica in the final measurements. In Figure 4.6 water fraction of less than 2.5 are used. Filtering water with a fraction less than this greatly reduces the amount of high CO_2 concentration over Africa (Figure 4.6). Figure 4.6 shows the amount of data remaining when using DOF values greater than 0.5 and 0.4 in addition to using the water filter. DOF values greater than 0.5 remove significant amount of data especially at higher latitudes, values of 0.4 or greater improve the amount of data available to analyse. The data is not filtered using the cloud fraction as the data remaining is limited (Figure 4.2) and no comparisons can be made with the amount of data remaining.

The filters used for the AIRS-LSQ data to reduce the uncertainties over Africa and Antarctica are; DOF > 0.4 and water fraction < 2.5.

4.3 Global CO$_2$ data.

4.3.1. Global AIRS-LSQ CO$_2$ data.

Global AIRS-LSQ column CO$_2$ (CO$_2$) is calculated for the atmospheric heights in the troposphere from the tropopause to 496.6 hPa, and filtered as described in section 4.2. Data is plotted from August 2003 through December 2004, with the exception of October 2004 (no data available). Filtering the CO$_2$ data reduces the retrievals over several regions, such as Antarctica, northern Africa and India, these regions were found to have a high concentration of water in the atmosphere and small information content (DOF). During the winter months in northern hemisphere (November through February), the data at higher latitudes is sparse due to the increased amounts of water in the atmosphere and generally low quality data available within this region.
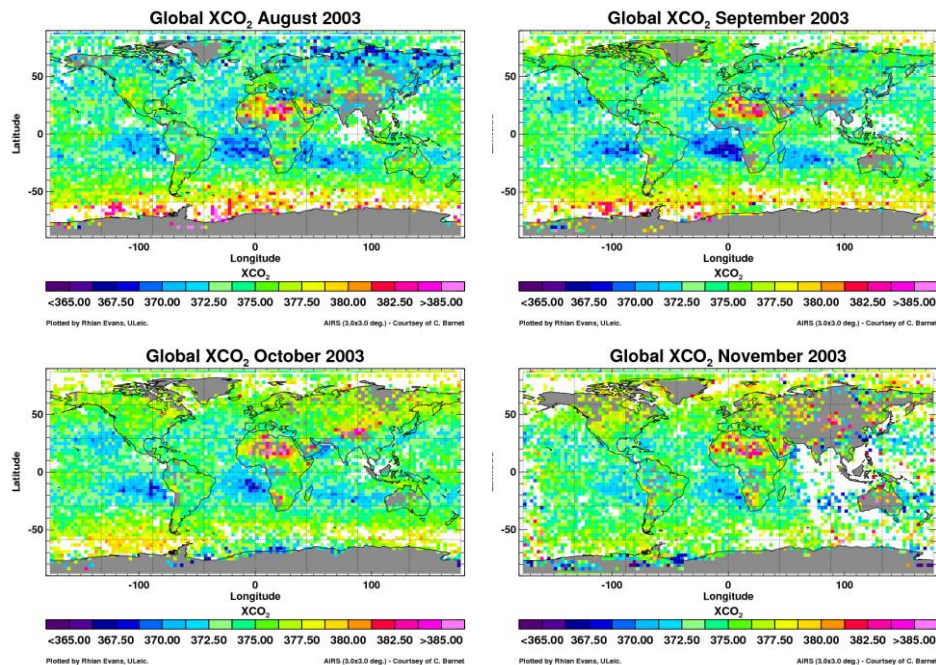
Figure 4.7a; Global column CO$_2$ retrieved by the AIRS-LSQ method for August 2003 to November 2003.
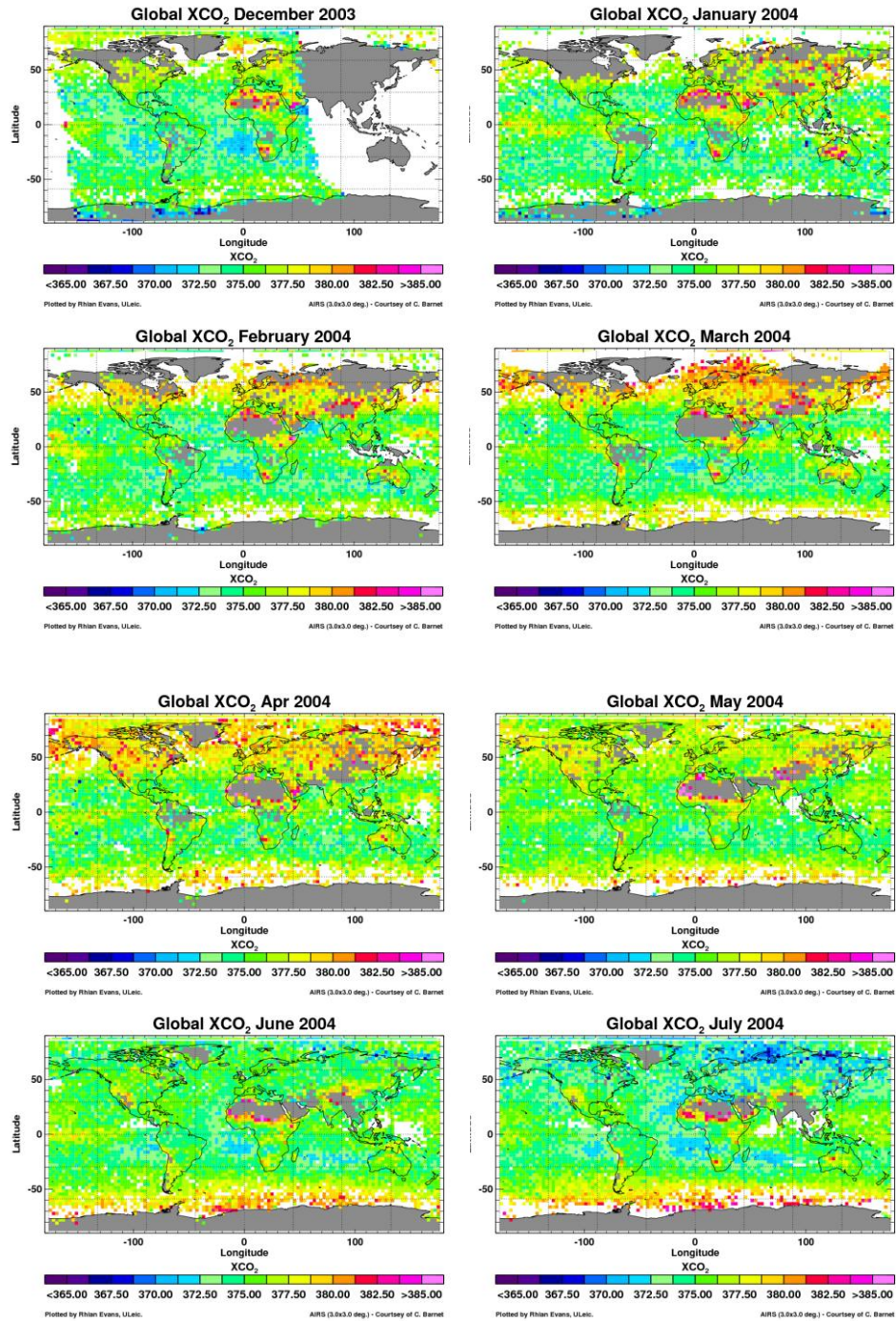
Figure 4.7b; Global column CO_2 retrieved by the AIRS-LSQ method for December 2003 to July 2004.
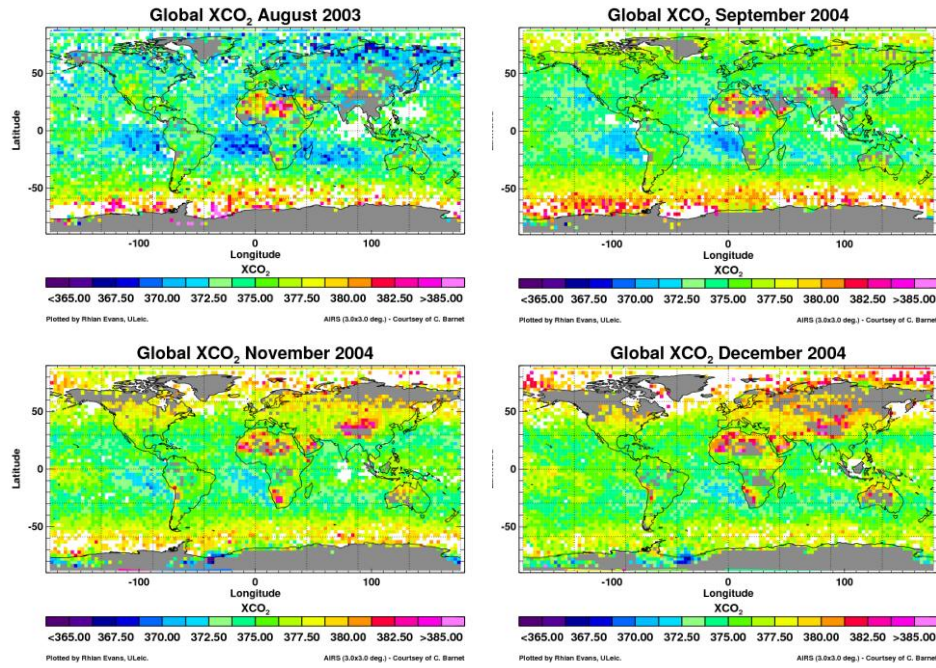
Figure 4.7c; Global column CO_2 retrieved by the AIRS-LSQ method for August 2004 to December 2004. (no October 2004 data available).

The AIRS-LSQ results show greater concentration variations of CO_2 in the upper troposphere compared to those retrieved via the 4d-var method, indicating that the LSQ method is more sensitive to CO_2 variations. These results show that the upper troposphere is influenced by the surrounding surface emissions and absorptions, rather than a well mixed mean value of the surrounding area, these effects are not as visible in the 4d-var retrievals (Figure 3.3).

Progressing through the monthly data, the CO_2 concentration in the atmosphere increases November through April, after which CO_2 concentrations begin to decrease with the lowest values occurring between July and August. This effect is more noticeable in the northern hemisphere, as there is a greater land mass with greater vegetative coverage which emits and absorbs CO_2 and also increased anthropogenic emissions which contribute to the tropospheric CO_2 levels. The southern hemisphere shows a smaller change over the sixteen months shown in Figure 4.7 which could be due to less land mass coverage influencing CO_2 absorption and emissions and a smaller contribution of anthropogenic CO_2 compared to the northern hemisphere. AIRS-LSQ measurements are sensitive to the middle-upper troposphere, therefore variations in the lower tropospheric CO_2

concentrations are unlikely to have an immediate effect on the CO_2 concentrations in the upper troposphere due to the time taken for the CO_2 to transport to the upper troposphere [Park et al., 2007]. Time taken for CO_2 to mix from the surface to the upper troposphere can take several days to weeks, which could explain why there aren't any considerable variation in the CO_2 concentration throughout the sixteen months in the southern hemisphere. The northern hemisphere emits greater amounts of CO_2 than the southern hemisphere which can explain why in conjunction with the time taken for CO_2 to mix through to the middle-upper troposphere that the amplitude of the southern seasonal cycle is small and is roughly in phase with the seasonal cycle in the northern hemisphere.

4.3.2 SCIAMACHY GLOBAL CO$_2$ DATA

Global CO_2 columns retrieved form SCIAMACHY is calculated using the (FSI) WFM-DOAS method (see section 2.3). Global SCIAMACHY CO_2 is retrieved for 2004 (Figure 4.8), the data has greater sensitivity to measurements than AIRS in the lower troposphere, between 1 and 5 km (Section 2.4) [Barkley et al., 2007; Buchwitz et al.,2007; Schneising et al., 2008]. Data retrieved in the lower troposphere shows greater CO_2 variation than the upper troposphere caused by the changes in the land types and anthropogenic emissions.
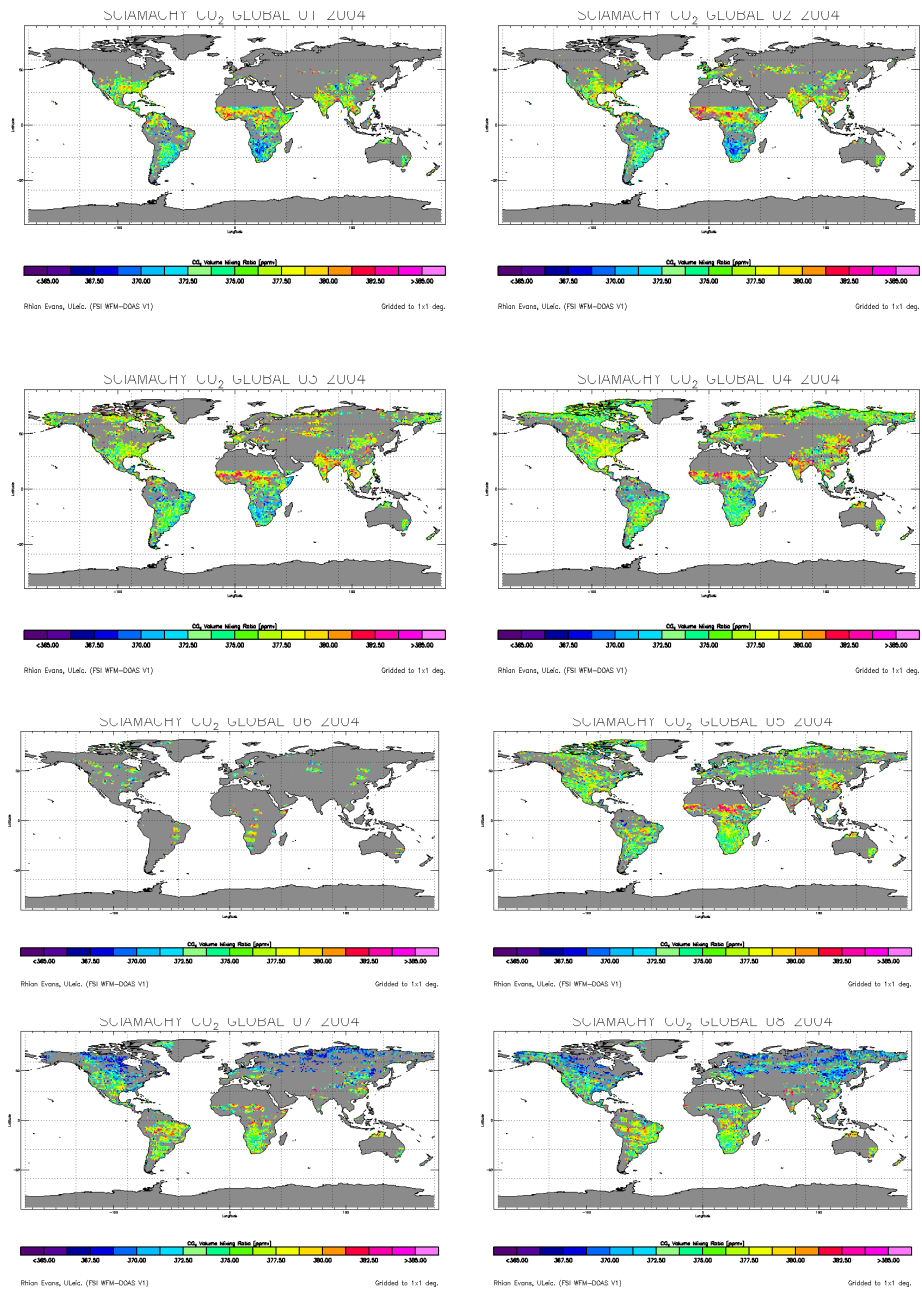
Figure 4.8a; Global column SCIAMACHY CO_2 data January through August 2004.
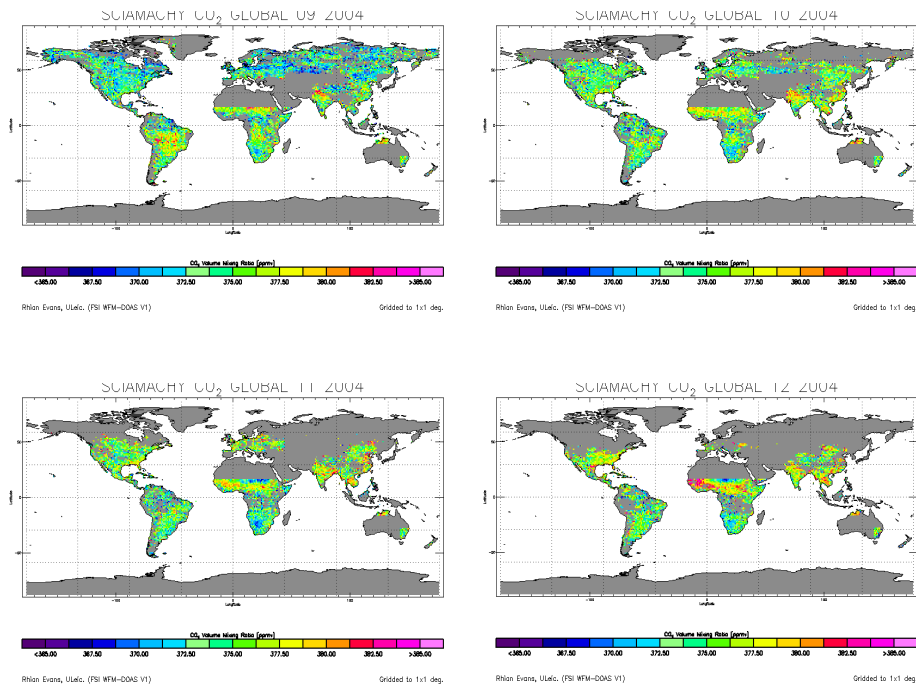
Figure 4.8b; Global column SCIAMACHY CO_2 data September through December 2004.

Only selected regional data are available for 2004 due to the time required to process each pixel. The CO_2 concentration shows substantial variations over the Earth, there is also a clear north-south divide which is more prominent in July through September, with lower CO_2 values in the northern hemisphere compared to the southern hemisphere. Clear CO_2 changes can be seen over the land which is best demonstrated in July and August over North America and January through May over Africa. The variation in the amplitude of the seasonal cycle in the lower troposphere is far greater than the amplitude in the middle-upper troposphere as the changes in surface fluxes are caused by the variations in vegetation and anthropogenic emissions. Surface fluxes are not detected in the lower troposphere as the CO_2 mixes throughout the atmosphere so sinks and sources are not easily detected in the upper troposphere.

4.3.3 Global AIRS-LSQ and SCIAMACHY CO$_2$ seasonal cycles for 2004

Global seasonal cycles retrieved by AIRS-LSQ and SCIAMACHY (Figure 4.9) show that the global and northern hemispheric data are roughly in phase in the two tropospheric regions. The seasonal cycle measured in the southern hemisphere produces seasonal cycles which are vastly different in the two tropospheric regions with the AIRS-LSQ data producing a seasonal cycle similar to those measured in the northern hemisphere but with a reduced amplitude of 1.33 ppmv compared to 3.59 ppmv measured in the northern hemisphere. SCIAMACHY seasonal cycle in the southern hemisphere is representative of the local seasonal change with CO$_2$ concentrations increasing in June (winter) and decreasing in October (Spring/summer).
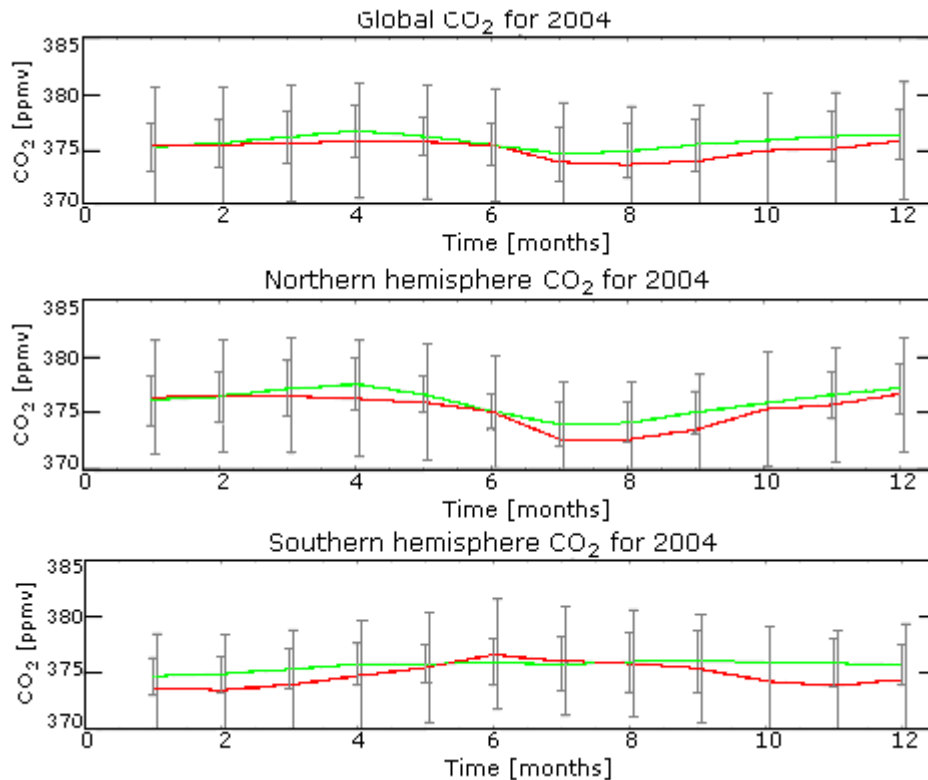
Figure 4. 9 Seasonal cycles measured by AIRS-LSQ (green) and SCIAMACHY (red) for 2004. Top: global cycle, middle: northern hemisphere, bottom: southern hemisphere.

Correlation value between the AIRS-LSQ and SCIAMACHY are greatest in the northern hemisphere producing a value of 0.893 and produces a negative correlation in the southern hemisphere -0.437, with an overall global correlation of 0.776. These values show that the CO_2 fluxes in the northern hemisphere are dominant throughout the troposphere especially in the upper troposphere.

4.3.4 SCIAMACHY – AIRS-LSQ CO_2 global data August 2003 – December 2004.

Global data retrieved by SCIAMACHY and AIRS-LSQ in the lower and middle-upper tropospheric regions respectively, the two data sets show great variations in the CO_2 measurements. AIRS-LSQ data shows little global variation whereas SCIAMACHY data shows significant variations over the land, showing sinks and sources over the continents. Validation between the two data sets is of no benefit as the CO_2 variations at the surface cannot be detected by AIRS; the data in the upper troposphere has been well mixed, representing an average value of the CO_2 from the surrounding area. However, both data sets are column averaged CO_2 which are sensitive to different regions in the troposphere. Therefore subtracting the AIRS-LSQ tropospheric column data from the SCIAMACHY CO_2 data should result in the data remaining which have an increased sensitivity to the lower atmosphere at altitudes below 496.6 hPa. The data remaining are the CO_2 column values from the surface to 496.6 hPa, with no influence of the average seasonal cycle of the upper troposphere on the CO_2 column data, thus the remaining data would only be sensitive to the variations in the surface fluxes.
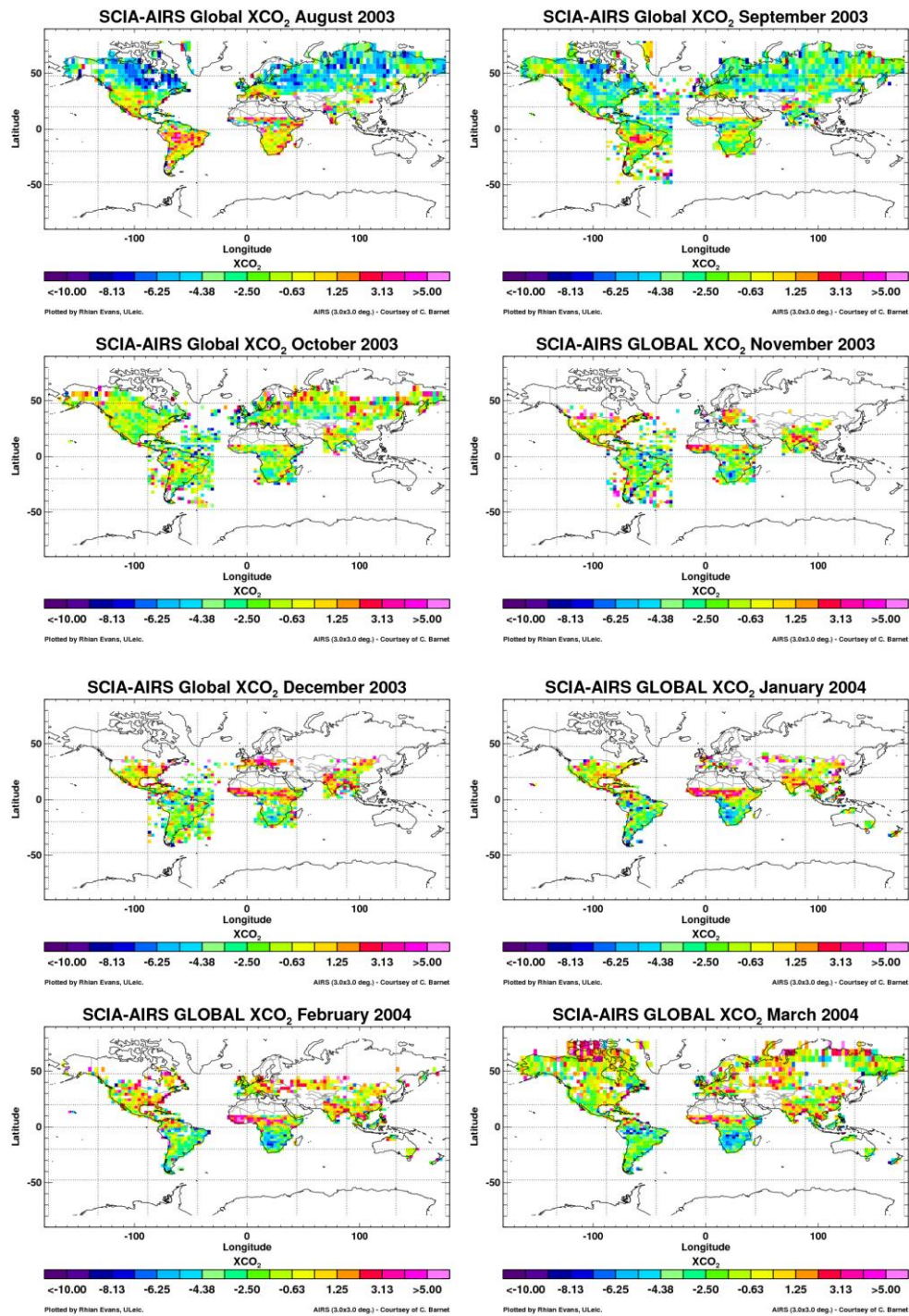
Figure 4.10a Global SCIAMACHY – AIRS-LSQ CO_2 data August 2003 to March 2004. Blue indicating less CO_2 in the lower troposphere and Red indicating more CO_2 in the lower troposphere compared to the upper troposphere.
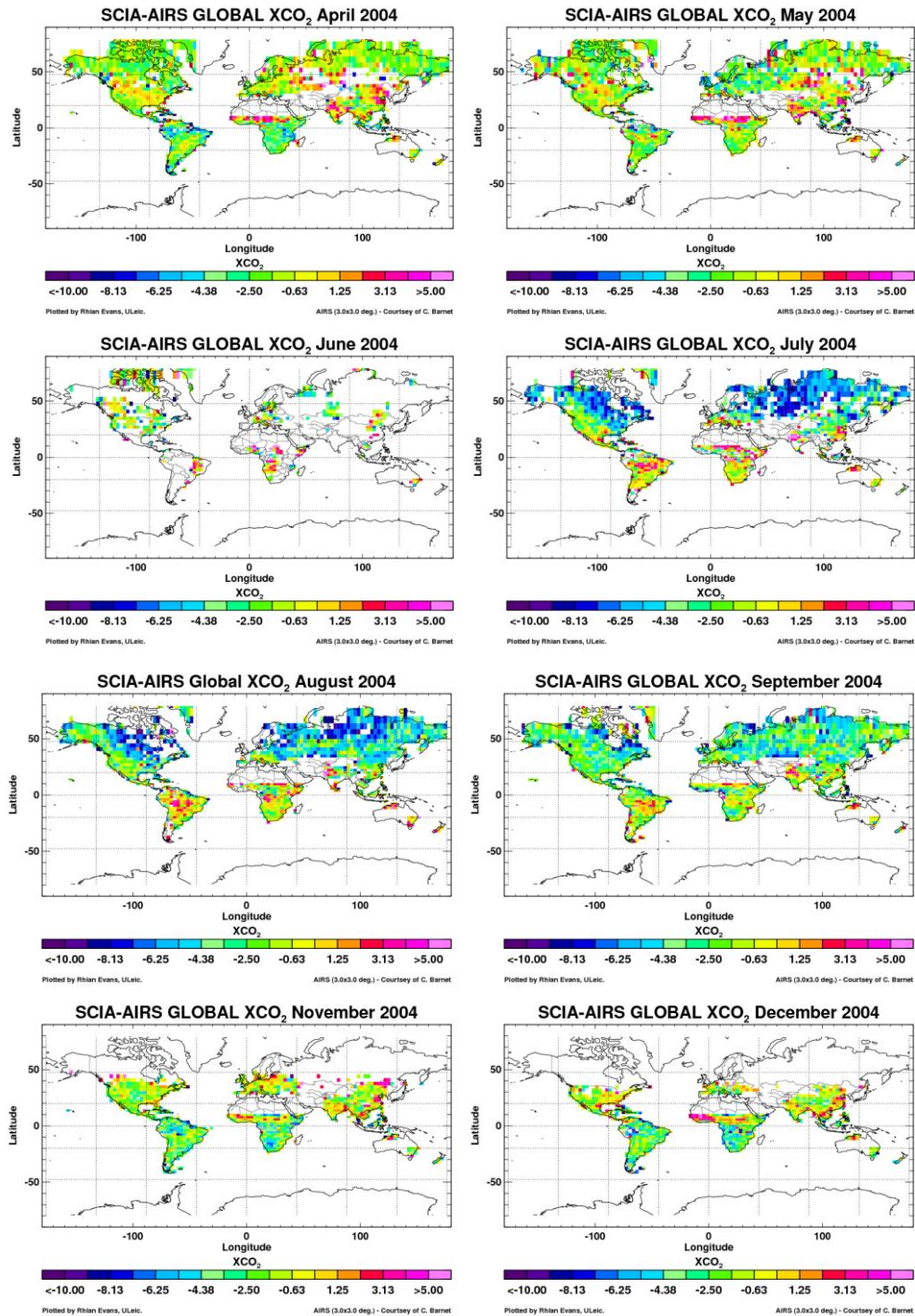
Figure 4.10b Global SCIAMACHY – AIRS-LSQ CO_2 data April 2004 to December 2004. Blue indicating less CO_2 in the lower troposphere and Red indicating more CO_2 in the lower troposphere compared to the upper troposphere.

The new CO_2 column plotted on a 3° x 3° grid as shown in Figure 4.10, where AIRS-LSQ CO_2 has been subtracted from SCIAMACHY CO_2 leaving the CO_2 from the surface to 496.6 hPa which is sensitive to the surface CO_2 flux. The

seasonal cycle is seen in the subtracted column, where a clear north/south hemispheric divide which is more prominent July through September as was shown in the SCIAMACHY data. Clear sinks (negative values) and sources (positive values) are seen which vary throughout the seasons possibly with changes in local vegetation. There are continuous anthropogenic emissions throughout the year, but there are not seen in these plots due to the low resolution. The subtraction of AIRS-LSQ from SCIAMACHY CO_2 produces seasonal cycles similar to those measured by SCIAMACHY. Subtracted data shows that the greatest flux variations occur in the lower troposphere. The upper troposphere shows little structure compared to the lower troposphere, as the CO_2 is well-mixed in the upper troposphere which is why the definition of the sinks and sources created by the surface fluxes are lost.

4.4 Regional comparisons of AIRS-LSQ and SCIAMACHY data.
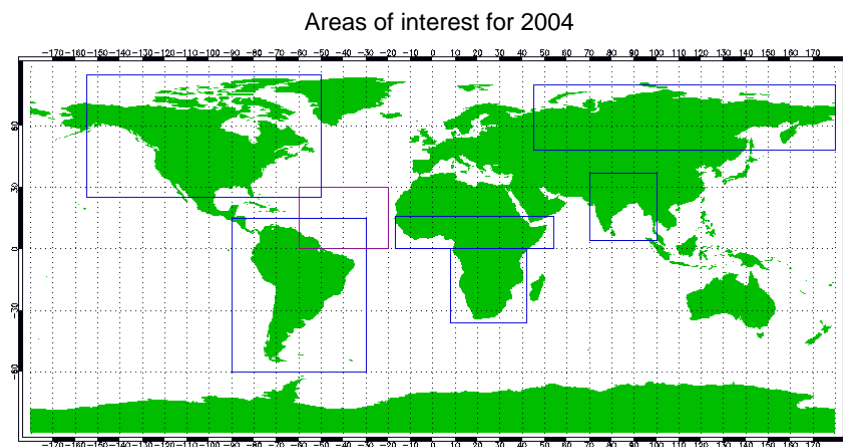
Figure 4.11: Areas for comparing AIRS-LSQ and SCIAMACHY data for 2004.

Six land areas and one oceanic scene have been selected to look at in greater detail the similarities and differences in the seasonal cycles produced by the SCIAMACHY and AIRS-LSQ CO_2 data. The areas investigated are North America, South America, central Africa, Southern Africa, India, Siberia and a section of the Atlantic ocean.

Region	latitude (min)	longitude (min)	latitude (max)	longitude (max)
North America	45.0°	-170.0°	84.0°	-51.0°
Siberia	48.0°	45.0°	80.0°	180.0°
Central Africa	0.0°	-6.0°	15.0°	54.0°
India	4.0°	70.0°	37.0°	100.0°
South America	-60.0°	-90.0°	15.0°	-30.0°
Southern Africa	-36.0°	8.0°	0.0°	42.0°
North Atlantic	0.0°	-60.0°	30.0°	-20.0°

Table 4.2 Region coordinates of the data investigated

4.4.1 North America.
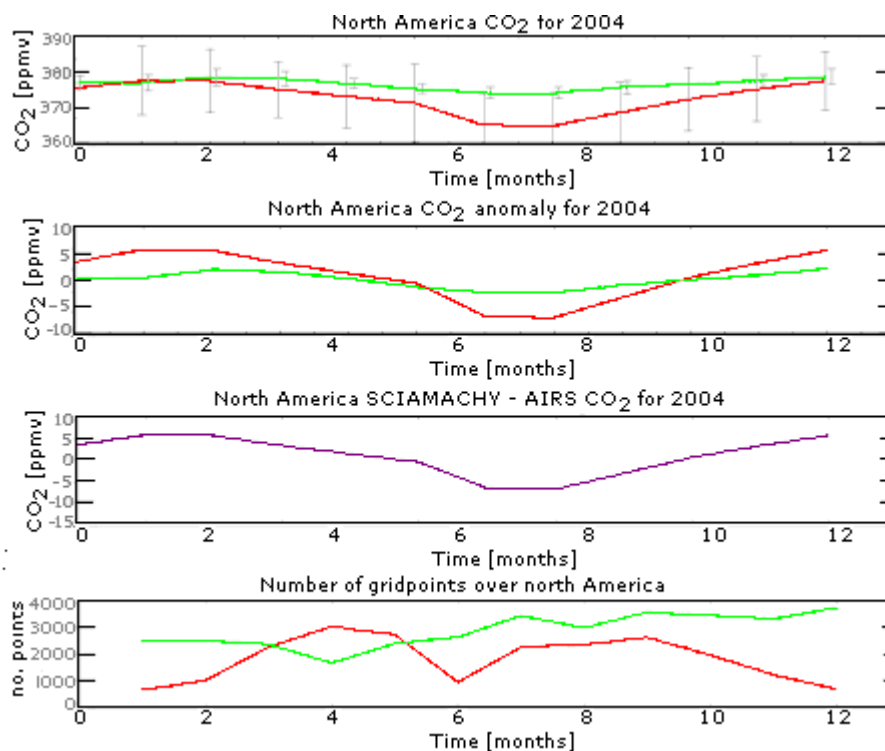
Figure 4.12. Seasonal cycles of SCIAMACHY (red) and AIRS-LSQ (green) for North America, 2004. First box; seasonal cycles of AIRS-LSQ and SCIAMACHY CO_2. Second box; Seasonal cycles of AIRS-LSQ and SCIAMACHY minus their yearly mean value. Box three the difference between AIRS-LSQ and SCIAMACHY CO_2 data. Box four the number of grid points retrieved by AIRS-LSQ and SCIAMACHY for the comparison.

The seasonal cycle measured over North America in both the upper and lower troposphere shows that the CO_2 concentration increases from August through March which are the winter months for this region. The CO_2 steadily decreases

April through August which is the spring/summer months where the volume of vegetation increases thus absorbing more CO_2. The amplitude of the seasonal cycle produced by SCIAMACHY is far greater than the AIRS-LSQ seasonal cycle as expected due to SCIAMACHY having sensitivity to the surface fluxes and AIRS-LSQ measuring CO_2 which has dispersed through the atmosphere and hence measuring a weaker seasonal cycle. There is also a phase difference between the two CO_2 measurements, where AIRS-LSQ maximum value lags SCIAMACHY's maximum during the winter months, and then the data is in phase during July. This could be due to the sharp decrease of CO_2 in the lower troposphere in June and July. The sudden decrease in the lower tropospheric CO_2 impacts the CO_2 concentrations in the upper atmosphere.

Subtracting AIRS-LSQ CO_2 from SCIAMACHY CO_2 shows the CO_2 flux in the lower atmosphere, where winter months produce a positive flux and summer months have a negative flux. The subtraction of data also shows that the measurements in the lower troposphere dominate the values detected by SCIAMACHY. Figures 4.8 and 4.10 show how the CO_2 concentration during the summer months (June to September) vary across north America, with CO_2 values greatest in the south western and lower in the north east. This indicates that the east and west regions act as a source and sink respectively which are likely caused by the local vegetation type and coverage [Barkley et al., 2007].

4.4.2 South America.

Figure 4.13. Seasonal cycles of SCIAMACHY (red) and AIRS-LSQ (green) for South America, 2004; see caption 4.12 for further details.

The seasonal cycle produced over South American is extremely weak and peaks in the lower troposphere during the region's winter months (around June), which is expected. A faint seasonal cycle which is in phase with the northern hemisphere cycle is measured by AIRS-LSQ, which is likely due to the dominance of the CO_2 emissions from the northern hemisphere mixing in the upper atmosphere, where it is fairly homogeneous (Section 4.3.3). In Figure 4.8 and 4.10 CO_2 data over south America is fairly consistent throughout the year. However over the rain forest between July and September there is a marked increase in CO_2 emissions, which are caused by decreased vegetative growth due to the dry season and forest fires. The amplitude of the seasonal cycle measured by SCIAMACHY is small due to the small flux changes over the area as a whole, with the exception of the rapid change in the CO_2 emissions over the rain forest which is a localized and small

120

area. Apart from the slight increase in CO_2 June to August the rest of the data retrieved for 2004 shows little structure, showing no other sinks or sources outside the rain forest area.

4.4.3 Central Africa.

Figure 4.14. Seasonal cycles of SCIAMACHY (red) and AIRS-LSQ (green) for Central Africa, 2004; see caption 4.12 for further details.

The AIRS-LSQ data shows a modest seasonal cycle which is representative of the northern hemisphere's cycle, as expected. SCIAMACHY on the other hand has a highly varied seasonal cycle, a general increase which peaks in June and falls to a minimum in September. The variations within the cycle could be due to the varieties of vegetation which grow at different times of the year. The increase of CO_2 measured in the lower troposphere in June could be caused by forest fires, as it is the beginning of the dry season, but it is difficult to determine if this is the

true value due to the lack of data retrieved by SCIAMACHY (Figure 4.8). In the tropical region there are two distinct seasons which are the wet and dry season, the dry season begins in June and ends in September, which is where the vegetation has its greatest growth rate.

4.4.4 Southern Africa.
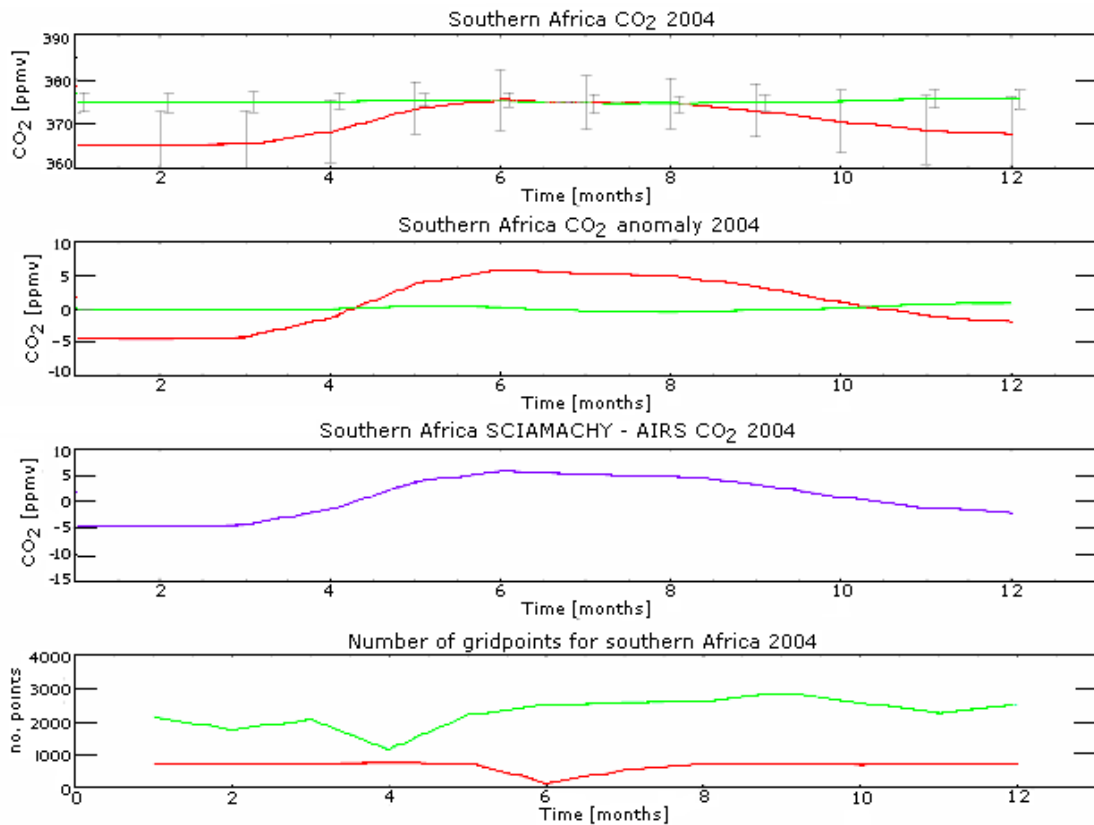
Figure 4.15. Seasonal cycles of SCIAMACHY (red) and AIRS-LSQ (green) for Southern Africa, 2004; see caption 4.12 for further details.

The amplitude of the seasonal cycle produced by SCIAMACHY is 10.3 ± 7.0 ppmv indicating that the regional vegetation has a profound influence on the amount of CO_2 emitted and absorbed. Atmospheric CO_2 concentration decreases between July and February the area's summer season, which is where the local vegetation grows and absorbs the CO_2 creating a regional sink. March through July, the CO_2 concentrations dramatically increase in the surrounding atmosphere creating a CO_2 source.

The southern African region primarily lies within the tropic of Capricorn which experiences tropical seasons, however some of the area lies within a temperate climate. The southern hemisphere spring/summer lies between October and June, the seasonal cycle produced by SCIAMACHY atmospheric CO_2 levels decrease within this period and increase July through September where the vegetation decreases. The seasonal cycles measured in the upper and lower troposphere are 5-6 months out of phase. The AIRS seasonal cycle (figure 4.15) resembles a seasonal cycle typically found in the northern hemisphere, this similarity could be due to the dominance of the northern hemispheric CO_2 emissions within the southern hemisphere (figure 4.9). Within the upper troposphere CO_2 is well mixed, were as the lower troposphere is dominated by the surface fluxes, which are clearly shown by Figure 4.15.

4.4.5 Siberia.
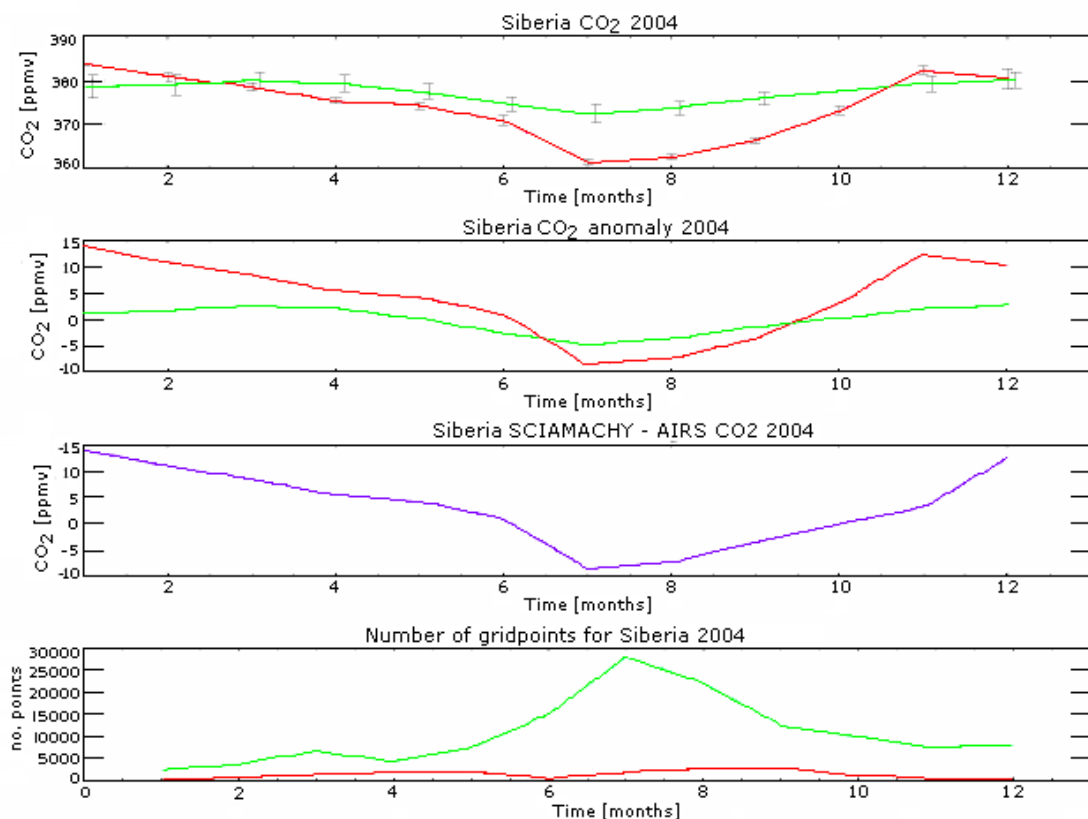
Figure 4.16. Seasonal cycles of SCIAMACHY (red) and AIRS-LSQ (green) for Siberia, 2004; see caption 4.12 for further details.

Seasonal cycles measured over Siberia show a distinct decrease of atmospheric CO_2 between May and August in both the AIRS-LSQ and SCIAMACHY measurements. A phase difference between the two measurements is observed, where AIRS-LSQ lags SCIAMACHY measurements by approximately a month. Amplitude of the SCIAMACHY measurement is around 22.60 ± 7.62 ppmv which is significantly greater than the 7.69 ± 1.85 ppmv amplitude measured by AIRS-LSQ. Clearly the surface fluxes have a profound effect on the CO_2 concentration measured in the lower troposphere, which are translated to the upper troposphere but are less pronounced due to mixing throughout the troposphere. Siberia is primarily covered with forest which during the spring/summer seasons absorbs large quantities of CO_2 which can be seen from June through September in the lower tropospheric measurements.

4.4.6 India.
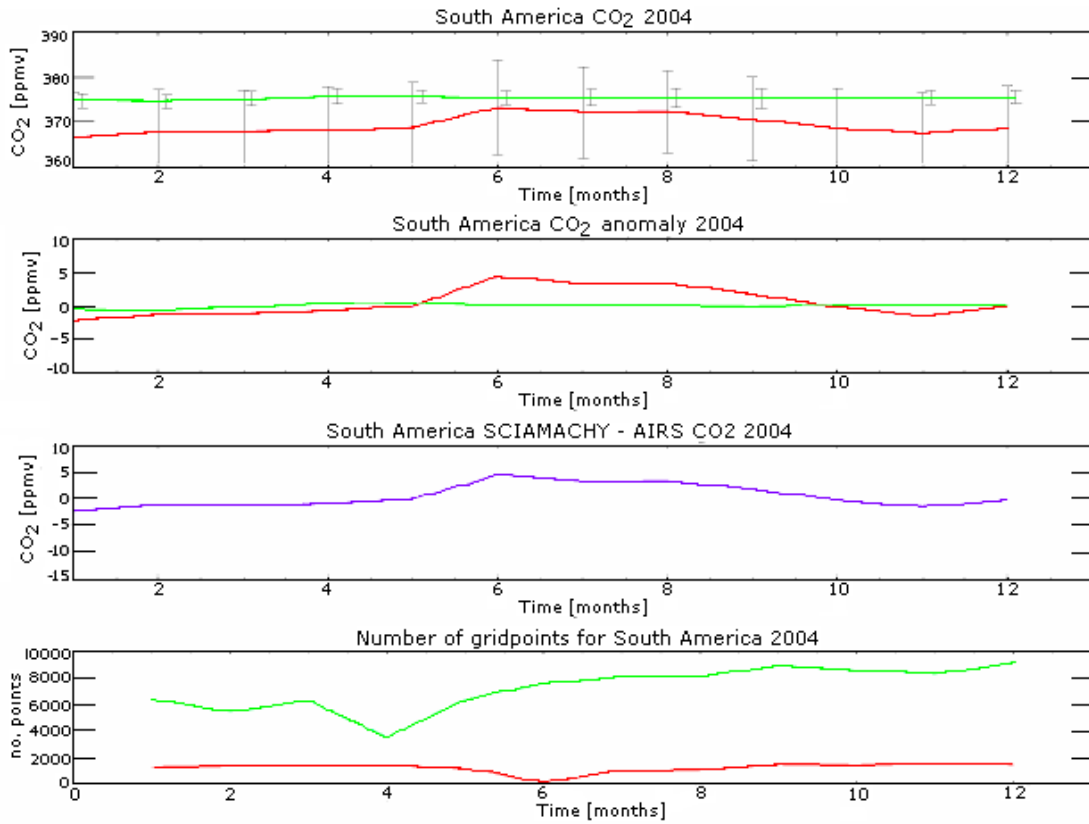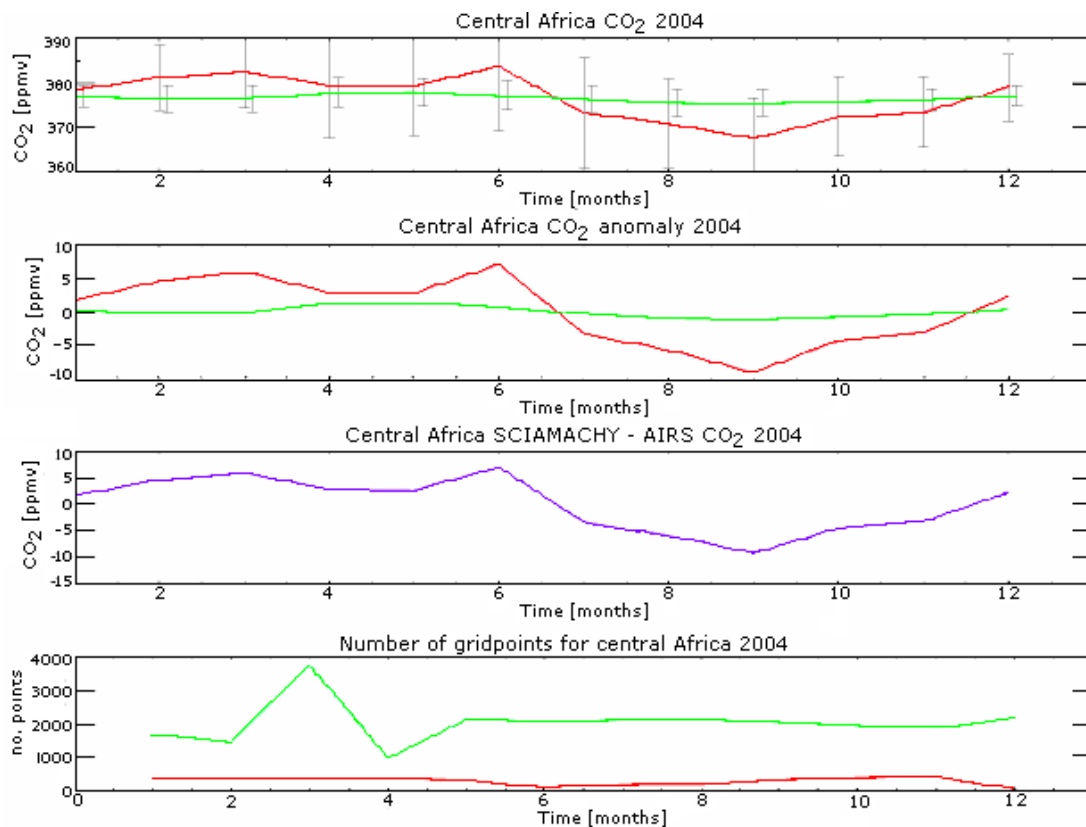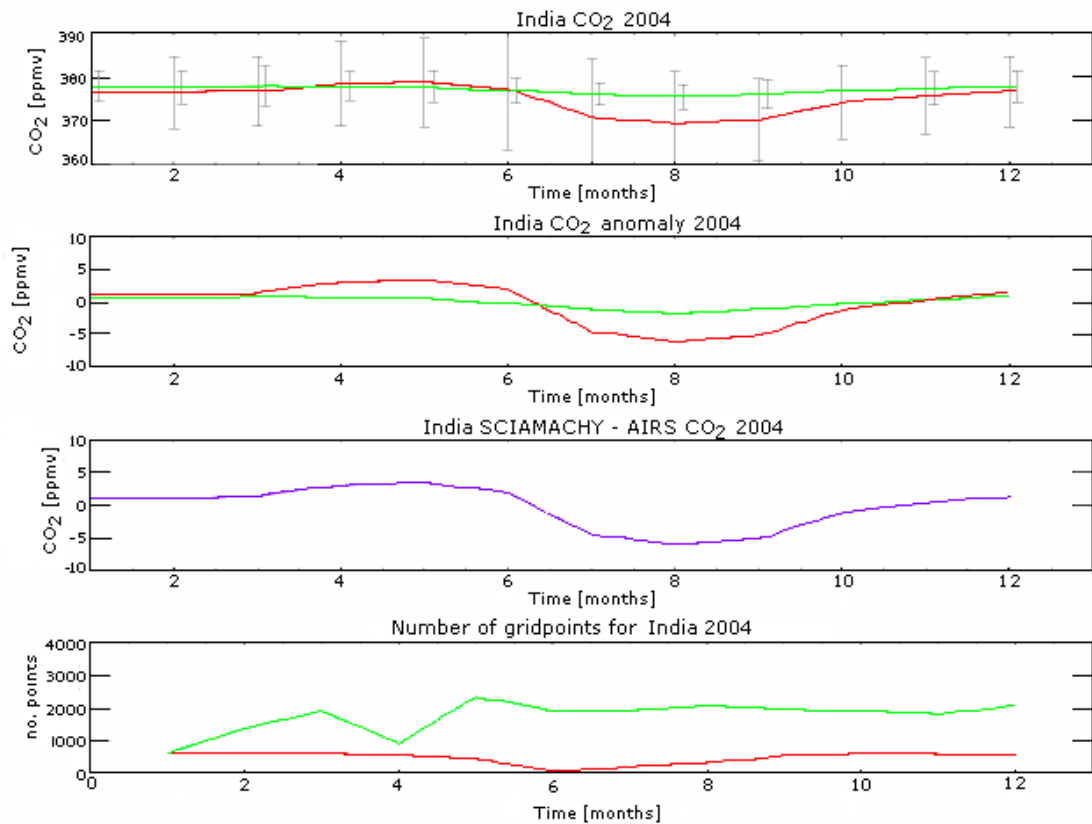

Figure 4.17. Seasonal cycles of SCIAMACHY (red) and AIRS-LSQ (green) for India, 2004; see caption 4.12 for further details.

AIRS-LSQ barely measures a change in the CO_2 throughout the year, an amplitude of 2.44 ± 3.43 ppmv is measured with a peak in May and a minimum during August. SCIAMACHY has a distinct seasonal cycle peaking between April and June, which rapidly decreases June through September. The two seasonal cycles are in phase both with their maximum around May and minimum in August. India lies within the Inter Tropical Convergence Zone (ITCZ) where large amounts of precipitation fall between June and August, which is also when the growing season for local vegetation is greatest.

4.4.7 Summary of the regional SCIAMACHY & AIRS-LSQ comparisons.

The amplitudes of the seasonal cycles produced by SCIAMACHY are significantly greater than those measured by AIRS-LSQ. Those produced by AIRS-LSQ barely show a change in the monthly concentration throughout the year, depending on where the measurements were taken, the amplitudes vary between 1.21 ± 1.72 ppmv (south America) and 7.69 ± 1.85 ppmv (Siberia). The greater the latitude in the northern hemisphere the greater the amplitude of the seasonal cycle as is seen over north America and Siberia. With decreasing latitude in the southern hemisphere the amplitude of seasonal cycle becomes increasingly weaker. In contrast to the AIRS-LSQ measurements SCIAMACHY retrievals are sensitive to the surface fluxes as is seen by the change in flux in each region. Amplitude of the SCIAMACHY's seasonal cycle measurements vary between 6.74 ± 9.72 ppmv and 22.60 ± 7.62 ppmv (Siberia) which is a significant variation in the flux. Measurements in the northern hemisphere produce the greatest amplitude, while those measured in the southern hemisphere are smaller. Within the northern hemisphere there are many contributions to the atmospheric CO_2 concentration, such as vegetation, land change and anthropogenic sources. In the southern hemisphere the amount of anthropogenic sources are significantly less. Subtracting the AIRS-LSQ column CO_2 from the SCIAMACHY column CO_2 in each region produced a seasonal cycle which is similar to the measured cycles produced by SCIAMACHY. Subtracting the upper column from the whole data

column shows us that the column when measured as a whole is influenced by the surface variations, where in the upper troposphere the CO_2 is fairly well mixed and only small CO_2 variations are seen. The subtracted data can provide a better representation of the surface CO_2 fluxes over large areas with greater accuracy, without the influence of the background values on the surface fluxes.

4.4.8 Regional correlation plots of AIRS-LSQ vs. SCIAMACHY
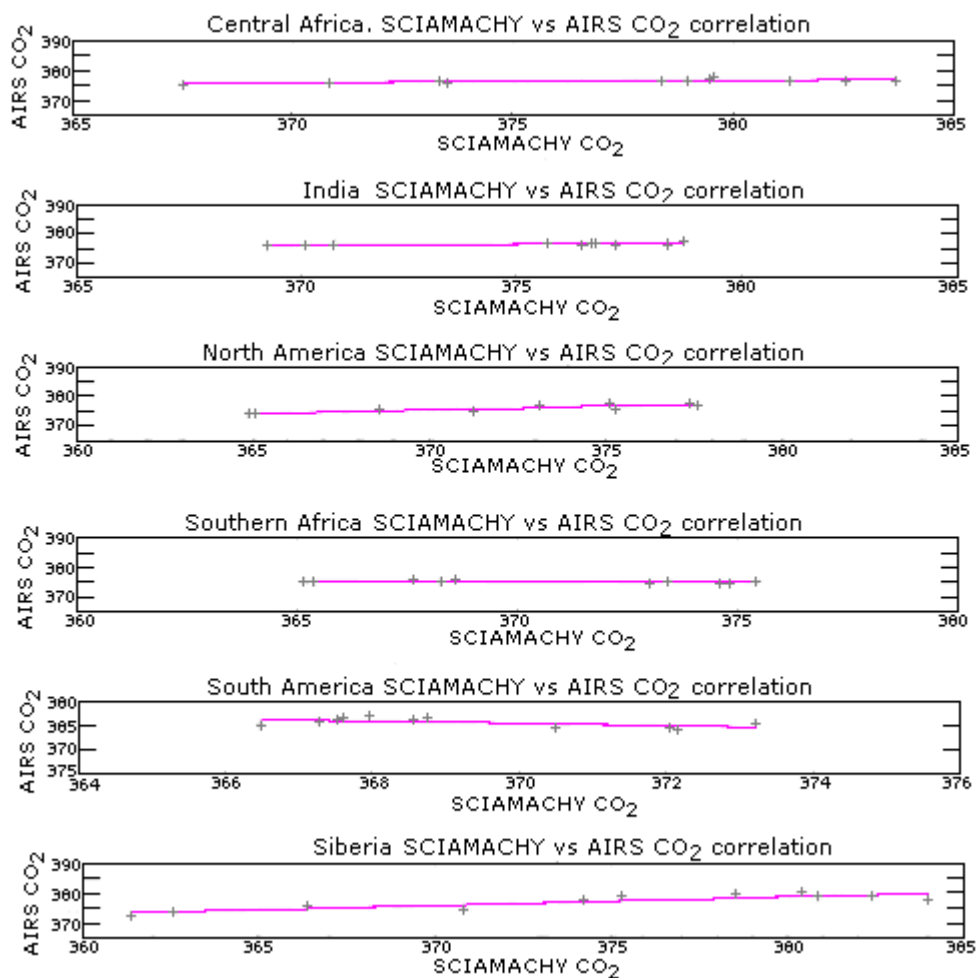
Figure 4.18. Regional correlation plots of AIRS-LSQ CO_2 vs SCIAMACHY CO2 for 2004.

Region	Correlation
Central Africa	0.66106
India	0.770095
North America	0.884705
Southern Africa	-0.340311
South America	-0.590611
Siberia	0.87443

Table 4.3 Correlation values of AIRS-LSQ and SCIAMACHY CO_2 data over 6 regions for 2004.

Comparisons between AIRS-LSQ and SCIAMACHY data indicate that the CO_2 mixing ratios measured in the upper troposphere are greater than those measured in the lower troposphere as result of large surface fluxes, which are not measured by AIRS-LSQ.

Correlation values between AIRS-LSQ and SCIAMACHY data are greater at higher northern latitudes (north America and Siberia) and decreases with latitude (India and central Africa). The data correlations of the regions in the southern hemisphere are negative due to the measurements in the mid-upper troposphere being influenced by the greater CO_2 emissions and absorptions in the northern hemisphere. The upper tropospheric data for all regions produced a seasonal cycle which is representative of that found in the northern hemisphere. Surface fluxes dominate the atmospheric concentration in the lower troposphere, but it is clear from the seasonal cycles that the changes in the CO_2 concentrations in northern hemisphere manipulate the structure of the seasonal cycle in the upper troposphere.

4.4.9 Northern Atlantic SCIAMACHY and AIRS-LSQ CO$_2$ data for 2004
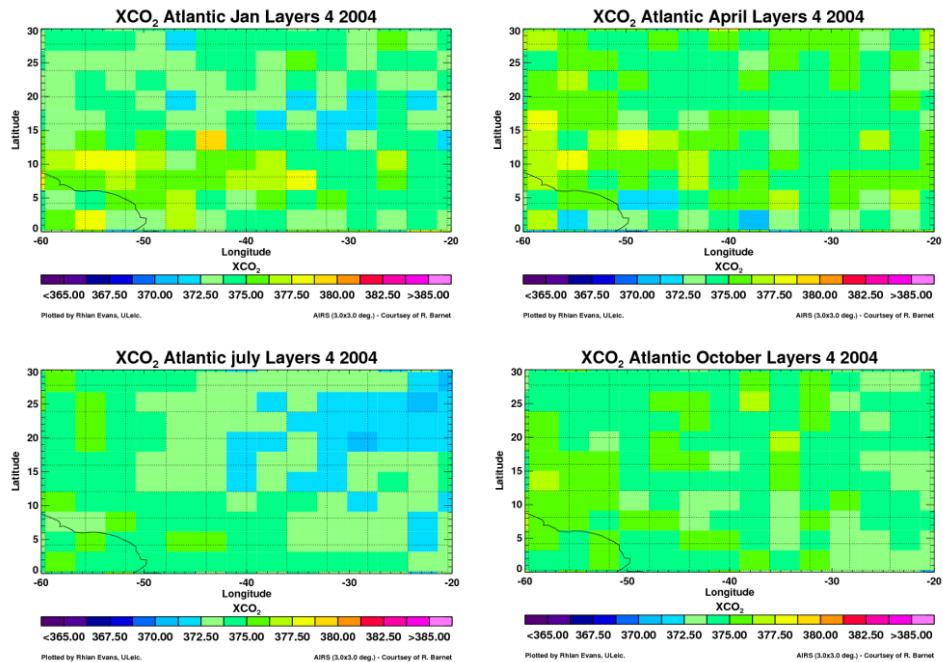
Figure 4.19. AIRS-LSQ CO$_2$ data over the north Atlantic
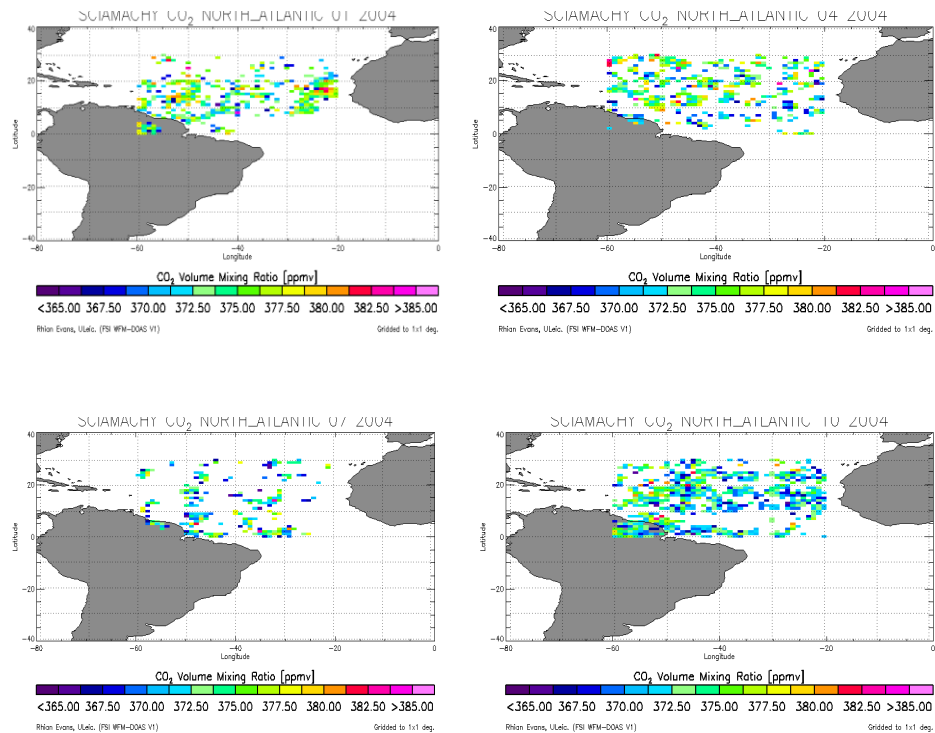
Figure 4.20. SCIAMACHY CO$_2$ data over the north Atlantic
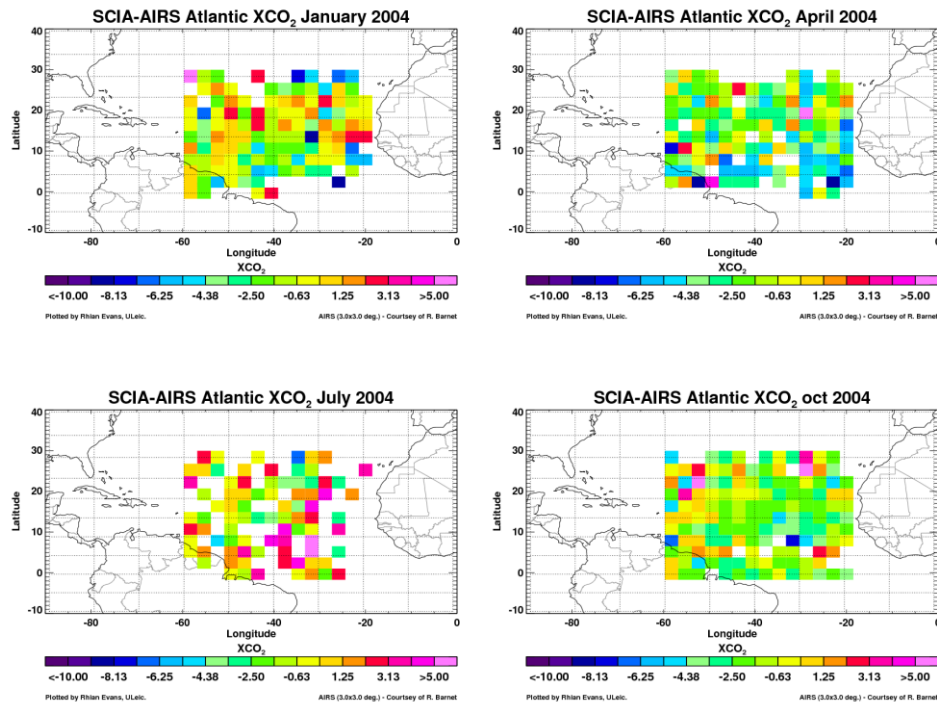
Figure 4.21. SCIAMACHY - AIRS-LSQ CO_2 data over the north Atlantic.

AIRS-LSQ measurements over the northern Atlantic show little variation in the CO_2 concentration as expected in the upper troposphere. Oceans tend to upwell CO_2 into the atmosphere at the equator and absorb CO_2 at the poles where the water is cooler. SCIAMACHY data retrieved is sparse and is highly variable, measuring CO_2 over the oceanic regions are inaccurate due to low albedo values. Determining if this region is a source or sink is difficult due to lack of retrieved data, where measurements are taken they do not show any specific regions of high or low CO_2 concentration. Subtracting the upper tropospheric data (AIRS-LSQ) from the column CO_2 data (SCIAMACHY) produces data sensitive to the lower troposphere which are highly variable with no visible structure. Retrieving CO_2 over the oceans produces highly variable results from which deducing if there are sinks and sources is difficult. To determine if there are any localized sources or sinks within the Atlantic ocean measured, greater accuracy of the measurements retrieved are essential.

4.5 Validation of AIRS-LSQ and SCIAMACHY data.

Ground data are retrieved from WMD WDGCC (http://gaw.kishou.go.jp/wdcgg/).
Data represent measurements taken from the surface up to 3.81 km (Mt.
Waliguan), which are representative of localized surface fluxes. Each measure the
immediate surroundings around the instrument, at specific altitudes. Satellite
retrievals measure an area or 'footprint' which are much larger than the area
measured by the ground instruments. CO_2 values used from the instruments are
centered on the coordinated of ground instruments. AIRS-LSQ data are calculated
on a 3 x 3 degree grid which represents an area much larger than the ground based
instrument, therefore large errors between the values are expected. However,
AIRS-LSQ measures in the mid-upper troposphere where the CO_2 is well mixed, a
reasonable correlation when comparing AIRS-LSQ measurements with aircraft
data in the upper troposphere is expected. Correlation values between AIRS-LSQ
column data to ground in-situ measurements are expected to be small, as AIRS-
LSQ data is retrieved in the upper troposphere with the lowest retrieval at 496.6
hPa (around 5.5 km) used in this thesis.

Aircraft measurements are available at various altitudes, different altitude
retrievals are available over each region, ranging from ground measurements up to
8 km in the atmosphere. Aircraft data are compared with AIRS-LSQ CO_2 and
AIRS-LSQ data at specific heights (or layers: L4 (496.6 hPa − boundary layer)
and L3 (300.0 − 496.6 hPa)) are made to validate the AIRS-LSQ data. Each
AIRS-LSQ measurement represents the area measured by the aircraft.

Comparisons of in-situ and SCIAMACHY CO_2 data are also made to determine
the accuracy of the data retrieved by the satellite.
Data from August 2003 to December 2004 are processed from AIRS-LSQ,
SCIAMACHY and in-situ measurements, from which seasonal cycles are
produced and compared. Correlation values are calculated to determine how
accurate the satellite data is compared to the in-situ data.

4.5.1 Satellite and ground based measurements.

4.5.1.1 In-situ comparisons AIRS-LSQ CO_2 and ground data

AIRS-LSQ column data are plotted over each region where in-situ measurements are available and seasonal cycles of each instrument's retrieval are plotted. From AIRS-LSQ and SCIAMACHY comparisons, the AIRS-LSQ data and the ground based measurements are expected to be out of phase and AIRS-LSQ amplitude to be much smaller, due to CO_2 mixing through the atmosphere. Figure 4.22 shows comparisons of the AIRS-LSQ CO_2 (green) and ground (blue) measurements from 10 regions, where the majority of cycles show that seasonal cycle of AIRS-LSQ are much smaller than the in-situ measurement, with the exception of Niwot ridge, Mt Waliguan and Cape point, where the amplitudes produced are similar. The towers used to observe CO_2 concentrations measure at different altitudes, Niwot ridge, Mt Waliguan and Cape point measurements are taken above 3 km all other locations measurements are below 1.4 km. The CO_2 measured at higher altitude have had a greater time to mix through the surrounding area, where a measurement representative of the surrounding area is obtained. Measurements below 1.4 km are more sensitive to the surface CO_2 fluxes within the immediate area, AIRS-LSQ measures CO_2 over a large area, and is unable to detect variations in the lower troposphere. The difference in amplitudes of the ground measurements between 0.03 km and 1.32 km and AIRS-LSQ measurements are greater than those compared to ground measurements taken at higher altitudes.
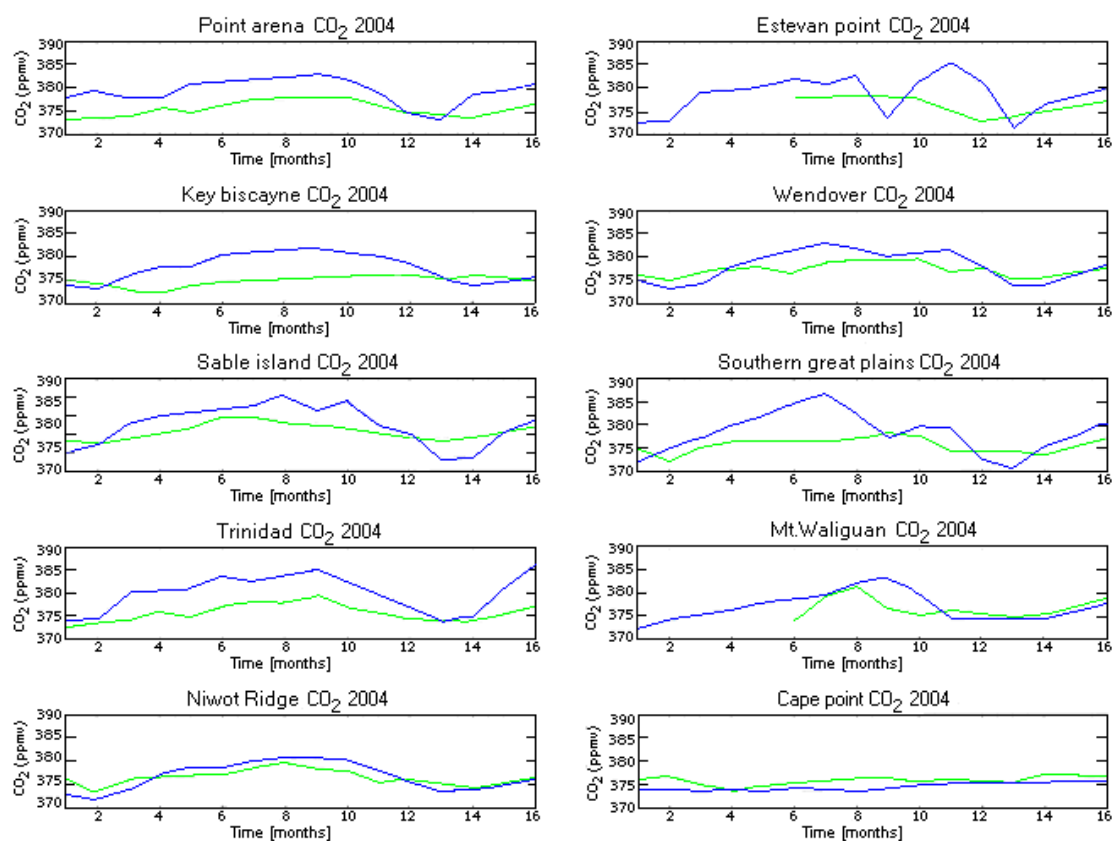
Figure 4.22: Seasonal cycles August 2003 – December 2004 for AIRS-LSQ CO_2 (green) and Ground data (WDCGG, NOAA/ESRL Global Monitoring Division: http://gaw.kishou.go.jp/wdcgg/) (blue).

132

4.5.1.2 AIRS-LSQ retrieved data (496.6hPa to the boundary layer) vs. ground based measurements.
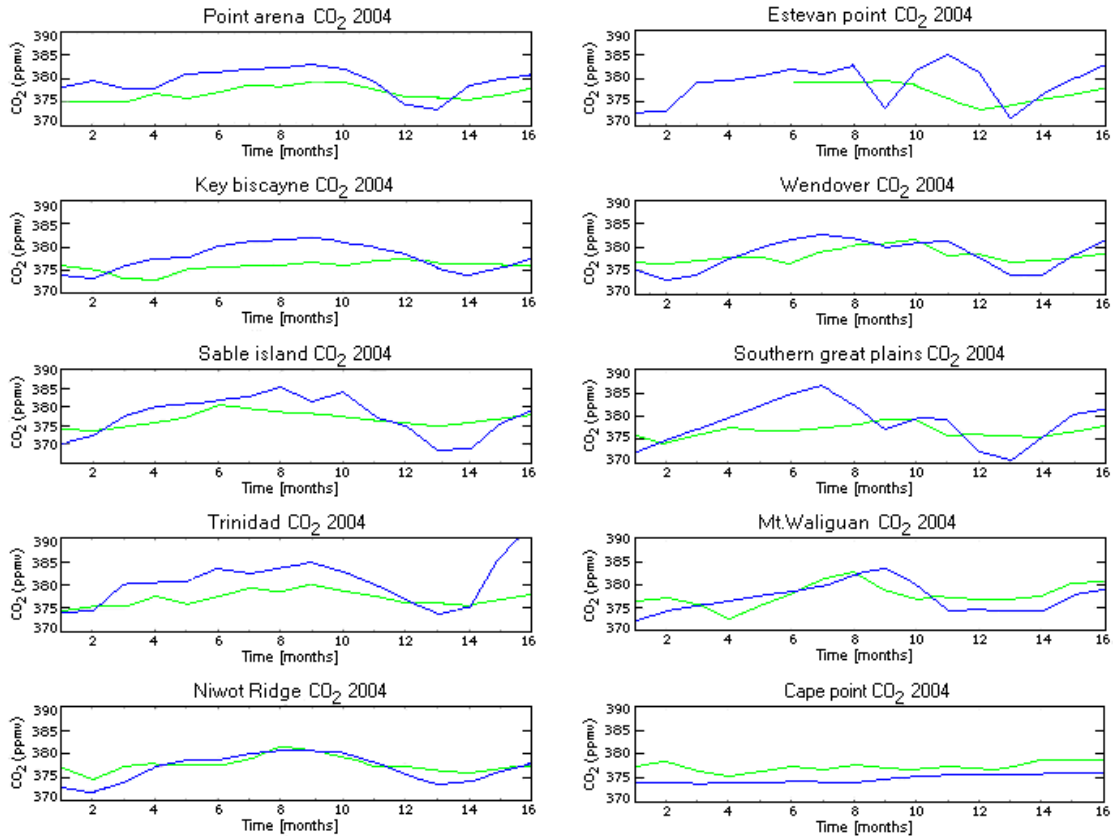
Figure 4.23: Seasonal cycles August 2003 – December 2004 for AIRS-LSQ layer 4 data (496.6 hPa – boundary layer) (green) and Ground data (WDCGG, NOAA/ESRL Global Monitoring Division: http://gaw.kishou.go.jp/wdcgg/) (blue).

AIRS-LSQ data retrieved between 496.6 hPa and the boundary layer are compared to ground data. The seasonal cycles are shown in Figure 4.23, these cycles are similar to those produced by the AIRS-LSQ CO_2 column. Layer 4 represents the CO_2 concentration in the atmosphere below 5.5 km. Differences between the ground based and satellite measurements are still seen in the seasonal cycle amplitudes, as the instrument's retrievals are sensitive at different altitudes.

There are similarities between the seasonal cycles of the two AIRS-LSQ data sets (CO_2 and Layer 4). However the CO_2 concentration in layer 4 is slightly greater than the CO_2 calculated in the column data, and this is best seen in Niwot ridge, Cape point, Mt. Waliguan, and Wendover.

4.5.1.3 SCIA vs. Ground data
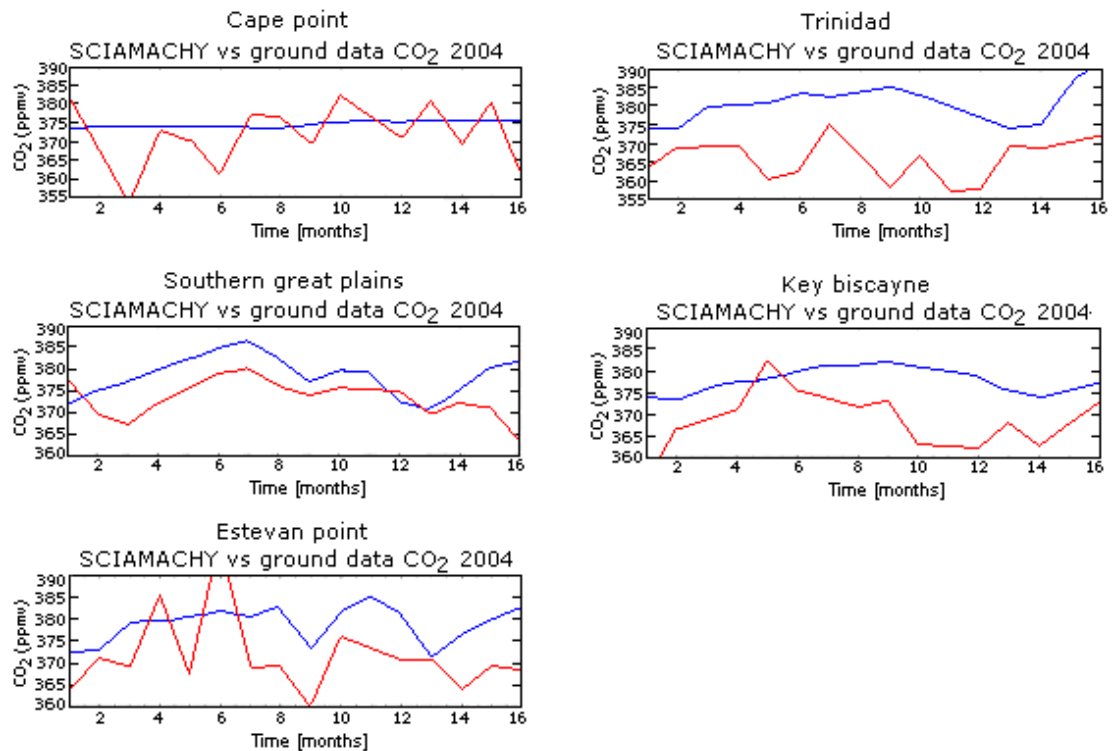
Figure 4.24 SCIAMACHY CO_2 (red) vs in-situ ground data (NOAA: http://gaw.kishou.go.jp/wdcgg/) (blue).

Data retrieved from SCIAMACHY was not available for all the regions used for the AIRS-LSQ comparisons. The seasonal cycles produced by SCIAMACHY and ground data (Figure 4.23) show that SCIAMACHY data is unpredictable over the 3 x 3 degree area, however a seasonal cycle can be seen over Southern great plains but data is too erratic to deduce any conclusions over such a small region. To attain better results for comparisons with in-situ measurements, the data retrieved from SCIAMACHY needs to be of greater spatial resolution. The areas measured by SCIAMACHY are vast, which is the likely cause of the erratic CO_2 fluxes. Measuring an area which has the same or similar land usage would produce better comparison results, as the different land usages absorb and emit various amounts of CO_2 which can vastly alter the atmospheric concentration of CO_2.

Region	Correlation value		
	AIRS-LSQ CO$_2$	AIRS-LSQ L4	SCIAMACHY CO$_2$
Cape point	0.225	0.231	-0.257
Estevan point	0.195	-0.290	0.403
Key biscayne	0.235	0.212	0.481
Mt waliguan	0.546	0.636	-
Niwot ridge	0.848	0.857	-
Point arena	0.642	0.676	-
Sable island	0.847	0.807	-
Southern great plains	0.616	0.581	0.333
Trinidad	0.789	0.739	0.227
Wendover	0.781	0.612	-

Table 4.4 :Correlation values of ground based measurements (WDCGG, NOAA: http://gaw.kishou.go.jp/wdcgg/) with AIRS-LSQ tropospheric CO$_2$ column, AIRS-LSQ layer 4 data (496.6 hPa – boundary layer) and SCIAMACHY column data for August 2003 – December 2004.

Correlation values calculated for ground data and satellite data as shown in table 4.4. AIRS-LSQ data above 496.6 hPa (CO$_2$ column) and below 496.6 hPa (layer 4) are compared to the ground data, correlation values are similar for both AIRS-LSQ data over each region. Correlation values were expected to be greater between Layer 4 than the CO$_2$ column compared to the ground data as layer 4 is representative of CO$_2$ lower in the atmosphere. Results show that only 4 regions analyzed show a greater correlation with the AIRS-LSQ layer 4 data than the CO$_2$ column data. This could be due to the CO$_2$ being consistently mixed throughout the atmosphere above the boundary layer or that the CO$_2$ concentration in the lower atmosphere is influenced by surrounding fluxes causing greater variations in the atmospheric concentration.

Correlation values of the SCIAMACHY and ground data are poor, due to the SCIAMACHY data being erratic over such a small area as seen in figure 4.23. Measuring a smaller area surrounding the in-situ location could help produce a more accurate comparison. SCIAMACHY data are sensitive between 1 and 5 km where the atmospheric CO$_2$ is subject to surface CO$_2$ flux variations, which could be anthropogenic or natural emissions and absorptions from the surrounding area. AIRS-LSQ represents an area of the atmosphere where the CO$_2$ is well mixed and the in-situ represents a localized area where the CO$_2$ concentrations are influenced

by the immediate surroundings. Comparing CO_2 data with different instruments which measure CO_2 at altitudes with different sensitivities do not provide accurate results, only approximate results as the area of each measurement are vastly different.

4.5.2 Satellite and aircraft comparisons.

4.5.2.1 AIRS-LSQ CO_2 and Aircraft data of various heights
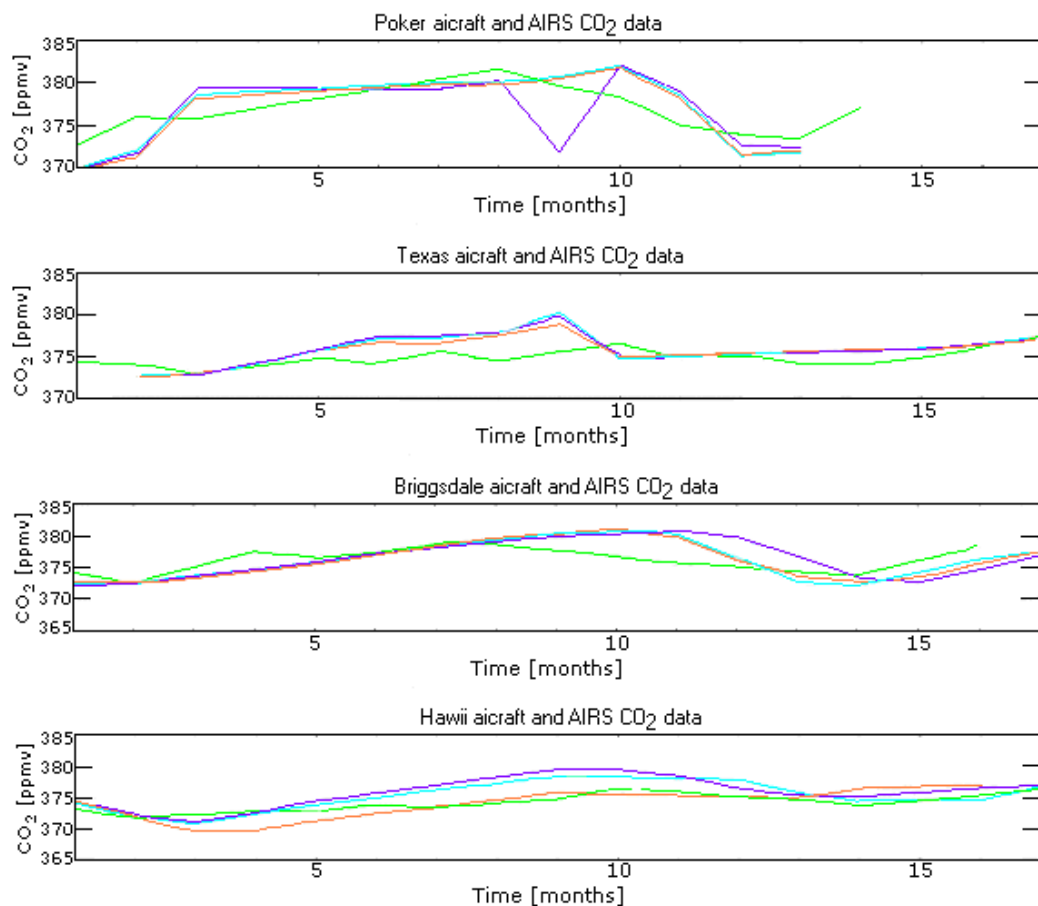
Figure 4.25; Seasonal cycles of AIRS-LSQ tropospheric column CO_2 (green) and aircraft data NOAA/ESRL: http://www.esrl.noaa.gov/gmd/ccgg/iadv/, (purple-8.5 km, blue – 7.5km, orange – 6.5 km, pink – 5.5km) between August 2003 and December 2004).

AIRS-LSQ CO_2 data represents the tropospheric column down to 496.6 hPa, the aircraft measurements used are from 5.5 km and greater, these aircraft data are

used to validate the AIRS-LSQ column data, where AIRS-LSQ measures the area covered by the aircraft.

Seasonal cycles of the AIRS-LSQ CO_2 and aircraft data over each location are in phase over Hawaii, Briggsdale and Poker, Alaska the AIRS-LSQ data peaks up to three months before those measured by the aircraft. Texas measurements show that AIRS-LSQ maximum value lags the aircraft data by approximately one month. These phase differences between the data sets could be caused by the difference in the area each instrument measures, AIRS-LSQ covers a much greater area than the aircraft, and hence the AIRS-LSQ data will have averaged CO_2 concentrations over a greater region, whereas the aircraft data is more localized. From the all locations measured the amplitude produced by the AIRS-LSQ data are up to 5 ppmv smaller compared to the aircraft data. The AIRS-LSQ data produced similar CO_2 values and seasonal cycles as the aircraft, indicating that AIRS-LSQ CO_2 data represents the mid-tropospheric region as is measured by the aircraft.

4.5.2.2 AIRS-LSQ layer 4 vs. aircraft CO$_2$.
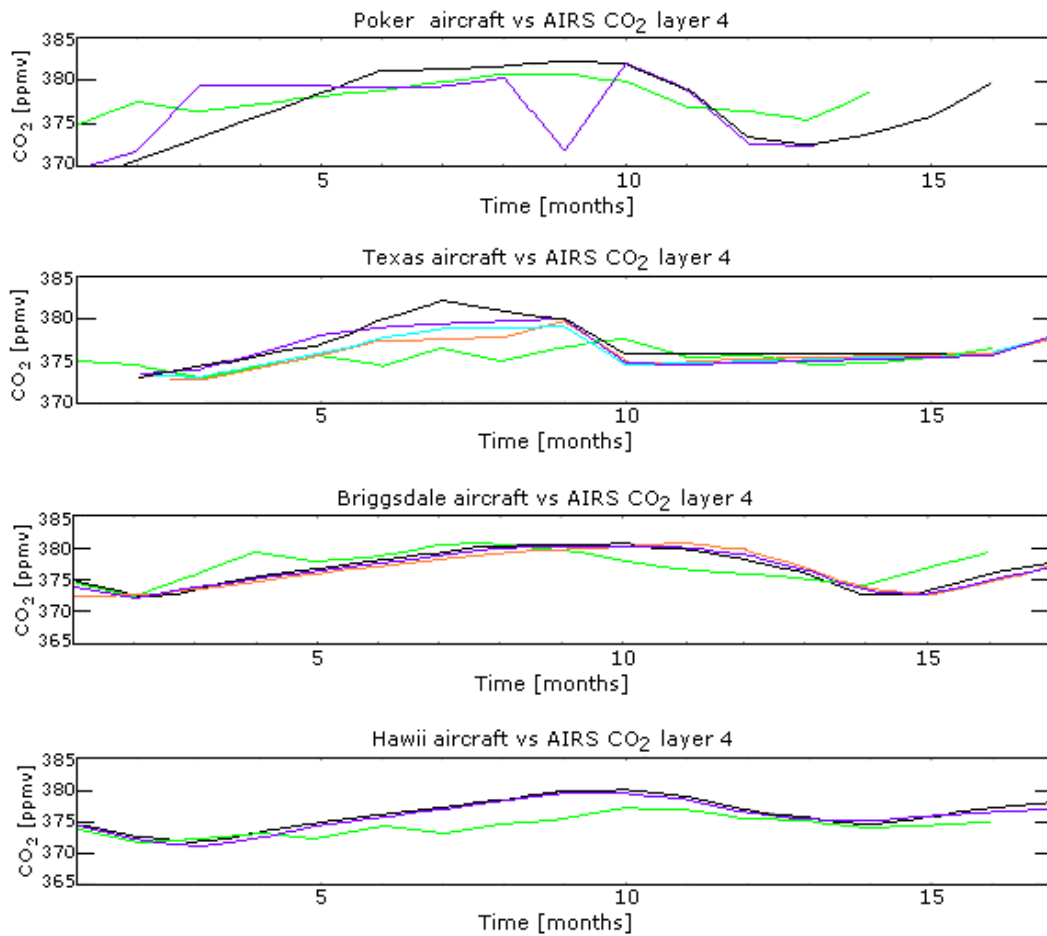
Figure 4.26: AIRS-LSQ layer 4 (496.6 hPa – boundary layer) CO$_2$ data (green) vs. aircraft CO$_2$ data NOAA/ESRL: http://www.esrl.noaa.gov/gmd/ccgg/iadv/ (pink- 5.5 km, blue – 4.5 km, black – 3.5 km, orange – 2.5 km).

AIRS-LSQ layer 4 data measures tropospheric CO$_2$ between 469.6 hPa and the boundary layer; aircraft data used to validate the AIRS-LSQ data are taken from 5.5 km and below. Results show that the seasonal cycles peak within a month of each other, results are similar to those produced between the CO$_2$ AIRS-LSQ column and aircraft data. Amplitudes produced by the AIRS-LSQ are between 2 and 7 ppmv smaller than the aircraft data.

4.5.2.3 AIRS-LSQ layer 3 vs. airplane CO$_2$.
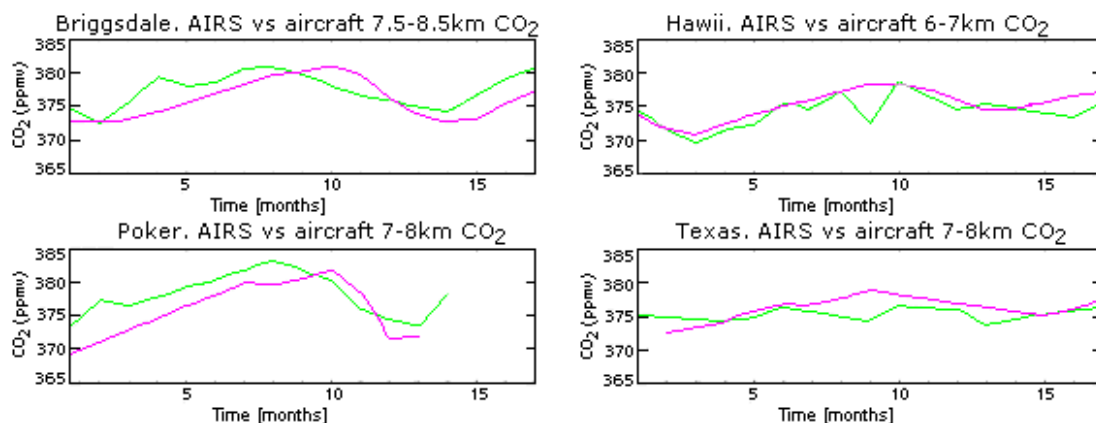
Figure 4.27. AIRS-LSQ (496.6-300 hPa) CO$_2$ data (green) vs in-situ airplane:
http://www.esrl.noaa.gov/gmd/ccgg/iadv/ CO$_2$ data (pink)

AIRS-LSQ layer 3 data are sensitive to tropospheric data between 300.0 and 496.6 hPa which represents an atmospheric altitude between 5.5 and 9.5 km. Seasonal cycles show that the AIRS-LSQ data lag the aircraft data at most by one month. Amplitudes of the two data are approximately the same, indicating that the AIRS-LSQ and the aircraft data within this region are reasonable.

4.5.2.4 SCIA vs. airplane CO$_2$ data.
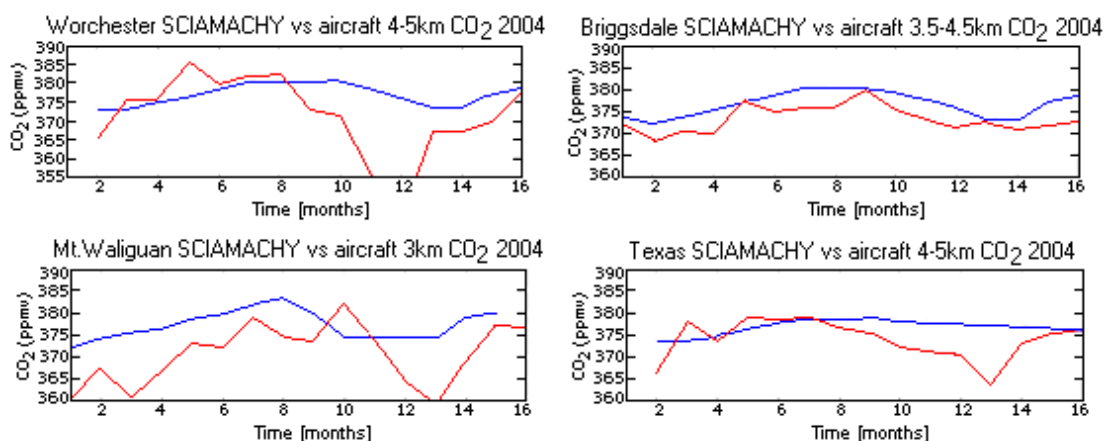
Figure 4.28. SCIAMACHY CO$_2$ (red) vs. airplane: http://www.esrl.noaa.gov/gmd/ccgg/iadv/ data from the lower troposphere (blue)

139

Both the AIRS-LSQ and aircraft data over each location analyzed show little variation in their respective seasonal cycles for both their amplitudes and their months of reaching max and min values over the various tropospheric heights. The data from each instrument show that with increasing altitude the CO_2 concentration decreases as is seen by the seasonal cycles produced. Overall the comparisons show that the AIRS-LSQ and aircraft data produce similar results indicating that the AIRS-LSQ data is sensitive to retrievals in the mid-upper troposphere.

4.5.3 Correlation of AIRS-LSQ and aircraft data.

Region	AIRS-LSQ CO_2	AIRS-LSQ L4	AIRS-LSQ L3	SCIAMACHY CO_2
Park falls 3.5-4.5km	0.857	0.842		
Briggsdale 2.5-3.5km	0.862	0.852	0.711	
Briggsdale 3.5-4.5km	0.888	0.884	0.757	0.749
Briggsdale 4.5-5.5km	0.824	0.825	0.699	
Briggsdale 5.5-6.5km	0.770	0.774	0.704	
Briggsdale 6.5-7.5km	0.722	0.731	0.651	
Briggsdale 7.5-8.5km	0.708	0.720	0.617	
Poker 4-5km	0.555	0.607	0.558	
Poker 5-6km	0.576	0.551	0.313	
Poker 6-7km	0.249	0.597	0.671	
Poker 7-8km	0.762	0.797	0.689	
Hawii 4-5km	0.905	0.905	0.727	
Hawii 5-6km	0.903	0.906	0.745	
Hawii 6-7km	0.906	0.789	0.739	
Hawii 7-8km	0.810	0.788	0.739	
Texas 0-1km	0.396	0.458	0.221	
Texas 1-2km	0.441	0.501	0.263	
Texas 2-3km	0.448	0.531	0.113	
Texas 3-4km	0.579	0.634	0.232	
Texas 4-5km	0.588	0.644	0.259	0.649
Texas 5-6km	0.655	0.700	0.254	
Texas 6-7km	0.666	0.708	0.218	
Texas 7-8km	0.668	0.705	0.274	
Mt Waliguan 3.8km		0.636		0.791
Estevan point 5-6km			0.673	
Worchester 4-5km				0.549

Table 4.5. Correlation values of AIRS-LSQ data (CO_2, layer 3 and layer 4 against aircraft data at various altitudes (NOAA/ESRL: http://www.esrl.noaa.gov/gmd/ccgg/iadv/)

AIRS-LSQ and aircraft data are correlated (table 4.5) for all AIRS-LSQ and aircraft data available, to determine where the AIRS-LSQ measurements are most sensitive in the troposphere. The Briggsdale comparison shows that the all AIRS-LSQ data used produced good correlations, with the best result occurring for aircraft data between 3.5 and 4.5 km. This result is unexpected as the AIRS-LSQ instrument is not sensitive to measurements within this region. Layer 4 retrievals decrease in this region, but the CO_2 and layer 3 data do not. Poker, Alaska data show great correlation at 7-8 km for all AIRS-LSQ data, Hawaii correlated best with Layer 3 and 4 at 5-6 km and at 6-7 km with the CO_2. Texas produced variable results, with the CO_2 best comparison at 7-8 km, layer 3 at 6-7 km and layer 3 over various layers. For comparisons best results were found to be at higher altitudes, except for Briggsdale. Seasonal cycles for the AIRS-LSQ data varied little within different tropospheric regions, whereas the aircraft data the CO_2 concentration generally decreased with increasing altitude. As AIRS-LSQ varied little over the different altitudes used, when correlating these with the aircraft data which did vary with altitude, its clear why the correlations tended to be greatest at the same aircraft altitudes.

4.6. Summary.

Although AIRS-LSQ and SCIAMACHY data cannot be directly compared as each instrument measures different regions in the atmosphere, they provide information of the CO_2 structures within their tropospheric regions. SCIAMACHY provides information of the flux variations in the lower troposphere and AIRS-LSQ provides information of the mean global CO_2 values in the upper troposphere. These two data show that CO_2 is not well mixed throughout the troposphere, AIRS-LSQ data shows that CO_2 is fairly well mixed in the upper troposphere, but still there are areas of high and low concentrations. The lower tropospheric CO_2 is in a constant state of flux due to continuous changes in vegetation, land and anthropogenic sources.

Results showed that SCIAMACHY data can measure CO_2 changes over large areas, but are unable to detect changes on a smaller scale as is shown by the in-situ

comparisons. AIRS-LSQ and SCIAMACHY provide us with a general view of the CO_2 patterns within the upper and lower troposphere, but are unable to detect variations on a small scale to the low spatial resolutions of the instruments.

Measurements taken by SCIAMACHY over small areas with similar land usage, and similar vegetation type could show a more stable seasonal cycle than those measured over small areas with variable land usage and vegetation. Comparisons of SCIAMACHY measurements with in-situ data over areas such as park falls which consist of a large area of similar vegetation provide a good correlation [Schneising et al., 2008, Barkley et al., 2007]. Due to the low resolution of SCIAMACHY in-situ comparisons are best done over areas which have little variation of land usage.

Future missions to measure surface CO_2 fluxes are underway, two satellites are scheduled for launched in January of 2009, these are Orbiting Carbon Observatory (OCO) and Greenhouse gases Observing SATellite (GOSAT). Both these instruments are designed to measure atmospheric CO_2 with greater accuracy, OCO mission is to ascertain representative values of column averaged dry air CO_2 mole (CO_2) [Crisp et al., 2003]. GOSAT mission is to estimate the greenhouse gases sources and sinks on sub-continental scales [Hamuzuki et al., 2008]. OCO will measure CO_2 at 1.61 and 2.06 μm measuring approximately 3 km^2 at nadir, whereas GOSAT has a wider spectral coverage measuring between 0.76 and 15 μm and has a footprint of 8 km^2 at nadir.

Chapter 5

Tropospheric CO_2 comparisons with vegetation types over Africa for 2004.

5.1 Introduction.

In chapters 3 and 4, AIRS-LSQ and SCIAMACHY data were used to determine if there were any similarities in the CO_2 concentrations in the upper and lower troposphere globally and regionally. From the data analysed the CO_2 was found to be well-mixed in the mid-upper troposphere and concentrations in the lower troposphere were dependent on the season (summer/winter) and land coverage where the retrievals were made.

In this chapter, CO_2 retrieved from SCIAMACHY and AIRS-LSQ (LSQ method, see chapter 4) are compared to fractional vegetation data from NESDIS/AVHRR [Gutman, and Ignatov, 1997] over five different vegetation types in Africa to determine the influence of these vegetation types on the tropospheric CO_2 concentration.

Carbon dioxide in the lower troposphere is in a constant state of flux owing to emissions and uptake of CO_2 at the surface, these fluxes can be detected by SCIAMACHY, however AIRS-LSQ does not measure these fluxes, as the CO_2 is homogeneously mixed in the upper troposphere. CO_2 takes approximately 26 days to mix through the tropical tropopause layer [Park et al., 2007], CO_2 measured in the upper troposphere is likely to be a combination of CO_2 emitted from a large surface area and also could be up to 30 days older than the CO_2

143

measured at the surface and lower troposphere. The upper tropospheric seasonal cycle is expected to resemble the seasonal cycle measured in the lower troposphere over each region, but is likely to produce a smaller amplitude variation and lag the lower tropospheric cycle up to 3 months (see chapter 4) due to the time taken to mix through the troposphere. To determine whether the CO_2 in the upper troposphere originates from the same region as the CO_2 measured in the lower troposphere the Numerical Atmospheric dispersion ModEl (NAME), a reverse model is used to calculate the path of the CO_2 from the upper troposphere back in time to where it's likely to have originated from.

5.2   Vegetation types.

Vegetative indices represent integrative measurements of vegetative biophysical properties (greenness), which provide information on the type and quantity of vegetation within an area. Vegetative indices are derived from ground, air and space borne sensors [Didan et al., 2002]. There are many different methods of calculating the vegetative indices these include; Normalized differential vegetative index (NDVI), Enhanced vegetative index (EVI), Leaf area index (LAI), Fraction of photosynthetically active radiation (FPAR), Fractional green vegetation (FGV) and many others. All methods calculate the amount of green vegetation within a specified region through measuring the amount of radiation absorbed and emitted within specific spectral bands. Using NDVI vegetation types are calculated and plotted (figure 5.1). The main vegetation types located in Africa are; shrublands, savannahs, woody savannahs, evergreen broadleaf and grasslands, these will be used to determine if there is a correlation between the CO_2 concentration and vegetation type.

5.2.1   Normalized difference vegetation index (NDVI)

Live green vegetation absorbs solar radiation which is in the red region of the visible part of the spectrum between 0.4 and 0.7 μm. This is also known as the

photosynthetically active radiation (PAR) spectral region (when measuring the light absorbed by plants). Leaf cells reflect solar radiation in the Near InfraRed (NIR) spectral region between 0.7 and 1.1 μm, so plants appear bright in the NIR region and relatively dark in the visible red spectral region [Gates et al., 1980]. Normalized difference vegetation index (NDVI) is the measured difference between the NIR reflected and the visible red absorbed in their respective spectral regions.

$$NDVI = \frac{(NIR - RED)}{(NIR + RED)} \qquad (5.1)$$

NDVI is the ratio of reflected to incoming radiation varying between -1 and +1. An area of dense canopy vegetation will have a typical value between 0.3 and 0.8, while clouds and snow fields will be characterized by negative values.
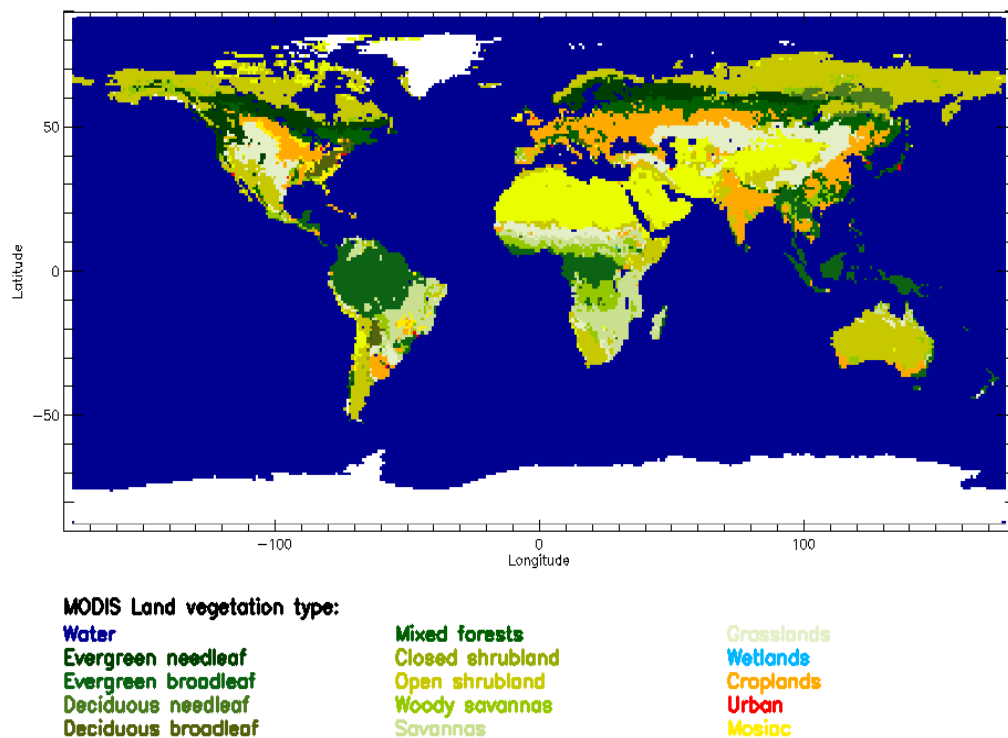
Figure 5.1; MODIS global land vegetation type, map is plotted from the Land Ecosystem Classification Product which is a static map generated from the official MODIS land ecosystem classification data set, MOD12Q1 for year 2000, see http://modis-atmos.gsfc.nasa.gov/ECOSYSTEM/index.html.

The Moderate-resolution Imaging Spectroradiometer (MODIS) instrument measures light in 36 spectral channels (non-continuously) over a wavelength interval of 0.4 – 14.4 μm. Two channels are imaged at a nominal ground resolution of 250 m at nadir, five channels at 500 m and the other 29 bands at 1 km and a swath of 2330 km (cross track) by 10 km (along track at nadir). Global coverage is achieved every one to two days. MODIS measures in the NIR and visible spectral regions from which the NDVI can be calculated (Equation 5.1) and is plotted in Figure 5.1 on a 1° x 1° grid.

5.2.2 Fraction of photosynthetically active radiation (FPAR)

FPAR is the fraction of photosynthetically active radiation (PAR) or red visible light absorbed by green vegetation. Green FPAR refers to the fraction absorbed by green leaves after the removal of the contribution of the surrounding woody material to the PAR absorption.

$$FPAR = 1 - \frac{(PAR_{below.canopy})}{(PAR_{above.canopy})} \qquad (5.2)$$

PAR cells measure the amount of transmitted light. FPAR is the difference of transmitted light above canopy and below canopy PAR values.

5.2.3 Leaf Area Index (LAI)

Leaf Area Index (LAI) is the ratio of the total upper leaf surface area of vegetation percentage divided the surface area of land on which the vegetation grows. Wavelengths used are in the Red and Near infrared regions of the spectra. Values calculated are typically between 0 and 6, where 0 represents bare ground and 6 is classed as dense forest.

$$LAI = \frac{upper\_leaf\_surface\_area}{Surface\_area\_of\_land} \qquad (5.3)$$

LAI is used to predict the NPP (net primary productivity) and is also used as a reference tool for crop growth.

5.2.4 Enhanced Vegetative Index (EVI)

The Moderate-resolution Imaging Spectroradiometer (MODIS) on board Terra measures the plant growth on a global scale. EVI improves upon the quality of the NDVI product. It is calculated in a similar way to the NDVI but doesn't become saturated as easily as the NDVI product when viewing areas containing large amounts of chlorophyll such as rainforests.

$$EVI = G \times \frac{\rho_{NIR} - \rho_{red}}{L + \rho_{NIR} + C_1 \rho_{red} - C_2 \rho_{blue}} \tag{5.2}$$

Equation 5.2 is used to calculate the EVI, where red, NIR, blue are reflectances in their respective sensor bands, L is the canopy background and C_1 and C_2 are the coefficients for aerosol. EVI method uses the blue spectral band to correct for the aerosols measured in the red spectral band [Didan et al., 2002]. NDVI is chlorophyll sensitive whereas EVI is responsive to canopy structural variations and measurements are reduced in residual atmosphere influences.

5.2.5 Fractional green vegetation.

Fractional vegetation is the percentage of green vegetation covering a region, which is essentially the NDVI values multiplied by 100. NDVI values ≤ 0.07 are set to zero and values ≥ 0.57 are set to 1.0 (NDVI values between 0.07 and 0.57 increase linearly from 0.0 to as fractional vegetation) [NOAA/NESDIS: www.osdpd.noaa.gov/PSB/IMAGES/gvi.html]
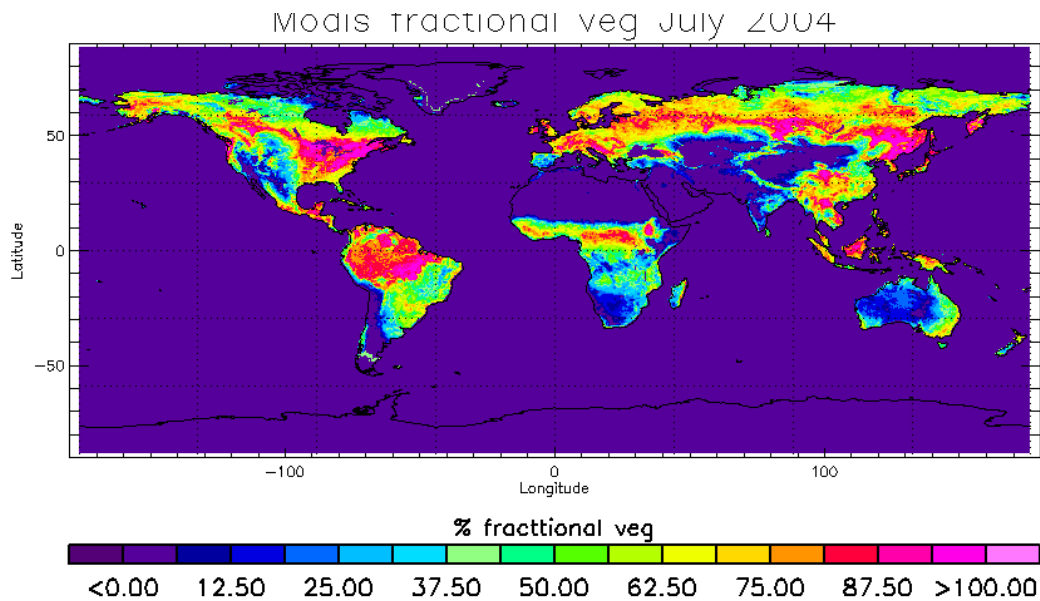
Figure 5.2; Global map of fractional green vegetation NESDIS AVHRR for July [Gutman, and Ignatov, 1997]
The global. 0.144 deg, monthly annual cycle of vegetation greenness fraction dataset was developed by the
NESDIS GCIP group (NESDIS Land Sciences: Gutman and Tarpley). The data is a composite of a 5-year
(1985-1990) global mean of satellite AVHRR vegetation index.

The NOAA (National Oceanic and Atmospheric Administration) AVHRR
(Advanced Very High Resolution Radiometer) instrument has five detectors, two
of which are sensitive to the NIR and Visible wavelengths. The photosynthetic
capacity of the vegetation is calculated from the intensity of light measured by
AVHRR from the Earth's surface. The size of an AVHRR pixel is equal to a
surface area of 1 km^2. The larger the reflected radiation in the NIR compared with
to the absorbed red visible spectrum, the more likely the area measured is to be
forest. If the reflected light is smaller than the absorbed light the vegetation
measured is likely to be sparse and consist of grassland or desert.

Fractional green vegetation data calculated from AVHRR is plotted on a 0.144
degree grid, data are a composite of a five year (1985 – 1990) global mean values
from the AVHRR vegetation index [Gutman et al., 1997]. The values are
percentages of the green vegetation ranging from 1 – 98 over land and 0 over
water.

5.3 African vegetation and fractional green vegetation.

Five vegetation types are chosen over Africa to determine how the CO_2 varies over the different vegetation types throughout the year, in the upper and lower troposphere in 2004. As seen in chapters 3 and 4 when retrieving CO_2 over small areas the flux variations are significant, to reduce the variable fluxes of CO_2, large areas surrounding the vegetation types were analysed.

MODIS Land vegetation type:

Water	Mixed forests	Grasslands
Evergreen needleaf	Closed shrubland	Wetlands
Evergreen broadleaf	Open shrubland	Croplands
Deciduous needleaf	Woody savannas	Urban
Deciduous broadleaf	Savannas	Mosiac
		Snow/ice
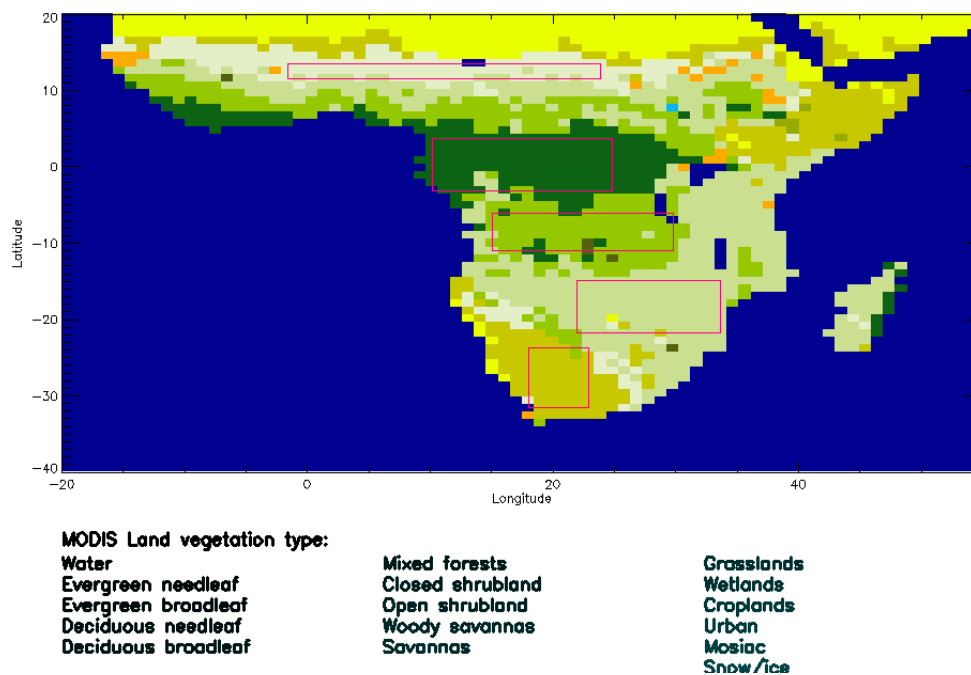
Figure 5.3; Africa vegetation plotted from MODIS land vegetation type. Five areas highlighted represent different vegetation types to be analysed. http://modis-atmos.gsfc.nasa.gov/ECOSYSTEM/index.html.

Figure 5.3 shows the five areas chosen, these are; grassland, evergreen forest, woody savannas, savannas and shrubland. Fractional green vegetation over each vegetation type, (measured by MODIS) is compared to AIRS-LSQ and SCIAMACHY CO_2 data measured over an equal area to determine how the CO_2 changes throughout the year.

Fractional vegetation from AVHRR is plotted over Africa (Figure 5.3). As is seen the vegetation dramatically changes throughout the year. The greatest percentage of vegetation is over the savannahs and rainforests which are located at and around the tropics. Vegetation fraction decreases outside the tropics ($> 30°$) as the type of

vegetation changes from forestry to shrubland which has a significantly lower concentration of green vegetation.
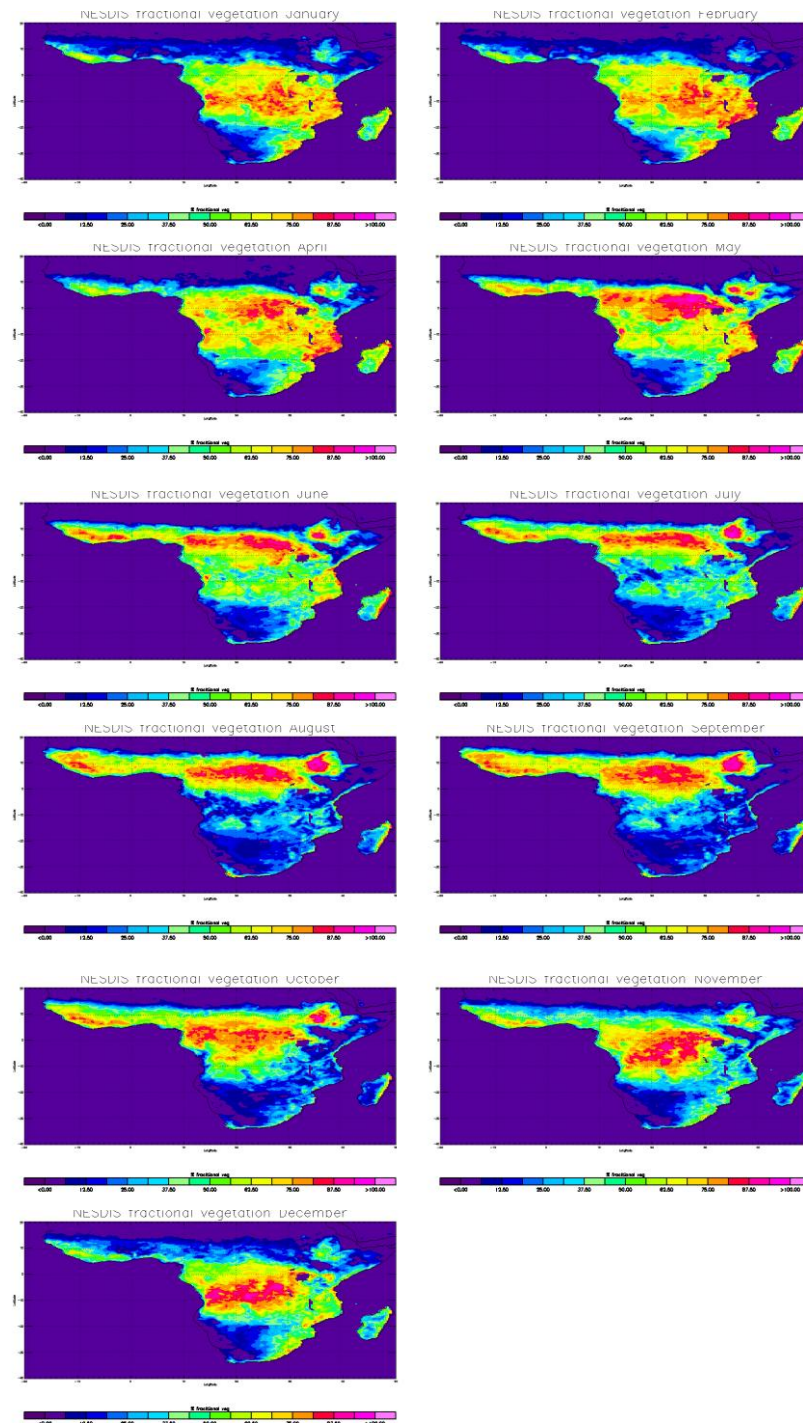
Figure 5.4; Monthly fractional vegetation NESDIS AVHRR [Gutman, and Ignatov, 1997] plotted over Africa. The global. 0.144 deg, monthly annual cycle of vegetation greenness fraction dataset was developed by the NESDIS GCIP group (NESDIS Land Sciences: Gutman and Tarpley). The data is a composite of a 5-year (1985-1990) global mean of satellite AVHRR vegetation index.

The Fractional green vegetation (FGV) varies throughout the year with the maximum concentration of FGV in the northern hemisphere is between June and September and the southern hemisphere concentration is greatest between January and April.

The FGV around the equator varies less than the values at higher latitudes as the climate changes with increasing latitude. A temperate climate is typically found at higher latitudes and a bimodal climate (wet and dry seasons) is found around the tropical regions. Some tropical regions have more than two seasons depending on their location compared to the Inter Tropical Convergence Zone (ITCZ). In some regions the ITCZ passes over twice yearly. The ITCZ is located in the northern hemisphere in June and at its highest latitude in the southern hemisphere during October. The ITCZ passes through some regions twice yearly where some tropical regions have two wet and two dry seasons each year. Vegetative growth is greatest in the tropics during the wet seasons, which can be seen in Figure 5.3 where FGV concentration increases and decreases twice throughout the year in the lower latitudes surrounding the equator.

5.4   CO$_2$ comparisons with fractional vegetation over Africa.

Monthly mean tropospheric CO$_2$ are retrieved by SCIAMACHY and AIRS-LSQ (LSQ method) for 2004 and are compared to the fractional green vegetation (FGV) retrieved by NOAA/NESDIS [Gutman et al., 1997]. Each instrument measures the same area;

	Minimum Longitude	Minimum latitude	Maximum longitude	Maximum latitude
Shrubland	12°	-36°	21°	-27°
Savannah	18°	-24°	30°	-18°
Woody Savannah	12°	-15°	27°	-9°
Evergreen broadleaf	6°	-6°	24°	3°
Grassland	-9°	12°	21°	15°

Table 5.1; coordinates of the vegetation analysed in Africa for CO$_2$ and FGV comparisons.

5.4.1   Shrublands.
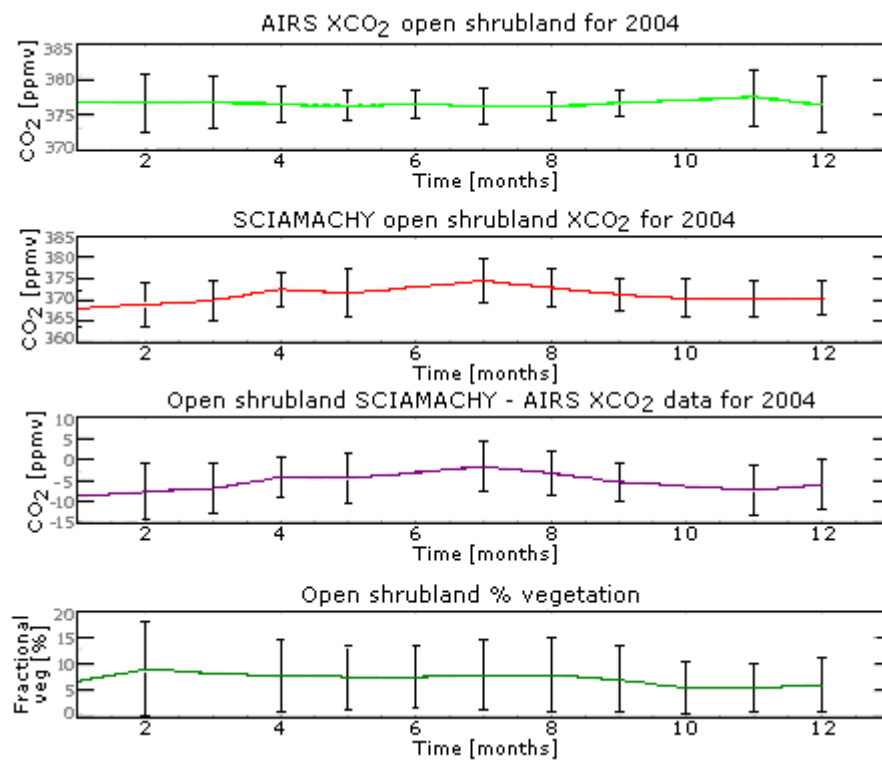
Figure 5.5; Shrubland 2004 AIRS-LSQ and SCIAMACHY CO_2 comparisons with fractional vegetation from NOAA NESDIS. First box; CO_2 seasonal cycle measured by AIRS-LSQ. Second box; CO_2 seasonal cycle measured by SCIAMACHY. Third box; difference between AIRS-LSQ and SCIAMACHY CO_2 seasonal cycles. Fourth box; fractional vegetation percentage.

There is little green vegetation to be found within shrubland area, the area examined has a maximum FGV of 8.96, which compared to the other regions examined is small. The AIRS-LSQ and SCIAMACHY CO_2 data are out of phase, with CO_2 peaking in July in the lower atmosphere and November in the upper atmosphere. The CO_2 and FGV seasonal cycles are not in phase nor are they anti-correlated, suggesting in this region there is no relation between the FGV and the atmospheric concentration in the upper or lower atmosphere.

5.4.2 Savannahs.
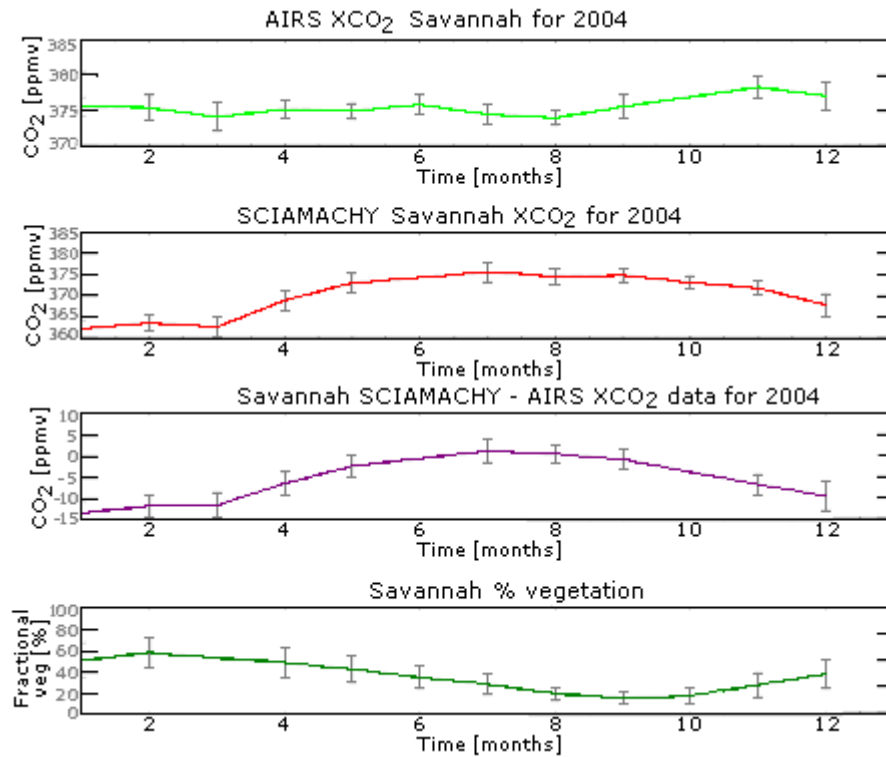
Figure 5.6; Savannah 2004 AIRS-LSQ and SCIAMACHY CO_2 comparisons with fractional vegetation from NOAA NESDIS. See caption of figure 5.5 for more details.

Savannahs typically consist of open tropical grassland with some scattering of shrubs and trees. CO_2 measured in the upper troposphere show that there is little variation throughout the year, showing only a slight increase in the atmosphere concentration in November. CO_2 in the lower troposphere indicates a long gradual increase in concentration between April and July, then slowly decreasing through the remainder of the year. The AIRS-LSQ CO_2 amplitude is 4.37 ± 1.52 ppmv and SCIAMACHY is 13.47 ± 2.09 ppmv, the variation in CO_2 in the lower troposphere is much greater then the variation in the upper troposphere. The FGV shows a steady decline from February through September producing an amplitude of 42.61 ± 11.25 ppmv. The seasonal cycles produced by the FGV and SCIAMACHY are approximately 6 months out of phase, while the CO_2 in the atmosphere increases the FGV decreases, but the change in FGV appears to have little overall effect on the CO_2 concentration in the upper troposphere.

5.4.3 Woody savannahs.
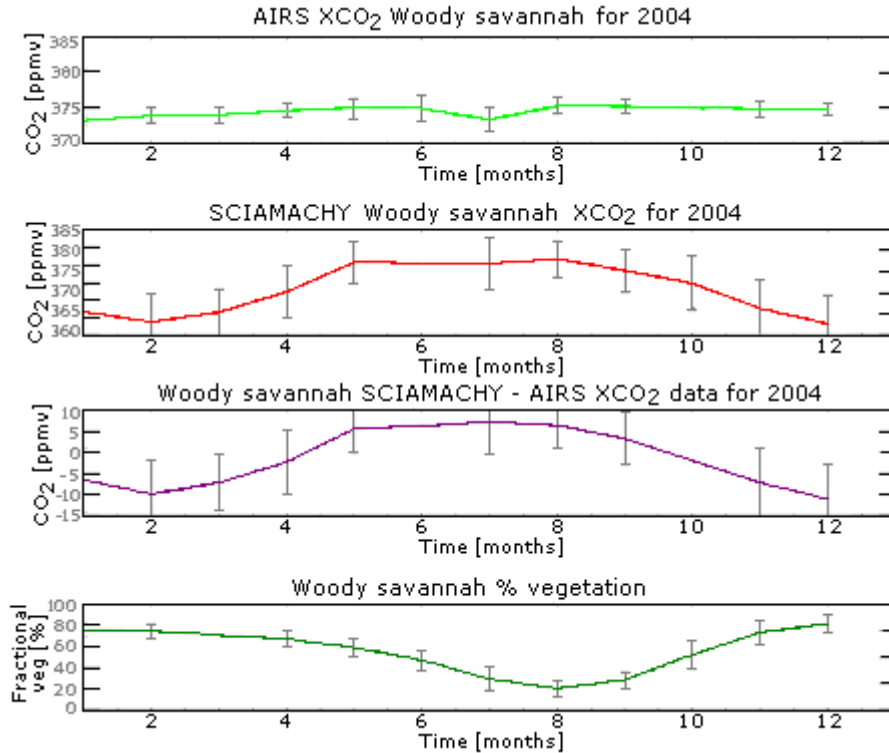
Figure 5.7; Woody savannah 2004 AIRS-LSQ and SCIAMACHY CO_2 comparisons with fractional vegetation from NOAA NESDIS. See caption of figure 5.5 for more details

Woody savannahs have a denser tree and canopy population compared to the savannahs. The CO_2 in the lower troposphere varies by 18.41 ± 7.07 ppmv throughout the year with CO_2 peaking around August (which is the regions winter months). The FGV is at its lowest value of 20.25 in August which is when the CO_2 concentration in the lower atmosphere peaks with a value of 376.70 ± 5.22 ppmv. The change in the percentage of FGV throughout the year is 61.43 which is significant as this drastic change in the FGV produces a large change in the CO_2 concentration in the lower troposphere, but has little to no effect on the CO_2 concentration in the upper troposphere where the seasonal amplitude measured is 2.14 ± 1.16 ppmv.

5.4.4   Evergreen broadleaf.
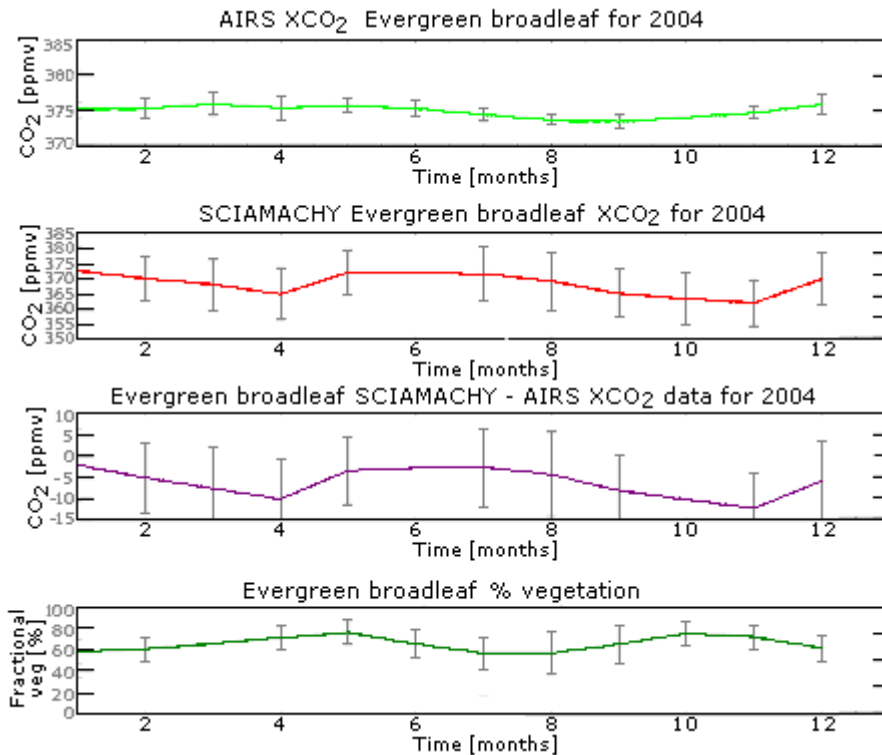
Figure 5.8; Evergreen broadleaf 2004 AIRS-LSQ and SCIAMACHY CO_2 comparisons with fractional vegetation from NOAA NESDIS. See caption of figure 5.5 for more details

The upper tropospheric seasonal cycle measured over the broadleaf region is representative of the northern hemispheric cycle peaking in May and reaching its minimum in September. Broadleaf rainforest is located near the equator which is why the seasonal cycle in the upper troposphere shows a strong resemblance to the northern hemispheric cycle.   The seasonal cycle measured in the lower troposphere is not representative of the seasonal cycles typically measured in the northern or southern hemispheric regions. The seasonal cycle measured produces two minima throughout 2004 one in April and the other in November.   The climate in the tropics are bimodal based on a summer wet season and a winter dry season, summer is between June and September and winter is typically between December and March). However the ITCZ crosses the broadleaf rainforest twice yearly, once in May and again in October, the passing of the ITCZ over a region corresponds with the local wet season. The vegetation grows during the wet

seasons, which is seen in Figure 5.8 where the FGV peaks twice, the double peak of FGV also produces a double dip in CO_2 concentration around the same period.

5.4.5 Grassland.
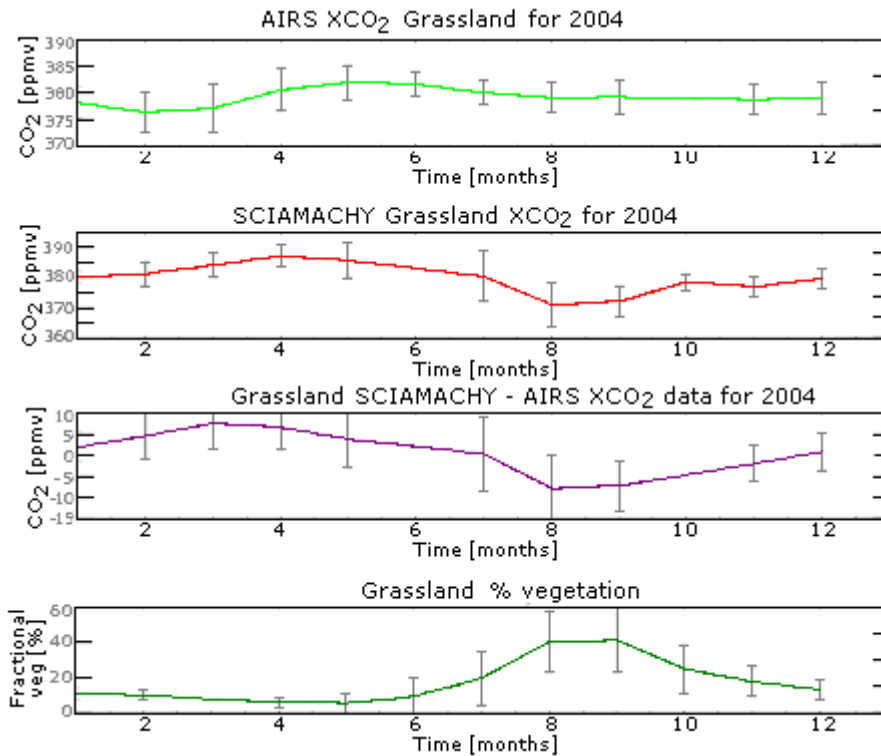
Figure 5.9; Grassland 2004 AIRS-LSQ and SCIAMACHY CO_2 comparisons with fractional vegetation from NOAA NESDIS. See caption of figure 5.5 for more details.

The grasslands are located in the northern hemisphere, the seasonal cycles in the upper and lower troposphere clearly show cycles representative of the northern hemisphere. The FGV shows a sudden increase from June through August which corresponds to the decrease in the lower tropospheric CO_2 concentration.

From the five vegetation regions analysed it's clear that a change in FGV causes a change in the CO_2 concentration in the lower troposphere. The variations in the lower tropospheric CO_2 and FGV have little to no effect on the CO_2 concentration in the upper troposphere.

5.4.6 Correlation values of fractional vegetation and atmospheric CO_2 over Africa
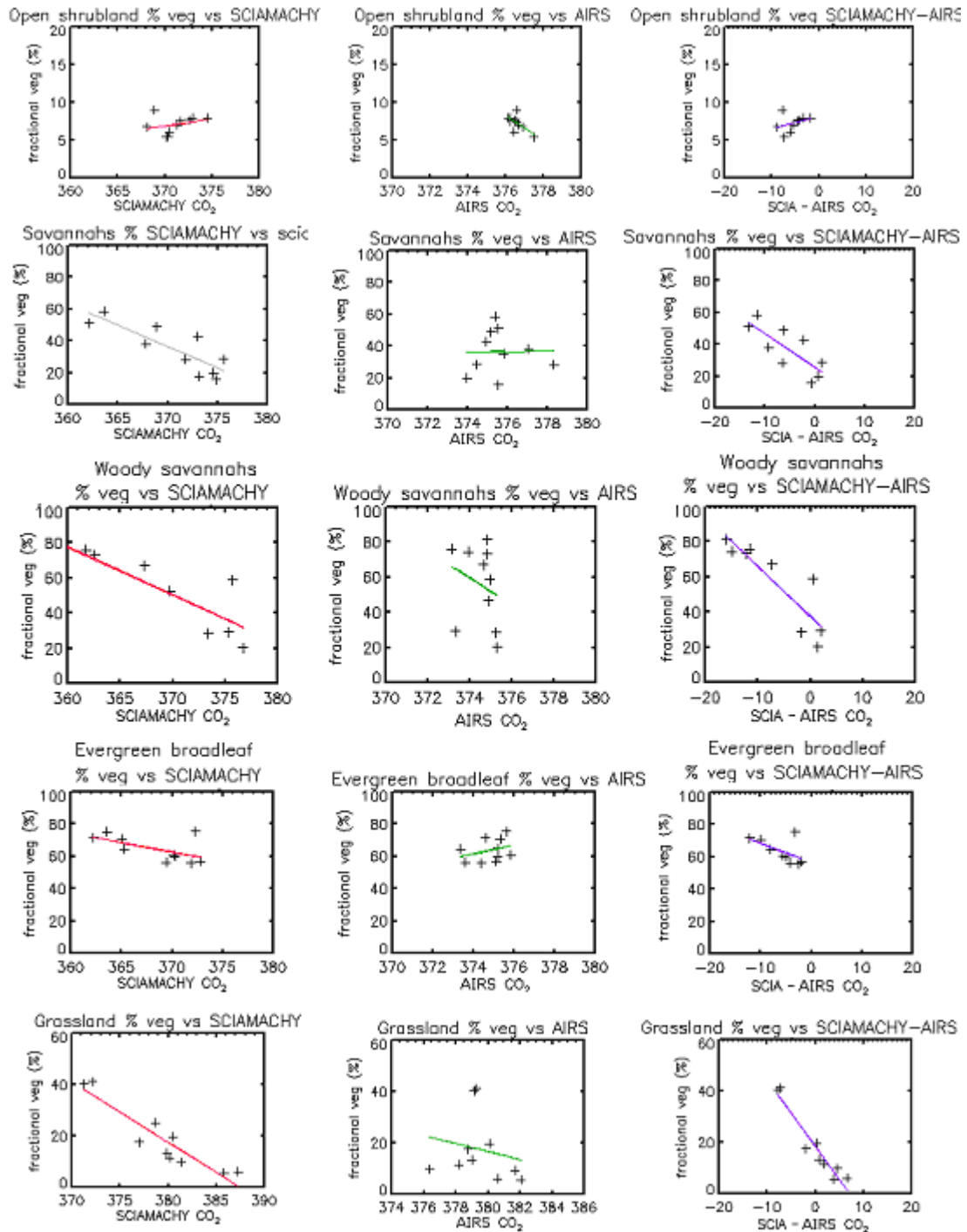
Figure 5.10; correlation plots of Fractional vegetation and satellite data; SCIAMACHY (left, red), AIRS-LSQ (middle, green) and SCIAMACHY-AIRS-LSQ (right, purple) CO_2 for 2004.

	SCIAMACHY CO_2	AIRS-LSQ CO_2	SCIAMACHY-AIRS-LSQ CO_2
Shrublands	0.287	-0.643	0.334
Savannah	-0.833	0.009	-0.776
Woody savannah	-0.875	-0.261	-0.878
Evergreen broadlands	-0.575	0.321	-0.569
Grasslands	-0.926	-0.203	-0.961

Table 5.2; Correlation values of Fractional vegetation and satellite data; SCIAMACHY , AIRS-LSQ and SCIAMACHY-AIRS-LSQ CO_2 for 2004.

Correlation values between the CO_2 data and the type of vegetation are shown in Table 5.2. CO_2 in the lower atmosphere (SCIAMACHY data) shows that four out of the five vegetation types there is a strong anti-correlation. CO_2 in the lower atmosphere is clearly influenced by the FGV on the surface, as increasing the percentage of FGV in turn absorbs more CO_2 from the surrounding atmosphere. Shrublands show a slight positive correlation with the SCIAMACHY data, the fraction of vegetation when at maximum is 8.96 and its seasonal cycle amplitude is 3.56 ± 6.2 which is comparatively small to the amplitudes produced by the other vegetation types. The small value of FGV in the shrublands is insignificant which has little impact on the surrounding tropospheric CO_2 concentration.

The correlation between CO_2 in the upper troposphere and the FGV is highly varied, with good anti-correlation over the shrublands, but correlations over the four other regions are small. The grasslands are located in the northern hemisphere where the seasonal cycles in the upper troposphere are strongly in sync with the northern hemispheric seasonal cycle, peaking around May and reaching minimum around November. The grasslands growth period is between June and August which happens to correspond with the decrease in the CO_2 concentration in the upper troposphere. Shrublands also show a reasonable anti-correlation with the FGV, this could be due to the small change of FGV through the year and small changes in the upper troposphere, and it is unclear why the FGV and the upper tropospheric CO_2 should anti-correlate so well.

Comparing the FGV to the subtracted CO_2 (SCIAMACHY − AIRS-LSQ) data produced similar results to those measured against the SCIAMACHY results. As the subtracted data shows no significant change from the results found by the

comparisons made to the SCIAMACHY data it is unclear whether these results represent the region better or worse than using the SCIAMACHY data alone. From the data produced from subtracting the two data it is clear that the CO_2 concentrations in the lower troposphere dominate throughout the atmosphere, as the fluxes are much greater in the lower troposphere due to the effect the vegetation has on the CO_2 in the surrounding troposphere.

	Fractional vegetation amplitude	AIRS-LSQ amplitude	SCIAMACHY amplitude	SCIAMACHY - AIRS-LSQ amplitude
Shrublands	3.52	1.37	6.41	7.07
Savannah	42.61	4.37	13.47	14.69
Woody savannah	61.43	2.14	18.14	18.14
Evergreen broadlands	19.46	2.55	10.60	10.25
Grasslands	35.71	5.70	16.00	15.31

Table 5.3; Amplitudes of the seasonal cycles produced by Fractional vegetation, SCIAMACHY , AIRS-LSQ and SCIAMACHY-AIRS-LSQ CO_2 for 2004.

Unique seasonal cycles were produced over each vegetation type measured, both for the CO_2 concentration and the FGV measured. It is clear from the correlation values and the seasonal cycles plotted that the FGV and CO_2 (in the lower troposphere) are out of phase with each other, indicating that the change in FGV affects the CO_2 concentration. Table 5.3 shows the amplitudes of the FGV and CO_2 values, it can be seen that the greater the amplitude (difference between maximum and minimum value) of FGV the greater the amplitude of CO_2 in the lower troposphere, with the exception of the savannah.

It is clear from the comparisons that the vegetation has a profound effect on the CO_2 in the lower troposphere not only by influencing the shape of the cycle but also its amplitude. Comparisons of vegetation types and CO_2 concentrations within the surrounding areas are important in determining the amount of CO_2 that different vegetations can absorb and emit. Understanding the fluxes of CO_2 over different vegetation types will help produce more accurate CO_2 models which will help determine future climate changes.

5.5 Origins of the carbon dioxide in the upper and lower troposphere.

As seen in section 5.4 the seasonal cycles measured in the upper and lower troposphere are significantly different, which suggests that the CO_2 disperses through the atmosphere and is well mixed as it travels up through the troposphere.

When measuring the CO_2 in the upper troposphere, are the measurements retrieved representative of the surface fluxes directly beneath the area or are they influenced by emissions from the surrounding area?

To determine if the CO_2 measured in the upper troposphere and lower troposphere is emitted from the surface directly beneath where the column is retrieved, a dispersion model is used. Numerical Atmospheric Dispersion Model (NAME) follows the path of the CO_2 back in time to determine the probable origin of the CO_2 which can help determine if the CO_2 originated from the surface beneath the tropospheric column measured by the satellites or if the CO_2 was emitted from the surrounding area.

Carbon dioxide measurements are retrieved in the upper and lower troposphere over 4 regions in Africa each consisting of a different type of vegetation. Name is used to determine if the CO_2 measured in the tropospheric regions (1 and 9 km) are emitted from the surface beneath.

5.5.1 The Unified model

The Unified model (UM) is the atmospheric and oceanic numerical modelling software developed and used by NAME. The UM can support global and/or regional domains and is applicable for a wide range of spatial and temporal scales for which it is used for numerical weather prediction and climate modelling. Weather prediction is calculated through inputting observational data into the UM where the data is assimilated and a weather prediction is completed.

5.5.2 Numerical Atmospheric Dispersion Model (NAME)

The Numerical Atmospheric Dispersion Model (NAME) is a Langrangian particle model, it uses a 3 hourly, 3 dimensional (3D) meteorology fields from the complex numerical weather prediction model, in a 'Unified Model' (UM) [Cullen, 1993], to move particles (CO_2) around the model [Manning et al., 2003].   The 3D flow is interpolated to the location of each particle at every time step (15 minutes). A random walk technique [Thompson, 1987] is used where each particle moves under the influence of the mean flow, wind meander and sub grid-scale turbulence. The random walk scheme uses a velocity variance and Langrangian timescale profiles which are calculated from empirical fits to the observational data to simulate the turbulent motion.

The Met Office Unified Model (UM) global version is used to calculate the wind fields and other meterological data, using a 60 km horizontal resolution and 50 vertical levels [Cullen et al., 1993]

Convection from randomly mixing particles with covariance clouds simulates the enhanced mixing calculated by the model. Entrainment which is the movement of the particles between the boundary layer and the free troposphere is modelled separately. NAME has been used for a range of applications including air quality forecasts, regional atmospheric chemistry modelling and international dispersion experiments [Manning et al., 2003]. Further details are given in appendix 2.

5.5.3   Input parameters for the model.

In real time, the point at which the particles are released is where the particle is located 'now' and the model is run backwards from this point, for example 5 days, at which the output of the model was calculated within the parameters specified by the user, where the particles were 5 days ago and the concentration of particles located there.

The model is set up for the individual's needs. For this study a 1 x 1 degree grid is used to analyse particles released over specified areas in Africa during August.

The particles can be released at any integer value within the height parameters specified in the model, which are between 1 and 10 km from the surface. The atmospheric height which is to be examined at the end of the result is specified which the model used could be between 0 and 10 km from the surface. The number of days for the model is to be run, that is back in time from the release date is also specified.

The release date for the particles is the 30th of August, which are run backwards for 10 and 20 days for each of the 4 regions and analysing the amount of particles between 0 and 4 km at the end of the model run. Particles are released from an initial height of 1 km for one analysis and at 9 km for another. Basically particles which are at 1 km and 9 km on August 30th are run backwards 10 and 20 days to determine how many particles originated from an altitude between 0 and 4 km.

Looking at where the particles were 10 and 20 days back in time it can be determined if they were emitted from the specified area or from another region. Knowing if the data measured by the satellites originated from the surface or from another region will help determine how the CO_2 mixes through the atmosphere and help locate with greater accuracy where the sinks and sources are located. The CO_2 mixes throughout the atmosphere. When calculating the location of sinks and sources, errors on the exact location are introduced owing to the homogeneous mixing of CO_2 throughout the CO_2 column measured by the satellites. NAME will also help determine if measuring the CO_2 in the upper troposphere provides any relevant information from the surface fluxes directly beneath the measurements.

The four areas analysed which consist of different vegetative types, where the CO_2 movements are calculated over Africa are; savannahs, woody savannahs, evergreen broadleaf forest and grasslands. The seasonal cycles of these areas are plotted in section 5.4, the results show that the CO_2 concentration in the lower troposphere is influenced by the seasons and the type of vegetation within the surrounding area. Larger seasonal cycles were measured with larger variations in the fractional green vegetation (FGV) value, but the variations of FGV and the CO_2 measured in the lower troposphere have little to no effect on the upper

tropospheric CO_2 concentration. The lack of influence from the FGV and CO_2 concentration in the lower atmosphere suggests that the CO_2 from the lower troposphere does not translate to the upper troposphere directly above as CO_2 is uniformly dispersed throughout the troposphere, which the satellite measures a mean CO_2 concentration value of the surrounding region.

NAME is used to look at particles in the upper troposphere (9 km) and lower troposphere (1 km) at day 'zero'. The model is run backwards 10 and 20 days from day 'zero', with particles starting from an altitude of 9 km and 1 km. The model then calculates how many particles originated from the area of interest which is the surface directly below the release of the particles at day 'zero'. The amount of particles which emanated from the area of interest between 0 and 4 km are calculated and plotted. These results will enable us to determine if the CO_2 concentration measured by the satellites originated from the surface directly beneath or if they originated from some other region.

5.5.4 Results: 10 days back from release date.

Particles released on the 30th of August 2003 from 1 and 9 km in the atmosphere, ending on the 21st of July. All results look at the atmospheric region between 0 and 4000 meters.
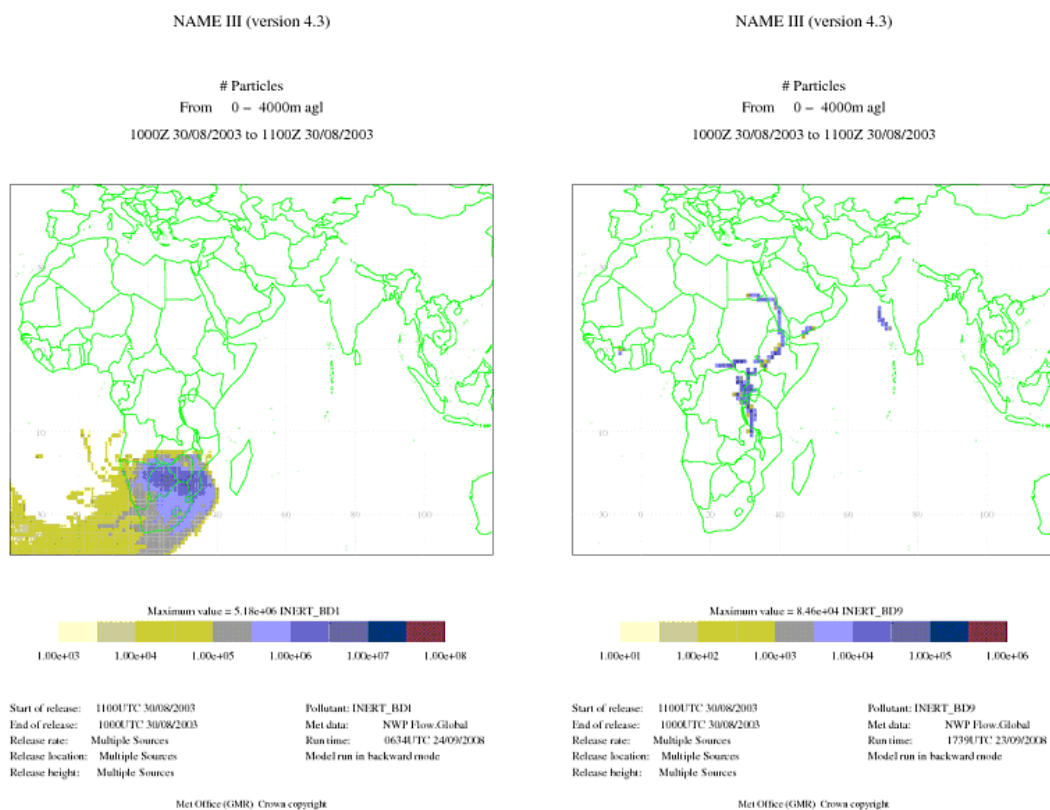
Figure 5.11; Particle released over savannahs, south Africa, left: release at 1km, right released at 9 km.
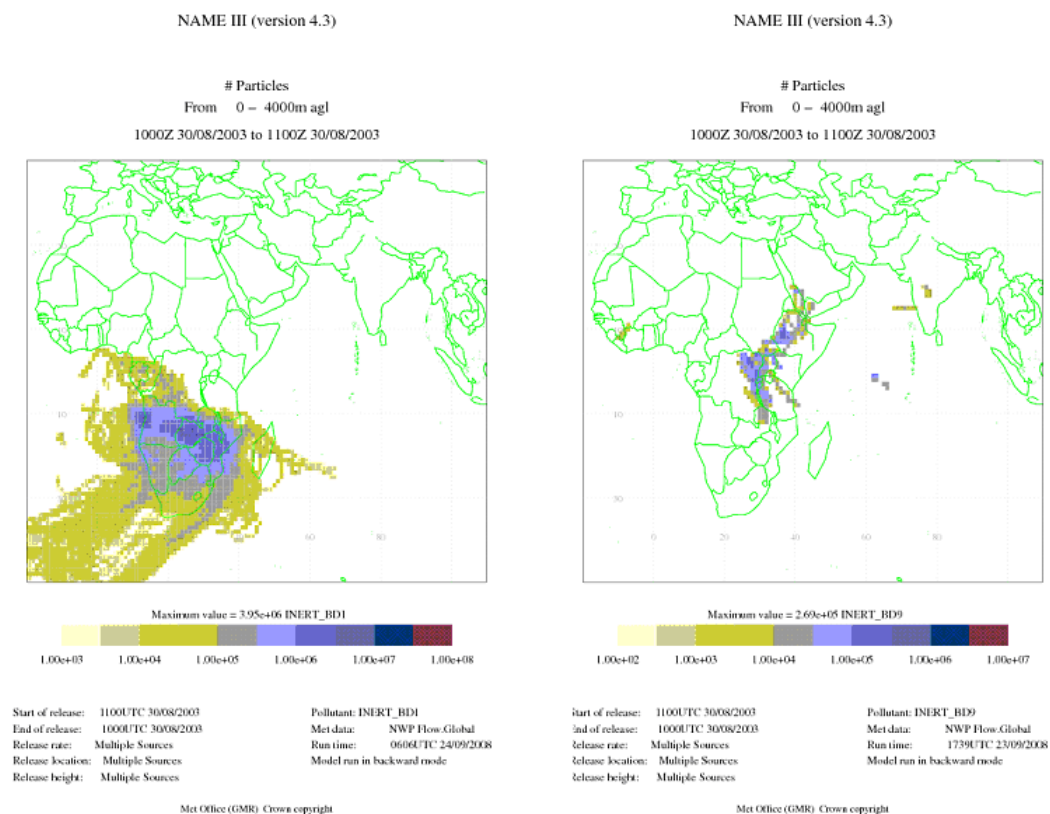
Figure 5.12; Particle released over woody savannahs, south Africa, left: release at 1km, right released at 9 km.
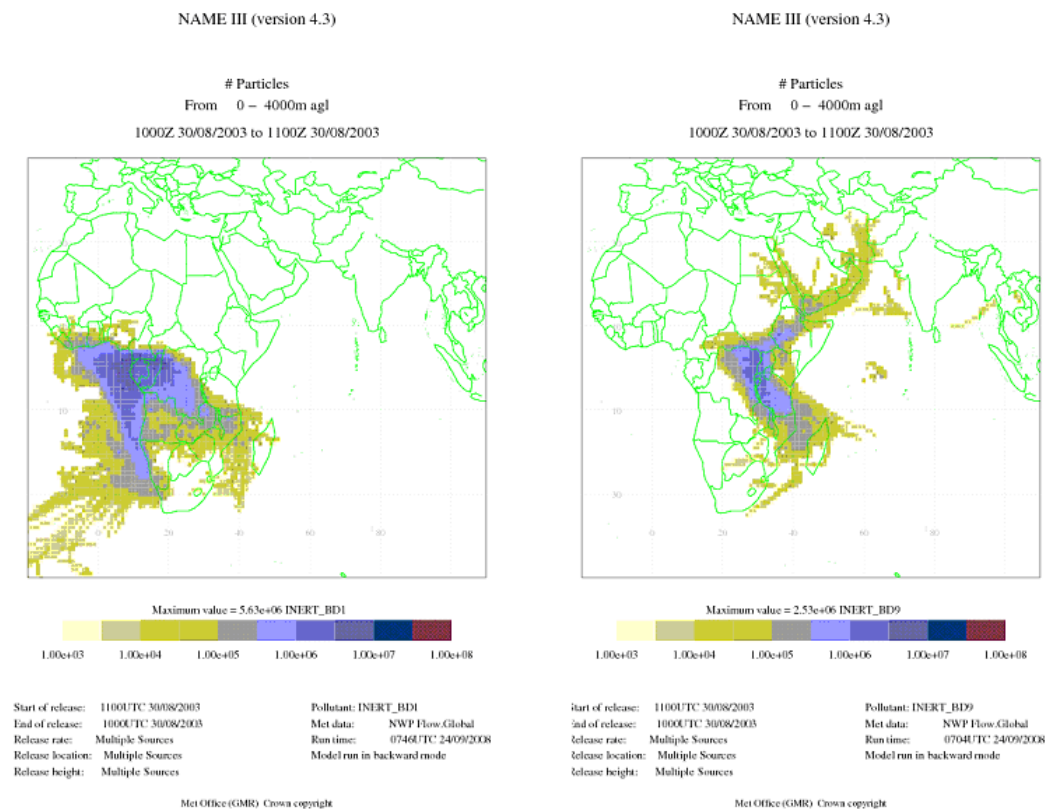
Figure 5.13; Particle released over Evergreen broadleaf, south Africa, left: release at 1km, right released at 9 km.
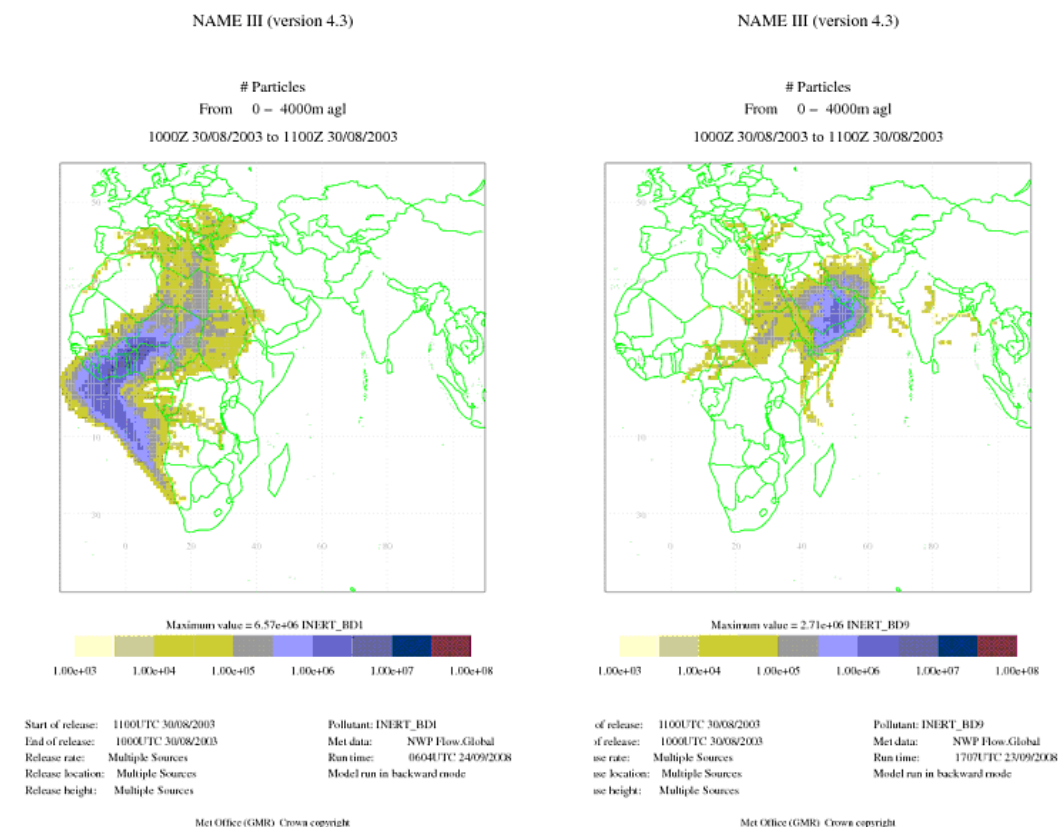
Figure 5.14; Particle released over grassland, south Africa, left: release at 1km, right released at 9 km.

Figures 5.11 through 5.14 show the concentration of particles measured between 0 and 4 km after 10 days, when the particles are released from 1 and 9 km. These figures show that the concentration of particles measured at 1 km above the area are considerable, compared to those released at 9 km.

The particles released at 9 km indicate that they did not originate from the surface directly beneath. These particles look to have originated from various surrounding regions. The number of particles emitted from the area within the lower troposphere over savannahs and woody savannahs vegetation are negligible, suggesting that the CO_2 emitted from any part of the surface does not reach the upper troposphere within 10 days at these latitudes. At lower latitudes, which are over the evergreen forests and grasslands, the number of particles emitted from the surface are numerous and some may have originated from the surface directly beneath the release points.

In all the regions with the particle released at 1 km shows that the CO_2 within the area specified does originate from the surrounding atmosphere. However the CO_2 measured over the grasslands show that they originate from the west coast of Africa.

5.5.5 Results: 20 days back from release date.
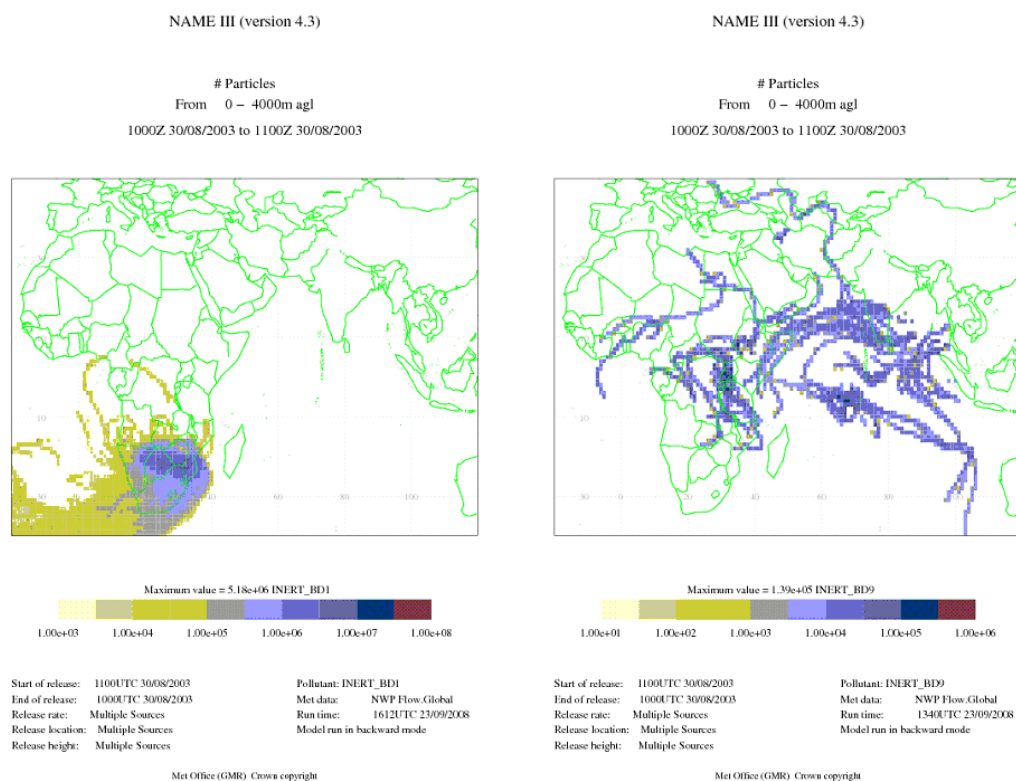
Figure 5.15; Particle released over savannah, south Africa, left: release at 1km, right released at 9 km.
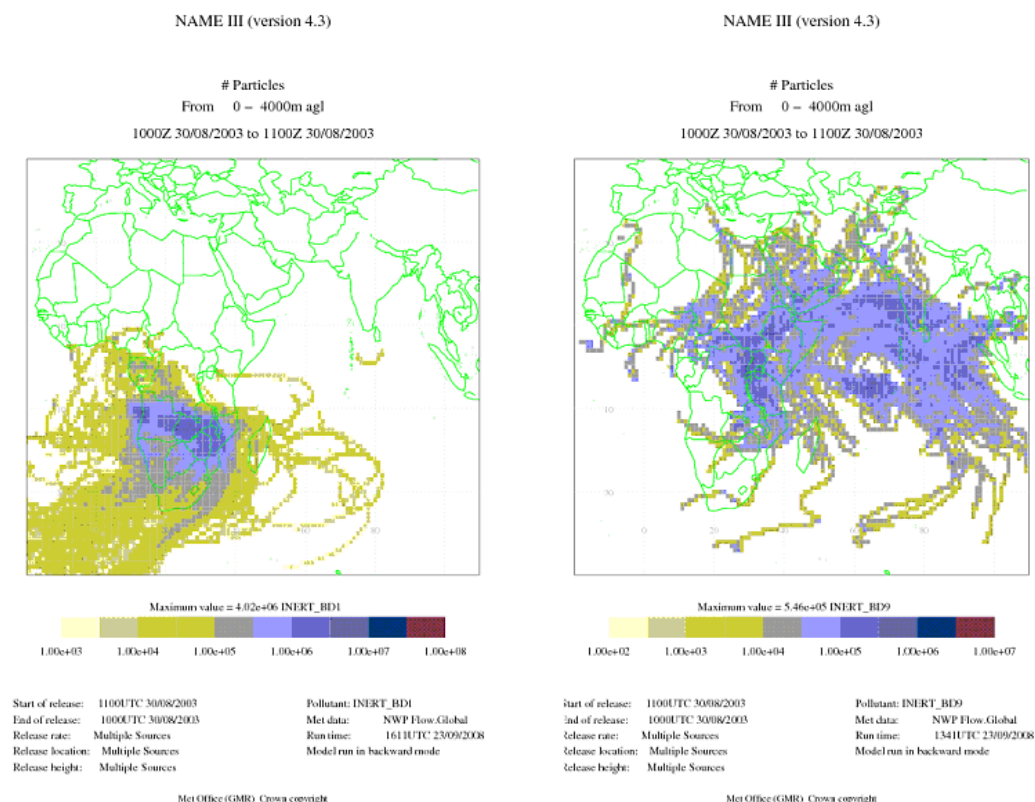
Figure 5.16; Particle released over woody savannah, south Africa, left: release at 1km, right released at 9 km.
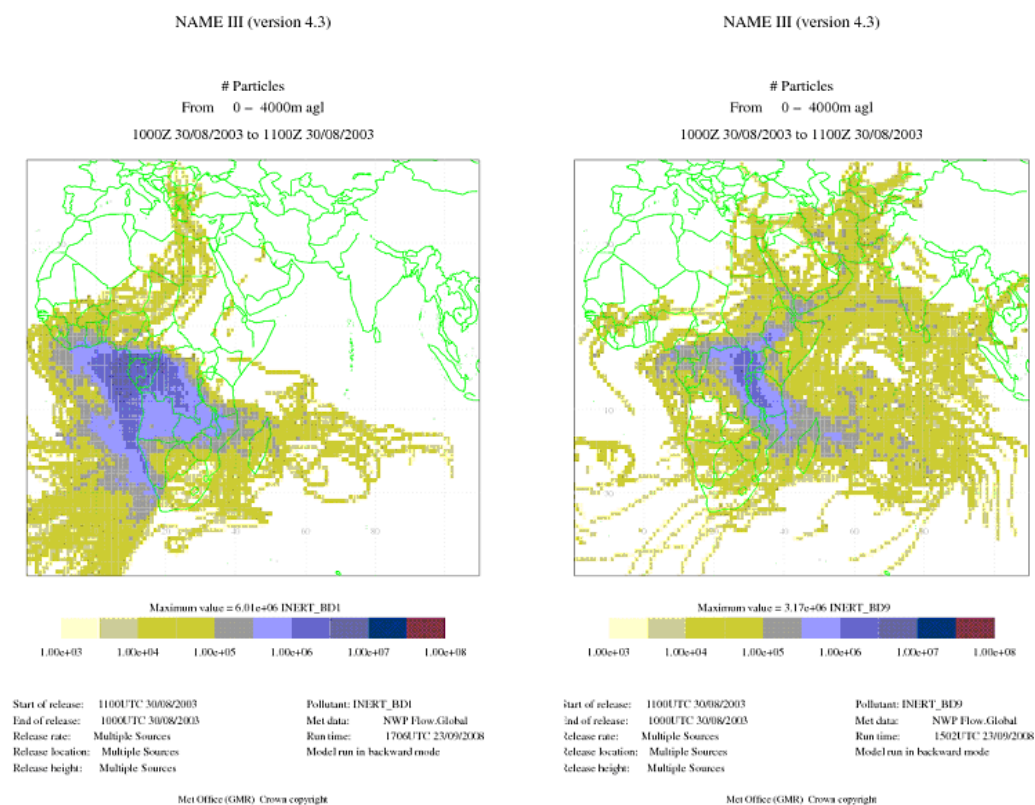
Figure 5.17; Particle released over evergreen broadland, south Africa, left: release at 1km, right released at 9 km.
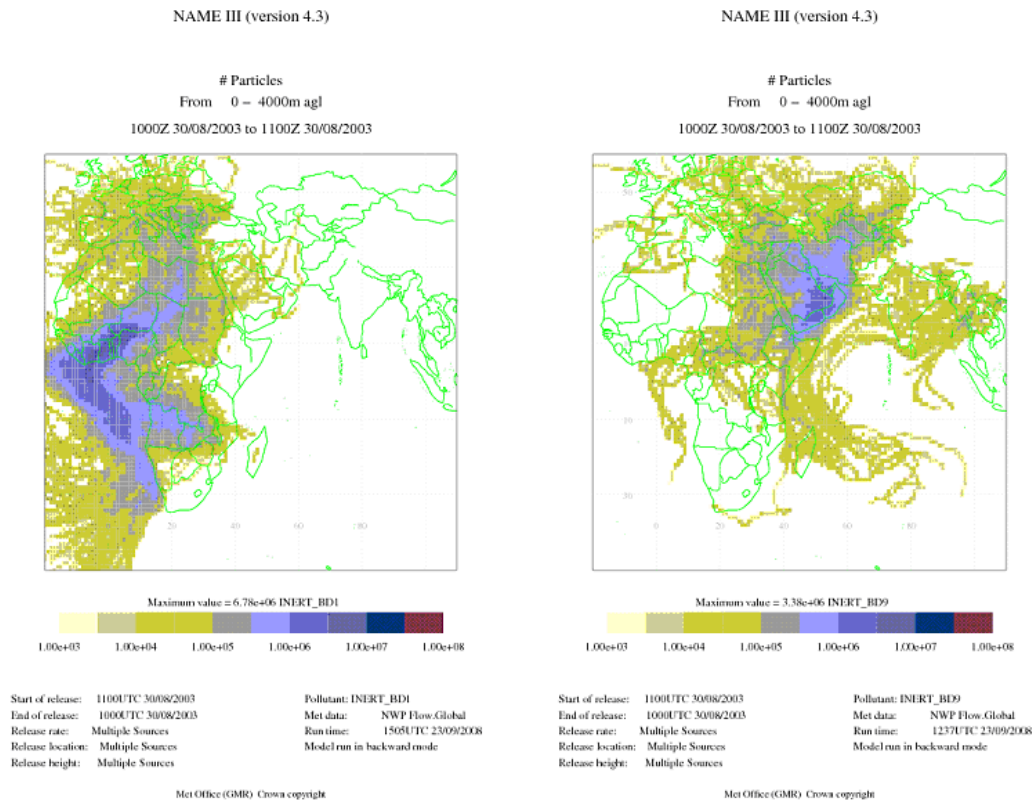
Figure 5.18; Particle released over grassland, south Africa, left: release at 1km, right released at 9 km.

Figures 5.15 through 5.18 represent particles released from atmospheric heights of 1 km and 9 km over the 4 vegetation regions used in 5.5.4, Name is run backwards for 20 days to determine where the particles emanated from.

Releasing the particles at 1 km shows that the majority of the particles originated from the area beneath the location measured. The vegetation types investigated are savannah, woody savannah and evergreen broadleaf, which showed that the majority of particles released at 1 km did originate from the surface below. The grassland area indicates that the particles origins are varied, some are within the vegetations location, but most of the particles originate from the west coast of Africa.

Back tracking the particles 20 days over the vegetation types, shows highly variable results with the majority of particles originating from surrounding areas. The number of particles originated between 0 and 4 km over the savannah region which reached an altitude of 9 km directly above the area is zero. There were particles that were emitted from the lower tropospheric region that reached an atmospheric height of 9 km but they originated from numerous regions, which are

likely caused by convection and winds moving the particles in from the surrounding areas.

The majority of particles measured at 9 km emanating from the lower troposphere (0 to 4 km) over the 20 day period are shown to have originated from east Africa and India. The probable cause of the particles coming from this area are due to convection and wind patterns moving the particles from the east over the areas of interest measured.

Some emissions from the evergreen broadleaf region measured at 9 km emanated from the surface beneath, but there are significant amounts of particles from surrounding regions measured at the upper tropospheric region.

5.5.6 Results: 30 days back from release date measured at 1km.

Measuring the amount of particles at 1 and 9 km which were released between 0 and 4000 meters showed that the majority of the particles measured at 1 km were emitted from the surface directly beneath the area of interest, whereas the particles measured at 9 km were likely to have originated from the surrounding areas. The atmospheric height of origin of the particles when released from an altitude of 1 km is between 0 and 4000m which is a significant area. To determine with greater accuracy how many particles were emitted from the surface, the model is set to release particles from an altitude of 1 km and run back 30 days and is to measure how many originated from the area of interest, between an altitude of 0 and 1 km.

The four areas of interest are; savannahs, woody savannahs, evergreen broadlands and grasslands in Africa. Particles are released at an altitude of 1 km, the model is then run backwards 30 days to determine the quantity of particles likely to have originated between 0 and 1 km.

NAME III (version 4.3)

Particles

From   0 – 1000m agl

1000Z 30/08/2003 to 1100Z 30/08/2003

Maximum value = 1.85e+06 INERT_BD1

1.00e+02   1.00e+03   1.00e+04   1.00e+05   1.00e+06   1.00e+07

Start of release: 1100UTC 30/08/2003   Pollutant: INERT_BD1
End of release: 1000UTC 30/08/2003   Met data: NWP Flow.Global
Release rate: Multiple Sources   Run time: 1349UTC 29/11/2008
Release location: Multiple Sources   Model run in backward mode
Release height: Multiple Sources

Met Office (GMR) Crown copyright

Figure 5.19; particle released over savannahs, south Africa. Particles released at 1km and followed back 30 days

NAME III (version 4.3)

Particles
From   0 – 1000m agl
1000Z 30/08/2003 to 1100Z 30/08/2003

Maximum value = 2.59e+06 INERT_BD1

1.00e+03   1.00e+04   1.00e+05   1.00e+06   1.00e+07   1.00e+08

Start of release: 1100UTC 30/08/2003   Pollutant: INERT_BD1
End of release: 1000UTC 30/08/2003   Met data: NWP Flow.Global
Release rate: Multiple Sources   Run time: 1640UTC 28/11/2008
Release location: Multiple Sources   Model run in backward mode
Release height: Multiple Sources
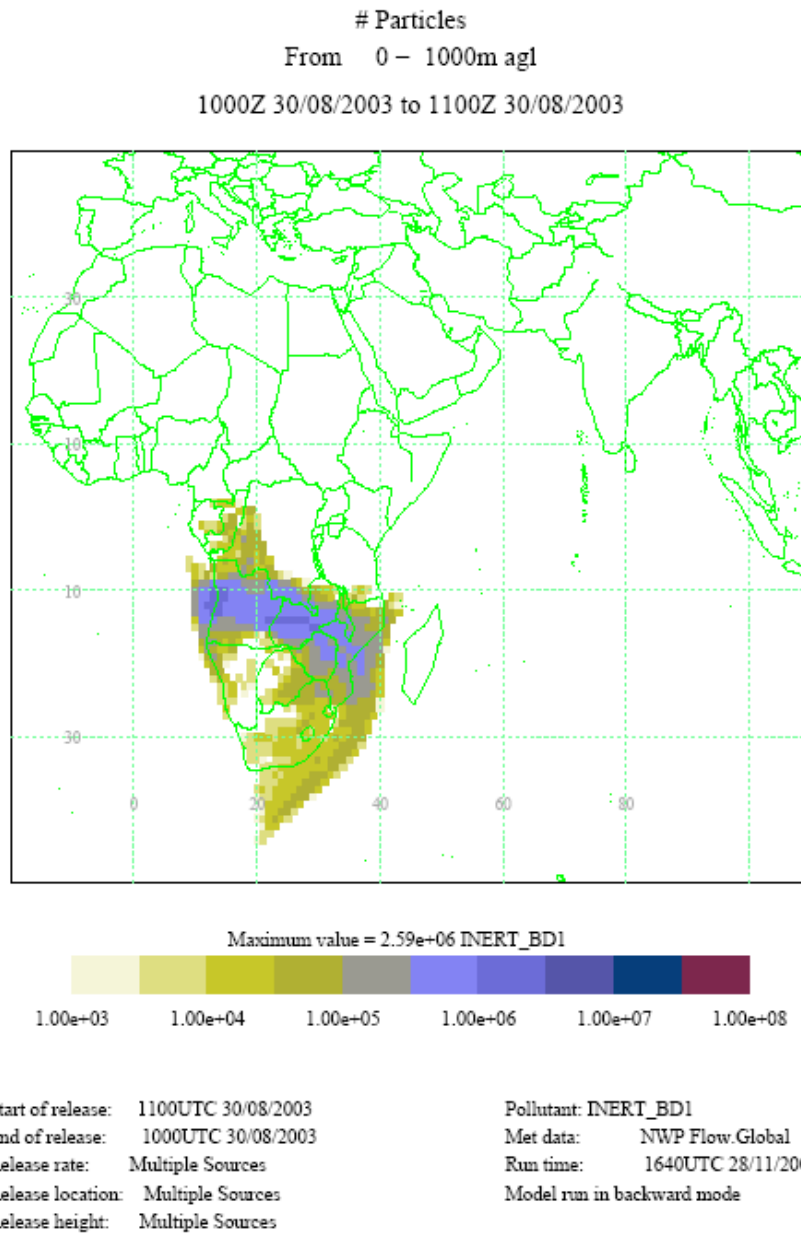
Met Office (GMR) Crown copyright

Figure 5.20; particle released over woody savannahs, south Africa. Particles released at 1km and followed back 30 days

NAME III (version 4.3)

Particles
From   0 – 1000m agl

1000Z 30/08/2003 to 1100Z 30/08/2003

Maximum value = 3.00e+06 INERT_BD1

1.00e+03   1.00e+04   1.00e+05   1.00e+06   1.00e+07   1.00e+08

Start of release: 1100UTC 30/08/2003   Pollutant: INERT_BD1
End of release: 1000UTC 30/08/2003   Met data: NWP Flow.Global
Release rate: Multiple Sources   Run time: 1325UTC 29/11/2008
Release location: Multiple Sources   Model run in backward mode
Release height: Multiple Sources
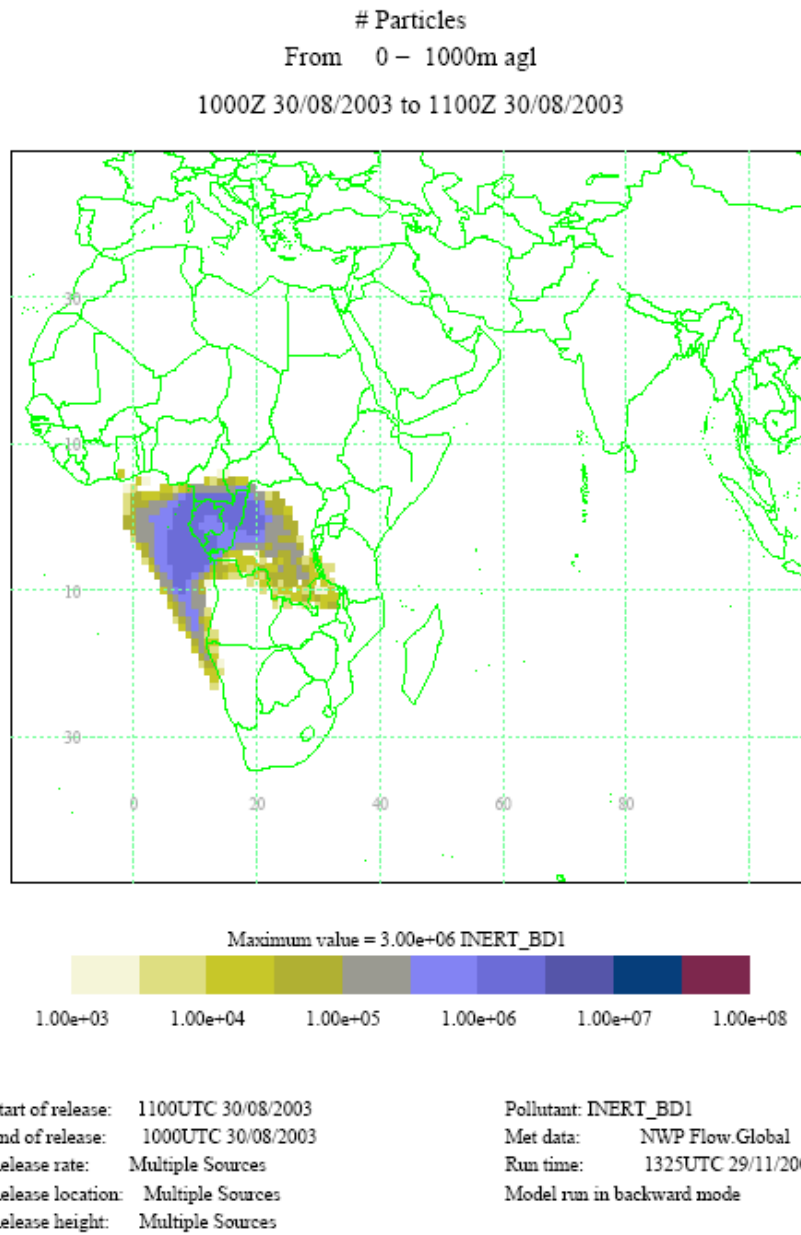
Met Office (GMR) Crown copyright

Figure 5.21; particle released over evergreen broadland, south Africa. Particles released at 1km and followed back 30 days

NAME III (version 4.3)

Particles
From   0 - 1000m agl
1000Z 30/08/2003 to 1100Z 30/08/2003

Maximum value = 4.00e+06 INERT_BD1

1.00e+03   1.00e+04   1.00e+05   1.00e+06   1.00e+07   1.00e+08

Start of release: 1100UTC 30/08/2003   Pollutant: INERT_BD1
End of release: 1000UTC 30/08/2003   Met data: NWP Flow.Global
Release rate: Multiple Sources   Run time: 1626UTC 28/11/2008
Release location: Multiple Sources   Model run in backward mode
Release height: Multiple Sources

Met Office (GMR) Crown copyright
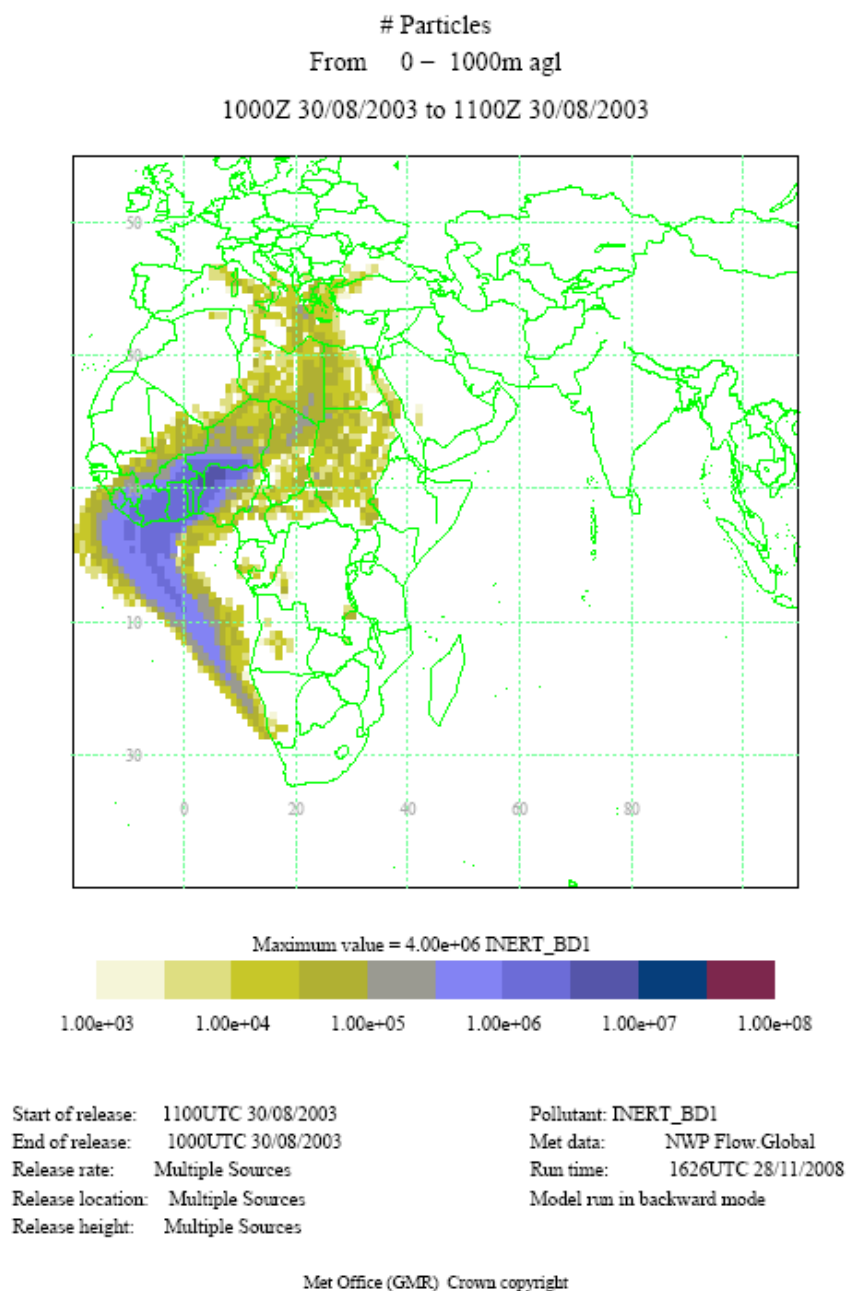
Figure 5.22; particle released over grassland, south Africa. Particles released at 1km and followed back
30 days

The four areas of interest show similar results to those produced measuring
between 0 and 4000 meters. The quantity of particles are similar to those
measured between 0 and 4000 meters, however the particles between 0 and
1000 meters are more concentrated.   The higher scatter area of particles

174

measured between 0 and 4000 meters indicates that the particles are mixing through the troposphere and the amount of particles likely to have been emitted from the surface directly beneath is reduced.

These results show that with increasing altitude (9 km) the likelihood of the particles being emitted from the surface directly beneath the area of interest decreases, and the probability of particles from neighbouring areas to be measured increases. Most importantly, it is seen that the majority of particles originate from the boundary layer in specific regions.

5.6 Conclusions.

The correlation between the vegetative green fraction (FGV) and the CO_2 concentration in the lower troposphere shows that a change in FGV prompts a change in CO_2 concentration, increasing the FGV value induces a decrease in CO_2 concentration in the surrounding region. The AIRS-LSQ measurements in the upper troposphere showed varied results, with poor correlations over the savannah, woody savannah and evergreen broadleaf area. The AIRS-LSQ measurements are sensitive to mid to upper tropospheric CO_2 measurements, which are where the CO_2 concentrations are thoroughly mixed, and are shown by the small amplitude variation of CO_2 throughout the year. Surface fluxes influence the seasonal cycles measured in the lower troposphere, which are not translated to the upper troposphere as the CO_2 is well mixed and an average CO_2 value of the surrounding areas are measured.

NAME is an important tool in determining how particles are distributed through the atmosphere and likely points of origin. When measuring CO_2 concentrations from satellite data it's imperative to take into consideration the likely origin of the particles. Measuring column CO_2 data not only measures the surface fluxes directly beneath the measurement, but also the surrounding CO_2 fluxes which are continuously mixing throughout the troposphere. The fluxes from neighbouring areas can have a significant affect on satellite

measurements, a strong anthropogenic source could effect a number of surrounding areas.

The SCIAMACHY and AIRS-LSQ data show that the FGV has a significant influence on the CO_2 concentration in the lower troposphere but has little to no direct effect on the concentrations measured directly above owing to the atmospheric mixing, through convection and wind. Using NAME to determine where the particles originated from will help verify if the CO_2 in the upper troposphere measured by AIRS-LSQ originated from the surface directly beneath or if it's a mean value of the CO_2 concentration from the surrounding regions.

Name results show that the CO_2 concentrations measured in the lower troposphere mainly originate from the surface below the area of interest, this is also evident as the seasonal cycles produced from SCIAMACHY data showed that the CO_2 concentration is dependent on the amount of FGV at the surface below. In the upper troposphere (9 km), NAME results showed that the particles originated from a multitude of regions, which is why the seasonal cycles produced from the AIRS-LSQ data showed little similarities to the CO_2 measured in the lower troposphere.

Combining the AIRS-LSQ, SCIAMACHY, FGV and NAME clearly showed that the CO_2 concentrations measured in the lower troposphere are those emitted from the surface area directly beneath the region measured. The upper troposphere CO_2 concentrations are a mixture of CO_2 concentrations from a multitude of surrounding regions of the area measured. The horizontal transport of the surrounding CO_2 into the areas to be measured is likely to influence the concentration of CO_2 measured by satellites.

Satellites such as SCIAMACHY which retrieve column CO_2, are not only likely to measure the surface fluxes but also a mixture of the surrounding CO_2 fluxes in the upper troposphere. AIRS-LSQ is sensitive to upper tropospheric CO_2 only. Subtracting the upper tropospheric (AIRS-LSQ data) column from the whole tropospheric column (SCIAMACHY data) will reduce the amount of CO_2 fluxes from surrounding areas, leaving the lower tropospheric column which is more likely to represent the surface fluxes with greater accuracy. When looking at tropospheric column data the CO_2 concentrations from surrounding areas must be

taken into account as these can significantly effect the measurements. The differences in seasonal cycles produced in the two tropospheric regions (AIRS-LSQ and SCIAMACHY retrievals) are likely caused by the mixing of the CO_2 from surrounding regions in the upper troposphere.

Subtracting the AIRS-LSQ column data from the SCIAMACHY column data, reduced the column to one which arguably represents the lower troposphere. This removes the background CO_2 concentrations, which as shown by NAME are imported from the surrounding regions and do not represent the CO_2 emitted by the surface directly beneath. The subtracted column showed that correlations between the FGV and the column (Table 5.3) were anti-correlated (with increasing FGV the CO_2 decreases owing to absorption by the vegetation). The results indicate that subtracting the mean background value, (which as shown by NAME the particles originate from areas outside the region of interest) produces a good representation of the CO_2 fluxes at the surface without the influence of the CO_2 particles from the surrounding regions.

Chapter 6

Conclusions and future work

6.1 Carbon dioxide in the atmosphere.

The atmospheric concentration of carbon dioxide has been steadily rising over the past 150 years from 280 to 380 ppmv in 2005 [Tiwari et al., 2005]. It is important to measure and monitor the concentration and distribution of the CO_2 within the atmosphere as CO_2 is a greenhouse gas which traps in thermal radiation which contributes to increasing the mean global temperature.

SCIAMACHY and AIRS provide vital information on the global distribution of CO_2 in the upper and lower tropospheric regions. Using the two satellites in conjunction with in-situ and model data, the distribution and concentration of CO_2 through the troposphere can be determined with greater accuracy. SCIAMACHY's measurements showed that the CO_2 in the lower troposphere is in a constant state of flux which is dependent on the seasons and the land type. AIRS data are impacted by the surface fluxes, but not necessarily from the surface directly below where the measurements are retrieved. The time taken for the CO_2 to traverse through the troposphere can take anywhere from hours to days to months, by which time the CO_2 is more completely mixed through the atmosphere. Satellites which are sensitive to measurements at higher altitudes are likely to measure the mean CO_2 concentration of the surface fluxes from the surrounding regions, which could be significantly different from the measurements retrieved at lower altitudes.

Satellite measurements in conjunction with in-situ measurements can provide invaluable information in determining the location of the sinks and sources with

greater accuracy. Determining how the CO_2 is distributed throughout the atmosphere is vital in determining where the greatest emissions are and where the sinks are located and if they can be increased to absorb more CO_2 from the atmosphere. Likely sinks are forests and oceans. If the satellites can determine over which areas the greatest amount of CO_2 is removed from the atmosphere, steps could be made to increase the magnitude of the sinks to remove more CO_2 from the atmosphere.

6.2 Measuring atmospheric carbon dioxide.

6.2.1 AIRS and SCIAMACHY CO_2 comparisons.

Measuring column CO_2 from SCIAMACHY and AIRS provides valuable information about how the CO_2 is distributed through the atmosphere. SCIAMACHY's retrievals are sensitive to CO_2 measurements in the lower troposphere, and AIRS retrievals are sensitive in the mid–upper troposphere. The SCIAMACHY retrievals provide information on the global surface fluxes whereas the AIRS data measures the mean CO_2 concentration of the atmosphere. By comparing the seasonal cycles measured from the two instruments, the time taken for the flux change at the surface to translate to the upper troposphere can be seen. Figures 3.7 to 3.17 & 4.12 to 4.14 show the seasonal cycles measured both in the upper and lower troposphere. The results showed that the AIRS seasonal cycle lags the seasonal cycle measured by SCIAMACHY in the lower troposphere by up to three months; the reader should note the two different AIRS products and two different years were used for comparison with the SCIAMACHY data, so the results are not directly comparable. The time lag in the upper tropospheric seasonal cycle shows that the CO_2 surface flux takes a significant amount of time to affect the mean upper tropospheric CO_2 concentration.

Correlation values between the AIRS and SCIAMACHY CO_2 column data were considerable in the northern hemisphere producing a value of 0.88 over North America. Regional comparisons in the southern hemisphere produced negative correlation values with South America (2004) producing the greatest anti-

correlation value of -0.59. Upper tropospheric seasonal cycles measured over the southern hemisphere showed cycles typical of those produced in the northern hemisphere, peaking between April and May and reaching minimum around September, thus the seasonal cycles measured in the southern hemisphere are out of phase in the upper and lower tropospheric regions. The seasonal cycles measured in the upper troposphere are clearly dominated by the CO_2 fluxes in the northern hemisphere, whereas the lower tropospheric cycles are influenced primarily by the land CO_2 fluxes.

6.2.2 Satellite and in-situ comparisons.

Measurements between satellite column CO_2 measurements and in-situ ground and aircraft data (which are measurements taken at specific altitudes) produced varied results. SCIAMACHY measurements over small areas were shown to be highly variable, producing correlation values between 0.19 and 0.85. Measurements produced by the AIRS instrument were fairly consistent when comparing the CO_2 data with aircraft data, producing correlation values up to 0.91. Amplitudes of the seasonal cycles measured by SCIAMACHY vary between 10.4 and 44.4 ppmv, the latter being a significant change of CO_2 over one region. These data suggest that either the resolution of the SCIAMACHY instrument is not sensitive enough to measure over small target areas with any accuracy, or that the fluxes within the regions measured are in a state of high flux causing the random results.

Comparisons of in-situ data with the AIRS retrievals produced reasonable results, seasonal cycles were smooth, (no random peaks or troughs measured) and the correlation values for 2003 and 2004 varied between 0.19 and 0.84, the low values can be attributed to the seasonal cycle lag (with respect to the surface seasonal cycle) and small amplitudes measured in the upper troposphere.

Measuring the atmospheric CO_2 daily with satellites and ground data at the same time of day (to avoid diurnal variations) could increase the accuracy of the

comparisons. The flux anomalies within the area measured by SCIAMACHY for the in-situ comparisons could be caused by the large area measured. The area measured could contain many different surface types, such as forestry, urban area and lakes, each of which contributes different quantities of CO_2 flux. Reducing the area measured by SCIAMACHY could reduce the anomalies in the retrievals attained.

6.2.3   Vegetation types and tropospheric carbon dioxide.

Chapter five showed comparisons of fractional green vegetation (FGV) with satellite CO_2 retrievals for both the upper and lower troposphere. The results show that, in general increasing the FGV decreased the CO_2 concentration in the surrounding tropospheric region, particularly in the lower tropospheric region. Different vegetation types produced different seasonal cycles, depending on their location (latitude) and the fraction of greenness (FGV). The greater the amplitude change of the FGV the greater the CO_2 amplitude measured in the lower troposphere (Figures 5.5 – 5.9). The influence of the annual amplitude variation and concentration of FGV on the CO_2 concentrations in the upper troposphere were negligible. AIRS data retrieved over each region showed little variation in the annual seasonal cycle; correlations between the AIRS CO_2 retrievals and the FGV over the majority of the regions were low.

Subtracting the AIRS from the SCIAMACHY CO_2 column retrievals, the data remaining represents the CO_2 fluxes in the lower troposphere, these data showed good anti-correlation with four of the vegetation types. These four vegetation types were the same vegetation types for which SCIAMACHY produced agreeable results, indicating that the subtracted data are a good representation of the CO_2 concentration in the lower troposphere.

6.2.4 Numerical atmospheric dispersion model (NAME).

NAME is a useful tool in examining the origins of particles in the atmosphere. Determining where particles from various tropospheric heights originated from helps determine how long the particle has been at a specific location and if the column data measured by the satellite is truly measuring the fluxes produced by the surface directly beneath or are they from another area.

Examining particles emitted in the upper and lower troposphere to determine if they were emitted from the surface beneath or if they are emissions from another area were determined in chapter 5. Results show that the particles measured in the lower troposphere were likely to have come from the surface within the column measured, the particles released in the upper troposphere showed to have multiple areas of emission. The time taken for the particles to reach the upper troposphere allows particles from various regions to mix owing to convection.

NAME could be used to determine the time taken for a particle to reach the upper troposphere which would help when measuring the column data in the upper troposphere if the CO_2 was emitted 5 days ago or 20 days ago, as the surface emission and absorptions concentrations vary daily and the time taken for the CO_2 flux to reach the upper troposphere affect the measurements retrieved by the satellites.

6.3 Future work.

The AIRS and SCIAMACHY data presented in this thesis shows that the SCIAMACHY data represents global CO_2 in the lower troposphere, where regional surface fluxes can be seen on a 3 x 3 degree grid, whereas the AIRS data represents the upper tropospheric mean global value. These data were combined, producing column data which represents CO_2 in the lower troposphere, this was achieved through subtracting the normalized AIRS column CO_2 from the normalized SCIAMACHY column. The results showed reasonable correlation with in-situ ground data. However the results can be vastly improved through re-

processing the AIRS retrievals through the same retrieval method as the SCIAMACHY. This would dramatically reduce the errors produced when combining the two retrieval methods.

The (FSI) WFM-DOAS retrieval method applied to the AIRS CO_2 channel data would produce a normalized CO_2 column, which would be subject to the same biases and errors the SCIAMACHY data are subject to [Barkley et al., 2006]. Subtracting the two columns using the same method would dramatically reduce the errors and the results produced would provide a more accurate representation of the CO_2 column in the lower troposphere. Systematic errors can also be reduced in the CO_2 column measurements through simultaneously retrieving the O_2 band (0.76 μm) by each instrument. Measuring the CO_2 and O_2 soundings simultaneously the dry air mole fraction (CO_2) can be calculated. XCO_2 (is the ratio of the CO_2 to O_2) will reduce the environmental uncertainties from the measurements, such as clouds, surface pressure, humidity and temperature [Crisp et al., 2004]. Time taken to process the data is significant, and selected target regions would be processed first, preferably over North America where the ground-based network for CO_2 retrievals is ample and the validation of the subtracted columns could be completed.

6.3.1 Future missions.

To improve upon the accuracy of measuring atmospheric CO_2 two new satellites are scheduled for launch in January 2009, these are the Orbiting Carbon Observatory (OCO) and Greenhouse gases Observing Satellite (GOSAT).

6.3.1.1 Observing Carbon Observatory (OCO).

The Orbiting Carbon Observatory (OCO) mission was intended to make the first global spaced based measurements of atmospheric CO_2 with precision, resolution and coverage needed to characterize CO_2 sources and sinks on regional scales.

OCO measures the intensity of reflected sunlight from the Earth's surface at specific wavelengths, CO_2 absorbs the reflected radiation at specific wavelengths, the OCO spectrometers will measure these change in the spectra, the level of absorption displayed in the spectra are indicative of the abundance of molecules in the region where the measurements were retrieved.

High-resolution spectroscopic observations of near infrared (IR) CO_2 absorption bands in reflected sunlight were selected as they provide high sensitivity near the surface where most of the sinks and sources are located.

Several factors besides the atmospheric CO_2 mole fraction contribute the CO_2 absorption intensity measured from space. These factors include the solar zenith angle, atmospheric temperature and humidity profiles, instrument pointing geometry and surface pressure. Clouds, aerosols and surface topography further complicate efforts to retrieve the CO_2 mole fractions from space-based CO_2 absorption measurements because they introduce additional uncertainties in the atmospheric optical path length. Accurate measurements are necessary to infer surface-atmosphere carbon fluxes from space based measurements.

OCOs objective is to retrieve global geographic distribution of CO_2 sources and sinks. The sinks and sources are not directly measured, assimilation of the retrieved data will produce column averaged dry air CO_2 mole fraction (XCO_2), which will infer the location of the sources and sinks.

OCO will retrieve XCO_2 from high-resolution spectroscopic measurements of reflected sunlight in the CO_2 bands at wavelengths near 1.61 μm and 2.06 μm and the O_2 A-band at 0.76 μm. O_2 is measured as a reference gas whose concentration is uniform and constant to calculate the dry air CO_2 mole fraction XCO_2 [Crisp et al., 2004].
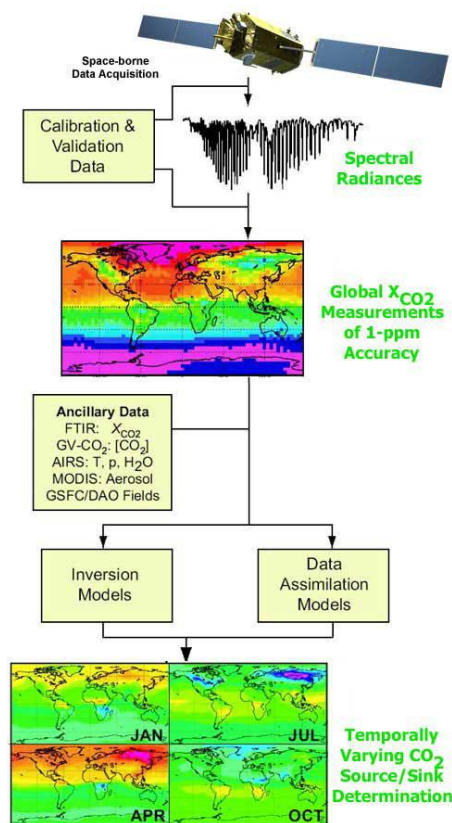
Figure 6.1; OCO instruments and retrieval and assimilation process.
http://oco.jpl.nasa.gov/science/dataproducts

OCO will acquire global data continuously over the entire daylight side of the Earth, XCO_2 global maps will be produced with an accuracy of 1 part per million (ppmv) on a 1 x 1 degree grid.

OCO will fly in a sun-synchronous orbit at an altitude of 705 km with a 1:15 pm equator crossing time. OCO will achieve full global coverage every sixteen days. An equator crossing is used to maximize the signal to noise of the XCO_2 measurements. And also the planetary boundary layer is deep and slowly varying, facilitating the efforts to validate the space-based CO_2 observations with ground based measurements.

6.3.1.2 Greenhouse Observing SATellite (GOSAT).

The Greenhouse gases Observing Satellite (GOSAT) will operate in a sun-synchronous polar orbit at an altitude of 666 km, with a local crossing time of about 1.00 pm (i.e. when the CO_2 column integral is about approaches its daily mean). The TANSO-FTS instrument will scan to $\pm$ 35° cross track and $\pm$ 25° along track, with a swath width of 790 km, with a nadir field of view of 10.5 km. Column measurements over the ocean will be made in a sun glint mode. Global coverage is achieved within 3 days providing 56,000 individual soundings. GOSAT is a satellite to monitor the carbon dioxide (CO_2) globally from orbit (Figure 6.2), and it aims to contribute to the international efforts to prevent global warming, such as the Kyoto Protocol.

The targets of the GOSAT mission are to measure 3-month atmospheric CO_2 column density with a 1% (4ppmv) relative accuracy in sub-continental spatial resolution and reduce the errors by 50% in identifying the GHGs sources and sinks in conjunction with ground based instruments on a sub-continental scale.
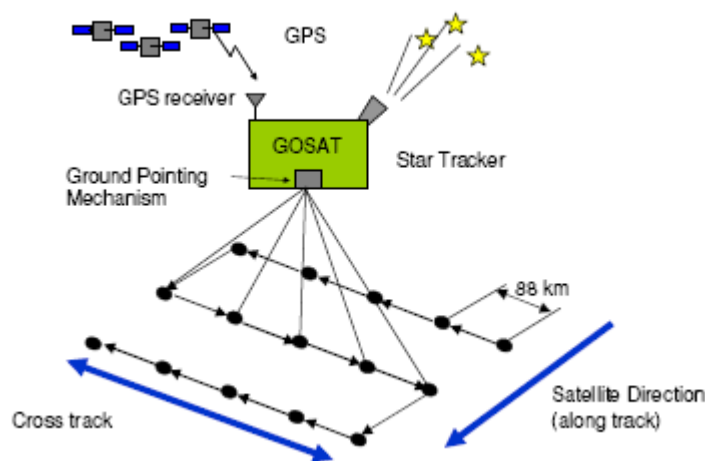
Figure 6.2; Viewing geometry of GOSAT. [Hamazakai, et al., 2004].

GOSAT is a Fourier Transform Spectrometer with high optical throughput and spectral resolution. The instrument detects the interferogram of solar short wave infrared spectra (SWIR) reflected on the earth's surface and thermal infrared

186

spectra (TIR) radiated from the ground and the atmosphere. The interferogram then are transformed with the fast Fourier transformation (FFT) algorithm into spectra, which include the absorption spectra of GHGs. GOSAT will measure the wide spectral range from 0.76 to 15 μm.

The main instrument on board GOSAT, is the Thermal And Near infrared Sensor for carbon Observation Fourier transform spectrometer (TANSO-FTS). This sensor measures reflected and scattered sunlight, at a spectral resolution of 0.2-0.5 cm^{-1}, in three channels (0.75–0.78 μm, 1.56–1.72 μm and 1.92–2.08 μm) and thermally emitted light (5.5–14.3 μm) in a fourth channel. The vertical column densities of CO_2 and CH_4 will be retrieved from the NIR channels (i.e. 1.6 μm and 2.0 μm bands) whilst the optical path length will be determined from the oxygen A-band (0.76 μm).

6.4 Conclusions

This thesis showed that the AIRS and SCIAMACHY instruments provides valuable information of global and regional transport and distributions of CO_2 through the atmosphere. Comparisons with in-situ data showed that the SCIAMACHY data retrieved is not sensitive enough to measure the surface fluxes at specific locations (for comparisons with ground based measurements). Comparisons of fractional green vegetation (FGV) with the SCIAMACHY data shows that different vegetation types can influence the surrounding CO_2 atmospheric concentrations, depending on the quantity of FGV. AIRS data, sensitive to upper tropospheric regions, measure the mean CO_2 atmospheric concentrations. SCIAMACHY retrievals were used to determine the concentration in the lower troposphere. Subtraction of the AIRS retrievals from the SCIAMACHY column data, results produced showed good correlations with in-situ measurements. Improvements can be made in calculating the lower tropospheric CO_2 concentration from the subtraction of the normalized column data (Section 6.3) these data could help determine the surface fluxes and locations of the sinks and sources with greater accuracy. SCIAMACHY and AIRS are

limited in their capabilities in measuring tropospheric CO2. OCO and GOSAT are specifically designed to measure the global atmospheric CO_2 concentrations. Using these new instruments, determining the locations of the sinks and sources and the distribution and transport of CO_2 within the tropospheric regions can be achieved with greater accuracy.

Appendix 1

Regional data for SCIAMACHY and AIRS data from 2003 and 2004.

2003 regional data

Region	Latitude min	Latitude max	Longitude min	Longitude max
Central Africa	0°	16°	-17°	54°
Gobi	35°	48°	96°	114°
India	4°	37°	70°	100°
North America	45°	84°	-170°	-51°
North Atlantic	20°	60°	-60°	-24°
Siberia	48°	80°	45°	180°
South Africa	-36°	0°	8°	42°
South America	-60°	15°	-90°	-30°
UK	42°	59°	-25°	14°

Table A: Coordinates for the regions investigated by SCIAMACHY and AIRS (Chapter 3)

Region	CO_2 minimum	CO_2 maximum	Mean CO_2	Amplitude	std dev difference	mean difference
Central Africa	365.43	383.73	374.32	18.30	4.67	3.99
Gobi	376.5	379.03	373.73	2.98	3.51	3.43
India	363.54	372.48	369.89	8.94	3.67	4.63
North America	364.91	376.41	369.51	11.50	3.95	6.95
North Atlantic	357.54	365.71	360.90	8.17	2.04	16.12
Siberia	361.58	382.92	368.56	21.34	5.89	6.33
South Africa	364.31	370.98	367.67	6.67	2.51	8.56
South America	365.11	368.38	365.19	3.27	1.65	9.66
UK	360.56	374.77	366.31	14.21	5.11	10.12

Table B: SCIAMACHY regional data for 2003 (Chapter 3) *All CO_2 values are in ppmv*

Region	CO_2 min	CO_2 max	Mean CO_2	Amplitude	correlation	CO_2 difference SCIAMACHY - AIRS
Central Africa	376.343	379.93	377.90	3.59	0.792	3.99
Gobi	376.23	379.81	377.48	3.59	0.219	7.59
India	376.52	380.52	377.92	4.0	0.495	8.27
North America	376.68	379.07	377.97	2.39	0.345	9.11
North Atlantic	375.79	378.79	365.99	2.99	0.644	5.08
Siberia	376.95	380.12	378.96	3.17	0.768	6.26
South Africa	376.62	378.10	377.36	1.48	0.868	8.71
South America	376.52	378.35	377.44	1.84	0.558	11.36
UK	374.88	379.08	376.43	4.2	-0.46	10.12

Table C: AIRS regional data 2003 (chapter 3) *All CO_2 values are in ppmv*

	minimum CO_2	Maximum CO_2	mean Year CO_2	CO_2 amplitude	Stddev
Central Africa	383.697	367.504	376.681	16.1924	9.6808
India	378.776	369.333	375.344	9.44235	9.80298
North America	377.596	364.854	371.932	12.7415	8.92834
Southern Africa	375.441	365.138	369.676	10.3024	7.00211
South America	373.212	366.475	368.775	6.73761	9.71503
Siberia	384.002	361.399	369.948	22.6029	7.6219

Table D: SCIAMACHY regional data 2004 (Chapter 4) *All CO_2 values are in ppmv*

	Minimum CO_2	Maximum CO_2	mean year CO_2	CO_2 amplitude	Stddev
Central Africa	377.941	375.439	376.632	2.50201	2.88535
India	377.963	375.525	377.17	2.43802	3.42864
North America	378.636	374.124	376.574	4.51199	1.80227
Southern Africa	375.717	374.433	375.09	1.284	1.91329
South America	375.675	374.469	375.263	1.20599	1.7169
Siberia	380.158	372.47	377.285	7.68799	1.84597

Table E: AIRS regional data 2004 (Chapter 4) *All CO_2 values are in ppmv*

Appendix 2

The Numerical Application modEl (NAME).

The NAME model was originally called the Nuclear Accident ModEl it was developed for emergency response purposes. NAME was implemented operationally for generating forecasts in the event of major atmospheric releases such as nuclear accidents and volcanic eruptions. Its applications were also used for a wide range of air quality problems, such as understanding PM_{10} transport to the UK [Malcolm et al., 2000] and following the trace gases over Mace Head [Ryall et al., 2001a]. NAME has been modified and has been re-named the Numerical Atmospheric Dispersion ModEl, which is used to predict the transport of airborne pollutants over range of a few kilometres to thousands of kilometres. NAME was produced and is used by the MET office and to forecast global weather and its other applications include simulating plume rise, boundary layers and upper level transport. Three dimensional trajectories of air parcels are used to compute air concentrations and ground deposits, (further information see www.metoffice.gov.uk/environment/name.html).

NAME uses a Lagrangian particle model, with three hourly 3-dimensional meteorology fields from the complex numerical weather prediction model, the unified model, UM [Cullen., et al 1993]. The unified model is used to move the abstract particles around the model's domain. At each fifteen minute time step the three dimensional model flow is interpolated to each particle position, this process is done using a random walk technique. Each particle in the model run moves under the influence of the mean flows, these include wind meander and sub-grid turbulence. To simulate turbulent motion, a random walk technique [Thomson., 1987] uses velocity variance and Lagrangian timescale profiles which are determined from empirical fits to observational data is used. Gaussian velocity distributions are assumed and the components of the turbulent motion are assumed uncorrelated. The model simulates the enhanced mixing particles within convective cloud.

At each time step a two dimensional field of the boundary layer height is calculated using a combination of the parcel method and the conventional gradient Richardson technique [Verver and Holtslag., 1992].

Improvements are currently being made to the NAME model which will be released within the next few years and will be the third upgrade (NAME III). NAME III will have enhanced capabilities, including improved modelling of short range dispersion, such as building effects on particle dispersion. It will also provide a unified approach to dispersion modelling applicable from local scales of a few meters up to a global scale, which can be used for emergency responses to environmental impact assessment.

References.

Alkhaled. A. A., Michalak. A. M., and Kawa. S. R.:Using CO_2 spatial variability to quantify representation errors of satellite CO_2 retrievals, Geophys. Res. Lett. 35, doi:1029/2008GL034528, 2008.

Aumann, H. H., Gregorich, D., Gaiser, S.: AIRS hyper-spectral measurements for climate research: Carbon dioxide and nitrous oxide effects, Geophys. Res. Lett, 32, L05806, doi:10.1029/2004GL021784, 2005.

Aumann, H. H., Broberg., S., Elliott., D., Gaiser, S., and Gregorich, D.: Three years of Atmospheric Infrared Sounder radiometric calibration validation using sea surface temperatures, J. Geophys. Res., 111, D16S90, doi:10.1029/2005JD006822, 2006.

Barkley, M. P., Frieß, U., and Monks, P. S.: Measuring atmospheric CO_2 from space using Full Spectral Initiation (FSI) WFM-DOAS, Atmos. Chem. Phys., 6, 3517–3534, 2006a.

Barkley, M. P., Monks, P. S., Frieß, U., Mittermeier, R. L., Fast, H., Korner, S., and Heimann, M.: Comparisons between SCIAMACHY atmospheric CO_2 retrieved using (FSI) WFM-DOAS to ground based FTIR data and the TM3 chemistry transport model, Atmos. Chem. Phys., 6, 4483–4498, 2006b.

Barkley M. P., P. S. Monks, R. J. Engelen (2006), Comparison of SCIAMACHY and AIRS CO_2 measurements over North America during the summer and autumn of 2003, Geophys. Res. Lett., 33, L20805, doi:10.1029/2006GL026807.], 2006c.

Barkley. M. P., Monks. P. S., Hewitt. A. J., Machida. T., Desai. A., Vinnichenko. N., Nakazawa. T., Arshinov. M. Yu., Fedoseev. N., and Watai. T.: Assessing the near surface sensitivity of SCIAMACHY atmospheric CO_2

retrieved using (FSI) WFM-DOAS, Atmos. Chem. Phys., 7, 3597-3619, 2007.

Barnet, C. D., M. Goldberg, L. McMillin, E. S. Maddy and M. T. Chahine 2005. Remote sounding of trace gases from advanced sounders. FTS/ HISE, *OSA technical Digest* (Optical Soc. Amer.) 3 pgs. (paper HMC3)

Barnet, C. D., M. Goldberg, L. M. McMillin and M. T. Chahine 2004. Remote sounding of trace gases with the EOS/ AIRS instrument. *SPIE* **5548** p. 300- 312.

Barnet, C. D., S. Datta and L. Strow 2003. Trace gas measurements from the atmospheric infrared sounder (AIRS). Optical Remote Sensing, *OSA Technical Digest* p. 89- 92.

de Beek R., Buchwitz. M., Noel. S., Burrows. J. P., Bovensmann. H., Bruns. M., Bremer. H., Bergamaschi. P., Korner. S., and Heimann. M.: Atmospheric carbon gases retrieved from SCIAMACHY by WFM-DOAS: improved global CO and CH_4 and initial verification of CO_2 over Park Falls (46_ N, 90_ W), Atmos. Chem. Phys. Discuss., 6, 363-399, 2006.

Bolin, B., Sukumar, R., P. Cais., W. Cramer., P. Jarvis., H. Kheshgi., C. Nobre., S. Semenov., W. Steffen, 2000: Global perspective. In IPCC, land use, land-use change and forestry. A special report of the IPCC {Watson et al]. Cambridge university press, Cambridge, UK, pp 23-51.

Bond, T. C., Streets, D. G., et al (2004)A technology- based global inventory of black and organic carbon emissions from combustion, J. Geophys. Res., 109, D14203, 10.1029/2003JD003697,2004.

Breon, F. M. and Peylin, Ph.: The potential of spaceborne remote sensing to contribute to the quantification of anthropogenic emissions in the frame of the Kyoto protocol, ESA study 15247/01/NL/MM, 2003.

Buchwitz, M. and Burrows, J. P.: Retrieval of CH_4, CO, and CO_2 total column amounts from SCIAMACHY near-infrared nadir spectra: Retrieval algorithm and first results, in: Remote Sensing of Clouds and the Atmosphere VIII, Proceedings of SPIE, edited by chafer, K. P., Comeron, A., Carleer, M. R., and Picard, R. H., vol. 5235, pp. 375–388, 2004.

Buchwitz, M., Rozanov, V. V., and Burrows, J. P.: A near infrared optimized DOAS method for the fast global retrieval of atmospheric CH_2, CO, CO_2, C_2O, and N_2O total column amounts from SCIAMACHY/ENVISAT-1 nadir radiances, J. Geophys. Res., 105, 15 231–15 246, 2000.

Buchwitz, M., de Beek, R., Bramstedt, K., N¨oel, S., Bovensmann, H., and Burrows, J. P.: Global carbon monoxide as retrieved from SCIAMACHY by WFM-DOAS, Atmos. Chem. Phys., 4, 1945–1960, 2004.

Buchwitz, M., de Beek, R., Burrows, J. P., Bovensmann, H., T.Warneke, Notholt, J., Meirink, J. F., Goede, A. P. H., Bergamaschi, P., K¨orner, S., Heimann, M., and Schulz, A.: Atmospheric methane and carbon dioxide from SCIAMACHY satellite data: initial comparison with chemistry and transport models, Atmos. Chem. Phys., 5, 941–962, 2005a.

Buchwitz, M., de Beek, R., N¨oel, S., Burrows, J. P., Bovensmann, H., Bremer, H., Bergamaschi, P., K¨orner, S., and Heimann, M.: Carbon monoxide, methane and carbon dioxide columns retrieved from SCIAMACHY by WFM-DOAS: year 2003 initial data set, Atmos. Chem. Phys., 5, 3313–3329, 2005b.

Buchwitz, M., de Beek, R., No¨el, S., Burrows, J. P., Bovensmann, H., Schneising, O., Khlystova, I., Bruns, M., Bremer, H., Bergamaschi, P., K¨orner, S., and Heimann, M.: Atmospheric carbon gases retrieved from SCIAMACHY by WFM-DOAS: version 0.5 CO and CH_4 and impact of calibration improvements on CO_2 retrieval, Atmos. Chem. Phys., 6, 2727–2751, 2006.

Buchwitz, M., Schneisind, O., Burrows, J. P., Bovensmann, H., Notholt, J.: First direct observation of the atmospheric CO_2 year-to-year increase from space, Atmos. Chem. Phys., 7, 6791-6735, 2007.

Cantrell, C. A.: Technical note: Review of methods for linear least-squares fitting of data and application to atmospheric chemistry problems, Atmos. Chem. Phys. Discuss., 8, 6409-6436, 2008.

Chahine, M., Barnet, C., Olsen, E. T., Chen, L., and Maddy, E.: On the determination of atmospheric minor gases by the method of vanishing partial derivatives with application to CO_2, Geophys. Res. Letts., 32, L22 803, doi:10.1029/2005GL024 165, 2005.

Chahine, M., Chen. L., Dimotakis. P., Jiang. X., Qinbin. L., Olsen. E. T., Pagano. T., Randerson. J., and Yung. Y .L.: Satellite remote sounding of mid-tropospheric CO_2, Geophys. Res. Lett, 35, L17807, doi:10.1029/2008GL035022, 2008.

Chan. D., Ishizawa. M., Higuchi. K., Maksyutov. S., and Chen. J.: Seasonal CO_2 rectifier effect and large-scale extratropical atmospheric transport, J. Geophys, Res, 113, D17309, doi:10.1029/2007JD009443, 2008.

Chedin, A., Hollingsworth, A., Scott, N. A., Serrar, S., Crevoisier, C., and Armante, R.: Annual and seasonal variations of atmospheric CO_2, N_2O and CO concentrations retrieved from NOAA/TOVS satellite observations, Geophys. Res. Letts., 29, NO. 8, 1269, 10.1029/2001GL014 082, 2002.

Chedin, A., Saunders, R., Hollingsworth, A., Scott, N. A., Matricardi, M., Etcheto, J., Clerbaux, C., Armante, R., and Crevoisier, C.: The feasibility of monitoring CO_2 from high-resolution infrared sounders, J. Geophys. Res., 108, 4064, doi:10.1029/2001JD001 443, 2003a.

Chedin, A., Serrar, S., Scott, N. A., Crevoisier, C., and Armante, R.: First global measurement of midtropospheric CO_2 from NOAA polar satellites:

Tropical zone, J. Geophys. Res., 108, NO. D18, 4581, doi:10.1029/2003JD003 439, 2003b.

Chevallier, F., Engelen, R. J., and Peylin, P.: The contribution of AIRS data to the estimation of CO_2 sources and sinks, Geophys. Res. Letts., 32, L23 801, doi:10.1029/2005GL024 229, 2005.

Christi, M. J., and Stephens, G. L.: Retrieving profiles of atmospheric CO_2 in clear sky and in the presence of thin cloud using spectroscopy from the near and thermal infrared: A preliminary case study, J. Geophys. Res., 109, D04316, doi:10.1029/2003JD004058, 2004.

Conway, T. J., P. P. Tans., L. S, Waterman., K. W. Thining., D. R. Kitzis., K. A. Masarie and N. Zhang, 1994: Evidence for interannual variability of the carbon cycle from NOAA/CMDL global air sampling network. J. Geophys research, 99, 22831-22855.

Cooke, W.F., C. Liousse, H. Cachier, and J. Feichter, 1999: Construction of a 1° x 1° degree fossil fuel emission data set for carbonaceous aerosol and implementation and radiative impact in the ECHAM4 model. J. Geophys. Res, 104, 22,137-22,162.

Crevoisier, C., Heilliette, S., Ch´edin, A., Serrar, S., Armante, R., and Scott, N. A.: Midtropospheric CO_2 concentration retrieval from AIRS observations in the tropics, 31, L17 106, doi:10.1029/2004GL020 141, 2004.

Crisp. D., Atlas. R. M., Breon. F. –M., Brown. L. R., Burrows. J. P., Ciais. P., Connor. B. J., Doney. S. C., Fung. I. Y., Jacob. D. J., Miller. C. E., O'Brien. D., Pawson. S., Randerson. J. T.,Rayner. P., Salawitch. R. J., Sander. S. P., Sen. B., Stephens. G. L., Tans. P., Toon. G. C., Wennberg. P. O., Wofsy. S. C., Fung. L. Y., Kuang. Z., Chudasama. B., Spague. G., Weiss. B., Pollock. R., Kenyon. D., Schroll. S.: The Orbiting Carbon Observatory (OCO) mission, COSPAR, doi:10.1016/j.asr.2003.08.062, 2004.

Cullen, M. J. P., The unified Forecast/Climate Model, Meteorol. Mag., 1449, 81-94, 1993

Denman, K., E. Hofmann and H. Merchant., 1996: Marine biotic responses to environmental change and feedback to climate, In : Climate change 1995. The sience of climate change [Houghton et al], Cambridge university press, Cambridge, Uk, pp 449-481.

Denman, K., et al., 2007: Marine biotic responses to environmental change and feedback to climate, In: Climate change 2007. The sience of climate change [Houghton et al], Cambridge university press, Cambridge, Uk.

Dils, B., De Maziere, M., M¨uller, J. F., Blumenstock, T., Buchwitz, M., de Beek, R., Demoulin, P., Duchatelet, P., Fast, H., Frankenberg, C., Gloudemans, A., Griffith, D., Jones, N., Kerzenmacher, T., Kramer, I., Mahieu, E., Mellqvist, J., Mittermeier, R. L., Notholt, J., Rinsland, C. P., Schrijver, H., Smale, D., Strandberg, A., Straume, A. G., Stremme, W., Strong, K., Sussmann, R., Taylor, J., van den Broek, M., Velazco, V., Wagner, T., Warneke, T., Wiacek, A., and Wood, S.: Comparisons between SCIAMACHY and ground-based FTIR data for total columns of CO, CH_4, CO_2 and N_2O, Atmos. Chem. Phys., 6, 1953–1976, 2006.

Dufour, E. and Breon, F.: Spaceborne estimate of atmospheric CO_2 column by use of the differential absorption method: error analysis, Appl. Opt., 42, 3595–3609, 2003.

Engelen, R. J. and McNally, A. P.: Estimating atmospheric CO_2 from advanced infrared satellite radiances within an operational four-dimensional variational (4DVar) data assimilation system: Results and validation, J. Geophys. Res., 110, D18 305, doi:10.1029/2005JD005 982, 2005.

Engelen, R. J., Andersson, E., Chevallier, F., Hollingsworth, A., Matricardi, M., McNally, A. P., Th´epaut, J.-N., and Watts, P. D.: Estimating atmospheric CO_2 from advanced infrared satellite radiances within an

operational 4D-Var data assimilation system: Methodology and first results, J. Geophys. Res., 109, D19 309, doi:10.1029/2004JD004 777, 2004.

Engelen, R. J., and A. P. McNally (2005), Estimating atmospheric CO_2 from advanced infrared satellite radiances within an operational four-dimensional variational (4D-Var) data assimilation system: Results and validation, J. Geophys. Res., 110, D18305, doi:10.1029/2005JD005982, 2005.

Fischer, H., M. Wahlen., J. Smith, D. Mastroianni and B. Deck, 1999: Ice core records of atmospheric CO_2 around the last three glacial transitions: Sciance, 283, 1712-1714.

Font. A., Morgui. J. A., and Rodo. X.: Atmospheric CO_2 in situ measurements: Two examples of crown Design flights in NE spain, J. Goephys. Res, 113, doi:10.1029/2007JD009111, 2008

Friedlingstein, P., Bopp, L., Ciais, P., et al., positive feedback between future climate change and the carbon cycle. Geophysical Research letters, 28, 1543-1547, 2001.

Friedlingstein, P., et al. Climate-carbon cycle feedback analysis from the C4MIP model intercomparison, J. Clim., 19, 3337-3353. 2006.

Gerber. S., Joos. F., and Prentice. I. C.: Sensitivity of a dynamic global vegetation model to climate and atmospheric CO_2, Global change biology, 10, 1223-1239, doi:101111/j.1365-2486.2004.00807., 2004.

GLOBALVIEW- CO_2: Cooperative Atmospheric Data Integration Project – Carbon Dioxide. CD-ROM, NOAA CMDL, Boulder, Colorado [Also available on Internet via anonymous FTP to ftp.cmdl.noaa.gov, Path:ccg/co2/GLOBALVIEW], 2005.

Gurney, K. R., Law, R. M., Denning, A. S., Rayner, P. J., Pak, B. C., Baker, D., Bousquet, P., Bruhwiler, L., Chen, Y.-H., Ciais, P., Fung, I. Y., Heimann,

M., John, J., Maki, T., Maksyutov, S., Peylin, P., Prather, M., and Taguchi, S.: Transcom 3 inversion intercomparison: Model mean results for the estimation of seasonal carbon sources and sinks, Global Biogeochemical Cycles, 18, GB1010, doi:10.1029/2003GB002 111, 2004.

Gutman, G. and A. Ignatov, 1997: Derivation of green vegetation fraction from NOAA/AVHRR for use in numerical weather prediction models. Manuscript available from Garik Gutman at ggutman@nesdis.noaa.gov.

Houghton, J. T., Ding, Y., Griggs, D., Nouguer, M., Van der Linden, P., Dai, X., Maskell, K., Johnson, C., IPCC, 2001:climate change 2001: The scientific basis. Contribution of working group I to the third assessment report of the International Panel on Climate Change, Cambridge university press, Cambridge, UK, New york, USA 881pp.

Houghton, J., Global Warming, Rep, Prog. Phys., 68, 1343–1403, 2005.

Houweling, S., Hartmann, W., Aben, I., Schrijver, H., Skidmore, J., Roelofs, G.-J., and Breon, F.-M.: Evidence of systematic errors in SCIAMACHY-observed CO_2 due to aerosols, Atmos. Chem. Phys., 5, 3003–3013, 2005.

Houweling, Breon, F.-M., Aben, I., Rodenbeck. C., Gloor. M., Heinmann. M., and Ciais. P.: Inverse modeling of CO_2 sources and sinks using satellite data: a synthetic inter-comparison of measurement techniques and their performance as a function of space and time, Atmos. Chem. Phys., 4, 523-538, 2004.

Huang, X.: Spatial and spectral variability of the outgoing thermal IR spectra from AIRS: A case study of July 2003, J. Geophys. Res., 110, D12102, doi:10.1029/2004JD005530, 2005.

Huete, A., Didan, K., Miura, T., Rodriguez, E. P., Gao, X., and Ferreira, L. G.: Overview of the radiometric and biophysical performance of the MODIS vegetation indices, Remote Sensing of the Environment, 83, 195–213, 2002.

IPCC: Climate change: The IPCC scientific assessment, J.T. Houghton, G.J. Jenkins and J.J. Ephraums., Cambridge University Press, Cambridge. 1990.

Intergovernmental Panel on Climate Change (IPCC) (2001), Climate Change 2001: The Scientific Basis, edited by J. T. Houghton et al., Cam-bridge Univ. Press, New York.

IPCC: Climate Change 2001: Synthesis Report: Third Assessment Report of the Intergovernmental Panel on Climate Change, Cambridge University Press, New York, 2001.

IPCC: 16 years of scientific assessment in support of the climate convention, IPCC, Geneava. 2004

IPCC: Climate Change 2007: Synthesis Report: Fourth Assessment Report of the Intergovernmental Panel on Climate Change, Cambridge University Press, New York, 2007

Indermuhle, A., T. F. Stocker., F. Joss., H. Fischer., H. J. Smith., M. Winton., B. Deck., D. Mastroianni., J. Tschumi., T. Blunier., R. Meyer., and B. Staulter, 1999: Holocene carbon cycle dynamics based on CO_2 trapped in ice at taylor dome, Antarctica, Nature, 398, 121-126.

Jain, A. K., Tao, Z., Yang, X., and Gillespie, C.: Estimates of biomass burning emissions for reactive greenhouse gases (CO, NMHCs, and NO_x) and CO_2, J. Geophys. Res, 111, D06304, doi:10.1029/2005JD006237, 2006.

Jiang. Z., Huete. A. R., Chen. J., Chen. Y., Li. J., Yan. G., Zhang. X.: Analysis of NDVI and scaled difference vegetation index retrievals of vegetation fraction, doi:10.1016/j.rse.2006.01.003, 2006.

Keeling, C. D., whorf T. P.,Wahlen, M., and van der Plicht, J.: Interannual extremes in the rate of rise of atmospheric carbon dioxide since 1980, Nature, 375(6533), 666–670, 1995.

Keeling,C.D., Whorf, T.P., 2000. Atmospheric CO_2 concentrations F Loa Observatory,Hawaii,1958   1999 (revised August 2000).CDIAC NDP-001 (http://cdiac.esd.ornl.gov/ndps/ndp001.html),Carbon Dioxide Information and Analysis Center, Oak Ridge, TN.

Keeling, C. D., and T. P. Whorf (2004), Atmospheric CO_2 records from sites in the SIO air sampling network, in Trends: A Compendium of Data on Global Change, Carbon Dioxide Inf. Anal. Cent., Oak Ridge Natl.Lab., U. S. Dep. of Energy, Oak Ridge, Tenn.

Keeling, C. D., R. B. Bacastow, and T. P. Whorf (1982), Measurements of the concentration of carbon dioxide at Mauna Loa Observatory, Hawaii, in Carbon Dioxide Review: 1982, edited by W. C. Clark, pp. 377– 385, Oxford Univ. Press, New York.

Keeling, C. D., J. F. S. Chin, and T. P. Whorf (1996), Increased activity of northern vegetation inferred from atmospheric CO_2 measurements, Nature, 382(6587), 146– 149.

Keeling, C. D., P. R. Guenther, G. I. Emanuele, A. Bollenbacher, and D. J. Moss (2002), Scripps reference gas calibration system for carbon dioxide-in-nitrogen and carbon dioxide-in-air standards: Revision of 1999 (with addendum), Scripps Inst. of Oceanogr., La Jolla, Calif.

Kettle, H., and Merchant, C. J.: Systematic errors in global air-sea CO_2 flux caused by temporal averaging of sea-level pressure, Atmos. Chem. Phys., 5, 1459-1466, 2005.

Kiehl, J. T. and Trenberth, K. E.: Earth's Annual Global Mean Energy Budget, Bulletin of the American Meteorological Society, 78, 197–208, 1997.

Kneizys, F. X., Abreu, L. W., Anderson, G. P., Shettle, E. P., Chetwynd, J. H., Shettle, E. P., Berk, A., Bernstein, L., Robert-son, D., Acharya, P., Rothman, L., Selby, J. E. A., Allery, W. O., and Clough, S. A.: The

MODTRAN 2/3 report and LOWTRAN 7 model, Tech. rep., Philips Laboratory, Hanscom AFB, 1996.

Knyazikhin, Y., Glassy, J., Privette, J. L., Tian, Y., Lotsch, A., Zhang, Y., Wang, Y., Morisette, J. T., P.Votava, Myneni, R. B., and R. R. Nemani, S. W. R.: MODIS Leaf Area Index (LAI) And Fraction Of Photosynthetically Active Radiation Absorbed By Vegetation (FPAR) Product (MOD15) Algorithm Theoretical Basis Document Version 4.0, 1999.

Lenton, T. M. and Huntinford, C., Global terrestrial carbon storage and uncertainties in its temperature sensitivity examined with a simple model. Global Change Biology, 9, 1333-1352. 2003.

Le Quere. C., Aumont. O., Bopp. L., Bousquet. P., Ciais. P., Francey. R., Heimann. M., Keeling. C. D., Keeling. R. F., Kheshgi. H., Peylin. P., Piper. S. C. Prentice. I. C., and Rayner. P. J.: Two decades of ocean CO_2 sink and variability, Tellus, 55B, 649-656, 2003.

Le Treut, H., R. Somerville, U. Cubasch, Y. Ding, C. Mauritzen, A. Mokssit, T. Peterson and M. Prather, 2007: Historical Overview of Climate Change. In: *Climate Change 2007: The Physical Science Basis. Contribution of Working Group I to the Fourth Assessment Report of the Intergovernmental Panel on Climate Change* [Solomon, S., D. Qin, M. Manning, Z. Chen, M. Marquis, K.B. Averyt, M. Tignor and H.L. Miller (eds.)]. Cambridge University Press, Cambridge, United Kingdom and New York, NY, USA.

Lintner, B. R., W. Buermann, C. D. Koven, and I. Y. Fung (2006), Seasonal circulation and Mauna Loa CO_2 variability, J. Geophys. Res., 111, D13104, doi:10.1029/2005JD006535, 2005.

Liousse, C., J. E. Penner., C. C. Chung., J. J. Walton, and H. Eddleman., 1996, A global three dimensional study of carbonaceous aerosols. J. Geophys. Res., 101, 19411-19432.

Lorenc, A. C. (1986), Analysis methods for numerical weather prediction, Q. J. R. Meteorol. Soc., 112, 1177– 1194.

Macatangay. R., Warneke. T., Gerbig. C., Korner. S., Ahmadov. R., Heimann. M., and Notholt. J.: A framework for comparing remotely sensed and in-situ CO_2 concentration, Atmos. Chem. Phys., 8, 2555-2568, 2008.

Maddy, E. S., C. D. Barnet, L. M. McMillin, M. Goldberg and M. T. Chahine 2005. Investigating the separability of temperature and CO_2 from operational hyper- spectral sounders. FTS/ HISE, *OSA Technical Digest* (Optical Soc. Amer.) 3 pgs. (paper HTuD10)

Maddy, E. S., and C. D. Barnet (2008), Vertical resolution estimates in version 5 of AIRS operational retrievals, IEEE Trans. Geosci. Remote Sensing, in press.

Maddy, E. S., C. D. Barnet, L. McMillin, M. Goldberg, and M. Chahine (2005), Investigating the separability of temperature and CO_2 from operational hyperspectral sounders, in Fourier Transform Spectroscopy/Hyperspectral Imaging and Sounding of the Environment FTS/HISE, Tech. Dig. CD, edited by Optical Society of America, p. HTuD10, OSA Technical Digest Series, Washington, D. C.

Malcolm, A. L., Derwent, R. G., and Maryon, R. H., Modelling the longrange transport of secondary PM_{10} to the UK, Atmos. Environ., 34, 881-894, 2000.

Manning,A. J., Ryall, D. B., and Derwent, R. G.: Estimating Euopean emissions of ozone-depleting and greenhouse gases using observation and a modeling back-attribution technique, J. Geophys. Res, 108, D14, 4405, doi:10.1029/2002JD002312, 2003.

Manning, A.C. and Keeling, R.F. (2006) Global oceanic and land biotic carbon sinks from the Scripps atmospheric oxygen flask sampling network, Tellus-B, 58B, 95-116, doi:10.1111/j.1600-0889.2006.00175.x.

Marland, G., T.A. Boden, and R. J. Andres, 2003. Global, Regional, and National CO_2 Emissions. In Trends: A Compendium of Data on Global Change. Carbon Dioxide Information Analysis Center, Oak Ridge National Laboratory, U.S. Department of Energy, Oak Ridge, TN, USA.

Marland, G. et al., Trends, Carbon Dioxide Information Analysis Center, Oak Ridge Nat. Lab., U.S.DOE, Oak Ridge, TN (2006).

Matricardi, M., F. Chevallier, G. Kelly, and J.-N. The´paut (2004), An improved general fast radiative transfer model for the assimilation of radiance observations, Q. J. R. Meteorol. Soc., 130, 153–173, doi:10.1256/qj.02.181.

Matsueda, H., Inoue, H. Y., and Ishii, M.: Aircraft observations of carbon dioxide at 8-13km altitude over the western Pacififc from 1933 to 1999, Tellus, 54B, 1–21, 2002.

McElroy,. "The Ocean Carbon Cycle". Main Article: "The Great Global Experiment," November-December 2002.
http://harvardmagazine.com/2002/11/the-ocean-carbon-cycle.html

McNally, A. P., and P. D. Watts (2003), A cloud detection algorithm for high-spectral-resolution infrared sounders, Q. J. R. Meteorol. Soc., 129, 3411 –3423, doi:10.1256/qj.02.208.

McNally, A. P., P. D. Watts, J. A. Smith, R. J. Engelen, G. A. Kelly, J.-N. Thepaut, and M. Matricardi (2005), The assimilation of AIRS radiance data at ECMWF, Q. J. R. Meteorol. Soc., vol. 132a, number 616. pp935-957. 2006

Miller. C. E., Crisp. D., Decola. P. L., Olsen. S. C., Randerson. J. T., Michalak. A. M., Alkhaled. A., Rayner. P., Jacob. D. J., Suntharalingam. P., Jones. D. B. A., Denning. A. S., Nicholls. M. E., Doney. S. C., Pawson. S., Boesch. H., Connor. B. J., Fung. I. Y., O'Brien. D., Salawitch. R. J., Sander. S. P., Sen. B., Tans. P., Toon. G. C., Wennberg. P. O., Wofsy. S. C., Yung.

Y. L., and Law. R. M.: Precision requirements for space-based XCO_2 data, J. Geophys. Res., 112, D10314, doi:10.1029/2006JD007659, 2007.

Nakazawa, T., Miyashita, K., Aoki, S., and Tanaka, M.: Temporal and spatial variations of upper tropospheric and lower stratospheric carbon dioxide, Tellus, 43B, 106–117, 1991.

Nakazawa, T., Murayama, S., Miyashita, K., Aoki, S., and Tanaka, M.: Longitudinally different variations of lower tropospheric carbon dioxide concentrations over the North Pacific Ocean, Tellus, 44B, 161–172, 1992.

Nakazawa, T., Sugawara, S., Inoue, G., Machida, T., Makshyutov, S., and Mukai, H.: Aircraft measurements of the concentrations of CO_2, CH_4, N_2O and CO in the troposphere over Russia, J. Geophys. Res., 102, 3843–3859, 1997.

O'Brien, D. M. and Rayner, P. J.: Global observations of the carbon budget, 2. CO_2 column from differential absorption of reflected sunlight in the 1.61μm band of CO_2, J. Geophys. Res., 107, NO. D18,4354, doi:10.1029/2001JD000 617, 2002.

Olsen. S. C., Randerson. T.: Differences between surface and column atmosphere CO_2 and implications for carbon cycle research, J. Geophys. Res. 109, D02301, doi:10.1029/2003JD003968, 2004.

Orr, J. C., Maier-Reimer, E., Mikolajewicz, U., Monfray, P., Sarmiento, J. L., Toggweiler, J. R., Taylor, N. K., Palmer, J., Gruber, N., Sabine, C. L., Quere, C. L., Key, R. M., and Boutin, J.: Estimates of anthropogenic carbon uptake from four three-dimensional global ocean models, Global Biogeochem. Cycles, 15, 43–60, 2001.

Parazoo. N., Denning. A., Kawa. S., Corbin. K., Lokupitiya. R., and Baker. I.: Mechanisms for synoptic transport of atmospheric CO_2 in the midlatitudes and tropics, Atmos. Chem. Phys. Discuss., 8, 12197-12225, 2008.

Park. S., Jimenez. R., Daube. B. C., Pfister. L., Conway. T. J., Gottlieb. E. W., Chow. V. Y., Curran. D. J., Matross. D. M., Bright. A., Atlas. E. L., Bui. T. P., Gao. R. –S., Twohy. C. H., and Wofsy. S. C.: The CO_2 tracer clock for the tropical tropopause layer, Atmos. Chem. Phys., 7, 3989-4000, 2007.

Peixoto, J. P., and A Oort, Physics of climate, 520 pp., Am. Inst. Of Phys., New York, 1992.

Petit, J. R., I Basile, D raymaud., C. Lorius., J. Joyzel., M. Stievenard., V. Y. Lipentov., N. I. Barkov., B. B. Kudryashov., M. Davis., E. Salzman and V. Kotlyaov. 1997. Pour climate cycles in Vostok ice core. Nature, 387: 359-360.

Petit, J. R., J. Jouzel., D. Raynaud., J. M. Barnola., M. Benders., J. Chuppellaz., G. Delayque., M. Delmotte., M. Legrand. 1999, Climate and atmospheric history of the past 420,000 years from the Vostok ice core, Antarctica. Nature, 399: 429-436.

Platt, U., Differential optical absorption spectroscopy (DOAS), in air monitoring by spectroscopic techniques, John Wiley, New York, 1994.

Platt, U. and Stutz, J.: Differential optical absorption spectroscopy (DOAS) Principals and Applications, Springer, New York, 2006.

Post, W. M., Peng, T. H., Emmanuel, W. R., et al., The global carbon cycle. American Sciantist, 78, 310-326. 1990.

Ramankutty, N. and Foley, J. A.: Estimating historical changes in global land cover: croplands from 1700 to 1992, Global biogeochem. Cy., 13, 997-1027, 1999.

Ramaswamy, V., Boucher, O., Haigh, J., Hauglustine, D., Haywood, J., Myhre, G., Nakajima, T., Shi, G. Y., and Solomon, S., 2001 Radiative forcing

of climate. In Climate change 2001: The scientific basis. Contribution of working group I to the third assessment report of the International Panel on Climate Change, Cambridge university press, Cambridge, UK, pp 349-416.

Rayner, P. J. and O'Brien, D. M.: The utility of remotely sensed CO_2 concentration data in surface source inversions, Geophys. Res. Lett., 28, 175–178, 2001.

Rodenbeck, C., Houweling, S., Gloor, M., and Heimann, M.: CO_2 flux history 1982-2001 inferred from atmospheric data using a global inversion of atmospheric transport, Atmos. Chem. Phys., 3, 1919–1964, 2003.

Rodenbeck, C., S. Houweling, M. Gloor, and M. Heimann (2003), Time-dependent atmospheric CO_2 inversions based on interannually varying tracer transport, Tellus, Ser. B, 55(2), 488– 497.

Rodgers, C. D. (2000), Inverse Methods for Atmospheric Sounding. Theory and Practice, World Sci., River Edge, N. J.

Rozanov, V. V., Buchwitz, M., Eichmann, K. U., de Beek, R., and Burrows, J. P.: SCIATRAN - a new radiative transfer model for geophysical applications in the 240-2400 nm spectral region: The pseudo-spherical version, presented at COSPAR 2000, Adv. Space Res., 29(11), 1831–1835, 2002.

Ryall, D. B., Derwent, R. G., Manning, A. J., Simmonds, P. G., O'Doherty, S.: Estimating source regions of European emissions of trace gases from observations at mace head, Atmos. Environment., 35, 2507-2523, 2001.

Saunders, R., Rayer, P., von Engeln, A., Bormann. N., Strow, L., Hannon. S., Heilliette. S., Lui. Xu., Miskolczi, F., Han, Y., Masiello, G., Moncet. J.-L., Uymin, G., Sherlock, V., Turner. D.S.: A comparison of radiative transfer models for simulating Atmospheric Infrared Sounder (AIRS) radiances, J. Geophys. Res., 112, doi:1029/2006JD007088, 2007.

Schneising., O, Buchwitz. M., Burrows. J. P., Bovensmann. H., Reuter. M., Notholt. J., Macatangay. R., and Warneke. T.: Three years of greenhouse gas column-averaged dry air mole fractions retrieved from satellite − Part 1: Carbon dioxide, Atmos. Chem. Phys. Discuss., 8, 5477-5536, 2008.

Scholes, M. and M.O. Andreae, 2000: Biogenic and pyrogenic emissions from Africa and their impact on the global atmosphere. Ambio, 29, 23-29.

Shia, R.-L., Liang, M.-C., Miller, C. E., and Yung, Y. L.: CO_2 in the Upper Troposphere: Influence of Stratosphere-Troposphere Exchange, Geophys. Res. Lett., 33, L14814, doi:10.1029/2006GL026141, 2006.

Strow. L. L., Hannon, S. E., De-Souza Machado. S. Motteler, H. E., and Tobin, D. C.: Validation of the Atmospheric Infrared Sounder radiative transfer algorithm, J. Geophys. Res, 111, D09S06, doi:10.1029/2005JD006146, 2006.

Susskind, J., C. D. Barnet, and J. Blaisdell (2003), Retrieval of atmospheric and surface parameters from AIRS/AMSU/HSB data in the presence of clouds, IEEE Trans. Geosci. Remote Sens., 41(2), 309– 409.

Takahashi, T., Sutherland, S. C., Sweeney, C., Poisson, A., Metzl, N., Tilbrook, B., Bates, N., Wanninkhof, R., Feely, R. A., Sabine, C., Olafsson, J., and Nojiri, Y.: Global sea-air CO_2 flux based on climatological surface ocean pCO_2, and seasonal biological and temperature effects, Deep-Sea Res. II, 49, 1601–1622, 2002.

Thomson, D. J., Criteria for the selection of stochastic models of particle trajectories in turbulent flows, J. Fluid Mech., 180, 529-556, 1987.

Tiwari, Y. K., Gloor, M., Engelen, R. J., Chevallier, F., Rodenbeck, C., Korner, S., Peylin, P., Braswell, B. H., and Heimann, M.: Comparing CO_2 retrieved from AIRS with model predictions: implications for constraining

surface fluxes and lower-to-upper troposphere transport, J. Geophys. Res.,
111, D17 106, doi:10.1029/2005JD006 681., 2006.

Trishchenko, A. P., Rublev, A., Uspensky, A. B., Udalova. N., Buchwitz, M.,
Rozanov, V., Rozanov, A., Zhuravleva, T., Wang, S., Trotsenko, A. N.,
Fernandes. R.: The potential and limitations of satellite observations for CO_2
retrievals over boreal forests.

Ustinov. E. A.: Atmospheric weighting function and surface partial
derivatives for remote sensing of scattering planetary atmospheres in thermal
region: general adjoint approach, doi:10.1016/j.jqsrt.2004.08.003, 2004.

Verver, G. H. L., and A. A. M. Holtslag, Sensitivity of an operational puff
dispersion model to alternative estimates of mixed-layer depth, in Air
Pollution Modelling and its Application, vol. IX, pp 315-321, edited by H.
van Dop and G. Kallos, plenum, New York, 1992.

Warneke. T., Yang. Z., Olsen. S., Korner. S., Notholt. J., Toon. G. C.,
Velazco. V., Schulz. A., and Schrems. O.: Seasonal and latitudinal variations
of column averaged volumne-mixing ratios of atmospheric CO_2, Geophys.
Res. Lett. 32, L03808, doi: 10.1029/2004GL021597, 2005.

Washenfelder, R. A., G. C. Toon, J.-F. B., Yang, Z., Allen, N. T., Wennberg,
P. O., Vay, S. A., Matross, D. M., and Daube, B. C.: Carbon dioxide column
abundances at the Wisconsin Tall Tower site, J. Geophys. Res., 111, D22
305, doi:10.1029/2006JD007 154, 2006.

Wright, J. and Colling, A. Seawater: Its composition, properties, and behaviour.
Pergamon Press, in association with the Open University (Oxford England and
New York) (ISBN 0080425186). 168 p. 1995.

Yang, Z. H., Toon, G. C., Margolis, J. S., and Wennberg, P. O.: Ground based
Inversion of CO2 column densities from solar spectra, geophys. Res. Lett, 29,
doi:10.1029/2001GL014537, 2002.